NELSON MANDELA UNIVERSITY

RESEARCH THESIS:

Enhancement of domestic solar photovoltaic unit productivity through the use of a cost effective tracking system

SUBMITTED IN FULFILMENT OF THE REQUIREMENTS FOR THE DEGREE OF:

Doctor of Philosophy: Engineering: Mechanical

IN THE FACULTY OF :

ENGINEERING, THE BUILT ENVIRONMENT AND INFORMATION TECHNOLOGY

AT THE

NELSON MANDELA UNIVERSITY

John Henry Cawood
Student Number: 213282909

Submitted: April 2021

Promoter : Prof. Russell Phillips

NELSON MANDELA UNIVERSITY

DECLARATION BY CANDIDATE

NAME: John Henry Cawood

STUDENT NUMBER: S213282909

QUALIFICATION: Doctor of Philosophy : Engineering ; Mechanical

TITLE OF PROJECT:

Enhancement of domestic solar photovoltaic unit productivity through the use of a cost effective tracking system

DECLARATION:

In accordance with Rule G5.11.4, I hereby declare that the above-mentioned treatise/ dissertation/ thesis is my own work and that it has not previously been submitted for assessment to another University or for another qualification.

SIGNATURE: 

DATE: 19 December 2020

ABSTRACT

The majority of new and existing small photovoltaic (PV) installations in South Africa are fixed-panel systems, largely due to the cost of photovoltaic panel components having reduced steadily in recent years where an increased requirement is met with a larger number of panels, whilst tracking system costs remain prohibitively expensive. Fixed installations realise only a part of their energy potential as they are truly effective for only short periods of the day.

The aim of this study is to investigate and build on the current technology of PV tracking systems with the aim of specifying a simple control and actuation system which performs the tracking function. The eventual purpose of this thesis is to reliably produce more energy from solar photovoltaic installations than similar installations using fixed panels. This would be achieved by the use of an effective and affordable tracking system which yields acceptable accuracy and reliability and opens the potential for the system to be further developed for other purposes. These alternative uses could be the control of sunlight into green buildings, control of dampers for building ventilation and cooling and Trombe wall air control. This study has investigated the potential of several passive and active methods to actuate a sun tracking system. A useful closed loop system, which uses low pressure hydraulics, was developed and tested. The prototype is detailed in the drawings, **Appendix D**.

Keywords: *solar power, photovoltaic systems, solar tracking, double axis*

ACKNOWLEDGEMENTS

The support and long term assistance of Prof. Russell Phillips is roundly appreciated, as well as the enduring patience of my wife for all the hours conceded to the sun.

“Truth is ever to be found in simplicity and not in the multiplicity and confusion of things” - *Isaac Newton*

CONTENTS

FIGURES

TABLES

PHOTOGRAPHS

APPENDICES

ABBREVIATIONS and SYMBOLS

PV	Photovoltaic
kWe	Installed capacity at full output
∅	Error angle in the East-to-West direction
θ	Error angle in the North-to-South direction
α	Compounded panel error angle
ß	Module error angle (90 - α)

1.0 SUMMARY:

Electronic tracking systems for photovoltaic (PV) systems are commercially available. They are accurate but expensive in relation to the components which they serve. One source in the USA (1) estimates the additional cost of a typical 4kWe installation at 57% for single axis and 100% for a dual axis tracking system, over the cost of a fixed system. These statements are made against assumptions of 35% to 40% improved production and states that payback periods could be up to 19 years when calculated as savings against US power costs.

The drawbacks of these devices in the Republic of South Africa (RSA) is a shortage of local technical support and poor operation in cloudy weather or in other diffuse sunlight conditions. Despite these disadvantages, single axis installations which track only the elevation of the sun, such as those used on large installations, display definite increases in energy production in comparison with fixed panel installations. Further improvements can be realised by adding a second axis of articulation to track the compass angle (azimuth) in addition to the elevation tracking, which increases production still further. It stands to reason that the expected benefit should outweigh the additional cost. The very wide range of reported improvements due to tracking, ranging from 10% to 75%, are not irrational, but that the diverse results are dependent on many variables such as light diffusion and angle of latitude of the test site (2). Conservatively, a 20% increase for the first tracking axis (polar tracking East to West) and a further 10% gain from the second axis (North elevation) appear to be achievable at the site, as borne out by the research.

Dual axis trackers constantly align their photovoltaic (PV) payload to the position of the sun and automatically also adjust for the gradual seasonal changes of both the azimuth and the zenith, due to their closed loop feedback control system.

This research attempts to simplify the actuation and feedback systems with the view to achieving acceptable accuracy with an affordable yet reliable tracking system.

2.0 INTRODUCTION:

The path of the sun observed from any place on earth and on any day of the year is well documented. The directional variations from sunrise to sunset, as well as the elevation of the sun vary with the angle of latitude of the observer, time of day and day of the year. Due to the arc shape of the solar path, the angular position of the sun angle changes with every passing minute at an average rate of around four minutes per degree of arc.

For simplicity, observations of the sun are taken relative to the site on earth, as if the sun travels the solar path and not that the earth travels about the sun. To simplify the complex arc of the solar path, the sun position is considered as the junction of two angles as seen by the observer, these being the azimuth angle and the elevation angle. Manipulation of the panel normal to these two planes ensures highly accurate co-ordinates of the sun's position.

For simplicity, cost and risk purposes, small installations in South Africa are generally fixed. They are mounted North facing and aligned to some elevated angle approximating the angle of latitude of the site but often just coincident with the roof angle. That useful power is generated from this setup is testimony to the forgiving nature of photovoltaic panels, as useful generation is obtained despite some considerable daily and seasonal misalignment, due partly to the ambient or background radiation. The panel alignment is sometimes biased for a greater benefit early or late in the day by a bias of the azimuth eastward or westward, also often installed to align below the equinox noon zenith to improve wintertime production. Due mainly to the angular error and reflection, the fixed panel is considerably underproductive in the early morning and late afternoon,

allowing the alignment to be optimal for just a few minutes per year, with only minutes of near-optimum exposure each day when the solar radiation approaches a right angle with the panel.

The solution is obviously to manipulate the panel to face the sun as squarely as possible for as long as possible on every sunshine day of the year.

The installer is faced with a choice of several tracking devices which track either or both of the solar coordinates and are commonly labelled single axis or double axis systems, although the single axis being tracked may be either the azimuth angle or the elevation angle. The articulation of the azimuth axis is also most often rotational about a vertical axis, rather than tilting.

Single axis tracking is usually in the elevation plane, which also requires the smaller articulation of the two axes and requires less land area due to the panels being arranged with minimal side clearance. Most large installations with dual axis tracking systems rotate the payload to track the azimuth and tilt to track the elevation (Rotate/Tilt). Applications of large dual axis installations and smaller off-grid installations, utilising single frame structures often tilt the payload in both planes (Tilt/Tilt).

These are the only methods of terrestrial dual axis payload articulation although they are described in literature by many different names and acronyms.

The drive to improve energy production from a defined size of installation is frustrated by the ever decreasing cost of photovoltaic panels reducing from R5-00/kWh in 2005 to around R0-60 in 2020 (3), however the landed costs of the auxiliary components - inverter units and battery storage - are still excessive

and prices are still escalating due to unfavourable foreign exchange rates. Additional choices such as the superior Lithium-ion type batteries and grid-tied inverter functions escalate the overall balance of installation cost by a further estimated 40%.

Dependent on ground albedo and light conditions at the site, an underslung additional panel, a bifacial or back panel, is reported to add up to 35% of production in stand-alone installations and another 30% to the cost of the single panel system (3). Back panel installations are also expected to benefit from tracking due to the reflected background albedo being aligned to the azimuth but no study could be found to quantify this theory at the time of writing.

A longer term motivation for tracked systems is the pollutant cost of producing panels with the view that optimised installations require less panel area per Watt hence less pollutants are created per unit of energy produced, whatever the future energy requirement and market pricing may be.

An example of a local situation is presented here -

In RSA, for a year 2020 rounded cost of R 4 615-00 per KWe for panel supply only, a single axis tracking kit with a limit of 1 kW payload is advertised online for R 4 360-00, or 94% of the panel cost per axis, even before adding the costs of the Balance of System (BoS) components and labour. At RSA retail prices for domestic power of R1.90/kWh for usage under 350kWh per month (4), the payback period for panels only is 20 months at 65% nett output for the fixed panels and 29 months for the single axis system and panels. Adding the second

tracking axis and estimating the BoS costs at 100%, the fully tracked 1kWe installation would cost around R27 000 and save around R340 per month at current prices. Scaling up, a useful sized 4kWe household system would cost R108 000 and pay for itself after 80 months. These estimations ignore other costs such as the power utility's monthly service charge and escalating power tariffs, which would shorten the payback period if taken into account.

The solution appears to be obvious – provide new installations with full tracking systems; however there are a few drawbacks to this option in RSA -

- They are costly.
- They are not yet well supported in RSA.
- They are affected by cloudy weather and other atmospheric conditions.
- They are complex devices reliant on electronics, gearing and electrical power. The integrity of each of these components are integral to the functionality due to their series arrangement, any component failure renders the entire system inoperable.
- They have limited appeal for some locations such as rooftops, due to their space requirement for full articulation.
- The structural integrity of the installation depends on the interface between framework and support structure so that the actuation device carries all transmitted loads. In windy areas some of the products on offer are too light for the task.

Contributing to this list is the African context; designs and solutions which perform satisfactorily in a more benign environment often do not stand the test

of time on this continent with its abundance of environmental factors such as heat, dust, humidity, aggressive insects, torrential rains and lightning.
All of the above contribute to the poor selection and availability of tracking systems in the local market, to the point where many installers claim that tracking systems provide no nett financial benefit and recommend fixed installations, using the low cost of the PV panels as motivation. The long term performance guarantee expected from the consumer undoubtedly has a negative effect on the price of the tracking option.

The intent of this research is to explore various options to enable acceptable tracking and the practicality thereof as regards functionality, cost, reliability and accuracy.

The research is consolidated to present a possible alternative to the electronic systems and proposes a electromechanical device to align a solar payload along the path of the sun without the use of electronic circuitry, speed reducers or gearing. The device is proven in one axis and a slave linkage system developed to approximate the second axis, before being refined to enhance maintainability, reliability, performance and longevity.

3.0 LIMITATIONS OF THE RESEARCH:

3.1 Movements of the payload

3.1.1 Azimuth movement type - rotate or tilt

For maximum exposure it is imperative that a dual axis movement is specified. Tracking of the elevation is always achieved through tilting of the payload however azimuthal tracking could be achieved with either tilting or rotating movements.

To showcase the wide range of articulation the author has chosen to use a rigid centre column and tilting movement for both tracking motions.

3.1.2 Range of movement of the payload

Articulation of 180˚ is not impossible but rather impractical due to the low energy density of early and late solar radiation which renders such large actuations for such little gain to be not feasible. For such a panel, a threshold angle of 30˚ above the horizons in the East/West (EW) plane is considered more practical and yields a somewhat simpler overall articulation. Similarly the range of articulation in the North/South (NS) plane range is relative to the EW elevation and the noon elevation which ranges seasonally between the solstices.

For proof of concept the prototype will demonstrate a range of around 120˚ articulation in the East to West plane.

The location of the test site is at 25.67138˚ East and 34.00190˚ South, which places the rounded-off panel angle limits for the solstices at 12° in summer

and 57° in winter and the equinoxes at 34°. By fixing the elevation at the angle of latitude introduces unacceptable errors in the early and late periods of the day and the error at noon ranges from zero at the equinox to 22.4° at the solstices, hence some articulation is required for daily elevation to earn the definition of a two axis movement. The elevation range must comply to the above limits which equate to solar elevations of 78° and 33° respectively at the summer and winter solstices.

3.1.3 Parking position

At sunset and sunrise, the double axis Tilt-Tilt actuated panel would ideally be required to face at almost right angles to the East or West to meet the azimuth angle of a rising or setting sun (i.e. meet the very low elevation angle as well as the morning azimuth angle). However, the limitation of articulation of 30° above east and west horizons requires that the panel attitude has some northerly component at these limits.

Within these limits, two main choices exist as to the type of tracking path -

- The first philosophy is the fold-away concept where the payload returns to the horizontal position overnight. This attribute is desirable in stormy climates as the night-time resting profile poses a slim profile for storm winds, however the system needs to perform an unproductive half a cycle of movement to meet the rising sun and again to return to park position after the solar day.

  This concept is complex and implies some form of antagonistic drive to balance the payload without external stimulus. The actual driving force

is the amount by which one of the antagonistic forces exceeds the other and necessitates large unproductive forces.

- The second option is a gravity return system, which is simpler and has the advantage of being ready without unproductive early morning response. Tracking commences to follow the path of the azimuth whilst tilting to the daily zenith angle, then continuing this motion to the westerly position at sunset. During the night, the motive source cools or drains away and the structure returns to the East facing rest position under gravitational force.

The chosen compromise is a gravity system which has some form of storm lockout and a rigid structure to weather the forces imposed on the large profile. The antagonistic drive approach will be explored for academic interest.

3.2 Limits of the system

3.2.1 Accuracy target

An overall target is the deviation from perfect alignment to be within 10%. Neither axis require a bias due to the payload shape being almost square. Hence, as an angular measure, 10% implies an accuracy of 90% or 0.9 being the Cosine of the compounded error angle. This concept is shown in **Figure 3.2.1 a), b) and c)** where the error of alignment manifests as a shadow from a perpendicular pin on the payload. This method can be used as a quick reference on site to estimate the accuracy of the alignment. Perfect alignment creates no shadow from the pin i.e. Cosine 0° = 1.

Figure 3.2.1 a) - Using shadow to measure misalignment

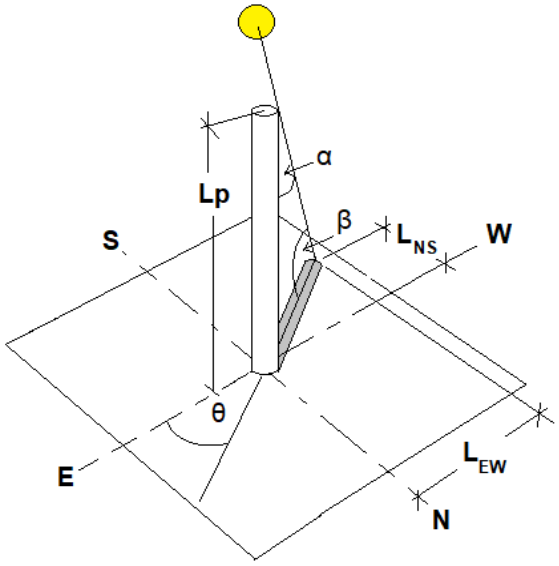

In **Figure 3.2.1 a)** the relative error in elevation is shown as angle β and the compounded correction of elevation is angle α. The azimuthal correction is shown as angle *θ*. Angle ∅ is not shown for simplicity.

The misalignment can be viewed as two components of the shadow being an EW component (L_{EW}) and a NS component (L_{NS}). The opposite side of this triangle is the length of the shadow L_S.

The triangles denoting the correction angles can produce polar corrections given the pin length L_P, The shadow length L_S and the azimuthal correction angle *θ* -

EW correction angle = ∅ = $Tan^{-1}(L_{EW} / L_P)$

NS correction angle = *θ* = $Tan^{-1}(L_{NS} / L_P)$

Figure 3.2.1 b) illustrates the effect of correcting only angle ∅, causing the shadow to fall along the North/South axis, similarly **Figure 3.2.1 c)** illustrates

the correction of only angle θ which causes the shadow to fall on the East/West axis.

Figure 3.2.1 b) - East/West error corrected only

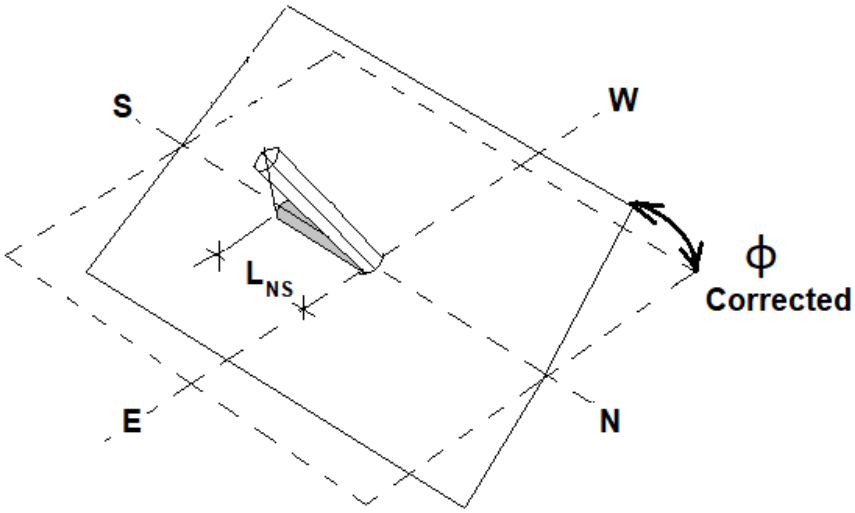

Figure 3.2.1 c) - North/South error corrected only

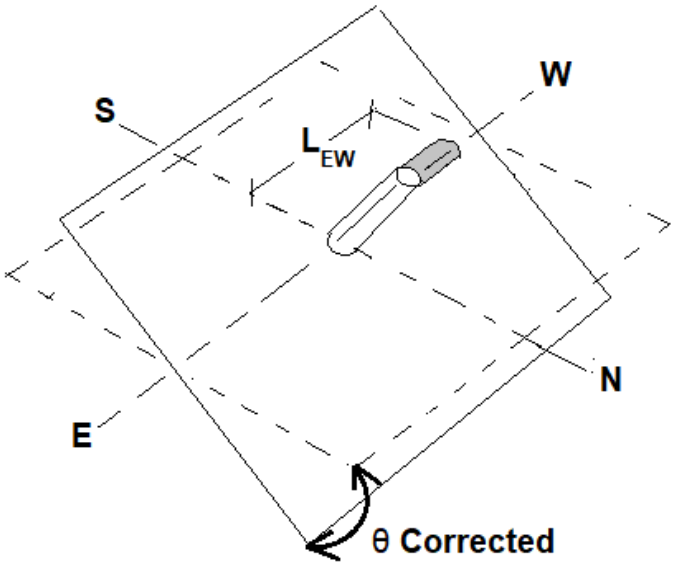

The pin is considered to be of negligible diameter, however the dimension L_S can be reduced by the radius of the pin to improve accuracy of measurement of small misalignments.

3.2.2 Compounded error and misalignment components

Applying any of the corrections ∅ or θ individually leaves a residual shadow in the South or East direction, hence the corrections must be compounded to eliminate any shadow.

To meet the performance criteria of 90% accuracy, the product of these two angles' Cosines must meet or exceed 0.9, hence -

Compounded error in two planes = Cos ∅ x Cos θ =0.9

For an equal error in both planes, Cos ∅ = Cos θ = $\sqrt{0.9}$ = 0.948

This implies the error angle range to be 18° in both planes on either side of zero error. However, the error angle would not always be equal in two planes hence, should one plane be perfectly aligned, i.e. Cos ∅ = 1 then the other plane has an admissible Cos θ alignment error of 0.9, equivalent to 25.8°.

Figure 3.2.1(d) illustrates the relationship of the permissible errors.

3.2.2 Linear array and matrices

The above philosophy for a single panel holds true for arrays and matrices but for one additional complexity, which is shading from one panel row to the next row and adjacent panels.

This thesis considers a single panel with tilting actuation in two planes, hence no allowance is made for shading effects.

3.2.3 Physical dimensions

For this thesis, a system comprising a single panel set of 4m^2 was proposed, equivalent to a pair of 325W panels on a fixed frame. The extent of the construction of equipment shall be limited to the stage of a satisfactorily working prototype, albeit with some upgrades during the evaluation phase. The optimisation of the construction of the intended device for the purpose of manufacture is considered but implementation is out of the scope of this research.

Figure 3.2.1(d) Limits of misalignment - permissible error curve

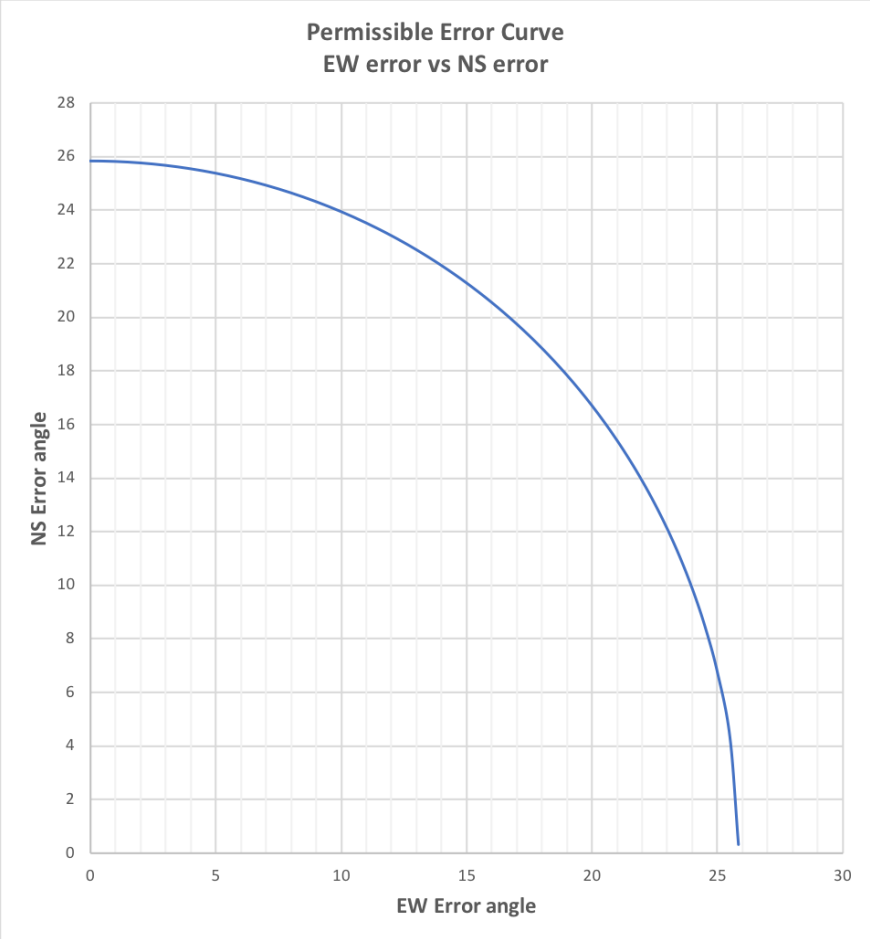

3.3 Power, energy and resources

3.3.1 Material sources and resources

The bulk of the materials and fabrication resources can be sourced from Nelson Mandela University (NMU) facilities. The balance of materials, equipment and any specialised services are sourced by the researcher.

3.3.2 Energy sink

For evaluation of energy production the system must be loaded hence the university must have capacity to absorb the power supplied and allow the system to perform to its limits. It is planned to connect the panels in parallel across a resistance heater and measure the power produced across the resistance during several solar days, alternately fixed on some days and tracking on other days, corrected for the solar insolation on each day.

3.3.3 Control inputs

The control inputs are limited to those of a passive physical nature i.e. changes in the natural phenomena of temperature, shade and pressure as opposed to algorithm based positioner solutions or electronic comparator devices. Simplicity is paramount.

3.3.4 Power source

Power is sourced from the apparatus by whatever means available and not from external power inputs.

Due to the large number of possible motive energy sources that can be explored, this thesis is based mainly on the manipulation of water and air to

provide the work required, whether directly sourced from the system or generated independently by passive means and stored.

3.4 Metrology

The basis of the accuracy measurements will be done utilising two matched solar cells and recording the output current from each.

3.4.1 Orientation of solar cells and utilisation of data

The first cell is mounted horizontal and records a current which can be compared to horizontal radiation measurements recorded elsewhere on site. The second cell is mounted flat on the payload platform and measures the current produced during the day along the tracked path.
Comparison of the summation of these two current recordings indicate any improvement of the production of the tracked cell over the horizontal cell. The full payload output current can be predicted using the horizontal cell output, modified to reflect the momentary radiation value and the panel rating.

The payload platform is then fixed facing North at an elevation set to the angle of latitude. Comparative current data between the two cells provides a comparison of the fixed panel against which the tracked panel can be compared, referenced to the radiation and day of the year.

3.4.2 Load data and comparisons

The resistance heater considered above is connected across a Wattmeter and the output signal logged as instantaneous Watts generated.

Synchronous readings of the daily Insolation are also logged for comparison purposes in units of W/m^2.The ratio of power to insolation, corrected for panel area, yields the overall effectivity of the system. The results are plotted to illustrate any gains of tracking over fixed systems.

3.4.3 Data acquisition and storage

The data is collected using synchronised single channel USB dataloggers which are retrieved at the end of each phase and the data stored and backed up to a portable hard drive. Excerpts of the testing phase are provided in the thesis, full data is tabulated in the appendices.

4.0 PROBLEM STATEMENT:

A need exists for an economical control and actuation system which can manipulate a photovoltaic panel to track the solar path reliably and economically, to acceptable accuracy.

Sub-Problem 1: Control system and actuation

- Research the potential of using differential temperature of gases to provide a control error signal.
- Research the conversion of the error signal to a differential pressure signal through heating and cooling.
- Research the potential of shading of a PV cell to provide a control error signal.
- Test and identify methods of using an error signal to do useful work in an actuator.
- Identify and solve the related issues of damping, feedback and positioning.
- Prove the control process, using a mathematical model with estimated physical dimensions and heat exchange values to simulate the various options of signal magnification.
- Confirm the process using a computational model of the heat exchange, feedback and damped responses.

Sub-Problem 2: Prototyping and Testing

- Conceptualise and design all components required to produce a prototype device based on the results of **Sub Problem 1** above. These components are expected to be structural, pneumatic and hydraulic in nature.
- Manufacture the prototype and assemble on the site provided by NMU.
- Perform the testing regimen as detailed in the Research Methodology Plan, **Chapter 6** below.

Sub-Problem 3: Final Specification

- Once testing is conclusive, consider every aspect of the prototype construction to improve ease and cost of manufacture.
- Produce a comprehensive final specification for the machine.

As evidenced by the conclusions to this work, the above actions were completed and are documented in this thesis and its appendices.

5.0 SIGNIFICANCE OF THE RESEARCH:

The objective of the research is to improve the productivity and hence cost effectivity of discrete PV installations through the use of a passive tracking system, by proving the concept with a prototype and by producing a final specification for a marketable device.

The significance of this research has a bearing on both environmental as well as financial aspects which have a further effect at the socio-economic level.

5.1 Environmental Impact of PV panels.

Photovoltaic cells produce no pollutants during operation but do require energy and create pollutants during their manufacture. According to Dai-Prá *et al* (5), the energy required to manufacture a solar module requires 8.5 years of operation to recover, whereafter the balance of a 25 year operating life can be considered clean energy production, chemical pollutants during manufacture not considered. The National Renewable Energy Laboratories of the USA (NREL) state that the carbon produced by PV manufacture, transport and installation is only 80g/kWh as opposed to 1000g/kWh for fossil fuel energy generation (6). Despite this fact, the availability of fossil fuels and the current state of the environment due to climate change and continued production of greenhouse gases compels us to use more renewable energy resources, amongst them the compromise of electricity generated by solar photovoltaic means. The impact of this alternative pollution can be reduced by producing the best possible output for every panel installed.

Assuming that a properly tracked system can conservatively produce 35% more power across its lifetime, by comparison the future demand could be met by 26% less PV hence manufacturing related pollutants could be reduced by 26%.

5.2 Financial Impact

A complete system comprises solar panels, an inverter unit, a storage device and cabling and installation with connection to the system by a licensed wireman. Local company Smart Energy SA offers several 3kW systems with prices ranging from R69 000 for the entry level grid-tied system. Using the NREL calculator (7), this system will produce 3573 kWh per annum, a saving of R6 788-00 and implying a payback period of 10 years. The calculator was set for single and double axis tracking estimates and returned savings of R9 000 and R12 170 per annum, suggesting payback periods reducing to 68 months.

There is as yet no administration cost from local authorities although City of Cape Town has stated their intention to pay 70c/kWh for grid feed and R1-90 for withdrawal.

On a socio-economic level, the research could impact positively on home owners and schools, whose power supply projects would benefit from a reduced footprint and more effective usage of assets. Another effect is to lower the cost of an effective system and widen the range of income groups who can afford to enjoy the benefits of this facility.

The research is significant to the Nelson Mandela University because it enhances an application of renewable energy and in so doing supports the renewable energy programme.

6.0 RESEARCH METHODOLOGY PLAN:

For clarity please refer to the Record of Activities, **Appendix A.**

To successfully realise the problem statement, the following methodology is planned –

6.1 Conduct Market Study

The market is researched to obtain technical and costing data on various tracking devices available.

Simultaneously, local providers and installers are interviewed about various aspects on the application of tracking technology in the local context and their observations and opinions are recorded.

6.2 Develop Prototype by Parts

6.2.1 Test rig

Design, fabricate, erect and maintain a suitable test rig which can be converted to trial several tracking variants.

As far as possible the components are made to be adaptable for use in the final complete prototype.

6.2.2 Trials of tracking variants

Cursory testing of several variants is done on the Primary axis to gauge response and practicality. The best performer of the trials will be pursued further. Non preferred variants are documented and recorded in the testing record in **Appendix B.**

6.2.3 Secondary axis activated

The success of the primary axis allows the complexity of the second axis to be included in the test rig without PV panels and some functional testing performed. A performance model, provided in **Appendix F**, is generated to predict performance.

6.2.4 Comparative testing

A pair of identical PV cells are mounted on the test rig, one vertical and one fixed to the payload plane. Current readings are collected over several months to establish a trend between the tracked plane and the vertical fixed plane.

6.2.5 Loaded and energised

The payload frame is fitted with two panels and these are connected to a load for evaluation of output. The articulation and balance are calibrated until response meets expectation. During this exercise, the East/West axis will be disabled for a period to produce a comparison with a fixed system, corrected for variability using daily insolation data. This concludes the testing of the functionality and accuracy of the drive system.

6.3 Develop Performance Model

The basic mathematical model in **Appendix F** is updated to match the actual results and eliminate any initial assumptions.

The model includes use of double panels and ground albedo.

6.4 Running activities

During normal running of the assembled system power data is collected routinely, accuracy is checked periodically and the results condensed to form a longer-term analysis.

Maintenance and any breakdown event is recorded, the cause determined and steps taken to prevent recurrence. During this phase the final specification will be drafted.

6.5 Finalise Thesis

A draft thesis is maintained throughout the project. The final specification is drawn up according to good engineering practises and material and cost information at that time. The thesis and associated documentation is submitted for scrutiny and evaluation to the Faculty.

A journal paper is drafted once the initial power testing results are compiled and submitted for publication during the thesis evaluation period.

A detailed costing exercise is undertaken under the assumptions of specific production volumes and manufacturing processes.

7.0 LITERATURE STUDY:

7.1 Local Practise

The overwhelming majority of small and medium installations in RSA are fixed systems, generally tilted to approximately the angle of latitude of the site and pointed true north in the southern hemisphere. Their power characteristic plot shows a pronounced bell-curve as the relative azimuth and elevation angles become progressively more advantageous until (true) noon and deteriorate in similar fashion thereafter, leaving the early and late parts of the solar day relatively unproductive. A popular installer has many examples where the panels are laid almost flat on the roofs of factories and shopping malls, as evidenced by the **Photo 7.1**, installed at latitude 29°South (Gateway Mall, Durban). The noon area aperture for a flat installation at this latitude ranges from 99% at summer solstice, through 87% at the equinox and only 62% at the winter solstice. Ironically, power requirements for lighting and heating are higher during the winter months due to shorter daylight hours and cooler days. This situation worsens with an increase in the latitude of a site as shown by Bahrami (8) and in Brazil by de Melo (9), for example a flat installation in Cape Town or Sydney at latitudes approaching 34°South has corresponding aperture areas of 98%, 83% and 56%. These figures are the best case scenarios as they only account for one direction of misalignment at solar noon. The East/West aperture area compounds these errors in the early and later parts of the day to yield a much lower daily aperture/time integral. Other influences such as sky clarity, humidity and coastal proximity also play a role in the strength of the insolation (9).

Photo 7.1 Flat mounted panels at Gateway Mall, KZN

"Gateway rooftop solar PV system. Photo courtesy of the SOLA Group (https://sola.africa/)".

7.2 Current Technology

7.2.1 Light source comparison

Tracking systems based on the error signal from different views of the same light source (10) currently dominate the tracking system market in one- or two-axis configurations. This system is a basic feedback control system which provides the input to a motorised actuation system to execute the control signals and align the payload with the ever-shifting solar angles of azimuth and elevation. See **Figure 7.2.1** which shows the possible articulation choices. The simplest type of tracker is a single axis control and is usually employed to tilt the payload to follow the sun's elevation above the horizon, whilst the direction of the payload is fixed at an angle approximately true north or south, dependent on the hemisphere of the site.

Figure 7.2.1 Choices for panel articulation

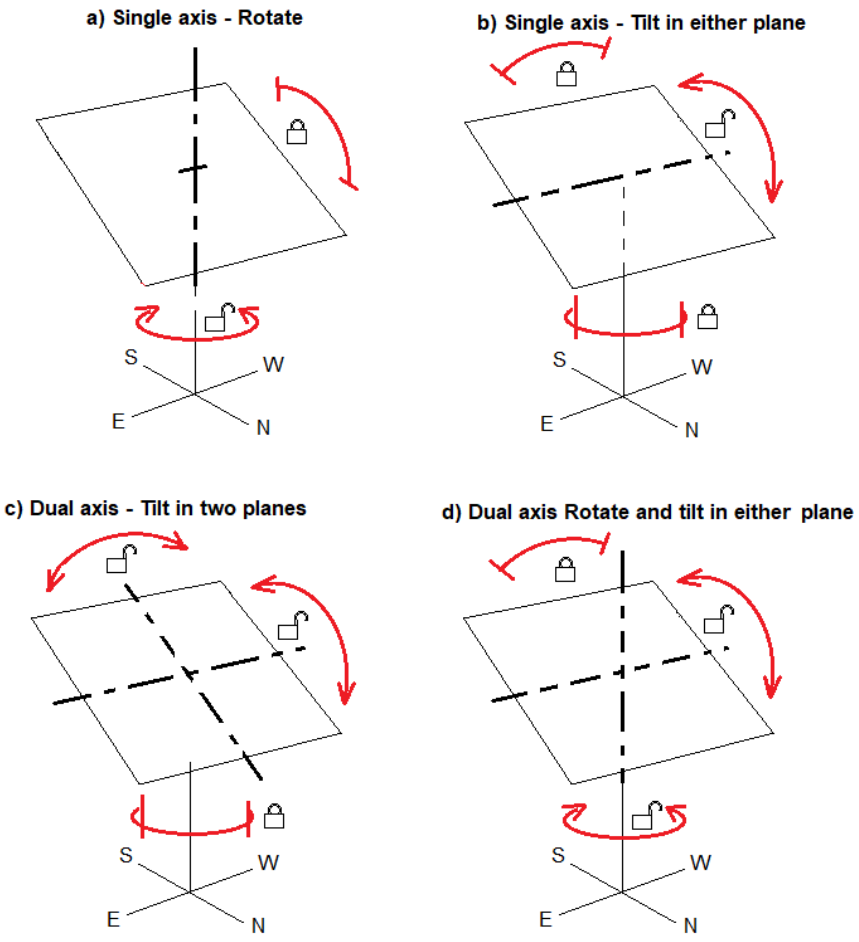

This provides the biggest payback for a single axis tracker in terms of power output and capital cost, according to Mousazadeh, but also advises against tracking of small systems due to the disproportionate energy requirement for tracking (11).

A second axis of control is available on more advanced trackers which supplements the above function with an additional East/West rotation. This two-axis system doubles the component count, cost and complexity of the of the single axis system but improves effectivity by around twice again of the improvement of the azimuth tracker (12).

Control systems, or devices whose purpose is to achieve a specific outcome by reacting to observed inputs, are of two basic types namely open systems and closed loop functions. Open systems control without regard to downstream effects (a pump whose speed is controlled by line frequency is oblivious to the level in the delivery side dam), whereas closed systems employ feedback to regulate the primary function, for example slowing the pump down when the dam level rises to a given height. The response of the controller can be modified in speed or extent to achieve a desired outcome. Clearly a tracking system requires feedback control to constantly follow the sun's path without any pre-programmed interrupts.

For this type of control, an error signal prompts a control response. The error is derived from a misaligned PV output from two light sensors with unequal outputs, due to one PV cell being more directly in alignment with the sun hence producing a stronger signal current. The logic maintains that the payload must move to benefit the poorer light signal and once a pre-determined error signal magnitude is reached i.e. a threshold start value, the power circuit to the motor is energised step-wise with the correct polarity to correct the alignment error. The payload moves and stops with the motor step and the feedback circuit re-evaluates the two source signals. This process is constantly repeated step-wise via the micro-controller until the two signals are similar or within a specified acceptable error tolerance i.e. acceptable error or ideally zero error signal. As the sun moves, the feedback error again increases until the threshold start voltage is again exceeded and the power circuit is stepped again. Damping and response are provided by motor speed

control, program wait commands and gearing. In this way, the tracker constantly re-adjusts itself to satisfy the error signal.

It can be appreciated that the mode of operation is not smooth but step-wise, resulting in a payload travel of many small start/stop operations.

An increased error signal tolerance increases the size of the stepped reactions and reduces the stress cycles, but at the cost of accuracy.

Considering that energy absorption is a continuous process, systems that respond in steps are only truly accurate for short periods of time, so that effectivity of the system is an average of the steps and overall effectivity of a PV panel is less than with a smooth or step-less system. Smooth response requires extremely small steps of feedback; it is most desirable to have constant (analogue) feedback.

One method to achieve this would be a similar system to the above motorised feedback system but with the improvement of a direct response to error i.e. in place of the error signal, both light sensors generate opposing magnetic fields within the same mechanical linkage. Once the fields are balanced the payload is in position, as the sun moves the changing magnetic field maintains the payload in optimum position (13). One problem prevents this system from being practically applied – the signal is too weak to do much work at all and must be amplified. Although this is achievable, the complexity persists in the form of induction actuators, amplifiers and external motive power requirements.

A further refinement which has found favour in the concentrator community is the addition of a computerised overriding controller, which uses date and time

to produce a desired position of the mirrors through the use of a heliostat algorithm. Where the simplistic optical system loses its way due to cloud or other interference, the computerised system takes control (14).

Despite all of the above, for the purpose of PV power generation, the background or ambient radiation provides a more forgiving environment for trackers in that exact alignment generates only slightly more energy than a closely approximated alignment, hence the limitation of a 90% alignment being deemed sufficient (12).

7.2.2 Bi-metallic strip passive trackers

This concept employs uneven heating of two or more bi-metallic strips to cause a deflection which is transmitted to the payload platform, tilting the platform towards the heat source. The strips have been employed in various orientations, some vertical and anchored to the ground, acting on the payload as proposed by Brito (15). Other designs use bimetallic strips horizontally mounted on the edges of the payload and acting against the centre column as suggested by Clifford (16).

Although the bi-metal deflection is almost proportional to the temperature change, the deflection is rather small and requires a large leverage ratio to achieve significant movement. The leverage acts to the disadvantage of the system when acted on from external forces, such as wind, when a small external force creates a large deflection of the payload platform.

Photo 7.2.2 A bi-metallic actuated single axis platform

7.2.3 Heated refrigerant passive trackers

This type of tracker has been utilised by the company Zomeworks who have installed in excess of 75 000 systems worldwide since their inception in the 1980's (17).

These are essentially a tilt/tilt type installation with the payload connected to the centre column via a universal joint. Thin tubes containing a liquid refrigerant gas are placed on opposite sides of the frame, either on two sides for single axis movement or four sides to create double axis pairs. Each tube is connected to a slim, high pressure actuator housed and anchored in the central column and connected to the payload platform via ball joints. The

tubes are framed inside curved reflectors to concentrate the radiation onto the tube surface. The misaligned panel causes one tube to heat more than the others, evaporating the refrigerant and causing a reaction to tilt the payload towards the heat source. As the cooler tube moves into alignment it begins to heat and the resultant gas pressure increase resists the movement. Ideally, the gas pressures all balance at perfect alignment and the system tilts along the solar path to maintain that equilibrium.

This system is totally passive but has some drawbacks. The leverage against the actuator, as with bi-metallics, is relatively large. The actuating pressures attained are also large, but exerted on relatively small bore actuator areas to conserve the available volume and achieve the desired travel, to meet a satisfactory range of articulation. For these reasons, this type of tracker is suitable for clear and windless days. On days with intermittent cloud, the system tends to oscillate constantly towards the park position and then try to catch up during a sunny patch. The time lag between heating and cooling tends to aggravate this problem. Other disadvantages of the system is the tendency to return to the horizontal overnight as the systems cool and pressures equalise. This causes a slow morning startup due to thermal inertia and the poor angle for heating the eastern refrigerant tube. Two positive aspects of this horizontal parking mode are the low profile presented to overnight storm winds and the fact that on cloudy days, the unresponsive panel stays horizontal and produces more power than a tracked system could provide, as discussed later. Zomeworks have discontinued manufacture of their passive tracker as electronic systems are more attractive in their simplicity and cost.

7.2.4 Shape Memory Alloys (SMA's)

Certain metal alloys of Iron, Copper, Gold, Nickel, Titanium and Zn have 'shape memory', which results in the alloyed material undergoing a transition between Austenite and Martensite when cooling, and the reverse reaction during heating. The mechanical effect produced when the metal is distorted cold is a strong reaction which causes the metal to revert to its original shape when heated. The best effect is obtained with Nickel Titanium alloys (NiTi) which is used for certain actuation duties. Poulek (18) utilised this feature to use a SMA actuator to track the sun using the thermal differential from a misaligned payload. His device actuated a single axis through the use of two bent leaf springs of Copper-Zinc-Aluminium alloy mounted antagonistically against a stator beam and inside a casing whose opening held a magnifying lens. A mirror surface was placed across the fulcrum between the springs. The wire springs, which were deformed cold, provided equal torque and hence equilibrium of the beam. Misaligned sunlight passing through the lens focussed on one spring which attempted to return to its original shape (Martensite to Austenite change) and generating greater torque force than its antagonistic twin, rotating the beam and improving the alignment. Once in alignment, the light focussed on the mirror and was reflected away from the springs, preventing further heating. Movement of the sun increased the misalignment and one of the springs would experience heating, again correcting the misalignment. In this way, Poulek's tracker 'locked-on' to the sun and maintained a good alignment across the day, within its 140° range.

7.3 Actuators

7.3.1 Common types

The most common type of actuator for small scale trackers is a linear screw type actuator with a geared drive as shown in **Photo 7.3.1**. This type of actuator allows very precise adjustment and has a large mechanical advantage, which prevents the system being manipulated by external forces.

Photo 7.3.1 Electrically actuated platform

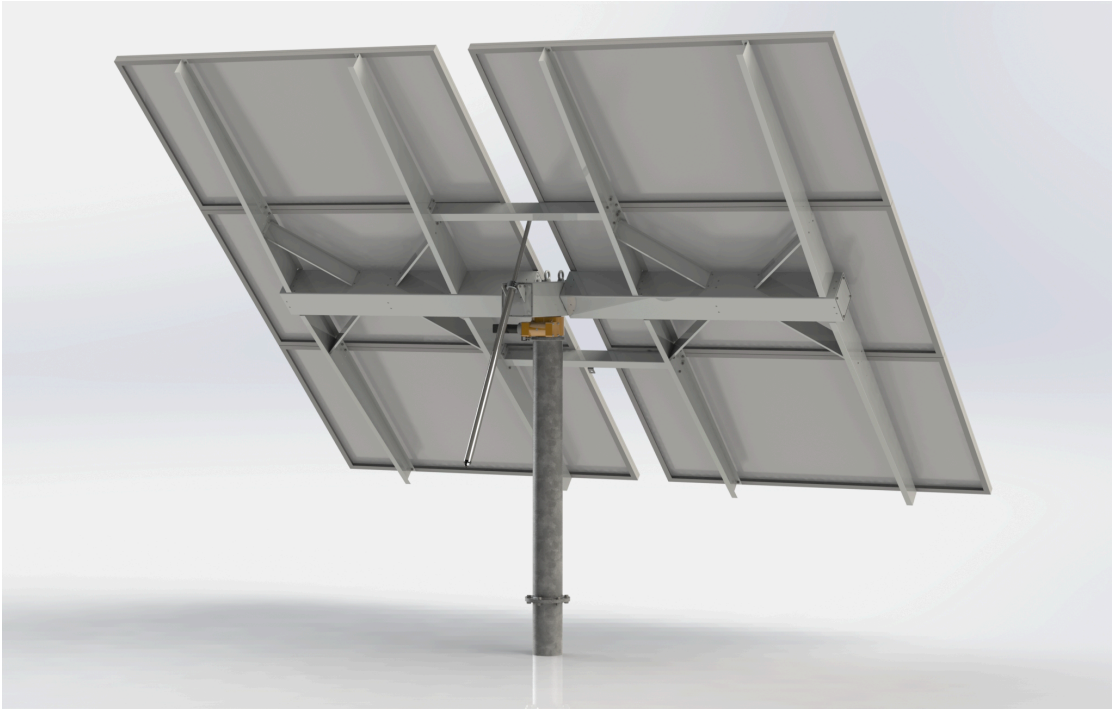

With compliments of Valdorex Greenpower

The disadvantages of this concept are -

- in some designs the actuator screw cannot be completely sealed against the elements, leading to contamination and wear.
- all external loads are transmitted to the anchor points via the screw threads, which have a limited shear area.

- at full extension the actuator is at its weakest and vulnerable to buckling under high externally applied loads.

This type of device is also available for multiple panel arrays as a heavy duty actuator system (19).

Lighter versions intended for small scale and domestic installations lack the industrial robustness of the equipment intended for commercial use and display many lower specification features. These are evident in the sheer lightness of construction, for example -

- casings are often thin steel pressings
- body tubes are light gauge aluminium tubing
- seals are standard nitrile rubber
- gearing is made of Nylon and Acetyl, not steel or bronze
- bearings are plain type bushings

Sector and worm drives are also offered for large scale solar farm installations for tilting of one or both axes (20). These are heavy duty devices with commensurate cost. A worm wheel is driven by a motor and drives a sector gear which is attached to the payload. The motion is not reversible so cannot be affected by wind or other external loads. These devices range from single payload actuators to multiple payload array drives. The model shown in the reference can operate up to 100 panels of $2m^2$ in single axis tilt configuration.

A recent commercial product for large scale PV arrays is the pneumatic bellows concept (21). A series of triangular rubber bellows are bonded together and mounted between the support column and the unbalanced payload. Pressurisation of the bladder extends the bellows portion and tilts the

payload platform. The payload is weighted to oppose the actuator and a bleed-off allows the payload to reset towards the default (morning) setting. Control is achieved by feedback from an optical comparator. An attempt to produce a bellows-derived actuation may be beneficial to the research.

For low friction actuation, a device which uses a rolling diaphragm (22) performs the role as a pneumatic or low pressure hydraulic cylinder. In place of the conventional piston and seal arrangement, a tubular diaphragm is used which is connected internally to the cylinder and, inverted within itself, has the other end connected to the cylinder rod. The space inside the diaphragm is pressurised with the motive fluid, which causes the rod to be extended and the diaphragm to be rolled out along the inside of the cylinder. The diaphragm is designed for high flexure and low extensibility thereby minimising rubbing action between the diaphragm and cylinder walls and delivering a highly efficient stroke. This device would certainly enhance the actuation of a solar tracking system, however the available models have large bore short stroke versions only for heavy duty applications.

Some developments in the use of rolling diaphragm actuators has been proposed in the medical field as a hermetically sealed spring with selective damping (23). These devices with their adjustable tension, silent operation and low frictional hysteresis are considered to be ideal tensioning devices for rehabilitation and permanent prostheses. The solar tracking actuator requires a stroke of at least 200mm to achieve 120° articulation without the actuator fouling on the centre column, use of the available device would require secondary linkages, increasing friction losses, cost and complexity.

Whilst a small bore, long stroke rolling diaphragm actuator may not be commercially available, some effort towards producing such a device could be beneficial.

A fluid driven tracking system is patented by Martinez (24) using two hydraulic actuators to actuate the two major tilt axes. The system uses conventional hydraulics and is unsuitable for domestic or small installation uses due to the size and cost.

7.3.2 Newer technology actuators

In their overview of novel actuation methods with a focus on robotic applications, Boyraz *et al* (25) investigates five types of actuation methods - shape memory alloys, fluidic elastomers, dielectric electro activated polymers, shape morphing polymers and electromagnetic actuators.

Of particular interest is the Fluidic Elastomer Actuation where a polymer 'muscle' is cast with voids, either interconnected (vascular) or isolated chambers as illustrated in **Figure 7.3.2** below.

The combination of fluidic pressurisation (or de-pressurisation or evacuation) of the various voids and vascular chambers causes the actuator to distort and do external work. In this way the actuator can extend, retract, bend curl, twist or perform any number of three dimensional movements.

This development is an evolution of the bellows concept (21) in that it could manipulate a payload in two planes using one actuator. This type of motion would require a column elastomer with four vertical rows of voids, pressurisation of two rows on any one side produces plain bending (flexing) whereas pressurisation and evacuation of diagonally opposed columns

produces flexure in the diagonal plane. For more precise positioning, several rows of voids at differing pressures increase the articulation in small increments across many angles. The fluid could be gaseous or liquid with the advantage that incompressible fluids would result in a firmer response, dependent on the elasticity of the material of the structure. Continuing this theme of pressurised geometric shapes, Blanes *et al* (26) proposed Additive Manufactured Polyamide actuator shapes to perform various motions. Their geometric shapes took the form of stacked toroids, serpentine tubes, spiral tubes and spheres. This work was intended to advance food handling robotics using small pressure and forces.

Figure 7.3.2 Fluidic Elastomer Actuation

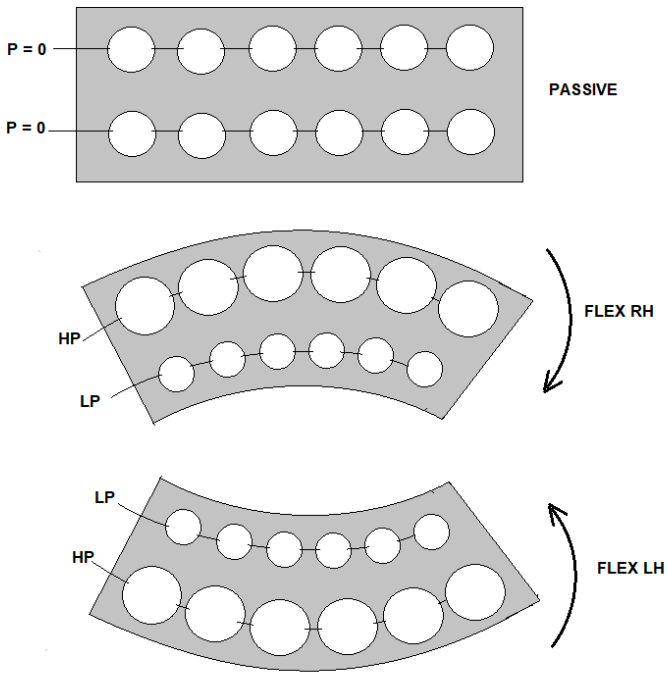

7.4 Potential gains due to tracking

Using a water pump as measurement of energy absorbed, Bione *et al* (27) realised a 50% increase in generated energy between fixed and tracked PV panels, using the same pumping equipment.

Baltas *et al* (28) found that fully tracked systems produced between 22.5% and 33% more energy than fixed systems, measured at three different sites. It was also found that by stepping the position of the array East to West in two stages daily and adjusting monthly for seasonal elevation changes, the installation produced 95% of the power of a fully tracked array.

Nann (29) found that a single axis tracked system produces almost as much energy as a dual axis for half the cost, a fact confirmed by Dickinson (30) on an annualised basis.

Estimated by Kalogirou (31), collector efficiencies of single axis tracking concentrator systems at the summer and winter solstices respectively would produce daily collection rates of 91.7% for polar East/West, 74% increasing to 86.2% for polar North/South tracking, 97.7% decreasing to 60.9% for a rotating fixed tilt type, all measured against a fully tracked system (100%). On this basis, a single axis polar East/West system appears to outperform any other single axis method. Annualised, the other single axis methods, rotating fixed tilt and northerly polar tilt produce very similar energy values.

Chang (32) produced a study using an east-to-west single axis tilt mechanism as compared to a horizontal panel, under varying latitudes and sky conditions. He found that the benefits were less than that of a single axis north-to-south tilt. Of greater interest is his claim that the tracked panel production increase

compared to the horizontal fixed panel varies from 12% to 134% between equator and the arctic.

Li *et al* (33) studied north-south tilted single axis trackers and concluded that the annualised energy generated was 96% of that of a fully tracked equivalent. When compared with fixed panels at optimum tilt angle they found that the improvement under high radiation conditions was 30% but in poorer conditions around 20%. It is not clear whether the effect of the background radiation or diffusion of the direct sunlight was the cause of this discrepancy.

7.5 Practicality of solar tracking in windy conditions

A payload suspended on actuators raises several concerns -

High wind loads can be experienced at any time of day, if the wind loading coincides with a large profile of a tilted panel array the coefficient of discharge of the wind force is magnified and the structure is abnormally stressed. Considering that all forces between the payload and the foundation are transmitted via the actuators raises the concern that the actuators need a higher safety factor than that required for normal operation.

The degree of motion is limited when considering mounting on a sloped surface such as a roof. The payload would need to be suspended above the roof to allow some movement and the wind reaction needs to be considered for the interface to the roof as well as the actuator, i.e. the stresses will be higher for the tilted profile than for panels mounted parallel and close to the roof surface.

Many studies have been done to determine the effects of wind on a tilted plane. Chu (34) determined that the maximum wind pressure occurred at an

inclination of 45° with wind facing 0° and 180°. The maximum inclination of the test device was 45°. It is most probable that a larger inclination will attract a larger wind load. Of greater concern was the yawing and pitching motions experienced when the wind direction was oblique. The wind creates alternating forces on opposite sides of the payload which could excite structural resonance with disastrous effects especially in an undamped structure. Chou *et al* (35) extended the study by monitoring elevations up to 80° and studied the pressure variations in two planes across a range of wind directions. The findings up to 40° concur with several other studies but a step change is experienced at inclinations above 50° producing a 'kink in the curve' and causing upliftment co-efficients which are very similar for 60° to 80° elevations.

The resonant problem is presented further by Rohr *et al* (36) when studied as a row or array of payloads in which each payload experiences a slightly higher deflection than its predecessor, resulting in 'galloping' arrays which stress and cause shearing of the common drive. This research is pertinent to single payloads as well, due to the same mechanism of vortex creation and vortex detachment lead to wildly undulating forces, as demonstrated in the paper's CFD renderings. A highly destructive form of resonance experienced in column mounted payloads is the torsional resonance about the vertical axis. Where this stiffness cannot be increased above wind shear excitation frequencies, the system needs to be flexible to allow deflection but with damping to absorb the resonant strain energy.

7.6 Cloudy or dusty environments

Cloud cover can confound optical trackers once the background radiation approximates or exceeds the direct radiation. Even considering perfect tracking through manual or algorithmic means, the tracked panel does not always exceed the performance of an equivalent fixed panel. As shown by Quesada (37), cloudy day results in Montreal, Canada, showed that the horizontal panel output exceeded the tracked panel output. On heavy overcast days it is more feasible to place the panel in a horizontal parked position than to attempt to track the sun behind the cloud cover. Elmer (38) reported that due to the diffuse light conditions in UK that tracking did not yield a significant gain. For reason of this diffuse sunlight, this situation should exist across northern Europe and Scandinavia.

It is a well known problem that dust accumulation on PV panels causes production losses. This fact is especially pertinent in low rainfall and dusty environments and at the mid-latitudes where the low panel angle far exceeds the repose angle for dust to slide off. Zorilla *et al* (39) studied the effects of dust coating of the glass of a fixed panel in a natural environment in Spain. During the rainy season even 1mm of rainfall was sufficient to restore the full effectivity of the panel, however in the dry summer months the losses exceeded 20% of expected output. Left to the elements, an overall loss of 4% of annual generation was experienced due to periods of dust contamination. Hussain (40) did practical experiments using different types of dust, ranging from chalk dust to rice husk. He concluded that the finer the contaminant, the higher the losses, largely irrespective of the nature of the dust but

acknowledged greater losses by dusts of red soil, then limestone and then fly ash. He also concluded that in desert areas, losses of up to 60% of output were possible. Logically, a payload that moves, whether it be rotating or tilting, stands a better chance of dislodging dust and finding a favourable aspect across the wind to keep itself relatively clear.

Cleaning of PV panels in dusty surroundings has received some innovative advances. Air and water cleaning systems are prevalent, however an effective dry cleaning method is a periodic static discharge which repels around 90% of the dust and can be regulated to perform autonomous cleaning periodically, at very small energy cost (41).

An innovative approach takes its cue from the lotus flower which emerges clean from the mud of its surroundings. Forbes (42) describes two innovative paint coatings which stay clean, one requires only water to stay clean in marine environments but the other, designed for transparent window surfaces, equally repels dust and water by employing nano-hairs which cause any contaminant to roll off the surface whilst the transparency remains unaffected.

A PV system to power streetlights was proposed by Zhang et al (43) who used four photo cells to track the payload in clear weather and a timer and stepper motor system for hazy conditions. The stepper motor advanced every few minutes when the photocell outputs were low.

A more sophisticated PLC based system was developed by Sungur (44). He programmed a PLC for a two axis solution for the position of the sun at each

minute of each day of the year and maintained accurate pointing in heavy overcast. As we have seen from Quesada, this performance is unnecessary when the background radiation equals or exceeds the direct radiation.

After evaluating five different tracking methods under three basic atmospheric conditions, clear, partly cloudy and heavy overcast, Koussa (45) discovered that under heavy overcast all tracking methods produced roughly the same amount of energy and the horizontal fixed panel performing the best.

7.7 Energy required for tracking

Not considering the additional burden of frost or snow, the amount of energy required to track a PV payload may be small, relative to the generation capacity of that payload. The reason for this is that whether the actuation is tilting or rotating, designers attempt to balance the payload so that the actuation forces required are balanced out to a large extent and the nett force required is little more than friction. Even a constant wind force will in most cases result in an almost even reaction about the axes, unless the velocity and angle of attack induce harmonic vibration, in which case the forces are large and alternating.

Lorenzo (46) describes the single axis Toledo plant in Spain (erected 1994) as having four payload sets of 250m^2, each driven by a 2.5hp (1.87kW) motorised drive. The drive capacity represents around 7% of installed capacity, but it must be noted that the drive only operates periodically and probably below 70% of its full rating, for reliability's sake. To estimate an accurate energy ratio between drive and installed capacity requires

knowledge of the drive time. Another method would be to know the energy requirement for one tracking cycle and divide that into the daily power generated to arrive at an energy usage percentage as a percentage of production.

Ahmad (47) declares a figure of 5.89% of generated power used by a two axis tracking system. A closer look at the research reveals that his PLC based controller used 5.84% of the power, the actual actuating motors used only 0.05%. It is also evident that the power was generated by two panels with a rating of 38W, which is impractically small.

The drive system in reference (20) specifies energy consumption for a single axis at 600kWh/MW_p/Annum. At its maximum load the unit consumes around 0.27% of the installed capacity.

7.8 Predicting the path of the sun

To begin to predict the position of the sun at a given site on the earth, some relevant site data is required, as the solar path changes each day and across the seasons. The most basic information is the site polar co-ordinates, latitude and longitude. The longitude is required to determine the solar noon at the site, when the sun reaches its daily zenith. The latitude dictates the noon elevation of the sun at the solstices and sets the limits for the noon elevation at the winter and summer equinoxes.

Many papers have been published of algorithms to produce a solar map for any particular site. An algorithm produced for the NREL by Reda and Andreas (48) produces a useful result valid for the years -2000 to +6000 with a claimed

uncertainty of 0.0003°. This is a complex calculation in sixteen parts and the result is irrefutably accurate.

For practical purposes, a website such as www.sunearthtools.com (49) will produce a polar plot of azimuth and elevation for any grid reference and for any particular day, including shadow effects for adjacent buildings. Such a plot for the test site is produced in **Figure 7.8** . The plot also shows the curves for seasonal limits. This plot was produced for the equinoxes on 21 March and 21 September. It is clear from the plot that, without shade from adjacent buildings, midsummer sunrise would occur at 29° South of East or Azimuth 119° but in midwinter this angle would be almost 29° North of East.
The plot is useful for setting up a tracking system as it references the elevation of the sun at any hour of the day on any day of the year.

7.9 Self actuating systems

In steam and thermal practise, there are several devices which self-actuate to achieve some form of control, using the medium being controlled as the actuation source. An example is a self-actuating temperature control valve whic

The system uses heat from the system being controlled to evaporate the fluid in the bulb and adjust the valve plug position to modify flow through the valve. Actuation is normally achieved by a light metal bellows and calibration is achieved by varying the volume in the sensor bulb (50). h uses a sealed bulb of fluid and a capillary tube to actuate a valve.

Figure 7.8 - Polar plot of the solar path at NMU North Campus

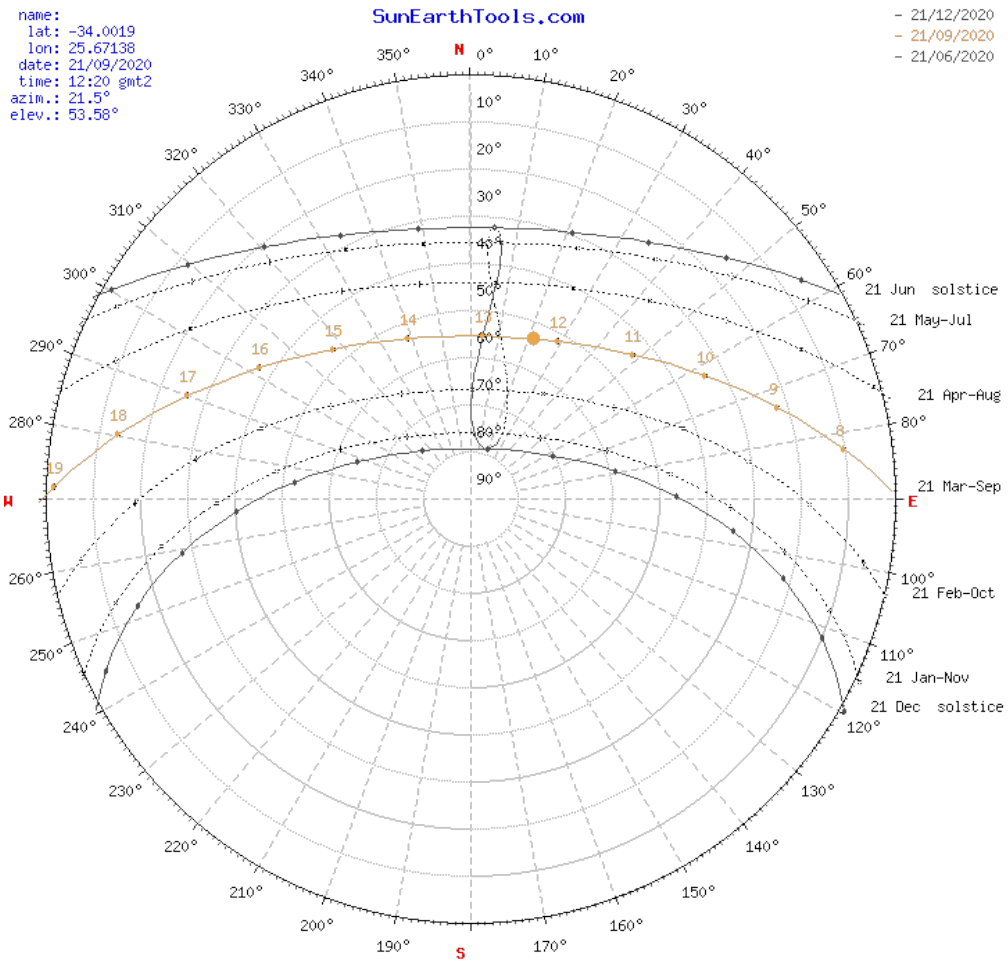

(Presented with permission from Creative Commons)

This principle is used across a variety of valve designs to regulate flow of cooling or heating fluids. The actuation strength and displacement is reliant on the volume of gas or vapor available and the temperature attained. For a large scale version of such a device, the same relationship is relevant and may be a workable solution for a passive solar tracker using thermal imbalance to correct alignment with the heat source i.e. the sun.

Another example of self actuation is the flue gas damper for fireplaces in cold climates. The damper is normally closed to exclude draughts with a small opening to allow a small fire to be started in the fireplace.

As soon as warm flue gases pass through the opening the damper begins to open itself. More heat causes a wider opening of the damper and the once the fire is out the actuator cools and the damper returns to the closed position.

These damper actuators are usually bi-metallic devices of various designs, of which there are around thirty registered patents in the USA alone. Other common uses for self-actuating devices are automotive cooling thermostatic valves (wax expansion), electric kettle automatic circuit breaker and refrigerator thermostats.

7.10 Powering the second axis

In the limitations of this thesis, a tilt/tilt dual axis system was decided on, based on initial research which indicated that useful gains could be made from the second tracking axis (51,52).

Mauro (53), He (54) and Hubach (55) all imagined that the first axis and the second axis could be combined to provide a rolling deck which remained normal to the sun. They concentrated on a four legged approach, one had four corner actuators with universal joints at each connection and worked on an algorithm to achieve two basic angles of correction. The other design was similar but each leg had a folding ‘knee’ to achieve the desired extension.

The work of Comsit (56) derived a position for the southerly tilting axis assuming an actuated rotating vertical primary axis. The linkages were on lockable sliders which allowed periodic adjustment for seasonal zenith and nadir positions.

No reference could be found to explore the possibility of using the idea of Comsit for a Tilt/Tilt configuration, i.e. actively tracking one tilting axis and passively tilting the second in a fixed but adjustable relationship. The actuation of a second axis from the first requires additional energy. The amount of energy required may be little more than the bearing friction and any damping or external (wind, snow) loading that may be present, should the system be well balanced to start with.

7.11 Summary of facts arising from the literature

Several pertinent facts have arisen from the initial research and interviews conducted

- There appears to be no consensus as to which tracking method is most effective and some research contradicts others, however it is noted that the research is done at diverse latitudes, on different continents, with differing atmospheric conditions and climates, all of which affect the annualised outputs. One aspect is certain, tracking systems of whatever nature, can increase solar electrical production by up to 35% (11,12) more than a fixed system, dependent on several variables. Using the logic of Chang (32) the NMU has the potential to collect 58% more energy than a fixed tilted payload, annually, using a perfectly tracked system. A pertinent statement is that of Kanyarusoke *et al* (51) who points out that the further the site is from the equator, the higher the benefit of the second axis of tracking.

- The method of tracking being considered, single axis, double axis, Tilt/Tilt or Rotate Tilt should take cognisance of the existing research in order to find the best solution for the intended locality.
- Perfect tracking alignment is not required in order to achieve significant improvements in production, as evidenced by the compounded error argument discussed in the project limitations; a 90% accuracy is achieved despite 18° misalignment in two planes. (28,29,30)
- Tracking systems are expensive in South Africa, often matching the cost of an entire fixed installation. Scarcity of local demand due to the negative aspects of quality, service, price and reliability places a further premium on these costs.
- Performance of the electronic systems (comparator and feedback types, with or without computational assistance), take good advantage of the available sunlight, although complexity and often questionable quality detracts from the benefits through unreliable performance. Lack of maintenance infrastructure and local know-how exacerbate the situation.
- Judging from the huge body of research into the subject as well as the numerous methods which have been devised to monitor and track the solar path, a system which delivers the benefits and negates the current problems would have far reaching demand in new and retrofitted installations.
- Tracked systems are considered by installers to be weaker than fixed systems since any external loading (wind, snow, birds) is transmitted to the support structure via the tracking actuation mechanism. This is not

necessarily true but rather depends on the design strength and suitability of the actuation devices.

8.0 SYSTEM CONCEPTS:

It is a goal of this project to achieve the tracking function in the simplest manner possible without resorting to external power, electronic control systems, time based algorithms, complex gear reductions and any other complexities which add cost and detract from longevity and reliability.

The largest required movement is in the primary axis from East to West. Once this axis has been mastered the smaller movement of the daily elevation can be addressed. As stated in the limitations, the choice of articulation is a dual axis Tilt/Tilt system.

8.1 Requirements for actuation and control

Actuation and control of a physical system requires work potential and limits to initiate and retard the rate of that work in comparison with a target position.

To move a structure from one position to a new position requires work where a force is exerted over a given distance. To do this work using a fluid, the force required is dependent on the pressure generated per unit area and the displacement is dependent on the effective volume of pressurised fluid available. To do the work using an unbalanced mass of fluid is dependent on the fluid density and volume displaced.

The force required to initiate movement is the sum of all resistances to motion including some form of damping, seal friction, bearing friction, opposition from an antagonistic cylinder, imbalance forces and other external influences such as wind. The chosen articulation is the tilting of a frame, so that the forces can be translated into moments of the frame about a central pivot, both positive and negative.

It is considered that movement is always slight, moving from one state of equilibrium to a new equilibrium, with some frictional hysteresis.

The temperature differential across a misaligned payload is proportional to pressure change, in a closed system, and the pressure differential thus created is utilised to correct the misalignment through antagonistic actuation. Positional control occurs when the pressures are balanced and no further work can be done to alter the platform angle.

In cases where the light source is interrupted, as on a cloudy day, the payload should remain static or recline slowly back to park position. Best productivity on an overcast day is achieved with a fixed horizontal panel, showing an improvement over a tracked panel (37,44) under these circumstances.

8.2 System variants considered

Actuation systems use various physical processes to do work on a system and control the position of the payload. Some examples are differential temperature, evaporation of refrigerant, change of state of wax, displacement of a mass or distortion of bimetallic strips. Some of these processes are passive and others are assisted. The mechanism for each actuation type differs widely from mechanical linkages to simple cylinders.

This chapter explores some of these passive actuation methods that were considered and tested and their potential to perform the tracking function.

8.2.1 Plain surface heating of a captive gas

This method as shown in **Figure 8.2.1** entails a hollow framework free to pivot in the planes required to follow the sun. The frame members are arranged to

face the compass directions and each member is hermetically sealed. All values of pressure and volume are initially equal.

The frame is partly shaded to receive sunlight only in its compass direction i.e. sun from the East only falls on the East member. The air trapped in the members is unevenly heated and the expanding air harnessed in an actuator which tilts the frame toward the sun. The opposite member is in communication with its own actuator which is arranged in conflict with the first i.e. antagonistically arranged so that the heated tube is tilted towards the heat source and control is exercised by the gradual exposure, heating and resistance from the opposite, cool, tube.

This system returns to park position when all gas volumes revert to their initial pre-charged state and the payload is horizontal. This requires the system to respond to the rising sun before actual tracking starts.

The warm actuator expands according to the general gas law from a condition (1) to a condition (2) -

$$(P_1V_1)/T_1 = (P_2V_2)/T_2 \quad \ldots\ldots (A)$$

The opposing actuator is slowly compressed at constant temperature according to Boyle's law to a different condition (3) -

$$P_1V_1 = P_3V_3$$

However, neglecting friction, the new pressure P_2 balances with the opposing pressure P_3 for equilibrium, hence for the cool side gas -

$$P_1V_1 = P_2V_3 \qquad \ldots\ldots (B)$$

As both volumetric changes supplement one another in a fixed volumetric ratio i.e. opposing pneumatic cylinders, -

$$V_2 + V_3 = 2V_1 \qquad \ldots\ldots (C)$$

Figure 8.2.1 - Plain surface heating of a captive gas

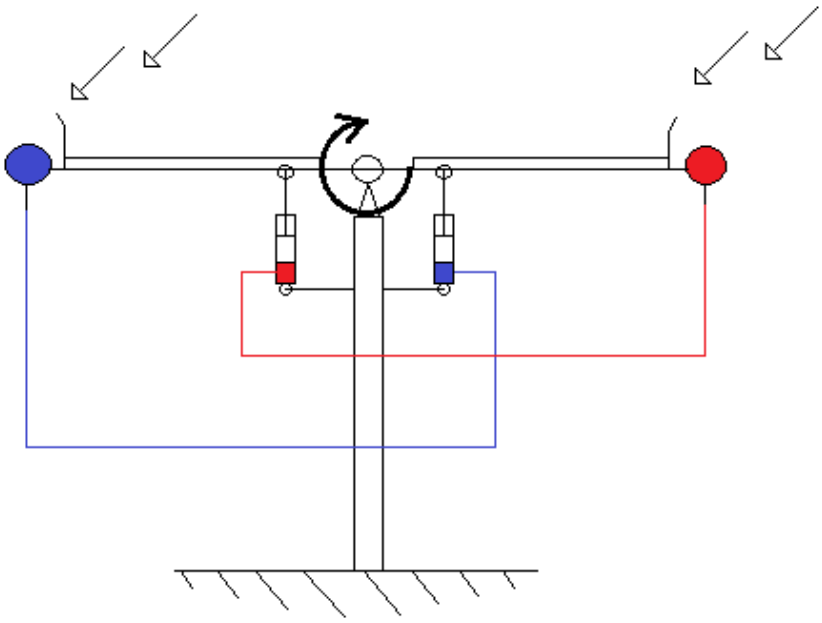

Manipulation of the above equations A and B by equating both sides to P_1V_1 leads to the statement -

$$V_3 = (V_2\ T_1)/T_2$$

Manipulation of equation C in favour of V_3 and equating both sides to cancel V_3 yields the solution for V_2 in terms of the known values -

$$\underline{\mathbf{V_2 = 2V_1/(1 + T_1/T_2)}}$$

The solution for V_3 is found as the difference from $2V_1$ and the equilibrium pressure P_2 is found from equation B.The work potential of this concept is limited to the differential temperature and initial charge pressure of the gas. A differential temperature of 20°C between the sensors would provide a pressure differential of 6.8 kPa(g) from an initial condition at NTP.

8.2.2 Enhanced heating of opposed captive gases using solar tubes

The system as described in paragraph 8.1.1 is upgraded to include two solar tubes which increases the maximum temperature above 150°C, with a corresponding pressure differential of 44kPa(g), as shown in **Figure 8.2.2**. The tubes would be mounted with preferential shade plates to ensure the East tube is exposed when the West tube is shaded, for antagonistic control and a rest position of a horizontal payload. The benefit of this system is the higher available gas pressure and potentially higher work capacity.

Figure 8.2.2 - Enhanced heating of opposed captive gases

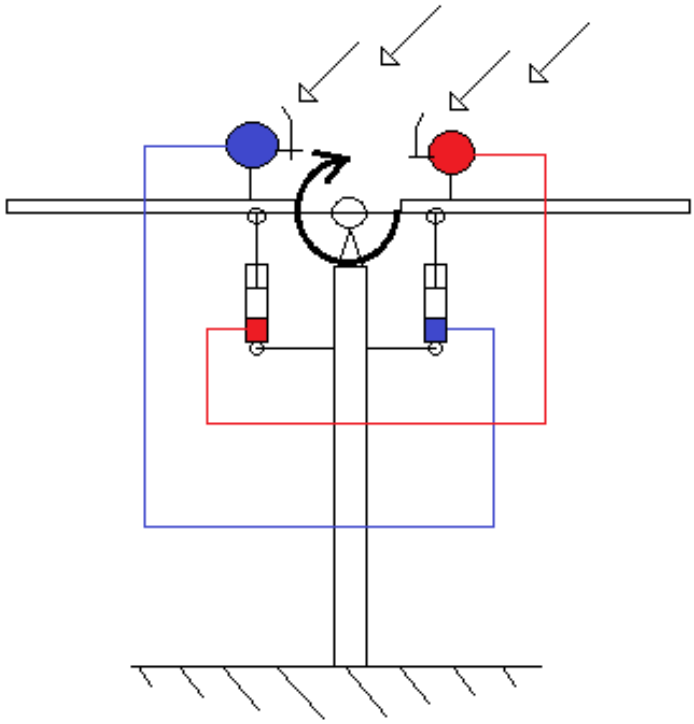

8.2.3 Enhanced heating of parallel captive gas volumes

A variation of the previous system is achieved by different arrangement of the same equipment, shown in **Figure 8.2.3**. The payload balance is disturbed to produce a bias to the East, so that the rest position becomes fully tilted to the

rising sun. The shade plates are both arranged to shade West to enable both tubes to heat at the same time and angle. The solar collector tubes are connected to the same cylinder to provide a reservoir of twice the volume of the previous arrangement but at the same pressure, alternately the second tube may be connected to the second cylinder rod-end to approximately double the moment with the same available expansion volume as before. The intent is that the solar tubes create a tilting movement away from the heat source which balances the heat-derived moment with the out-of-balance moment to track the sun until the motive moment is lost in late afternoon, at which the gas cools and the payload succumbs to the gravity moment and returns East for the next day. The pressure potential remains as with the previous concept but the available volume or actuator area is doubled. Multiple collector tubes increase the available volume further but add complexity.

Figure 8.2.3 - Enhanced heating of captive gas volumes in parallel

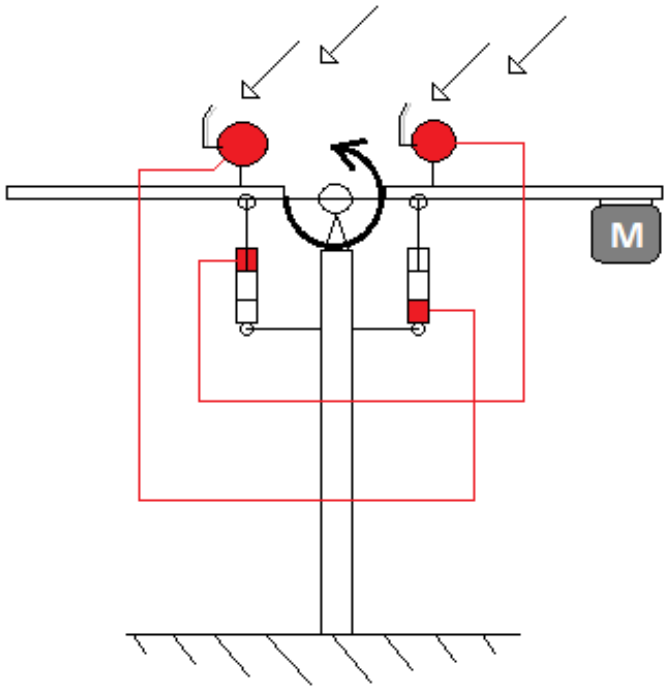

8.2.4 Gas expansion to displace a liquid weight

In a departure from using the heat derived pressure in a cylinder, the air is used to displace water from a fixed reservoir to a second reservoir on the payload platform with the intent of disturbing the equilibrium, as shown below in **Figure 8.2.4**.

Position control is again regulated by shade caused by the relative angle between sun and collector tube shade plate. As the tube is shaded the gas cools and allows fluid to siphon back to the fixed reservoir. The head pressure requirement is the height of the payload platform above the fixed reservoir and the gas volume that can be expanded at this pressure is the equivalent fluid volume which can be displaced to meet and exceed the bias mass.

Figure 8.2.4 - Gas expansion to displace a liquid mass

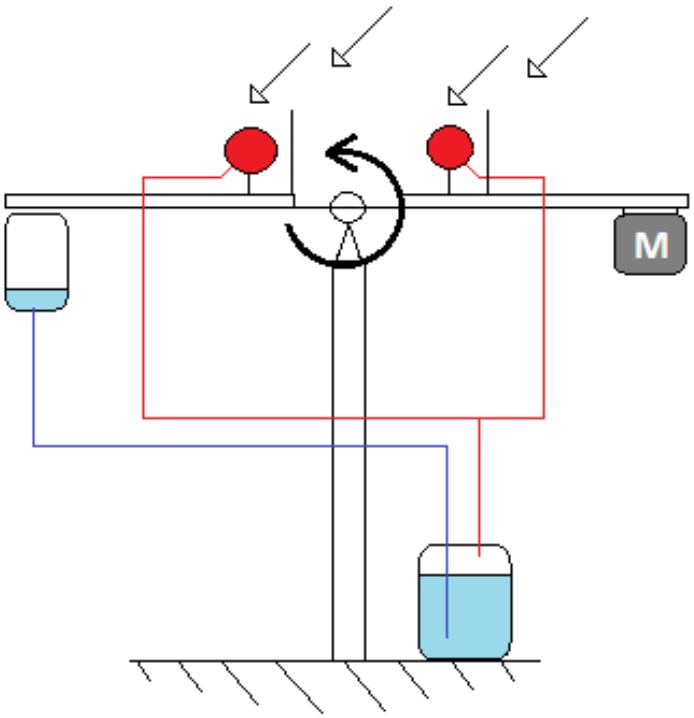

8.2.5 Auxiliary PV and pump in an electro-hydraulic combination

It was observed that the placement of PV cells in their panel configuration resulted in an almost zero panel output when a small section of the panel is shaded, despite the largest area of the panel exposed to strong sunlight. The current output of the panel is also relatively proportional to the unshaded area. See **Figure 8.2.5** below.

Using the above characteristic as a sun angle reference, a pump which is started by a cyclically shaded auxiliary PV panel pressurises a hydraulic cylinder which in turn is linked to the payload platform angle. The philosophy is that the pump speed increases as a function of the available current, again proportional to the degree of shade on the panel.

The pump constantly maintains a shade angle which holds the payload panel normal to the direction of the sun.

To prevent the pump running in a zero flow condition, a small leak-off ensures cooling flow through the pump and has the added benefit of allowing the platform to pass through the optimum angle twice per cycle.

At the end of day, the pump slows and stops and the leak-off flow allows the platform to revert to its easterly bias overnight.

Figure 8.2.5 - Electro-Hydraulic combination

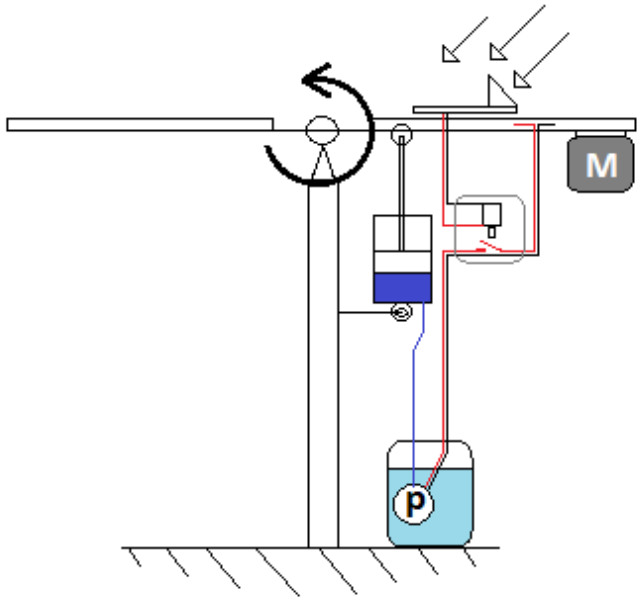

8.2.6 Auxiliary PV and pump in a disturbed balance arrangement

Similar to the above arrangement, this variant shown in **Figure 8.2.6** requires no cylinders or linkages. The auxiliary PV panel is fitted as before but in place of the cylinder a tank is fitted to the West side member. When the tank is empty, the bias weight keeps the panel at the East limit. The PV causes water to be pumped to the tank which in turn disturbs the balance of the structure and it tilts in favour of the increasing tank mass. As before, movement of the shade across the auxiliary panel causes the circuit to shut down and the frame slowly returns to the biased position as fluid siphons back to the reservoir. To ensure rapid response and retarded return, a check valve is required in the delivery line which is bypassed with a restricted bypass tube for return flow.

Figure 8.2.6 - Auxiliary PV and pump in unbalanced mass arrangement

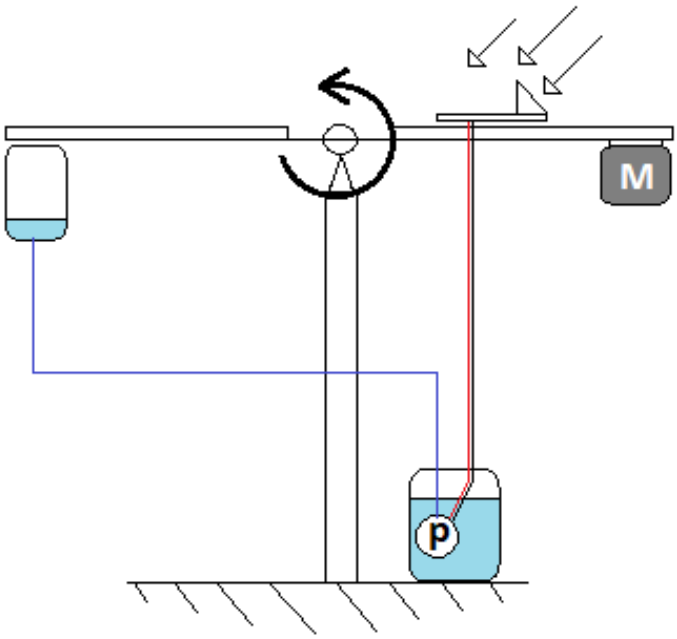

8.3 Amplifying a thermal error signal

Given sufficient amplification, the thermal pressure may possibly be utilised to do useful work. Methods of amplification are explored below.

8.3.1 Elevated pre-charge pressure

By raising the captive gas initial pressure increases the differential pressure once heated. The pre-charge pressure limitation is the sensor tube (pressure vessel) construction mass and proportionality ratios. An increase of pre-charge pressure will not increase the actuation stroke of antagonistically arranged actuators and cannot be realistically used in unopposed systems. The negative aspect of this method is the reality of the inevitable small leakage and the need for periodic recharging of the system, whereas systems which use barometric pressure may be self-recharging during the overnight cooling period through a check valve from atmosphere.

8.3.2 Greenhouse cover

Another form of amplification of the temperature input signal would be the greenhouse cover aspect of solar heated devices. A sensor tube with a glass cover will heat faster and more effectively to a higher temperature than a plain tube, also weather and wind effects are removed from the considerations or at least minimised.

8.3.3 Insulation

Insulation of the sensor tubes around the ‘dead’ or non-insolated surfaces will reduce radiation and convection losses and allow a higher temperature equilibrium, as well as shield the tubes from ground albedo which would affect the response. The gains in temperature will be offset in cooling response, which may have a positive effect on stability by introducing a measure of damping.

8.3.4 Use of solar tubes

In a departure from using the frame mounted air reservoirs, solar tubes can be mounted on the frame to provide much higher temperatures and pressures due to their enhanced vacuum insulation.

The super insulation provided by the vacuum tube does however hinder cooling response as the heat is not easily rejected. A potential solution lies in rejection of the heat outside of the tube, say at a protruding stub. In this way the irradiated solar tube generates much more heat than is rejected but cools faster when shaded.

8.3.5 Mechanical advantage

Utilising a given pressurised volume with which to do work also has the amplification opportunity of increased actuator area to increase force, however the moment of the actuation will remain constant when considered in the volumetric sense. An actuation force well above frictional resistance is preferable to a weaker force exerted over a longer stroke, where the frictional resistance may be at or near the applied force. The relationship between friction force and diameter of any pneumatic cylinder needs to be determined as a design guideline.

8.4 Practicalities to be considered

8.4.1 Friction effects

Pneumatic seals are dynamic in that increased pressure results in increased normal force between seal and cylinder wall, increasing frictional resistance to movement.

Friction effects cause a step-wise adjustment which is required to be small and dependent on the free movement and lubrication of the bearings of the mechanical structure. This situation is akin to the ‘chalkboard screech’ where movement is vibratory in nature due to motion opposed by alternatively static and dynamic friction co-efficients. The differential pressure increase across the stationary piston until the static friction is overcome, after which the displacement is exaggerated and movement overshoots due to momentum, finally losing motive force and stopping, which in turn invokes the static co-efficient of friction again. In pneumatic trade terminology, this phenomenon is

known as ‘stiction’ and causes jerky movement and over- and undershoot control response.

The stepping increments are also required to be small so as not to cause any noticeable inertial effects i.e. there are no start/stop inertial loads of the magnitude experienced with motors and gearing.

A possible solution to the frictional resistance and ‘stiction’ phenomenon at low pressures is by using a diaphragm actuator. Conventional diaphragm actuators generate large forces through their large area but have limited stroke and a non-linear pressure to displacement ratio and antagonistic resistance of the extended diaphragm. A hybrid device combining the hermetic and low friction properties of a diaphragm actuator with the linear properties of a pneumatic cylinder is the recent development of the rolling diaphragm actuator where the pressure fluid is supplied dynamically, unlike the similar air spring device which utilises a captive passive gas charge within the device.

8.4.2 Damping

A further consideration for response is that of damping. A simple restrictor in the impulse line between actuator and sensor will reduce the severity of any errant response but also reduce start-up response. Considering that the horizontal resting system parks in a neutral position overnight, it is required to respond to the rising sun through a large angle of movement, so that any response delay due to restriction will cause a loss of production in the morning. The sundown situation is different in that it does not matter whether the response from sundown to park position takes a long time, as production

has ended for the day. For this reason, it is considered that response and damping be biased toward an easterly response, thereby minimising wasted production time in the morning. This is effected by a dual path damping system comprising a feed line with check valve in parallel to a bypass circuit with restrictor. Flow can pass freely from the East sensor to the actuator, via the check valve, to effect fast response to the rising sun. The return flow is blocked by the check valve and flow is forced through the parallel circuit containing the flow restriction.

8.4.3 Air - over - Oil sealing

Due to the low density of gases, hermetic sealing across component sliding interfaces is not possible with conventional pneumatic cylinders without periodic topping up.

One method of reducing gas leakage is through use of an air-over-oil type hydraulic/pneumatic hybrid system. The oil leakage can be very well controlled due to higher viscosity and the 800x density increase over air hence near-perfect sealing of the actuator cylinders is possible. The amount of oil in the system may range from just sufficient to keep seals wetted or to an entirely hydraulic cylinder with the air-to-oil interface in a separate reservoir.

Any oil vapours absorbed into the air charge remain in suspension and periodically condense within the system, hence piping dead spaces and slopes are important.

A definite benefit of this partially hydraulic system is the ease with which the response can be damped as well as other hydraulic concepts that can be

applied. For example, external effects such as roosting of large birds or sudden gusts of wind can be resisted by introduction of a mechanical loading valve; any sudden surge of fluid causes the valve to snap shut and release again slowly once the disturbance has passed.

8.4.4 Volatile gas mixtures and chemical compatibility

Adjustment of temperature/pressure characteristics can be achieved by using gas mixtures. A variation of simply heated gases using a refrigerant or low boiling point medium, either as a pure compound or as an air-to-vapour mixture, allows some modification of the mixture's expansion characteristics through Daltons law of partial pressure of each compound.

An inexpensive route would be to use a common compound such as an Acetone vapour and air mixture along with commercial pneumatic cylinders. To ensure long term integrity of the mixture, the air-over-oil method would ensure that the cylinder seals provide a liquid seal and long term pressure integrity, however the acetone, thinner or alcohol refrigerant would tend to condense in the cooler volume of the cylinder and react with- or dilute the oil mixture. A viscous medium which is elastomer friendly is required to achieve the wet seal. Due to the insolubility of Glycerine in Acetone, these compounds are selected for the prototype testing with Glycerine as the wet seal medium and Acetone as the refrigerant motive vapour.

8.4.5 Cylinder orientation and restriction

The issue of 'stiction' remains, as well as the practical requirement for damping to resist external forces such as wind gust. The solution to both

these considerations may be found in the use of a double acting pneumatic cylinder where the unused volume is utilised for hydraulic damping. A further enhancement would be to mount the cylinder with rod side down to limit the gas sealing to only one (piston) seal. This allows the wet sealing medium contemplated above as Glycerine to ride on the piston and ensure a wet seal at all times. The damping action is achieved by the use of the rod-end volume as a reservoir for the same viscous compound for the wet seal, in communication with the opposite cylinder rod-end volume via a restrictor. The restrictor ensures that some back pressure on the pneumatic piston seal and pressure balancing reduces the seal interface force, reducing piston seal friction and permitting a smoother sliding action.

8.4.6 Adaptability for testing other mechanisms

A different method of control would be to use the sensor pressures as control forces only, i.e. by using a shuttle valve for control. The actuation energy needs to be sourced from outside the system, which is a departure from the intent of an independent operation. As a potential solution, a method of generating pressurised air within the system, using sunshine as input energy, would need to be explored to render a fully passive solution. To utilise such an air supply, a unique control is needed to respond to the very small sensor pressure changes during accurate tracking manoeuvres. The sensor pressures may be utilised as pilot operations for the use of a modified 3 position 5 port pneumatic control valve for each axis.

8.5 Summary of all the variants considered

8.5.1 Passive methods

The passive thermal methods considered in paragraphs 8.2.1 to 8.2.4 were tested using the Tilt/Tilt test rig. In all instances, response was found to be slow due to thermal inertia and external effects of cool wind over heated surfaces. Angular displacement was found to be quite small in most systems. In all systems, the strength of the response was found to fall far short of the external factors, especially wind force in this region.

8.5.2 Assisted actuations

The systems as described in paragraphs 8.2.5 and 8.2.6 displayed positive response, satisfactory displacements and resistance to external forces. It was decided to proceed with the primary tracking system using one of these methods.

9.0 PROTOTYPE DESIGN:

More than just a negation of existing system shortfalls, the design should contribute to the state of the art and advance the technology beyond what is commercially available and affordable.

The design process lists the negative and positive aspects of electronic motorised systems and then continues with a list of potential enhancements to improve the technology.

9.1 Current small electronic tracker systems

– Negatives

- High cost due to imports, exchange rates, foreign (EU and USA) labour cost, foreign royalties, layered commercial processes and import duties. Cost meets or exceeds the cost of the entire PV system.
- Insufficient service facilities for honouring guarantees and performing maintenance. A partial cause of the reputation for unreliability.
- Alternative quality systems sourced from eastern countries, another causal factor for unreliability.
- High complexity. Many components rely on one another in series to allow the system to work. A minor failure results in a full system failure.
- Systems are geared for large solar farm scale installations; options for small systems are few.
- All systems rely on electronic control and electrical power sourced from the panel.

In conclusion to the view of the existing systems, it is obvious that there is room for improvement of several aspects of the status quo.

Positives

- Accuracy is very good, reliability of higher spec systems is acceptable.
- Geared systems are not reversible, have high degrees of mechanical advantage and have good resistance to external forces dependent on their strength of construction.

9.2 Desired attributes of the proposed system

- Independent of external power supplies, minimal drain on the PV system.
- Non-Electronic solution insofar as computational components and circuitry, simplicity of any electrical requirement.
- Acceptable accuracy and acceptable response.
- Standard materials, locally available.
- Simple design solution for assembly by hand with minimal technical knowledge.
- Low technology manufacture.
- High reliability due to simplicity, corrosion resistance, weather resistance.
- Damped to resist external influences such as wind gust, monkeys etc.
- Long service life, lifetime lubrication.
- Small actuation forces required due to balanced payload design.

- Aesthetically not poorer than current structures.
- System may extend to several panels in series or matrix layouts.

To achieve the desired attributes, each point is discussed individually with its challenges and opportunities –

9.2.1 External Power

Electrical actuators essentially make use of small motors with large reduction drives. These drives are complex and expensive gearing systems. To minimise costs the gearing is often made from nylon and polymer materials, which have adequate strength if temperature and cleanliness requirements are consistently met.

To move away from external electrical power, another energy source is required to actuate the system and do work on the payload. The simplest method to produce a mechanical force is through movement of fluids, whether through heating and expansion or mechanically pressurised. A ready source of energy can be derived from the PV panel itself, provided the consumption is small.

9.2.2 Non-Electronic Solution

Electronics are generally susceptible to deterioration in the environmental conditions of heat, humidity, solar radiation, rain, dust and lightning. The use of sensor tubes to expand motive gases is a method immune to wind, rain, humidity but is reliant on solar radiation to operate. When the weather is wet and stormy, the PV system will not be effective anyway, so during heavy rain

and dark weather the system shall return to its parking position. Any electrical components need to be shielded against moisture, excessive heat and static discharge.

9.2.3 Accuracy and Response

Sensors are accurately and firmly fixed to the payload structure. As stated in the project limitations, the expected accuracy and response will allow the payload to reside within 10% of optimal alignment which results in a minimum effectivity of 90% averaged over all seasons.

9.2.4 Standard materials and local availability

The design must essentially concentrate on the use of locally sourced materials. Exotic materials and complex machining or the use of proprietary parts from international corporates should be avoided where possible. Specialised components for example exotic seals may be considered for their role in providing a long reliable life but for the most part the design philosophy should hinge on local supply, local fabrication and above all value addition to local materials. Due consideration in the design can meet these challenges to the benefit of local job creation, support of local commerce and the potential of foreign revenue.

9.2.5 Simple Design, hand assembly

The design philosophy is again stressed as having to epitomise the concept of simplicity meeting absolute functionality without compromise to structural

integrity or long term reliability. This is achieved through use of hand assembled structural joints, clip fittings, pressure locking mechanisms. Material selection of lightweight hollow sections and corrosion resistant heat treated alloys also aid achievement of this goal. Where possible, use of automotive materials such as rubber products, paint and hydraulic components is to be considered for this purpose, these generally having met high manufacturing standards and generally being immune to the weather environment and harsh treatment.

9.2.6 Low-Tech manufacture

By design, the system apart from the PV panel can be manufactured without dependence on large capital equipment and high technology. This allows manufacture to be done by several small business workshops delivering to an assembly hub. In this way, small operators are empowered and employment is distributed amongst many lower income entities rather than a high capital batching production line of a large business.

9.2.7 High Reliability and Long Service Life

The design process will focus on material selection for long life with the considerations of fatigue, wear and corrosion but moderated by cost. Another aspect to be considered is the sealed unit concept which eliminates joints and potential leakage by using permanent fixing methods.

9.3 Design Fundamentals

9.3.1 General Dimensions

The two test PV panels are sized at 325W rated capacity each and have the dimensions of 1m wide and 2m long. For a minimal actuation force and hence minimum work done to articulate through the full range, the unit will need to be well balanced. To meet this criterion the centre of gravity of the payload must pass through the pivot between payload and support structure. The problem arises that the centre of gravity of the panel and any support frame would pass within the depth of the panel. For this reason the configuration chosen is two panels arranged side by side with a central space wherein the pivot may be fitted in the centre of gravity. As the pivot will not occupy all of this central gap it is conceivable that some smaller PV panels may be fitted in the gap, if required.

The maximum articulation range chosen is 30° above the horizons in the East/West direction and a similar arrangement for North/South. This implies that the central gap would be in the order of 0.5m wide in order to avoid fouling between payload and support structure at the extremes. The general payload dimension is then 2.5m in width and 2.0m in length.

9.3.2 Rotational stability

The chosen configuration is a Tilt/Tilt arrangement. To keep each of the control actions from unduly affecting the other, it is important to prevent any rotation of the payload such as would be the case if a ball joint pivot is selected. The solution to this requirement is the selection or design of a Hookes joint which is capable of sufficient articulation to meet the angular

motion requirement and the required strength. The centre of the cross of this universal is required to be coincident with the payload CG. To attach to a payload frame, the centre cross may be unequally sized.

9.3.3 Weather resistance

The support structure may be a single upright column, whether solid, hollow or latticed. The length of the column must ensure that the corner of the frame cannot foul with the floor, hence the minimum height between floor and pivot is the diagonal between pivot and corner of the payload or 1.6m, which leaves a 100mm clearance at maximum articulation. The centre column and payload frame must be able to resist storm gusts with a safety factor of 2, the frame must also be checked for strength at least equivalent to the panels i.e. 2400N wind load and 5400N snow loading. Although the test site is not in a snowy climate it is not inconceivable to encounter some hail burden at some time in the future. An important consideration is the attachment of the support structure to the concrete slab at the test site. It would be advisable to place outriggers to reduce the point loads on floor bolts and also use an industrial epoxy under these to distribute the load.

9.3.4 Safety

As in all designs, intrinsic safety is a necessity. Apart from sufficient strength of structures, the design must cater for resistance to collapse or failure through looseness, vibration, corrosion or accident. During high winds or unexpected gusts the structure may move unexpectedly, so that a safety bolt facility must be provided to prevent movement when persons are in close proximity during maintenance or inspection.

9.4 Detailed design

The detailed design of the following components is attached in **Appendix C.**

9.4.1 PV interface frame

This frame is the carrier for the panels and is mounted to the central pivot. The prototype frame also serves as a set of five pressure vessels which provide structural strength and a reservoir for motive fluid, as well as performing duty as heat sensors. The final design uses unequal leg angle sections.

9.4.2 Centre support column

The support column was designed for the prototype although the design parameters also hold true for the final specification. The prototype column included a hermetically sealed space for use as bulk air receiver, as forward planning for alternative actuation fluid. The design also included considerations for the fragility of the rooftop test site, wind loading and corrosion. The final design utilises square tubing for the centre column. It has optional steel feet for mounting on an existing concrete slab, alternately a pre-cast site-assembled concrete base is specified.

9.4.3 Hookes joint

The payload interface frame must be radially stable to enable Tilt/Tilt panel tracking and resist external forces. The prototype used stock mild steel sections and common bearings. The final design reduces mass and cost by half without compromising strength.

9.4.4 North-South Linkage

The actuation of the elevation axis is powered by the azimuthal axis. It comprises a rigid linkage attached to the centre column by means of a second linkage whose ends are fitted with 3-axis ball joints. The mechanism is set up to meet the start and end of day azimuth angles and progressively revert to the noonday angle of the angle of latitude of the site.

9.4.5 Reinforced concrete (RC) foundation

A pre-cast foundation is proposed for installation at a greenfield site. The assembly consists of two identical and interlocking parts that are assembled in a compacted excavation and then backfilled. The centre column bolts onto this construction.

A second foundation proposal is for the site to be excavated and compacted, steel reinforcing is assembled in the excavation and some blind shuttering limits the cast volume. The mould is then cast and backfilled and backfill compacted to produce a single piece foundation.

9.4.6 Return mechanism

For a final solution that entails a gravity return, some mechanism is required to allow the system to return to the parking position at the end of the day. Two methods are considered -

- An electrical cut-out. A limit switch is activated at the end of the east-to-west tilt range, which resets once the system has reached parking

position, or once the payload trigger cell has been tilted beyond the light source.

- A hydraulic cut-out. A ball valve is mounted on a plate with an eccentric spring to create a détente which allows the valve to snap open or shut from an activating force. The activating force is a lever or cable connected to the east-to-west tilting beam. The valve opens at the end of stroke and allows the payload to revert to parking position, where the valve snaps shut and the hydraulic system is restored for the next operation.

10.0 TEST RESULTS - OVERVIEW

This chapter recounts the highlights of the various tests. A detailed record of testing is provided in **Appendix B.**

In line with the many possible variants considered, **Table 10** summarises the testing of each variant and their scoring against the desired criteria. Clearly the auxiliary PV and pump variant performed better than the other variants and prompted the decision to develop this concept.

Quantitative testing only became possible once the tracking system produced predictable and repeatable results. A set of two current sensing PV cells were employed, the first mounted on the tracked platform, the second mounted horizontal on the centre column. Data from these sensors was logged using synchronised, periodic current readings, which are representative of full size PV installations. Their comparative data reflects the improvement of the productivity of the tracked payload versus the horizontal fixed installation, tracked versus fixed tilted and fixed horizontal versus fixed tilted. The horizontal fixed sensor is representative of the conventional insolation measurements which are recorded by many organisations worldwide, providing a link between site data and historical site data.

10.1 Pressure sensors

During February 2019, a set of steel pressure vessel sensors was constructed from square tube with plate ends. The tubes were initially blackened with self-etching high heat paint, fitted with pneumatic valves and pressure transducers and pressurised to 5 Bar(g) at 24˚C. Under full sunshine in still conditions and

approaching 1000 W/m^2 vertical insolation, the two sensors generated 585kPa and 589kPa gauge pressure, implying an average gas temperature of close to 70˚C. The sensors were shaded in turn using cardboard tunnels with sufficient height to allow free convection for cooling. Pressures were measured at 5 minute intervals to indicate response time. The pressure differential diverged exponentially and settled to within 5% of the final 30-minute result within the first 10 minutes. Settled temperatures derived from gas pressures were typically 68˚C and 29˚C, a differential of 39˚C and which concurs with previous estimates of the available limits for a full-size actuation system.

10.2 Test rig tilting range

The original test rig comprised a payload platform from tubing, each member being a captive gas pressure vessel. The structure displayed a range of movement which would allow a panel angle of 70˚ to all four directions. This range reduces to a panel angle of 60˚ to East and West once the balancing slides are fully extended. (**See Appendix D page 38, Drawing P0000**)

10.3 Testing using thermal pressurisation

Original testing using the test rig pressure vessels fell short of expectations, despite the pressure of the closed vessels meeting the calculated value. Initial calculations indicated a larger available gas volume expansion than the tests produced. The error was found to be a combination of -

- the omission in the calculation of the lost mass of gas to actuation
- the constriction of the lost mass due to cooling in the actuator

- the effect of gradual ambient warming of the cool gas volume
- background radiation on the cool gas volume

Although the system did produce some useful expansion to do work, the available work was too small for practical purposes. Further pursuit of this method requires substantially higher temperatures and impractically large volumes to produce sufficient work potential.

10.4 Testing using enhanced thermal pressurisation

Using solar tubes and steel inserts produced temperatures around 150 ˚C and gauge pressures exceeding 40kPa.

Despite the higher temperatures the gas volumes were the limiting feature. The volume of heated gas in the steel pressure vessel inside the solar tube further limited the available gas volume despite the large improvement in temperature and pressure. The steel mass also drastically increased response time, taking around two hours to heat.

The steel tubes were replaced with longer aluminium tubes of similar cross section with no improvement in work potential other than a response time improvement to twenty minutes.

TABLE 10 - Performance rating of several variants of actuation

GROUP		COST				PERFORMANCE							VALUE			ENVIRONMENT			SCORE	%	COMMENT
CRITERIA		SIMPLICITY	SKILL OF CONSTRUCTION	STANDARDISED MATERIALS	LOCAL AVAILABILITY	ACCURACY	RANGE OF MOTION	FORCE OF ACTUATION	SPEED OF RESPONSE	SENSITIVITY	RESISTANCE TO EXTERNALS	PASSIVE FACTOR	FUNCTIONAL RELIABILITY	STRUCTURAL RELIABILITY	ENVIRONMENTAL EFFECTS	CARBON FOOTPRINT	RECYCLABILITY			(16 criteria are evaluated /10 points each and multiplied by their weighting)
WEIGHTING		7	7	5	5	9	6	9	8	7	6	6	7	7	8	8	5	- / 1100	%	
SYSTEM CONFIGURATION																					
Plain surface heating with Rolling Diaphragm actuator		7	5	3	5	2	2	2	2	3	3	8	2	6	6	7	5	460	41.818	Poor response, leakage, affected by external forces
Plain surface heating with double acting Radial Diaphragm actuator		6	5	4	6	3	2	2	2	3	7	8	4	8	6	7	5	524	47.636	Poor response, leakage, affected by external forces
Enhanced heating of opposed captive gas with steel inserts		5	5	4	7	4	3	2	1	3	4	8	4	6	5	6	5	481	43.727	Poor response, leakage, affected by external forces
Enhanced heating of opposed captive gas with aluminium inserts		5	4	4	7	5	3	2	4	4	4	8	4	6	5	6	5	514	46.727	Improved response but affected by external forces
Enhanced heating of parallel captive gas with aluminium inserts, single cylinder		5	4	4	7	4	3	3	4	4	4	8	4	6	5	6	5	514	46.727	No improvement over previous variant
Enhanced heating of parallel captive gas with aluminium inserts, two cylinders		5	4	4	7	4	3	3	4	4	4	8	4	6	5	6	5	514	46.727	No improvement over previous variant
Gas expansion to displace liquid weight		6	5	4	7	5	5	2	4	4	4	8	4	5	6	6	5	541	49.182	Improved range and response but cannot resist wind force
Auxilliary PV and pump in electro-hydraulic configuration		3	4	6	8	7	8	7	8	7	8	5	9	8	6	5	4	711	64.636	Large improvement in range, accuracy and response
Auxilliary PV and pump in a disturbed balance arrangement		4	4	5	8	7	8	6	7	6	7	5	9	7	6	5	4	676	61.455	Responsive but actuation force is too light for damping

10.5 Acetone Mixture volume tests

A separate apparatus was set up to investigate the effects of Acetone $(CH_2)_3CO$ vapour as an air mixture, using a solar tube with a steel insert with wick and connected to a pressure gauge and a 50mm pneumatic cylinder. The cylinder seal was blanketed with Glycerine to produce a wet seal. Pure acetone has a very low vapour pressure at low ambient pressures, hence the air mixture moderates this low temperature situation by a Daltons law addition of partial pressures and ensuring that the mixture pressure remains positive. These tests produced useful pressures and volumes. The side effect is that the vapour condenses above the Glycerine layer in the cylinder and remains there as an inert fluid, having neither the pressure or heat to become re-entrained. It was noted that the system pressure performance diminished as the liquid volume in the solar tube transferred to the cylinder.

These tests illustrate that an Acetone vapour pressure generator can produce good results under the following conditions -

- The actuator should be located above the vapour generator to ensure gravity return of the condensate. The slope of the tubing should allow drainage of condensate.
- The feed pipe should be large enough to allow dual direction flow of vapour and returning condensate.
- The cylinder being pressurised should be arranged such that any condensate formed inside can be effectively drained away.
- The feed line requires insulation to prevent significant heat loss to condensation with resultant pressure reduction.

- Acetone is reactive with aluminium hence materials such as nickel steels must be used.

10.6 Testing using shifting balance

This variant pumps water from a low reservoir to an eccentrically placed reservoir at the edge of the platform. The platform is weighted to face East overnight. The heated air from one solar tube aluminium insert displaces the water from the airtight low reservoir up to the variable mass reservoir which encourages tilting of the platform, in turn causing shading of the solar tube and a resultant cooling of the gas, causing drainage of fluid from the variable reservoir and reversing the tilt. The intent is that the alternate tilting increments follow the angle of the sun until sundown, when heating is lost and the fluid drains back to the reservoir, allowing the platform to return to its East bias by gravity.

This theory was tested during the week starting 16 March 2020. The platform was fitted up with two glass jars of 500 ml capacity, the first jar had been modified to accept pressurised air of 50 kPa via a sealed tube through the lid. A second sealed tube originated in the base of the jar and extended to the second bottle. This second bottle was hung from the platform at its western end and its lid was perforated to prevent airlocks. The platform was weighted to stay tilted to the East when the second bottle was empty.

A function test using only lung pressure easily displaced water to the second reservoir and effected a successful full tilting motion. The water was then allowed to siphon back to the airtight bottle with the air hose disconnected.

The air tube was connected to the aluminium insert on 17 March. The system responded as expected and water was pumped to the second reservoir, initiating some tilt. The air pressure was noted to increase to approximate the head difference and stabilised there for some time. The limiting factor is again the rapidly diminishing pressure and volume of the heated gas once it is used to do work.

This system relies on a delicate balance driven by heating and cooling, the heating having a response of twenty minutes and the cooling response somewhat slower. The system does perform some tracking although the result is difficult to measure due to effects of wind and passing clouds.

10.7 Shade positioned payload

A pump connected to a pneumatic cylinder provided a firm response which provides a powerful hydraulic thrust and which is damped to resist external influences. Positioning of the payload is effected by starting and stopping of the pump, triggered by the relative position of the sun and shade screen as shown in **Photo 10.7**.

The system was calibrated to respond within 5˚ either side of optimum when running a single axis polar East/West tracking method. The trigger system was further developed to react at a total angle of 4˚ using a 5 Volt PV cell and relay.

Photo 10.7 - Shaded trigger sensor

10.8 Testing the second axis control linkage

The initiative to actuate the second axis without duplicating the entire first axis system was tested and found to be productive.

The system uses a drop link pivoted vertically from the major arm of the Hookes joint and rotating a bell crank, which in turn lifts a ball jointed connecting rod, attached to a bridge across the centre beam frame and positioned at 180mm from the centre pivot. See **Figure 10.8(a) to (e)** for clarity.

Figure 10.8(a) - Mimic linkage for northerly tilt

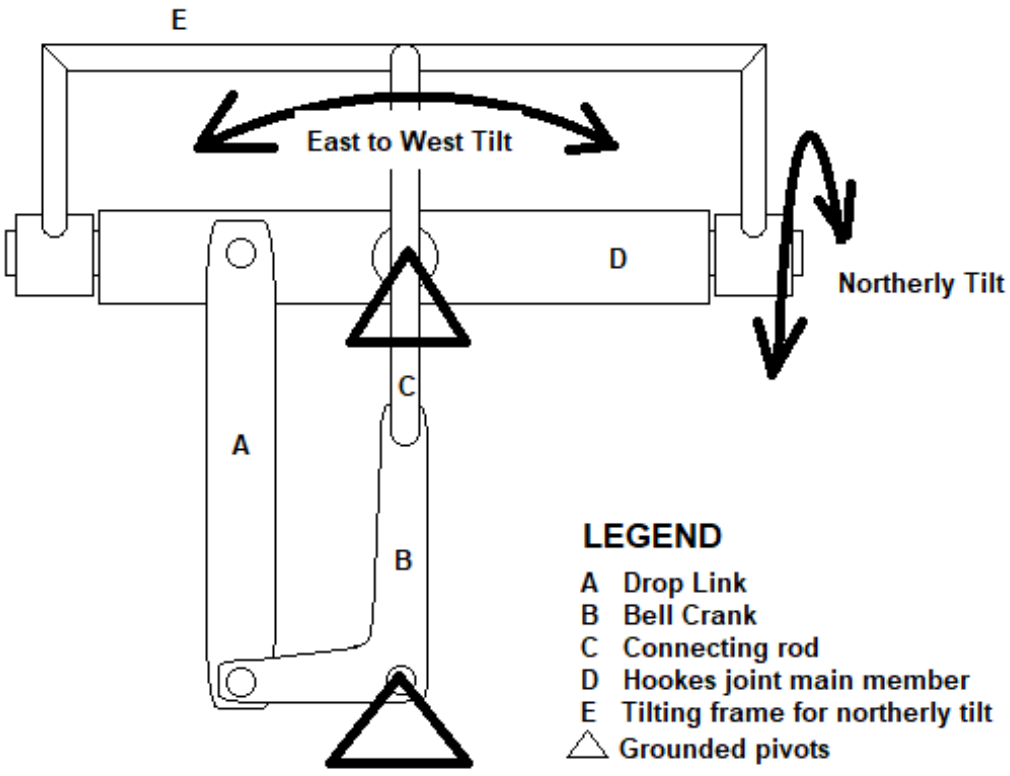

In this way the payload is tilted progressively up to the maximum noon position and then reduced progressively until sundown, when the payload is inclined at its maximum westerly position and retains some northerly tilt.

The system can be set at the median (equinox) position and remain unadjusted throughout the year. In this case the noon accuracy is precise at both equinoxes but reduces to 92.4% at noon on the solstices. Early morning and late afternoon alignment accuracy is dependent on the degree of articulation but remains above 90% within the active tracking range. The noonday accuracy changes daily by an average 0.08% between the limits of 92% and 100%.

Figure 10.8(b) - View from East at morning position

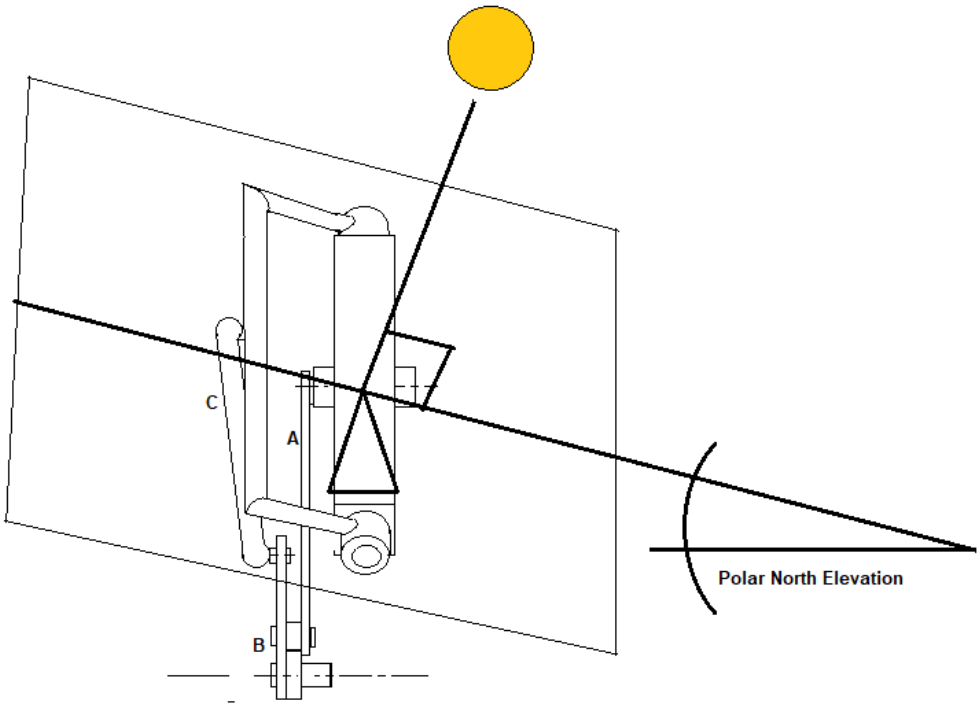

Figure 10.8(c) - View from South at morning position

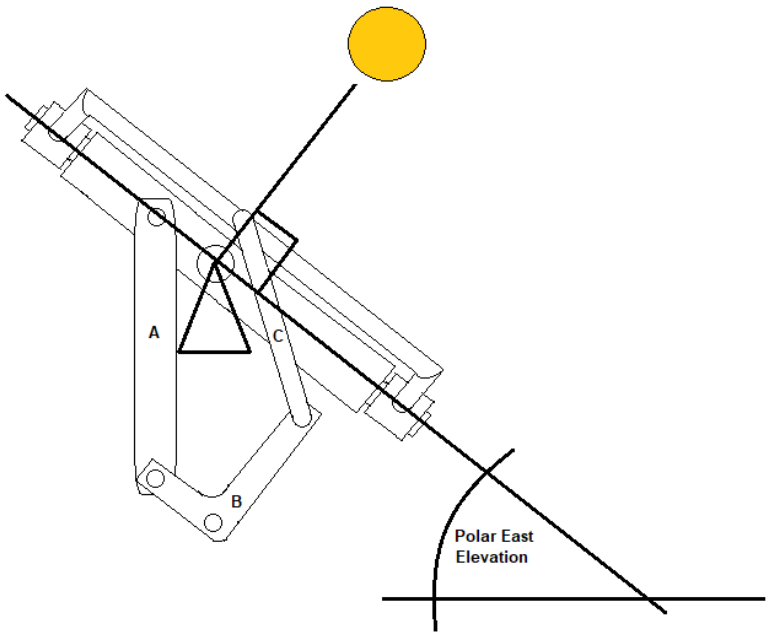

Figure 10.8(d) - View from East at noon position

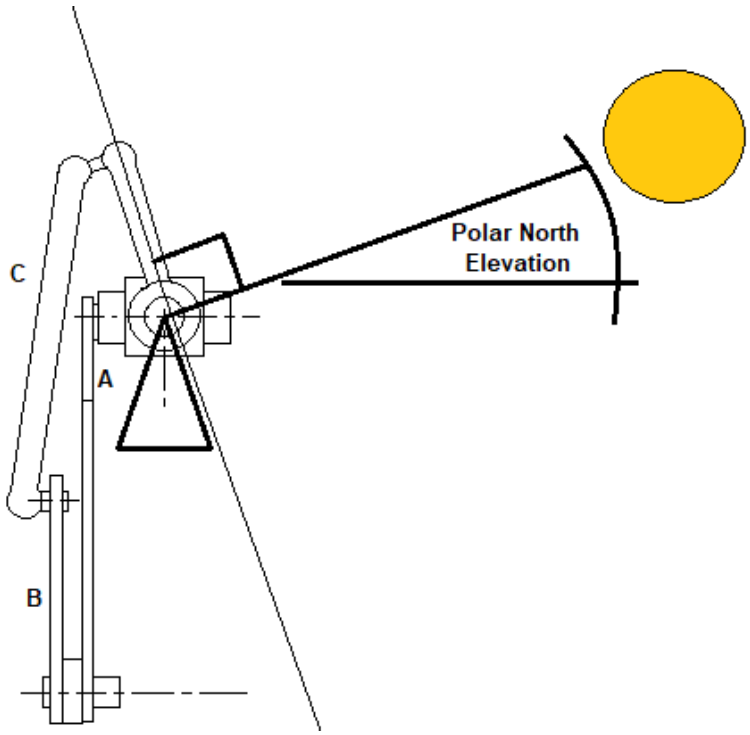

Figure 10.8(e) - View from South at noon position

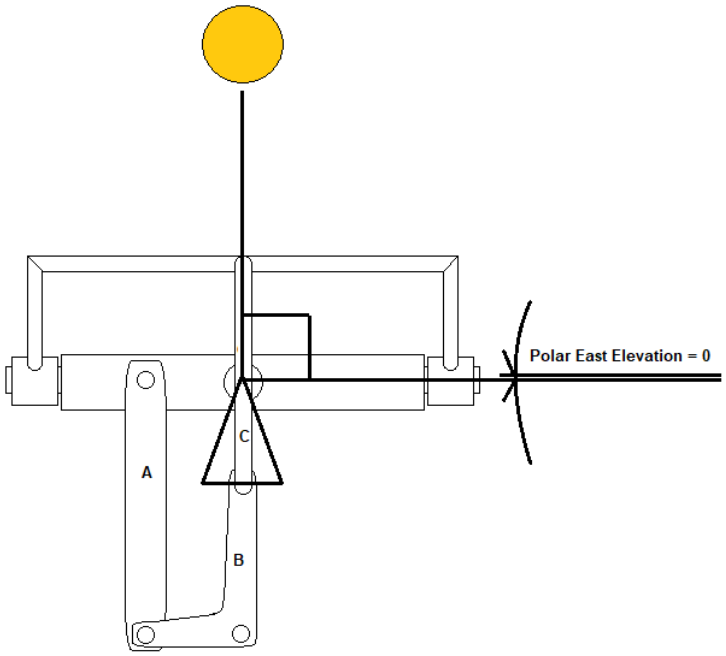

This tilting motion reverses as the platform returns to the morning position overnight, ready for sunrise with an easterly tilt and again with a northern tilt component.

The linkage was set up for the exact day of the year and observed to be 98% compliant, acting as an auxiliary to the hydraulic first axis drive and dependent on the accuracy of that actuation.

By effecting a linkage adjustment of around 7˚ twice yearly increases the mean annual noon accuracy to 97%.

The linkage drawings and components are detailed in Appendix C. A table of recommended bell crank drillings is provided for several ranges of latitudes in the southern hemisphere.

10.9 Estimating the pointing accuracy

The pin and shade method of checking absolute alignment was used to monitor the accuracy of the tracking function at a glance, in order to rapidly correct deficiencies on site without waiting for datalogger downloads and trends. A 10mm pin of 80mm length was placed normal to the payload. The pin was mounted on a pyramid of washers of known diameters. The length of the shade indicates the accuracy of the alignment at a glance. **Figure 10.9 (a)** and **10.9 (b)** illustrate the method.

10.10 Solar cell output comparisons - Tracked vs Horizontal

Testing of the performance of the platform started in earnest once a consistent tracking response was achieved during the first quarter of 2020.

The two comparator cells were mounted on a common board and connected to EasiLog current dataloggers to measure in the range 4 - 20 mA, with 20mA representing an insolation of 1000W/m^2. The cells were exposed for a period of one solar day and produced almost identical results, with a percentage deviation of 0.1%. This was neglected and the marginally under-reading cell mounted on the tracked plane, for any later benefit of doubt.

Figure 10.9(a) - Shade pin error angles illustrated

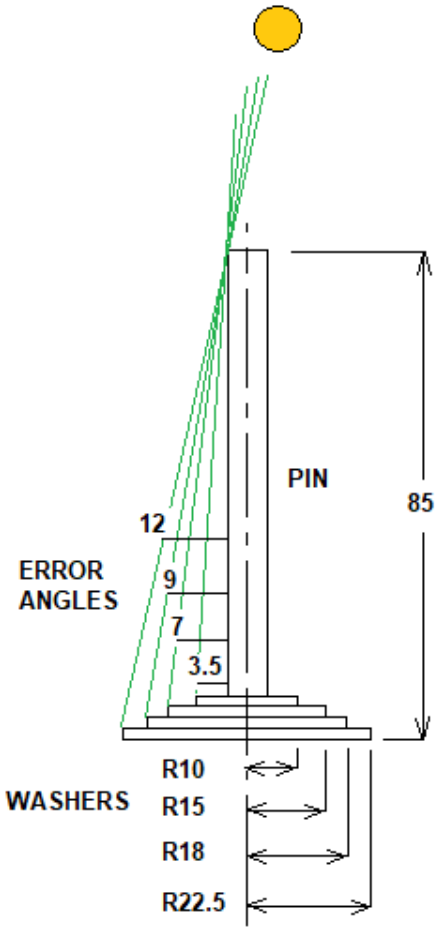

For this gauge, the error angle at the edge of each washer is calculated as -

α = Tan-1 (radius of washer / length of pin)

Figure 10.9(b) - Shade pin - from concept to reality

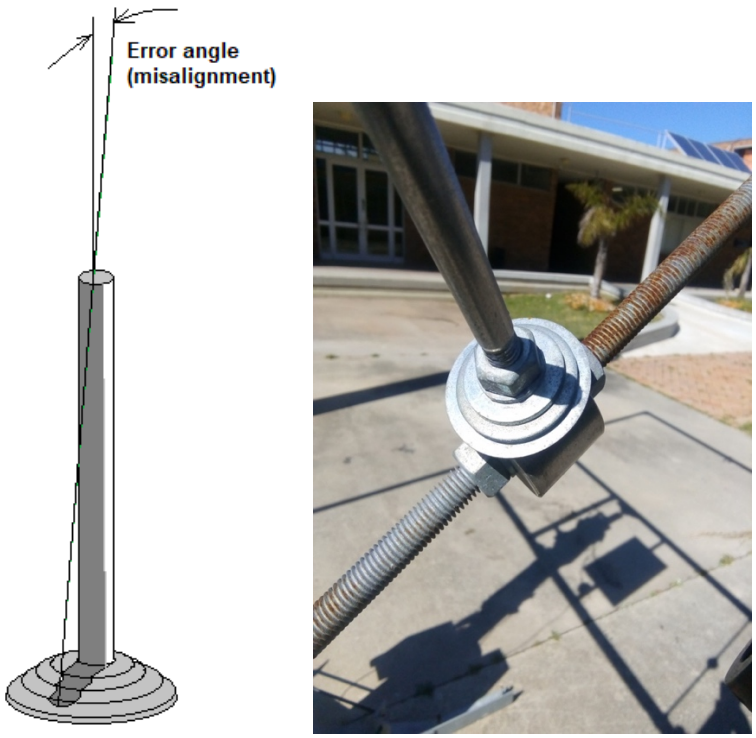

During the month of September 2020, the noon setting was fixed at 35° panel angle which approximates the equinox position of the noonday sun at the site. The results are shown in the current outputs of the tracked and fixed horizontal cells.

Examples are shown below in **Figures 10.10(a) and (b)** for these equinox period test results, two days are chosen for their full day cloudless conditions, 17 and 30 September 2020. Samples are shown for the period 06h00 to 17h00.

The tracked cell produced 17.449 Ampere seconds (As) for the day compared to the horizontal cell's 10.986As for the same period, an improvement of 58.82% over the horizontal.

Figure 10.10(a) - Comparison Tracked vs Horizontal 17 Sept. 2020

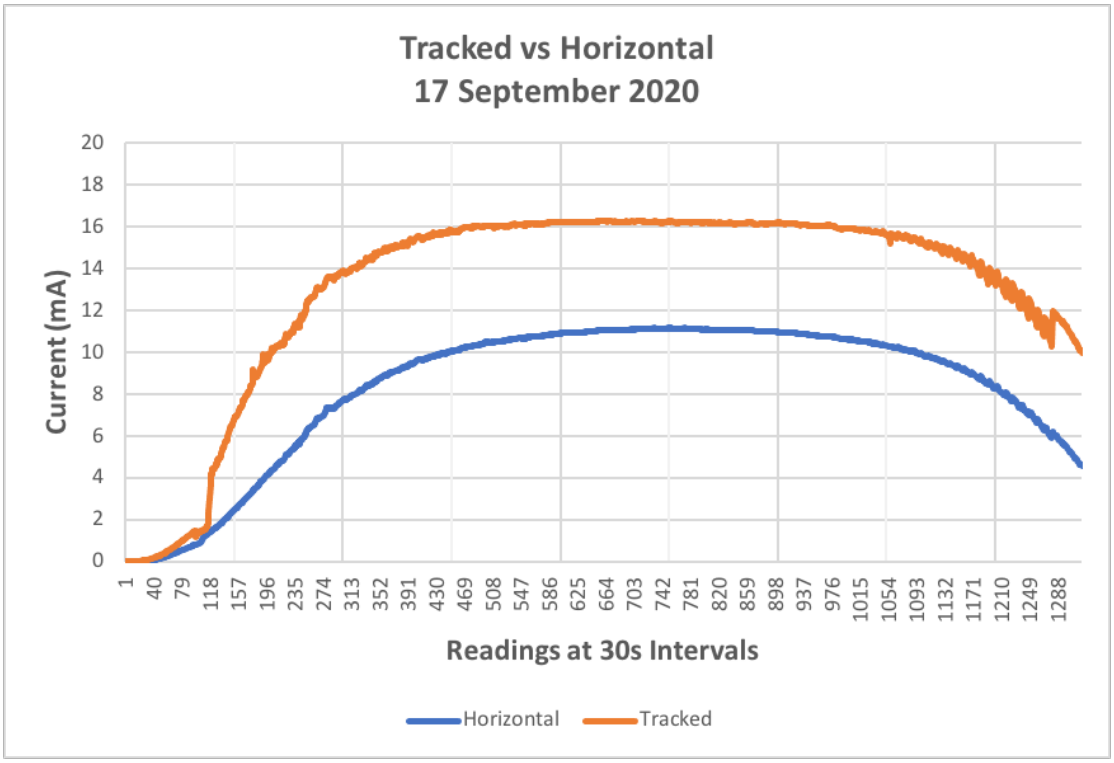

From the curve it can be seen that the current peak exceeds 16mA against the horizontal cell's 11mA. A similar condition was experienced on 30 September 2020 as shown. On this day the tracked cell produced 17.81As against the fixed cell's 11.31As, an improvement of 57.5%.

Of interest in these charts is the characteristic irregularities. The abrupt morning reaction of the tracked cell is due to the sun emerging over an adjacent rooftop. Due to the advantageous alignment at the start of the day, the initial ratio of currents produced is between 2::1 and 4::1 in the early morning, dependent on mist or low cloud at sunrise.

Figure 10.10(b) - Comparison Tracked vs Horizontal 30 Sept. 2020

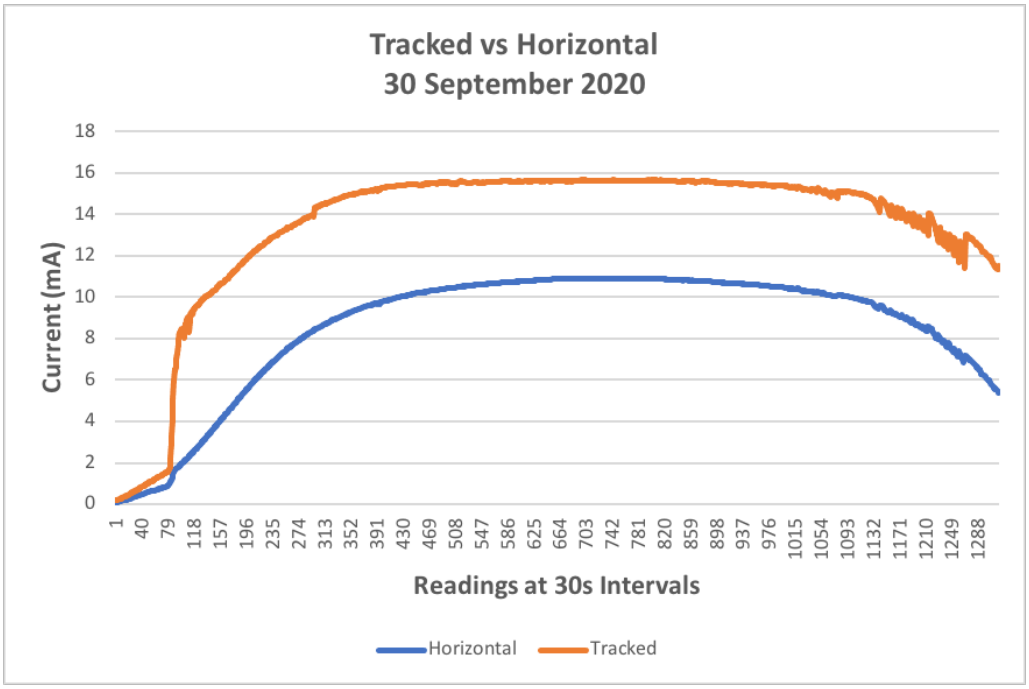

The cyclic pattern at the end of the day is due to the termination device which cuts the power and allows the payload to drift back to the east, but resets several times to keep the panel at maximum tilt position until no more sunlight is seen by the shaded sensor. At the end of day, the tracked output is still around 100% greater than the horizontal cell output.

Illustrating the findings of Quesada, Koussa and others, a heavy overcast day was monitored where the tracker was just able to function. As can be seen in Figure 10.10(c) the horizontal cell produces slightly more current than the tracked cell, although the tracked system responded earlier and reached peak

output around 90 minutes earlier than the static panel. This would contribute almost twice as much absorbed energy across this period.

Figure 10.10(c) - Comparison of rainy day 27 Oct. 2020

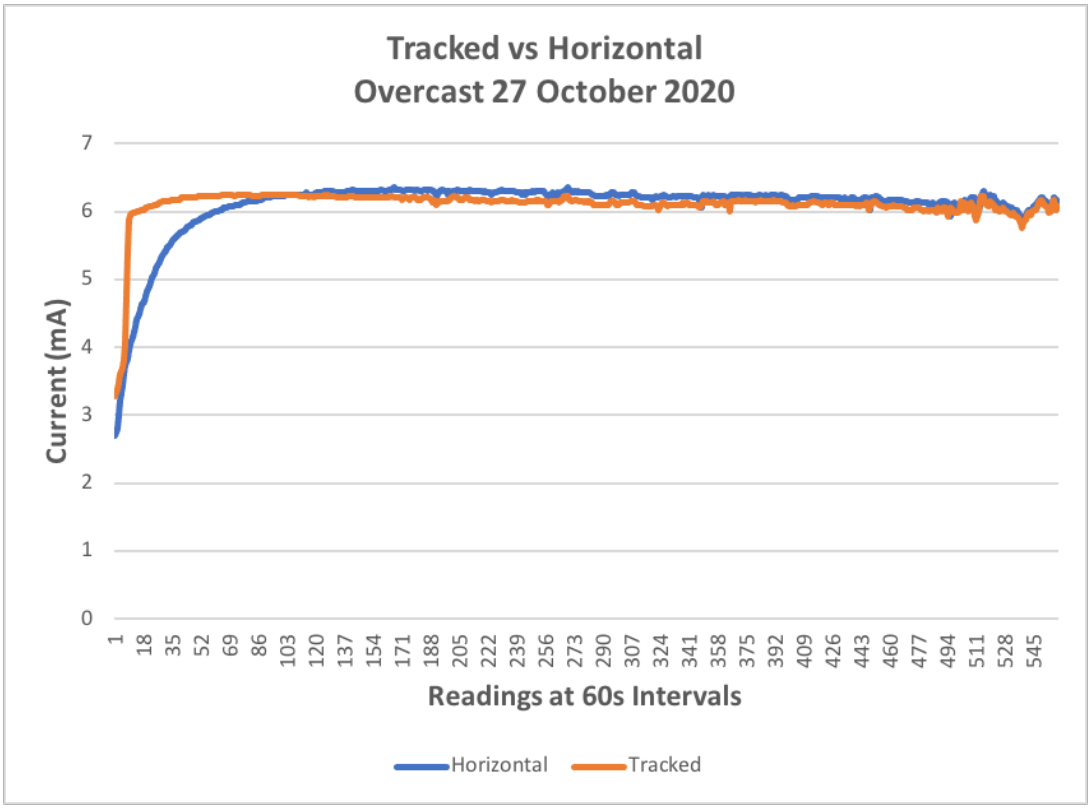

An unusual behaviour was noted on this occasion in that the payload was seen to ignore the direct position of the heavily overcast sun position and locked on to the area further west which appeared brighter and exhibited the appearance of having greater background radiation, thereby almost matching the horizontal cell output.

11.0 FINAL SPECIFICATION:

The specification reflects the final state of the test prototype. All drawings are to be found in **Appendix D**.

11.1 Construction

11.1.1 General Description

The specification describes the structures, parts, circuits and loops required to construct a sun tracking platform which will support 650We of solar photovoltaic panels. It details a Tilt/Tilt operation whereby the payload platform tilts in a wide range of angles using an unequal leg Hookes joint interface with a centre column, in order to meet the solar path squarely over a large part of the solar day.

11.1.2 Centre column and mounting method

The centre column is flange mounted with an option of bolting to slab or to a pre-cast foundation. The slab mounted option has welded foot braces which are interlaced with round bar ties to avoid torsional vibration in high winds. The foundation mounted option caters for a pre-cast reinforced concrete X-footing in two parts. Provision is made for wire-tie stiffeners on this option. The centre column uses a square section for its lower extremity to resist very high bending moments near the base in the event of storm winds. A structural tube section extends from the base to meet the Hookes joint. The bearings on the centre column are bolted onto a set of short channel sections welded rigidly to the tube column upper section. A bridge of inverted channel section is welded atop the bearing mounts as a structural torsion stiffener.

11.1.3 Payload Platform

This description is illustrated by **Figure 11.1.3.** The platform comprises a rectangular frame of unequal leg angle sections with the long flange vertical and the short flange horizontal facing outwards. The members are joined by diagonally drilled corner braces fabricated from equal leg angle. The frame is suspended on two backbone members of tapered channel section which are placed parallel on either side of the centre of the longest side. The backbone members are bolted to bearings via an optional centre of gravity height adjuster plate and which connects to the pin ends of the longer Hookes joint member via a pair of spherical bearings.

The shorter Hookes joint pin is held in a second pair of parallel spherical bearings mounted on the top of the centre column.

Figure 11.1.3 - General arrangement of Tilt-Tilt structure

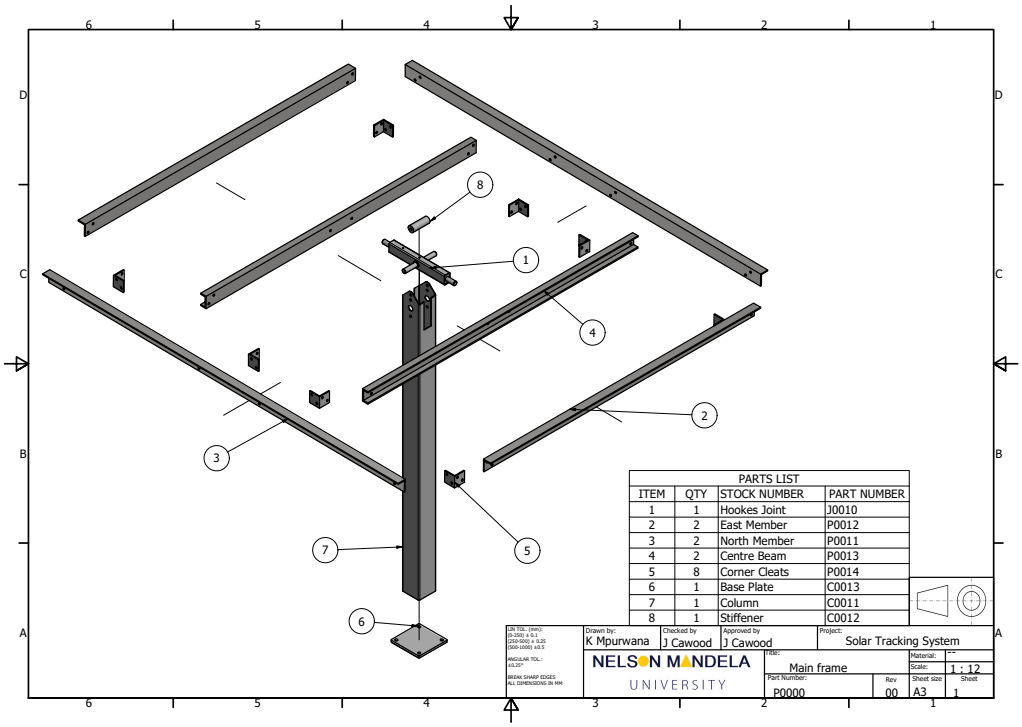

11.1.4 Fluid drive and actuation

The platform utilises a pneumatic cylinder which is repurposed as a hydraulic actuator. Hydraulic pressure is provided by a pump which is stopped and started by a positioning circuit. The positioning circuit is energised via a relay from a selectively shaded PV cell. Electrical power is tapped from the PV set through a DC voltage reducer.

The actuator is mounted on a pivot fixed to the centre column and acts against the longer Hookes joint member by means of an extended clevis. Actuation and positioning are provided in one plane only, the second axis is actuated by a mimic linkage to the first and tilts toward the northern direction as a function of the angle of the Hookes joint main member. The bell crank part of the mimic device has various drillings to adjust for improved performance at different latitudes or seasons.

11.2 Functional Description

11.2.1 Hydraulic Operation

The following description can be read with **Figure 11.2.1 Hydraulic circuit diagram.**

The hydraulic circuit contains a reservoir, a pump, an actuator and a return line which tees from the supply line and returns to the reservoir via a restriction and isolation valve.

When the pump runs, pressurised fluid extends the cylinder and lifts the Hooks joint member by means of the clevis extension. As the pump stops, the pressurised fluid in the cylinder is held by the pump discharge check valve, however a small volume of fluid bleeds out through the restrictor and returns

to the reservoir. With no further pump starts the platform returns to its original position after some delay by gravity.

The inlet to the cylinder is also restricted to provide some damping to the movement. The cylinder is double acting so the rod end is used as a damper against storm winds. The upper chamber is flooded and the entry is connected to the reservoir via another restrictor.

A small volume of air resides inside the cylinder to absorb any shocks such as from wind gusts. Excess air in the cylinder is displaced each night through the bleed restrictor when the piston recedes.

11.2.2 Electrical operation

The electrical circuit is illustrated in **Figure 11.2.2 Electrical circuit diagram** and has two discrete circuits - Power and Control.

The power circuit draws current from the panel voltage reducer direct to the motor positive terminal. The negative motor lead continues across the contactors of a relay and an isolation switch back to the power supply. When the isolator is closed and the relay normally open contactors are closed, the motor draws current and runs.

The control circuit draws power from a selectively shaded PV cell mounted on the payload frame and positioned to illuminate when a certain degree of misalignment is present. Once the cell is illuminated beyond 75% of its area, the resulting current is sufficient to energise the relay coil and pull the relay contactors closed, starting the motor.

Figure 11.2.1 Hydraulic circuit diagram

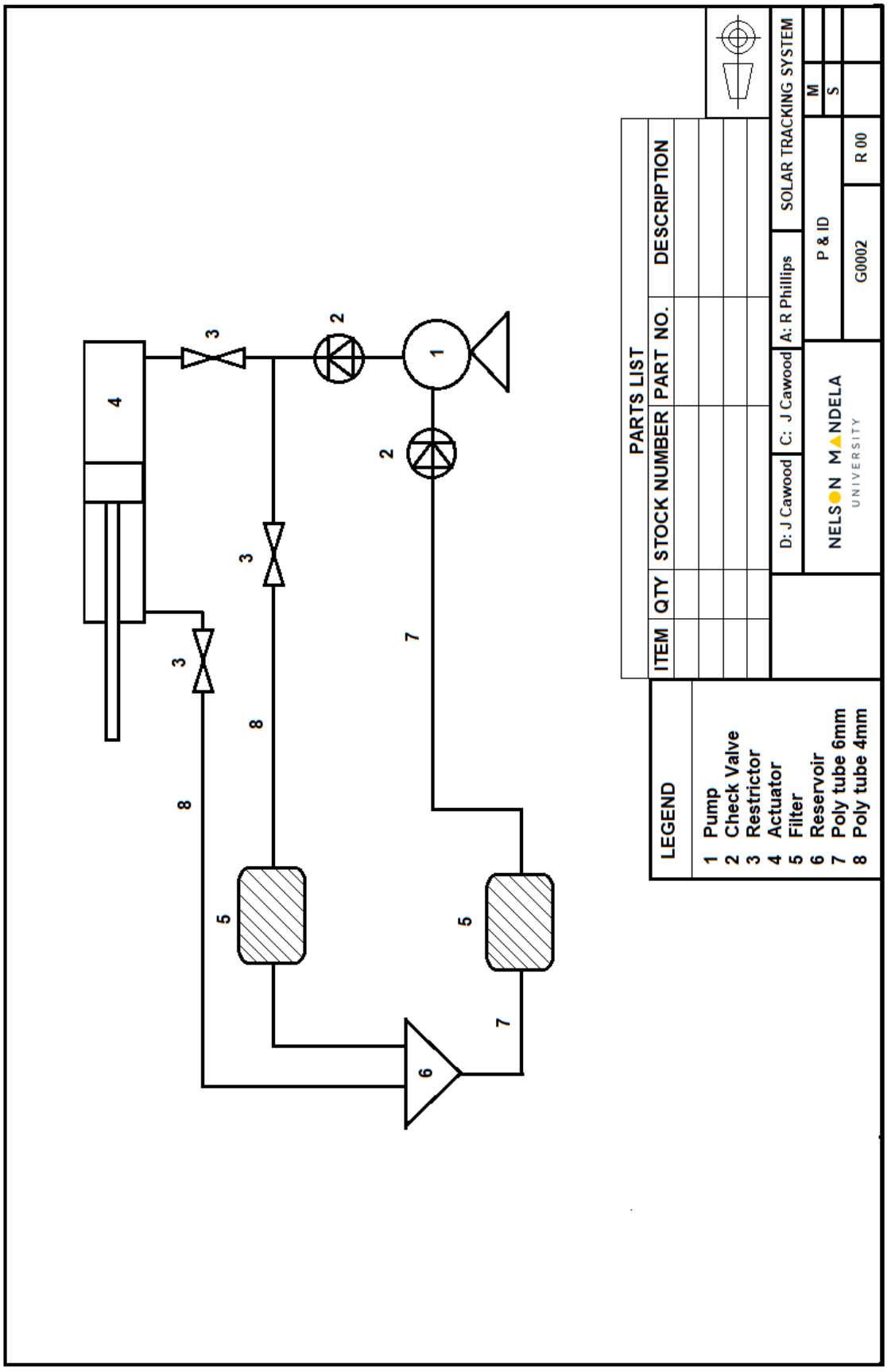

The running motor shifts the position of the payload platform and subsequently shades the control PV cell, opening the relay contactors.
In time, a combination of the changing position of the sun and the reclining action due to the leak-off valve, the control PV cell illuminates again and advances the payload another increment.

11.3 Performance

The pump specification is 120 litres per minute at 75 kPa. The pump is a positive displacement type and with restricted flow performs a full stroke of the cylinder in 3 minutes.
The restrictors are set to return from full extension over 120 minutes.
The motor starts approximately every 3 minutes and runs for 6 to 8 strokes.
The alignment with the polar East to West position is maintained within 2° for the operating range of the device.
The mimic device accuracy of the northerly tilt depends on the bell crank setting on the day but ranges above 90% alignment within the actuation range of the system when set at the equinox setting of the site.

11.4 Materials

The materials details can be found on the individual part and assembly drawings as well as the costing sheet in **Appendix E.**

Figure 11.2.2 Electrical circuit diagram

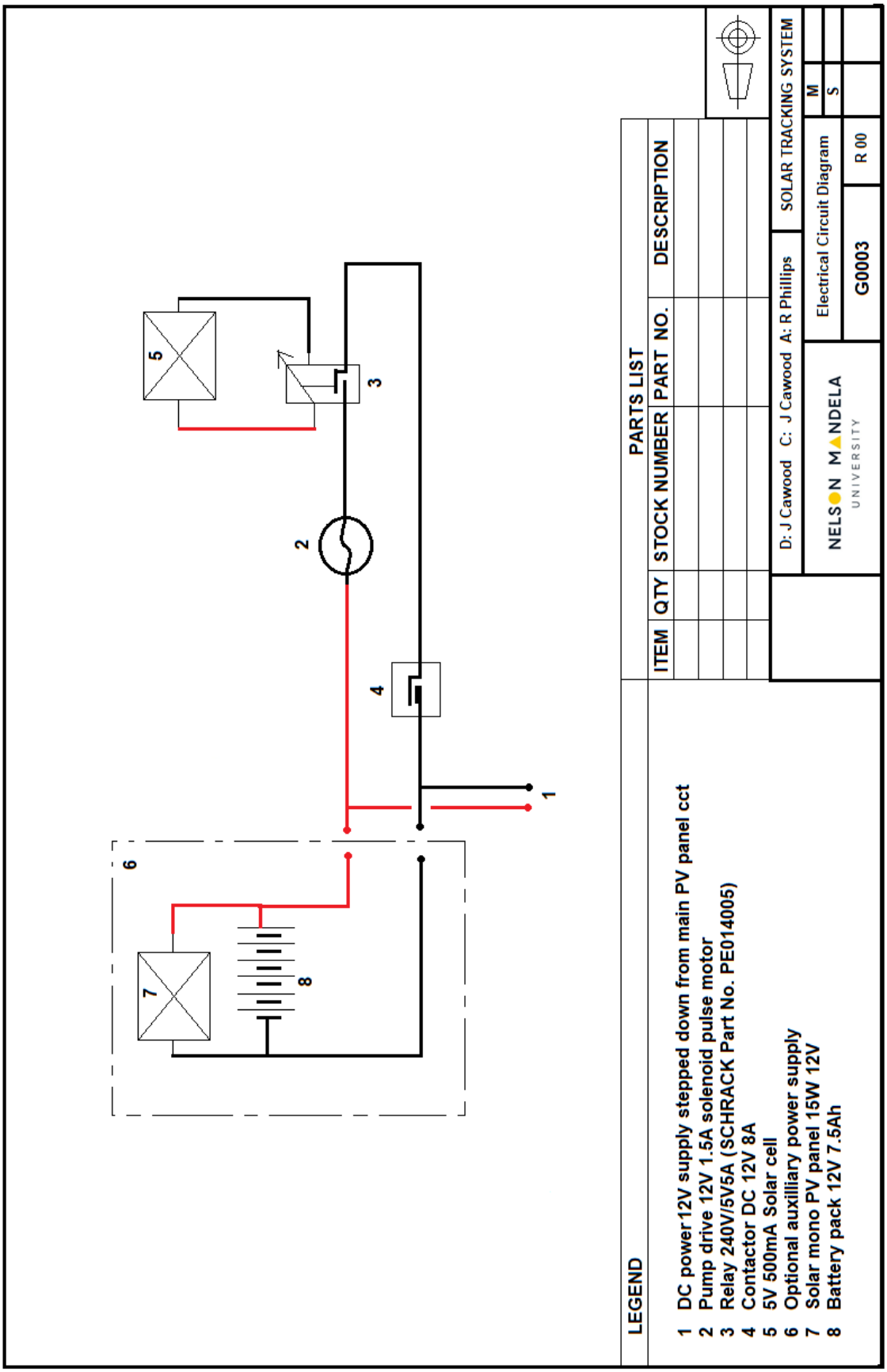

11.4.1 Commercial components

Pneumatic Cylinder

The cylinder is repurposed for low pressure hydraulic duty. The selection code is ‘SC-202005261124154646’ and the catalogue page is provided below in **Figure 11.4.1 (a).**

Hydraulic pump

The pump selected is a solenoid and plunger type 12V model pulse flow electric fuel pump manufactured by Motor Components LLC, USA under the trade name Facet ® Electronic Fuel Pump. The installation instructions are attached **Figure 11.4.1 (b).**

Miniature circuit breaking relay

The PE series relays provide reliability at low cost. The spec sheet is provided below in **Figure 11.4.1 (c).**

Rod end connectors

The mimic linkage requires spherical joints at the ends of the links. These are sourced through Bearing Man (Pty) Ltd and manufactured by IKO Nippon Thompson Co. Ltd. The part number is PHS 10EC.

Flange bearings

The four Hookes joint bearings are 25mm spherical bearings in a 2-hole flange mounting, supplied by Bearing Man (Pty) Ltd.

The Housings are designated FYT5 and the spherical insert YAR 2-2F.

Fasteners

Structural bolting is fixed using plated bolts and spring washers.

Linkages are for the most part lubricated bolt shanks in bushings, these are tensioned to the required clearance for minimal play and held in place using

Ny-Lok locking nuts. Captured O-rings maintain the lubrication in the swivel joints.

Figure 11.4.1 (a) SC Series Pneumatic cylinder

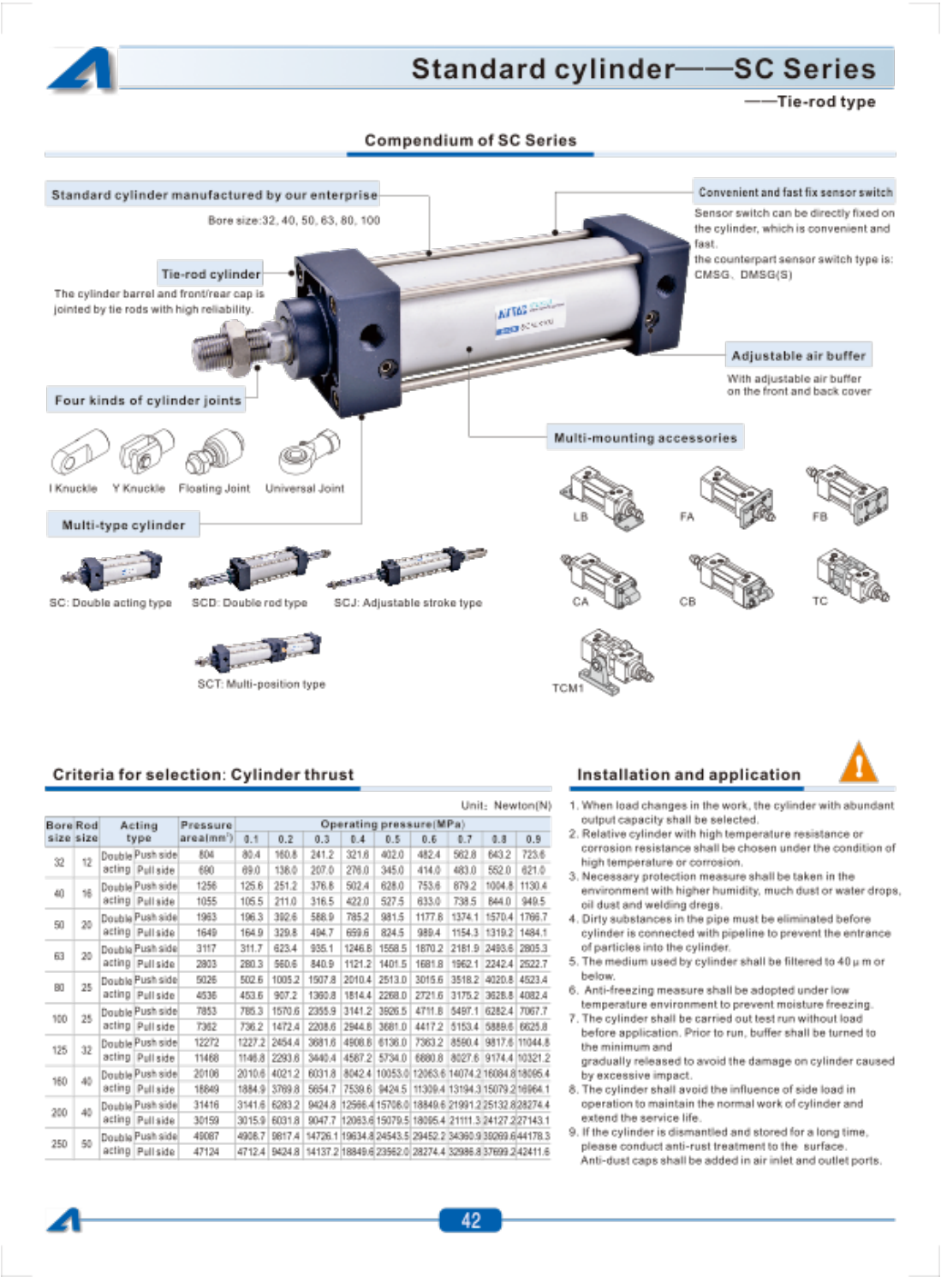

Standard cylinder——SC Series

——Tie-rod type

Compendium of SC Series

Standard cylinder manufactured by our enterprise

Bore size:32, 40, 50, 63, 80, 100

Tie-rod cylinder

The cylinder barrel and front/rear cap is jointed by tie rods with high reliability.

Convenient and fast fix sensor switch

Sensor switch can be directly fixed on the cylinder, which is convenient and fast.
the counterpart sensor switch type is: CMSG、DMSG(S)

Adjustable air buffer

With adjustable air buffer on the front and back cover

Four kinds of cylinder joints

I Knuckle Y Knuckle Floating Joint Universal Joint

Multi-mounting accessories

LB FA FB CA CB TC TCM1

Multi-type cylinder

SC: Double acting type SCD: Double rod type SCJ: Adjustable stroke type SCT: Multi-position type

Criteria for selection: Cylinder thrust

Unit: Newton(N)

Bore size	Rod size	Acting type		Pressure area(mm²)	Operating pressure(MPa) 0.1	0.2	0.3	0.4	0.5	0.6	0.7	0.8	0.9
32	12	Double acting	Push side	804	80.4	160.8	241.2	321.6	402.0	482.4	562.8	643.2	723.6
			Pull side	690	69.0	138.0	207.0	276.0	345.0	414.0	483.0	552.0	621.0
40	16	Double acting	Push side	1256	125.6	251.2	376.8	502.4	628.0	753.6	879.2	1004.8	1130.4
			Pull side	1055	105.5	211.0	316.5	422.0	527.5	633.0	738.5	844.0	949.5
50	20	Double acting	Push side	1963	196.3	392.6	588.9	785.2	981.5	1177.8	1374.1	1570.4	1766.7
			Pull side	1649	164.9	329.8	494.7	659.6	824.5	989.4	1154.3	1319.2	1484.1
63	20	Double acting	Push side	3117	311.7	623.4	935.1	1246.8	1558.5	1870.2	2181.9	2493.6	2805.3
			Pull side	2803	280.3	560.6	840.9	1121.2	1401.5	1681.8	1962.1	2242.4	2522.7
80	25	Double acting	Push side	5026	502.6	1005.2	1507.8	2010.4	2513.0	3015.6	3518.2	4020.8	4523.4
			Pull side	4536	453.6	907.2	1360.8	1814.4	2268.0	2721.6	3175.2	3628.8	4082.4
100	25	Double acting	Push side	7853	785.3	1570.6	2355.9	3141.2	3926.5	4711.8	5497.1	6282.4	7067.7
			Pull side	7362	736.2	1472.4	2208.6	2944.8	3681.0	4417.2	5153.4	5889.6	6625.8
125	32	Double acting	Push side	12272	1227.2	2454.4	3681.6	4908.8	6136.0	7363.2	8590.4	9817.6	11044.8
			Pull side	11468	1146.8	2293.6	3440.4	4587.2	5734.0	6880.8	8027.6	9174.4	10321.2
160	40	Double acting	Push side	20106	2010.6	4021.2	6031.8	8042.4	10053.0	12063.6	14074.2	16084.8	18095.4
			Pull side	18849	1884.9	3769.8	5654.7	7539.6	9424.5	11309.4	13194.3	15079.2	16964.1
200	40	Double acting	Push side	31416	3141.6	6283.2	9424.8	12566.4	15708.0	18849.6	21991.2	25132.8	28274.4
			Pull side	30159	3015.9	6031.8	9047.7	12063.6	15079.5	18095.4	21111.3	24127.2	27143.1
250	50	Double acting	Push side	49087	4908.7	9817.4	14726.1	19634.8	24543.5	29452.2	34360.9	39269.6	44178.3
			Pull side	47124	4712.4	9424.8	14137.2	18849.6	23562.0	28274.4	32986.8	37699.2	42411.6

Installation and application

1. When load changes in the work, the cylinder with abundant output capacity shall be selected.
2. Relative cylinder with high temperature resistance or corrosion resistance shall be chosen under the condition of high temperature or corrosion.
3. Necessary protection measure shall be taken in the environment with higher humidity, much dust or water drops, oil dust and welding dregs.
4. Dirty substances in the pipe must be eliminated before cylinder is connected with pipeline to prevent the entrance of particles into the cylinder.
5. The medium used by cylinder shall be filtered to 40 μ m or below.
6. Anti-freezing measure shall be adopted under low temperature environment to prevent moisture freezing.
7. The cylinder shall be carried out test run without load before application. Prior to run, buffer shall be turned to the minimum and gradually released to avoid the damage on cylinder caused by excessive impact.
8. The cylinder shall avoid the influence of side load in operation to maintain the normal work of cylinder and extend the service life.
9. If the cylinder is dismantled and stored for a long time, please conduct anti-rust treatment to the surface. Anti-dust caps shall be added in air inlet and outlet ports.

42

Figure 11.4.1 (b) Pump installation guide

Instructions in English, Español, and Français

English — **FACET-PUROLATOR SOLID STATE ELECTRONIC FUEL PUMP INSTALLATION INSTRUCTIONS**

The Facet-Purolator Solid State Electronic Fuel Pump is designed to replace the original equipment fuel pump on carburetor-equipped cars, trucks, agricultural equipment, marine pleasure craft, and generators. The solid-state design provides greater reliability, longer life, easy installation, freedom from hot weather vapor lock, and faster engine starting in cold weather. When properly installed, your fuel pump will provide a consistent, steady fuel supply to keep your vehicle running smoothly for many years to come even under severe driving conditions.

OPTIONAL ITEMS:
2 – 5/16-inch fuel line fittings
2 – 1/4-inch Hex self-tap screws
2 – 1/4-inch nuts
2 – 1/4-inch star washers

REQUIRED ITEMS:
1 – In-line fuel filter (74 micron) to be mounted on the pump's inlet port.
2 – Pump must be properly fused with a 3- to 5-Amp automotive-type fuse.

SUGGESTED TOOLS: Electric drill & 7/32-inch bit, tube cutter, hose clamp pliers, locking pliers, 7/16-inch wrench & fuel line plugs, hose clamps, wiring connectors, wire, 5/16-inch flex-hose.

PREPARATION
1 – Needed: (ABC) fire extinguisher within reach.
2 – Disconnect the vehicle battery, relieve fuel line pressure, then disconnect fuel line.
3 – Select mounting area where temperature won't exceed 140°F (60°C).
4 – Ensure the fuel pump electrical requirements match those of the vehicle electrical system.

OPTIONAL
Install an OIL PRESSURE SAFETY SWITCH during installation of this fuel pump and connect the **Red** power lead to the **P** contact. This stops pump operation if the engine stops and the ignition switch is **ON**. (Fig. 1)

INSTALLATION
NEGATIVE GROUND SYSTEM ONLY
1 – Select mounting location: a clean section of the frame away from an area susceptible to road hazard damage, exhaust systems, and must be within (12) vertical inches from the fuel tank (bottom).
2 – Position the pump in an upward direction at 45° away from the tank. Mark and drill (2) 7/32-inch holes into the frame aligned to the mounting bracket. (Fig. 2)
3 – Place the pump over the holes and start the first 1/4-inch self-tap screw into the frame. Start the second screw capturing the black (neg) lead into the other hole. Tighten both screws.

NOTE: Some installations may require fastening the bracket to threaded studs with 1/4-inch nuts.

4 – Install the fuel filter (74 micron) on the inlet. Reconnect fuel line and clean up spilled fuel.
5 – Connect the RED (positive) power lead to the OIL PRESSURE SAFETY SWITCH OR TO A RELAY CONTROLLED BY IGNITION. If this pressure switch is not available, connect to the ignition switch voltage supply terminal.
6 – Reconnect the battery terminals.
7 – Turn ignition switch to ON, and start engine. Observe the pump is operating by hearing a vibrating sound from it. Ensure there are no leaks in the fuel system.

Solid State Electronic Fuel Pump

POS AND NEG GROUND SYSTEM | PARA SER INSTALADA EN SISTEMA DE TIERRA POS Y NEG | POUR SYSTÈME DE MASSE POS ET NÉG

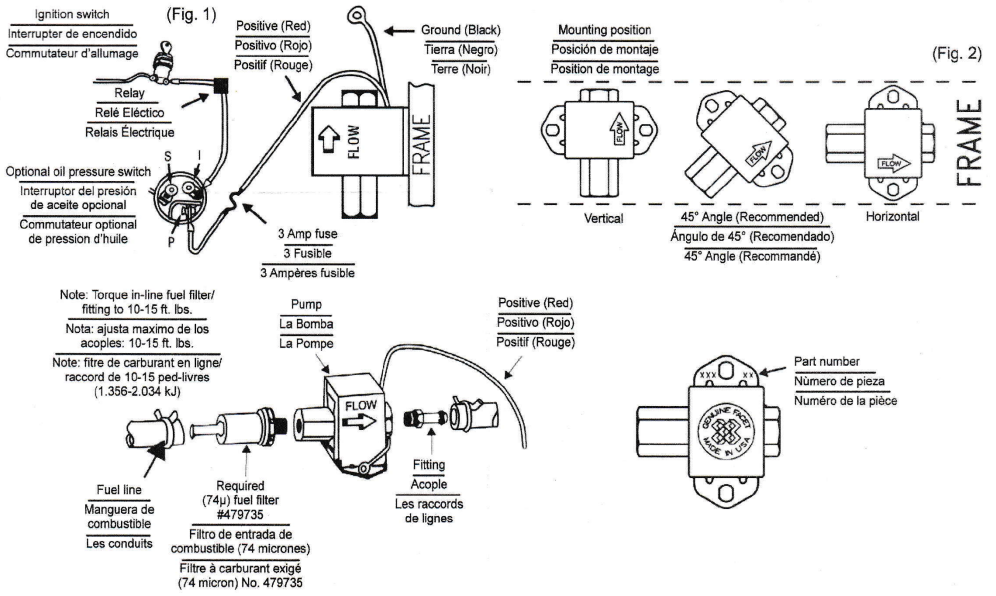

Figure 11.4.1 (c) Miniature PCB Relay

Miniature PCB Relay PE

- **1 pole 5 A, 1 form C (CO) or 6A, 1 form A (NO) contact**
- **Cadmium-free contacts**
- **Sensitive coil 200mW**
- **Ambient temperature 85°C**
- **Low height 10.0mm**
- **Plastic materials according to IEC 60335-1 (domestic appliances)**

F0169-C

Typical applications
Industrial electronics, white goods, measurement and control

Approvals

VDE Cert. No. 40011901, UL E214025
Technical data of approved types on request

Contact Data

Contact arrangement	1 form C (CO) or 1 form A (NO)
Rated voltage	250VAC
Max. switching voltage	400VAC
Rated current	5A (CO - types) 6A (NO - types)
Breaking capacity max.	1250VA (CO - types) 1500VA (NO - types)
Contact material	AgNi 90/10, $AgSnO_2$
Frequency of operation with/without load	360/72000 ops/h
Operate/release time	typ. 8/8ms
Bounce time, form A/form B	typ. 4/6ms

Contact ratings

Type	Contact	Load	Cycles
IEC 61810			
PE013	C (CO)	5A, 250VAC, cosφ=1, 85°C	$30x10^3$
PE014/PE015	C (CO)	5A, 250VAC, cosφ=1, 85°C	$100x10^3$
PE014	A (NO)	5A, 30VDC, 0ms, 85°C	$100x10^3$
PE015	A (NO)	1,5A, 30VDC, 900/h, 50% DF	$100x10^3$
PE034	A (NO)	6A, 250VAC, cosφ=1, 70°C	$50x10^3$
UL 508			
PE013	C (CO)	5A, 240VAC, resistive, 85°C	$30x10^3$
PE014/PE015	C (CO)	5A, 250VAC, resistive, 85°C	$100x10^3$
PE014	A (NO)	5A, 30VDC, resistive, 85°C	$100x10^3$
PE034	A (NO)	6A, 250VAC, resistive, 70°C	$100x10^3$
PE514	C (CO)	5A, 250VAC, resistive, 85°C	$10x10^3$

Max. DC load breaking capacity

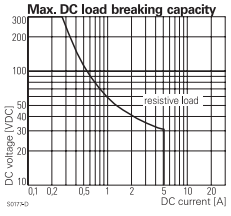

Electrical endurance

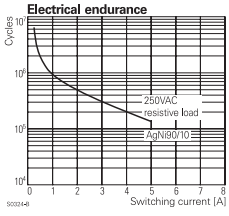

Mechanical endurance, DC coil	>15x10⁶ operations.

Coil Data

Coil voltage range	5 to 48 VDC
Operative range, IEC 61810	2

Coil versions, DC coil

Coil code	Rated voltage VDC	Operate voltage VDC	Release voltage VDC	Coil resistance Ω±10%	Rated coil power mW
3	3	2.25	0.3	45	200
5	5	3.8	0.5	125	200
6	6	4.5	0.6	172	209
9	9	6.8	0.9	405	200
12	12	9.0	1.2	685	210
24	24	18.0	2.4	2725	211
48	48	36.0	4.8	10970	210

Coil operating range DC

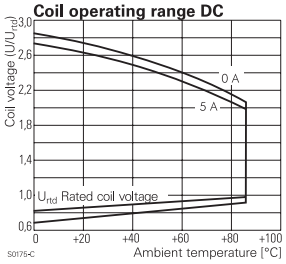

All figures are given for coil without pre-energization, at ambient temperature +23°C.
Other coil voltages on request.

Insulation Data

Initial dielectric strength	
between open contacts	$1000V_{rms}$
between contact and coil	$4000V_{rms}$
Initial insulation resistance	
open contact circuit	$>10x10^9\Omega$
coil-contact circuit	$>10x10^9\Omega$
Clearance/creepage	
between contact and coil	≥3.2/4mm
Material group of insulation parts	IIIa

01-2017, Rev. 0117
www.te.com

11.4.2 Proprietary parts

Centrifugal pump

The forward bladed centrifugal pump was developed for the prototype hydraulic actuation for many start/stop operations and long service life. Details of the pump construction are provided in the drawing series H, attached in **Appendix D**.

Hydraulic cylinder

A low cost hydraulic single acting hydraulic cylinder is detailed in **Appendix D**. This cylinder was manufactured at low cost and tested on the prototype for several weeks. The drawings are provided in **Appendix D** along with the casting mould to produce the piston seal. The seal is cast from a good quality silicone rubber and works well with the soluble oil and water fluid used in the prototype.

Shade sensor

A sheet metal pattern is provided in the drawings. The prototype version uses a 0.5mm galvanised steel sheet folded as indicated to house the trigger cell. The trigger cell is any single PV or set of cells which can produce 5V at 200mA. The arrangement is such that the full potential is only available once the final row of cells or PV circuit emerges from the shade.

11.5 Manufacturing Processes

11.5.1 Welding notes

Most welds are performed on mild steel BS43 or S235J structural steel and as such do not require any pre-heat or stress relief.

Welded parts to be galvanised are first welded and cleaned before galvanising.

Drawings do not specify weldment preparations. As a general rule -

- fitted parts to be welded will be relieved before welding e.g. the pin sleeve in the Hookes joint will have the hole lightly countersunk using a pencil grinder before welding,
- similarly the end pin abutments will be chamfered on the weld side before welding. This measure ensures that the fillet weld penetrates partway into the joint and reduces the stress raiser that could cause cracks in the future, as well as reducing the crevices which initiate crevice corrosion from the entrapment of rain and dew and the cycling up of concentrations of corrosive agents once these evaporate.
- Fillet welds on thin wall sections to be made in at least two passes, a root using a smaller gauge electrode and a filler cap using a heavier gauge electrode and where possible an iron powder filler rod for the cap.
- All welds on stressed joints to be peened after capping.
- Welding of Grade 8.8 bolting steel for the Hookes joint pins should be done with 120°C preheat and covered with insulating material after welding for slower cooling.

11.5.2 Surface finish

All carbon steel parts to be hot dipped galvanised prior to assembly.

Holes in structural steel to be drilled 1mm oversize during fabrication and cleaned 0.5 mm oversize after galvanising.

Where galvanising is cleaned for fits or holes are cleaned, a coat of cold galvanising coating such as Rustoleum® is to be applied to the area. This also applies to foundation bolts that are cut to size.

Fasteners to be electroplated or cad-coated for corrosion.

11.6 Assembly Guidelines

To facilitate easy assembly and delivery of components, the structures are broken into manageable modules which bolt together.

11.6.1 Assembly procedure - slab mounted

The structure is assembled from the base to the frame -

- The column square section is placed in the demarcated position.
- The outrigger feet are bolted to the square section
- The outrigger feet are bolted to the rooftop
- The centre column is dropped into the square section and bolted in position
- The UJ cross is assembled and placed in the NS brackets
- The NS bearings are fitted and aligned.
- The EW bearings are fitted to the cross.
- The EW bearings are attached to the carrier plates
- The centre columns are loosely bolted to the carrier plates.
- The adjuster mechanism is assembled on each carrier plate
- The centre column height is adjusted and bolts torqued.
- The East frame member is loosely attached to the centre column cleats
- Safety chains are hooked up to stabilise the structure.

- The West frame member is attached loosely to centre column cleats
- The North and South frame members are fitted with pinned elbows
- The North and South members are fitted to the East and West members.
- All corners are pinned and tubing properly routed.
- All bolts are tightened after final alignment is confirmed.

Balance checks and adjustments are made for the empty frame.

11.6.2 Assembly procedure - prefabricated footing

The site is marked and excavated to form a cross of 4m legs and 500mm wide by 400mm deep. The excavation is marked and levelled and compacted to around 30 kPa. It is advisable to pour a 25 to 50mm screed of 90/10 fine sand and cement to set the compaction. Assembly of the foundation follows -

- The first section is placed in the excavation with the tie bolts protruding.
- The top section is overlaid taking care to guide the tie bolts through the guide holes.
- Once located and before closing the joint, a 50 MPa grout mixture is packed into the joint by hand and the tie bolts tightened down whilst the grout is still wet, to form a firm joint.
- The centre column is then mounted on the tie bolts and the installation procedure follows the slab mounted guidelines above.

It is advisable to backfill the exposed prefabricated footing prior to placing any panels or allowing any significant wind drag area on the column.

11.7 General

11.7.1 Structure

The final structure comprises unequal leg angle sections in place of the prototype tubing construction. The strength calculations show improved resistance against wind and provide better resistance to crevice corrosion.

The Hookes joint is fabricated from rectangular tubing with welded inserts and abutments. This replaces the heavy and costly square bar prototype version whilst maintaining strength.

The vertical support is modified to use only tubing sections with a flange for fixing to the foundations.

All steel members are hot dipped galvanised and electroplated fasteners are used.

11.7.2 Foundation

A prefabricated RC foundation drawing is provided for windy areas or where the soil at the site is sandy and not conducive to simple compaction and a cast slab.

11.7.3 Panel sizing

The prototype was designed for 2 x 325W panels. Larger panels can be accommodated using C-strut extensions on the basic frame. Balance can be regained using underslung steel counterweights.

11.7.4 North/South axis bell crank positioning

The prototype bell crank arm drillings were designed to suit the test site in NMB. A table specifying the drilling positions is provided in the specification for the solstices and equinoxes of the intended installation site.

12.0 CONCLUSIONS:

As per the Problem Statement in Chapter 4, the goal of the research was to find an economical control and actuation system to track the solar path reliably and economically, to acceptable accuracy. Comparative testing of calibrated cells show up to 58% increase in power generated for the tracked platform across a solar day, when compared to a horizontal, fixed cell.

The greatest gains to be made are in the early morning and late afternoon, where fixed panels suffer from aperture area losses and glass reflectance losses.

The second tilting axis mimics the first axis through a bell crank linkage which improves the compounded alignment error by adjusting the northern tilt across the day. This linkage is manually adjustable to cater for seasonal elevation changes.

12.1 Actuation

The research has investigated the potential of using the differential temperature of captive gases to provide an error signal. This was achieved, however it was found that passive systems that rely on heating and cooling of gases produce inadequate response to be used as terrestrial tracking devices. This is due to the delayed response of heating and cooling as well as the disproportionately small energy values with which to do work. External influences of wind easily defeat these actuations.

The research also shows that although physical movement of a balanced payload requires very small amounts of energy to manipulate, a large amount of damping is required to maintain a smooth tracking response despite external forces of wind, birds, monkeys etc. The imbalanced load methods

require a high level of damping and so the residual force for actuation is small and inconsistent.

The hydraulic system provided the best response and consistency of all options considered. The use of low pressure hydraulics is novel as standard hydraulic systems use very high pressures typically ranging from 120 Bar to 200 Bar. This application functions on less than 1 Bar, hence it is clear that the use of commercially available hydraulic and pneumatic equipment is way over specified and extremely costly for this service.

The use of pneumatic equipment provides a better alternative in terms of off-the-shelf equipment and also allows for high quality standards and guarantees of performance and reliability, however the pneumatic equipment range is designed and manufactured for a working pressure up to 10 Bar, which is still excessive for this application but readily available in a range of sizes for many applications. The use of pneumatic equipment is the preferred option when erecting contracted installations, i.e. the guarantees are transferrable from supplier to end user, the cost implications are still significant.

12.2 Control

For devices which rely on heating and cooling, the control system would be purely proportional, i.e. the sensor surface exposed to the largest and most direct radiation would reach the highest temperature and antagonistically oppose the cooler sensor, thereby maintaining equilibrium through alignment with the sun.

The hydraulic solution required a feedback system whereby exposure of the trigger cell represented threshold misalignment and started the hydraulic

pump relay, the pump ran until the cell was again shaded, providing a small alignment overshoot. Hydraulic leak-off ensured that the system would gradually revert back to the first position unless the cell was again exposed. This system hunts back and forth within a small misalignment as long as there is sufficient sunlight to trigger the relay. At the end of day, the leak-off causes the platform to return to the morning position.

Here follows the conclusions on specific areas of the research -

12.3 Air sensors

In the uncovered form, captive gas sensors are sensitive in clear weather but their performance deteriorates rapidly with some light cloud cover and wind. Higher pre-charge pressures produce a better compliance to ideal performance with no significant lag in response.

Partly insulated sensors improve the overall performance through increased temperature response during heating but slow the cooling response noticeably.

Due to performance limitations caused by limited volumes and detrimental effects of wind cooling and light cloud, the differential pressure generated by plain heating is impractical as a motive energy source.

12.4 Pressure boosted air sensors

An air pre-charge increases the motive pressure, but a pressure around 5.0 Bar(g) is required to provide threshold performance. This pressure increases the likelihood of leakage and stresses the pneumatic components.

An air pre-charge containing doses of low boiling point hydrocarbons and spiritous compounds increases the temperature response. System repeatability suffers due to the tendency of the liquid compound to condense within the cooler zones of the actuators. Where condensate is trapped in the cooler zones, the heating pressure drops off. Where condensate returns to the pipe in a batch, the pressure spikes. Startup response is very small until the refrigerant boiling point is reached, at which time the pressure increases very rapidly. These characteristics make this aspect very difficult to control.

12.5 Chemical compatibility

Chemical dosage of the charge raises the problems of reaction with metals and elastomers. Mineral oils used for wet sealing are diluted by condensed spiritous solvents such as paint thinner and acetone, hence the wet seal fluid would need to be immiscible with mineral spirits, such as glycerine. Acetone dissolves the aluminium oxide layer on aluminium alloys and causes aluminium corrosion in the medium term, requiring nickel steel alloys for pneumatic components. Leaks in the test cylinders were found to be due to surface damage from acetone on the aluminium cylinder bore.

12.6 Enhanced heating with solar tubes

The solar tubes provide heating up to 160°C and responses are under 20 minutes using longer tubes and aluminium inserts. The use of the tube without a pressure insert allows for negligible mass and very quick response, however the construction of these tubes is too fragile to entertain any additional stress, as evidenced by the several breakages in pursuit of this goal.

The response of the aluminium inserts, although hugely improved over the steel inserts, is still too slow to provide accurate tracking control. As evidenced by the displaced mass using heated gas, the pressure and volume provided by even two tubes in parallel fall way short of the energy required for precise tracking and positive positioning against the elements.

12.7 Hydraulic actuation with shaded PV positioner

As shown in Figure 12.6, the prototype test rig utilised a water heater as a heat sink to absorb the power generated and the hydraulics and auxiliary battery were contained in PVC electrical cabinets and powered from a 10W PV auxiliary panel. A later heat sink utilised five resistance wires in parallel as a resistance heater heat sink.

This system is arguably not a pure passive system, yet the power is derived from nature and within the confines of the device without need of replenishment from an external source. The energy thus provided experiences three conversions to provide actuation. Despite these detractors, this system has the energy required for positive actuation. It is held firm against wind and other forces due to hydraulic blocking. The pneumatic cylinder variant is run on a soluble oil and water mix and requires the expense of cylinder with end fixings and anchor points.

The additional cost for the pump and LP hydraulic actuator matches the comparative costs of solar tubes, welded inserts and specialised actuators of the other variants, but with the benefits of ready availability of components, standard parts, absolute simplicity and the longevity and reliability desired in the original proposal.

Photo 12.6 Prototype test rig with water tank heat sink

12.8 Future research

12.8.1 Low pressure hydraulics equipment and applications

A market gap exists which could supply low pressure hydraulic actuators and pumps for service below 3 Bar. The research has investigated this requirement and produced a low pressure single acting hydraulic cylinder which performed leak free and reliably for several weeks in the test rig. Further pursuit of this market niche will benefit from further development.

The research also produced a miniature low flow high head centrifugal pump specifically for use with low pressure hydraulic applications and which also reveals a gap in the commercial market for this item, probably due to small prior demand. Low pressure hydraulics in the built environment offers many opportunities for automated actuation of architectural features such as sun blinds, ventilation dampers and solar tracking so that development of these components will be of benefit for future technologies.

12.8.2 Rolling diaphragm actuators

During the research, methods of actuation using hermetically sealed heated air gave rise to the design and construction of two versions of Rolling Diaphragm Actuators, devices which used the inflation of a blocked flexible hose against a follower to produce a linear output force. A small bore and long stroke linear rolling diaphragm actuator may prove to be useful in architecture for the automatic operation of blinds and dampers, also possibly in engines utilising waste heat. A short stroke radial rolling diaphragm actuator would be useful in agriculture and industry for high force and short stroke applications such as fork truck clamping operations for lifting pallets or removal of poles from the ground.

12.9 Conformance to requirements

This concludes the evaluation of the final product to the requirements stated in the Prototype Design and Limitations sections -

12.9.1 Prototype design requirements

- Non electronic solution. The system uses 12V electrical circuitry and components. The control circuit is a 5V circuit powered by a PV cell.. The use of power derived from the main panel would also be considered to be an electronic component in the circuit.
  Some electronic componentry (PV) is unavoidable.
  The system returns to its parking position when the sunlight levels are unproductive.
- The payload resides within the 10% margin of alignment during the tracked period, when set at the Equinox position for year round operation. Increased performance is achieved with seasonal settings i.e. between equinox and solstices.
- Construction is performed manually without specialised equipment and using hand tools. Manufacturing processes require welding and galvanising facilities - common in most partially industrialised areas. Materials with exception of PV panels are all locally sourced products of steel, fasteners, paint and concrete construction materials.
- The design simplicity is self-evident. Automotive components are used for the positive displacement pump option. The relay is imported at a value of R35-00. The actuator is locally manufactured, however the proprietary cylinder is available using both imported and local aluminium sections and local labour component.
- The Hookes joint design provides the required rotational stability.
  The framework can withstand 10kNm applied wind load (Calculated at the worst case scenario whereby the Cd of the wind loading is taken as

unity and the wind is considered at 160 km/h at 20°C and 1 Atmosphere barometric pressure, see **Appendix C**).

- Static loading is made from mass estimates of 130 kg (1275 N) for the suspended payload. Torsional stability is provided by tie rods across the support feet. Damping is provided in the form of hydraulic restrictors to prevent excessive movement during wind gusts.
- The North-South mimic linkage performs as expected and has two settings for seasonal adjustment.
- The cut-out and return mechanism functions as expected using a power cut-out limit switch and gravity return through restricted leak-off.

13.0 REFERENCES:

1 Lane C. Solar Reviews. *What is a solar tracker and is it worth the additional investment?* Weblog. Available from http://www.solarreviews.com/blog/are-solar-trackers-worth-the-additional-investment [Accessed 14th October 2020].

2 Lusson N. PV-Magazine. *Bifacial Modules: the challenges and advantages*. Available from www.pv-magazine.com . [Accessed 21 March 2021].

3 Lee, Chou *et al*. Sun Tracking systems : A review. *Sensors*. 2009;9(1): 3875 - 3890.

4 Nelson Mandela Bay Metro. *Tariff Book 2020-2021*. Available from: www.nelsonmandelabay.gov.za/datarepository/documents/2020-2021-nmbm-tariff-book_oswAh.pdf [Accessed 25 October 2020].

5 Dai-Prá LB *et al.* Comparison between the Energy Required for Production of PV Module and the Output Energy Throughout the Product Life Time. *Journal of Power and Energy Engineering.* 2015. 9(6): 592 - 597.

6 National Renewable Energy Laboratories. *Lifecycle Greenhouse Gas Emissions from Solar Photovoltaics*. Available from: www.nrel.gov.docs/fy13osti/56487.pdf [Accessed 24 October 2020].

7 National Renewable Energy Laboratories (NREL USA). *NRel's PVWatts® Calculator.* Available from: https://pvwatts.nrel.gov [Accessed 3 November 2020]

8 Bahrami *et al*. The effect of latitude on the performance of solar trackers in Europe and Africa. *Applied Energy*. 2016; 177: 896 - 906

9 de Melo *et al*. A study on the influence of locality in the viability of solar tracking systems. In: Joao Pessao. *Proceedings from the XXII Congresso Brasileiro de Automatica 9 - 10 September 2018.* CBA. 2018.

10 Singh, Kumar *et al.* An imperative role of sun trackers in photovoltaic technology: A review. *Renewable and Sustainable Energy Reviews.* 2018; 82: 3263 - 3278.

11 Mousazadeh H *et al*. A review of principle and sun tracking methods for maximising solar systems output. *Renewable and Sustainable Energy Reviews*. 2009; 13(8): 1800-1818

12 Helwa NH *et al.* Maximum Collectable Solar Energy by Different Solar Tracking Systems. *Energy Sources*. 2000; 22(1): 23-34

13 Pratt AD *et al*. An AI approach to using magnetic gradient tensor analysis for quick depth and property estimation. In: AEGC 2019. *Proceedings from the AEGC 2019. 2 - 5 September 2019. AGC Perth*. 2019.

14 Mashonor M *et al*. Evaluation of Genetic Algorithm based solar tracking system for Photovoltaic panels. In: IEEE Conference on Sustainable Energy Technologies. *Proceedings from the 2008 IEEE Conference on Sustainable Energy Technologies. 24 - 27 November 2008. Singapore*. 2008.

15 Brito M *et al.* Passive solar tracker based in the differential expansion of vertical strips. *Renewable Sustainable Energy*. 2019; 11(4).

16 Clifford M *et al*. Design of a novel passive solar tracker. *Solar Energy*. 2004; 77: 268 - 280.

17 Zomeworks inc. *Passive solar tracker.* Available from: http://zomeworks.com [Accessed 13 November 2020]

18 Poulek V. Self powered tracker for Low Concentration PV (LCPV) systems. Solar Energy. 2016; 127: 109 - 112

19 FTC Solar. *AP90 Single axis tracker.* Available from: http://www.ftcsolar.com [Accessed 19 September 2018]

20 Soltigua Corporation. *iTracker: Catching all the sun.* Available from: https://www.soltigua.com [Accessed 31 July 2020]

21 Machine Design. *Pneumatics Let Solar Arrays Generate More Power.* Available from: https://www.machinedesign.com/mechanical-motion-systems/article/21138630/pneumatics-let-solar-arrays-generate-more-power [Accessed 10 August 2020]

22 Hydraulics & Pneumatics. *What are rolling diaphragm cylinders and why use them?* Available from: http://hydraulicspneumatics.com/technologies/cylinders-actuators/whitepaper/21887537

23 Hashemi S. Low friction, long stroke rolling diaphragm cylinder for passive rehabilitation robots. In: ASME DMD 2017-3518; *Proceedings of the 2017 Design of Medical Devices Conference, 10 - 13 April 2017, Minneapolis, USA.*

24 Martinez C. Bidirectional solar tracker. US Patent. 2010/0095955, 22 April 2010.

25 Boyraz P, Runge D, Raatz A. An overview of novel actuators for soft robotics. *Sensors.* 2018. 7 (48) 1 - 21. Available from: www.mdpi.com [Accessed 27 July 2019]

26 Blanes C *et al*. Novel Additive Manufacturing Pneumatic Actuators and Mechanisms for Food Handling Grippers. *Actuators.* 2014; 3: 202 - 225.

27 Bione J, Vilela OC. Comparison of the performance of PV water pumping systems driven by fixed, tracking and V-trough generators. *Solar Energy*. 2004; 76(6): 703 - 711.

28 Baltas P, Tortorelli M. Evaluation of power output for fixed and step tracking PV arrays. *Solar Energy*. 1986; 37(2): 147 - 163

29 Nann S. Potential for tracking PV systems and V-troughs in moderate climates. *Solar Energy*. 1990. 45(6) 385 - 393.

30 Dickinson W. Annual available radiation for fixed and tracking collectors. *Mechanics of Composite Materials.* 1978; 15(2) 153 - 157

31 Kalogirou S. Solar thermal collectors and applications. *Progress in energy and combustion science*. 2004;30: 231 - 295

32 Chang T. Performance study on east-west oriented single-axis tracked panel. *Energy*. 2009; 34(10) 1530 - 1538

33 Li Z *et al*. Optical performance of inclined south-north single-axis tracked solar panels. *Energy.* 2010; 35(6): 2511 - 2516

34 Chu C, Tsao S. Aerodynamic loading of trackers on flat roofed buildings. *Journal of Wind Engineering and Industrial Aerodynamics.* 2018; 175: 202 - 212.

35 Chou C, Chung P. Wind Loads on a Solar Panel at High Tilt Angles. *Applied Sciences.* 2019; 9 : 1594 - 1606.

36 Rohr C, Bourke P, Banks D. Torsional Instability of Single Axis Tracking Systems. In: *Proceedings of the 14th International Conference on Wind Engineering. ICWE14 Porte Alegre - Brazil*. 2015.

37 Quesada G *et al*. Tracking strategy for photovoltaic solar systems in high latitudes. *Energy Conversion and Management*. 2015; 103:147-156

38 Elmer Z. Optimising solar tracking systems for solar cells. 4th Serbian-Hungarian Joint Symposium on Intelligent Systems. SISY. 2006; 167 - 180.

39 Zorrilla-Casanova J. Analysis of dust losses in photovoltaic modules. In: *World Renewable Energy Congress*. 8 - 13 May 2011. Linkoping, Sweden.

40 Hussain *et al*. An experimental study on the effect of dust on power loss in solar photovoltaic module. Renewables. 2017: 4(9). Available from https://doi.org/10.1186/s40807-017-0043-y

41 He G *et al*. Review of self cleaning method for solar cell array. *Procedia Engineering*. 2011; (16) 640 - 645

42 Forbes P. *The Gecko's Foot: How scientists are taking a leaf from nature's book.* New York: WW Norton and Company; 2006.

43 Zhang P *et al*. Numerical study on the properties of an active sun tracker for solar street light. *Mechatronics*. 2013; 23(8): 1215 - 1222.

44 Sungur C. Multi-axes sun tracking systemwith PLC control for photovoltaic panels in Turkey. Renewable Energy. 2009; 34(4) 1119 - 1125.

45 Koussa M *et al*. Measured and modelled improvement in solar energy yield from flat plate photovoltaic systems and under a range

of environmental conditions. Applied Energy. 2011; 88(5): 1756 - 1771

46 Lorenzo E *et al*. Design of Tracking Photovoltaic Systems with a Single Vertical Axis*. Progress in Photovoltaics: Research and Applications*. 2002; 10; 533 - 543

47 Ahmad S *et al*. Power feasibility of a low power consumption solar tracker. *Procedia Environmental Sciences.* 2013; 17; 494 - 502

48 Reda I, Andreas A. *Solar Position Algorithm for Solar Radiation Applications.* NREL. Report number: NREL/TP-560-34202,2003.

49 SunEarthTools.com *Tools for consumers and designers of solar*. Available from: www.sunearthtools.com/maps [Accessed 21 June 2020]

50 Spirax Sarco. Learn about steam. Available from: www.spiraxsarco.com/learn-about-steam/control-hardware [Accessed 15 August 2019]

51 Kanyarusoke K *et al*. Are solar tracking technologies feasible for domestic applications in rural tropical Africa? Journal of Energy in South Africa. 2015; 26(1): 86 - 95.

52 Bekker B. Irradiation and PV array energy output, cost and optimal positioning estimation for South Africa. Journal of Energy in South Africa. 2007; 18(2);16 - 25.

53 Mauro S *et al*. Design and test of a parallel kinematic solar tracker. Advances in Mechanical Engineering. 2015; 7(12); 1 - 16

54 He X *et al*. Solar automatic tracker based on parallel mechanism. Journal of Mechanical and Electrical Engineering. 2012. (01).

55 Hubach J. Solar Tracking Using a Parallel Manipulator Mechanism to Achieve Two-Axis Position Tracking. *Graduate Thesis-Mechanical Engineering.* 2019. Rose-Hulman Institute of Technology. © Joseph Otto Hubach.

56 Comsit M *et al*. Design of the linkages type tracking mechanisms of the solar energy conversion systems by using Multi Body Systems method. *Proceeds of the 12th IFToMM World Congress. 18 - 21 June 2007.* Besancon, France.

NELSON MANDELA UNIVERSITY

FACULTY OF ENGINEERING, THE BUILT ENVIRONMENT AND INFORMATION TECHNOLOGY

A - RECORD OF ACTIVITIES
APPENDIX TO THE RESEARCH THESIS -

'Enhancement of domestic solar photovoltaic unit productivity through the use of a cost effective tracking system '

John Henry Cawood
Student Number: 213282909

1.0 OVERVIEW

This work record serves as a summary of the actual work performed during the research period, whether productively contributing to the end result or not.
The purpose of the record is to capture any lessons learned which could be shared with future research along similar lines, to illustrate the quantity of effort exerted during the research, to serve as a record of potential future research and to record any milestones that may not directly have contributed to the final thesis. The summary below is compiled from the project diary log sheets.

2.0 INITIATION MAY 2018 - FEB 2019

(GOALS - Pre-study / Registration / Proposal / Acceptance)
This phase was entered with a strong personal pre-conception that heated gases would be the final solution, based on initial literature and assumptions. The proposal reflects this bias which did not bear fruit. The lesson learned here is to keep the option range wide until detailed knowledge indicates a clear direction for the research.

3.0 RESEARCH 1st PHASE FEB 2019 - MAY 2019

(GOALS - Options / Limitations / Provisional Costing / Provisional Schedule, Common apparatus fabrication / Generalised literature study)

Despite mounting indications to the contrary the heating theme was favoured at the cost of more viable options, affecting the literature study, schedule and costing.
Several months were dedicated to developing a small bore/long stroke Rolling Diaphragm actuator which required a research project of its own and may serve as a useful component in air engines or transmissions.
More time was spent pursuing an alternative Radial type actuator that was very effective when using an air source but could not be hermetically sealed for use with the captive heated gas concept, proving to be another device which would find uses in agriculture and factories as a rugged actuator for clamping and holding but failed to deliver the requirements for this thesis.
A further period was spent devising a thermal compressor and pneumatic relay system to provide a compressed air supply to enable and justify the work spent on

the actuator developments. These pursuits have merit for other purposes such as architectural features, building automation and remote valve and damper drives but failed to meet the brief of the thesis - simplicity, cost, effectivity and reliability.

4.0 SELECT OPTIONS MAR 2019 - MAY 2019

(GOALS - Begin draft thesis / collect relevant references / decision on final direction of research / firming up of limitations, schedule and cost)

The heated gas theme still dominated the work flow, encouraged by static results obtained with high pressure air and refrigerant mixtures. The test rig was built and achieved the desired outcomes in terms of structural functionality. The test rig design was influenced by a second personal bias towards a tilting concept, fuelled by literature which indicated tilting in two planes would be the most effective arrangement.

5.0 OPTION TRIALS MAR 2019 - MAY 2020

(GOALS - Trial testing of heated gas expansions, displaced mass testing and hydraulic systems)

The heated gas option proved to be unworkable despite many innovations to increase the work output of the process such as enhanced heating, acetone vapour generation and increased heated volumes. At this late stage, somewhat hurried research began in earnest to find viable alternatives to power the successful test rig. Some success was enjoyed by the use of shifting water weights and hydraulic actuation using a pump and shaded PV panel, which later developed into two circuits, power and control. Real response and actuation prompted rapid development of this option.

Research on site was halted during the pandemic but a scaled down apparatus was set up at home to pursue the solution.

6.0 RESEARCH 2nd PHASE APR 2020 - JUN 2020

(GOALS - Focussed literature study / detailed design / specialised equipment fabrication / Final proto building / Testing of chosen option)

In pursuit of the hydraulic option during level 5 lockdown, much equipment had to be manufactured from the home workshop. A hydraulic cylinder, an electrical relay and a centrifugal pump were examples of these, with parts manufactured from whatever could be found or salvaged from household equipment. The option proves to be successful and warrants further development. Further literature was researched in a more focussed direction to support the practical work.

7.0 CONSOLIDATION JUN 2020 - NOV 2020

(GOALS - Collate data / preliminary conclusions / equipment improvement or upgrade / Continue data collection to monitor changes / Edit Thesis and request comment)

This phase could only begin once useful data was available and saw rapid progress from April 2020. Small improvements to the prototype are still being effected until the outcome of the thesis evaluation, to be added as a postscript at final submission.

8.0 CONCLUSIONS SEP 2020 - JAN 2021

(GOALS - Complete appendices / package results / complete drawings / edit specification / submit Thesis for examination)

Thesis final draft completed 6 December 2020. Appendices compiled and finalised 12 December. Drawings completed 12 November.
Submission of complete document for examination by 15 December 2020. NMU revised calendar examination deadline 8 January 2021 due to the pandemic.

NELSON MANDELA UNIVERSITY

FACULTY OF ENGINEERING, THE BUILT ENVIRONMENT AND INFORMATION TECHNOLOGY

B - RECORD OF TESTING
APPENDIX TO THE RESEARCH THESIS

'Enhancement of domestic solar photovoltaic unit productivity through the use of a cost effective tracking system '

John Henry Cawood
Student Number: 213282909

CONTENT

1.0 PRELIMINARY TESTING

The concept of using the energy of a differential temperature 'error signal' to control and actuate a tracking system appears to be rather straightforward, however the physical device and assembly would be quite novel and required much development to produce a test model.

1.1 Temperature range and response

Initial testing started on 5 February 2019 with the temperature trials of a miniature sensor rod to investigate the temperature limits for a larger system.

A raw aluminium rod was fitted with a thermocouple and placed North/South on a glass surface for one solar day, see **Figure 1.1a**. For successive days, changes to simulate various absorption effects were tested on the same sensor, these being the selective surface coating, surface finish, glass cover and insulation between sensor and lower glass surface. The **Figures 1.1a and b** illustrate these attempts. Each change improved the overall temperature peak and heating response, culminating in a 78˚C temperature peak at insolation over 800 W/m^2 at ambient air temperature of 29˚C. This implies that a system is required whose maximum differential is within 49K.

Figure 1.1a

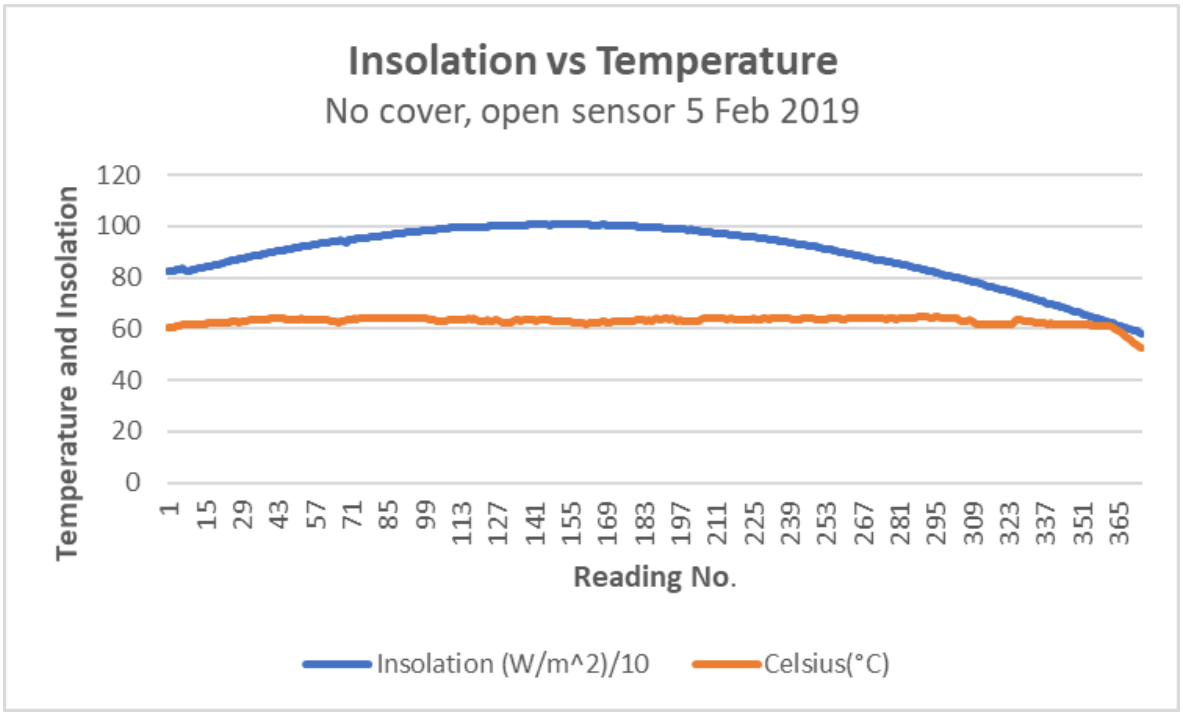

Figure 1.1b

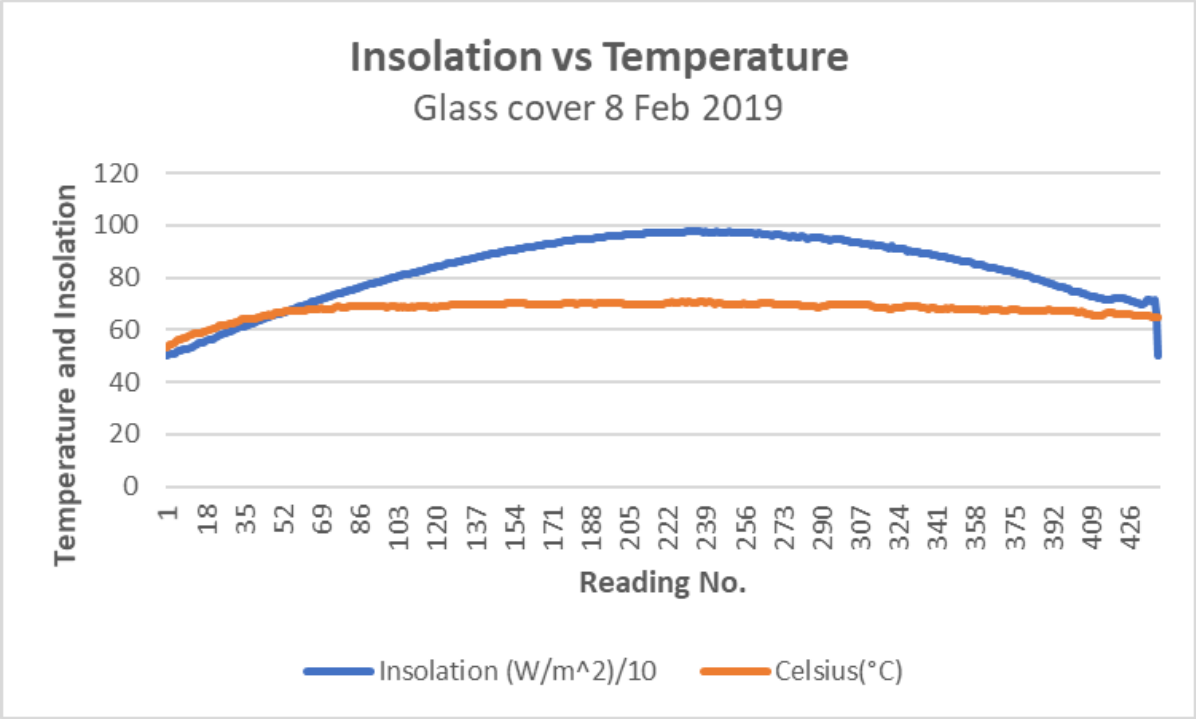

Figure 1.1c

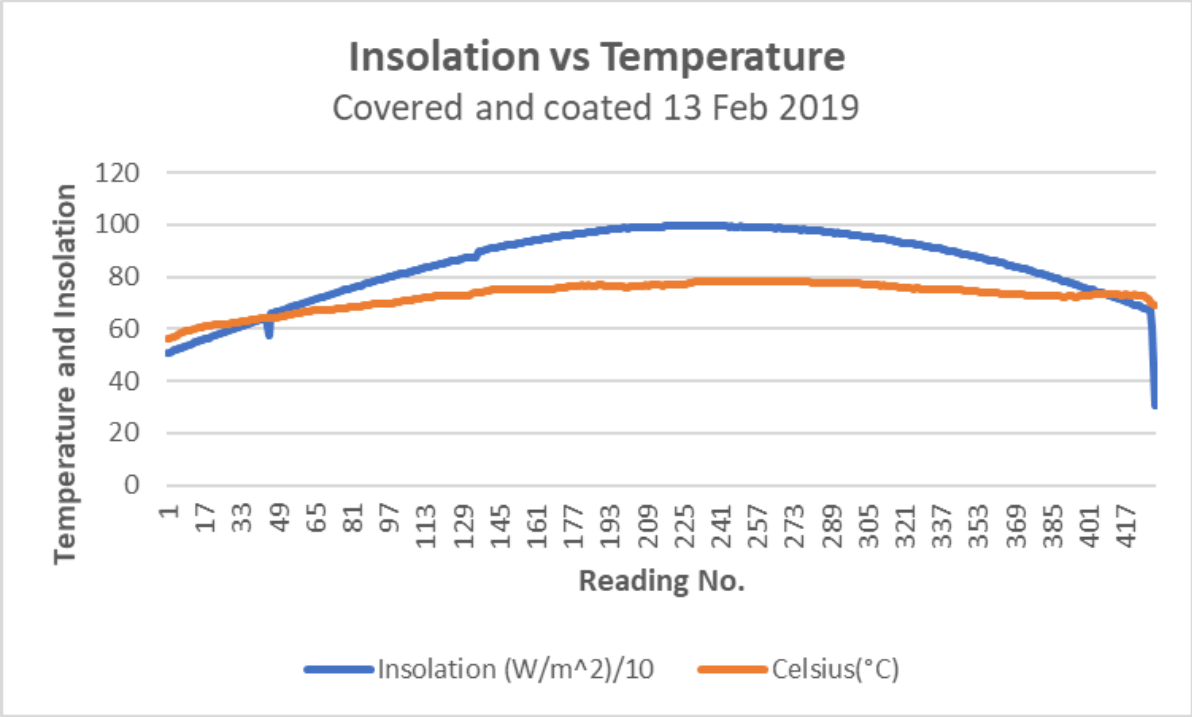

1.2 Effect of directional shading

A second range of tests was undertaken using a pair of ammonia blackened copper tube sensors using all the boundary accessories as used in the initial model tests but

with one sensor biased 60˚ to the east and the other biased 60˚ to the west. Temperature/time plots resembled those of the earlier tests and a clear definition was seen between the daily curves, with the easterly biased sensor peaking before noon and the westerly biased sensor peaking in the early afternoon. The differential between these curves was plotted but shows that the West biased sensor does not convincingly overtake the East sensor due to the increase in temperature from background radiation and the delayed cooling caused by backing insulation. Despite this, the temperature difference is a function of the degree of misalignment as evidenced by the early part of the curve. This is important if the error signal is to be used to provide the energy source for self-correction.

Figure 1.2

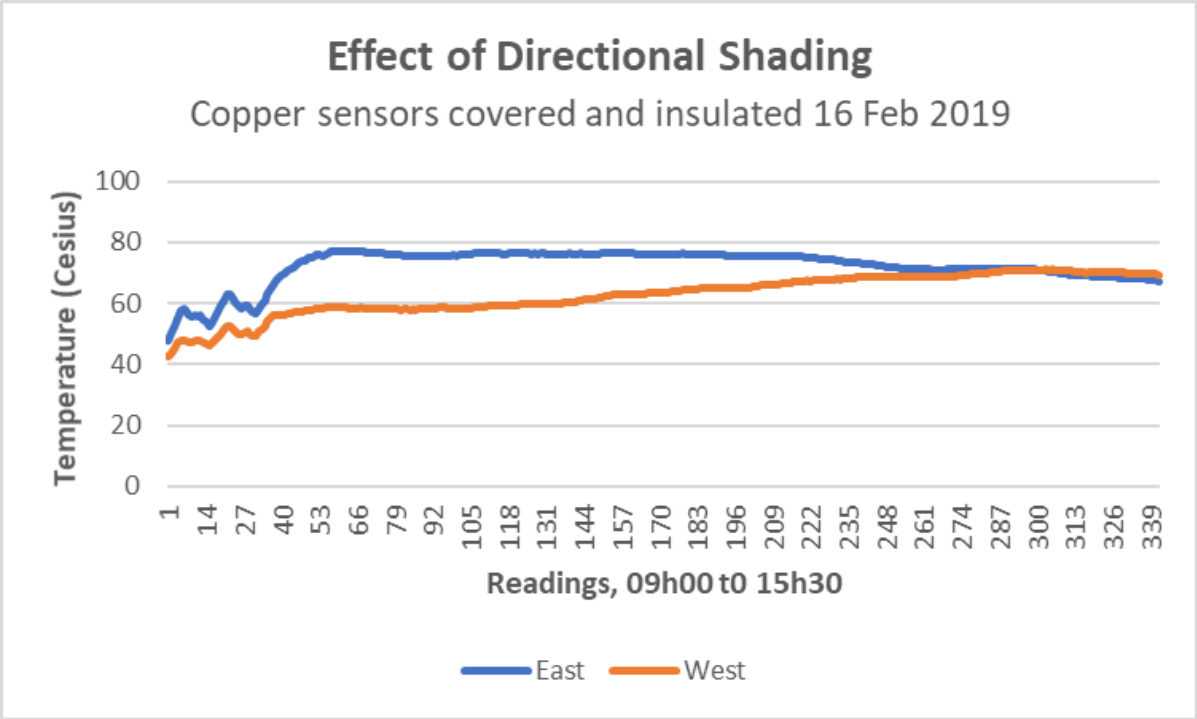

1.3 Pressurised sensor performance

Building on the above experimentation, a set of steel pressure vessel sensors was constructed from square tube with plate ends. The tubes were initially blackened with self-etching high heat paint, fitted with pneumatic valves and pressure transducers and pressurised to 5 Bar(g) at 24˚C. Under full sunshine in still conditions and approaching 1000 W/m2 vertical insolation, the two sensors generated 585kPa and 589kPa guage pressure, implying an average gas temperature of close to 70˚C. The

sensors were shaded in turn using cardboard tunnels with sufficient height to allow free convection. Pressures were measured at 5 minute intervals to indicate response time. The pressure differential diverged exponentially and settled to within 5% of the final 30-minute result within the first 10 minutes. Settled temperatures derived from gas pressures were typically 68˚C and 29˚C, a differential of 39˚C and which concurs with previous estimates of the available limits for a full-size actuation system.

1.4 Actuation from thermally derived pressure increases

A trial using the bare square tube sensors was attempted during early March 2019 using a conventional 50mm pneumatic air cylinder with 200mm stroke length. The sensor pressures were balanced and the cylinder stroke centred. The sensors were initially shaded in turn to gauge response and travel, however the ‘stiction’ phenomenon allowed only large step changes at the limits of expansion and often no movement at all where the differential pressure was too low to overcome friction. It was observed that directly after a change, if the movement was initially assisted it would continue very slowly without sticking, indicating that the dynamic friction co-efficient was much less than the static. The viscosity of the cylinder lubricant would also aggravate this damping effect. The surface temperature of the un-covered and uninsulated sensors did not exceed 63° Celsius whilst the daily insolation peaked at around 865 W/m^2.

A further minor development was the insulation of the sensors on two sides with 16mm expanded styrene foam, so as to create directionally preferential heating.

2.0 ACTUATOR TESTING

The answer to the low friction requirement appeared to be possibly found in the rolling diaphragm actuator (RDA) concept, however a search for commercially available components yielded nothing in the required range, the offerings limited to large bore short stroke models and very small scale items for surgical use. Due to commercial unavailability, a rolling diaphragm actuator was designed and built in March 2019 as a low-cost trial for evaluation using low pressure. The first actuator had internal diameter of 40mm and a stroke of 80mm with extended length of 460mm. It was successful at low pressures, the diaphragm inflated at 12kPa and once partially inflated offered minimal resistance to movement. A second identical

model followed a week later with a sleeve coupler to create an antagonistic pair for testing purposes and the pair were pressure tested at 300 kPa (gge).

2.1 First antagonistic testing

The two actuators were mounted on a stand with a tilting beam on a low friction pivot and the ability to articulate 60° below the horizon in both directions.
At the end of March 2019, the sensors were positioned horizontally along the North/South axis and rotated to allow one to be biased to the East and the other to the West. The actuators and their tilting beam were connected to the sensors and the whole system pressurised to 50 kPa (gge) and the tilting beam centralised to the cylinders, with a horizontal position, prior to sunrise. This series of tests was postponed due to problems with a swivel bearing in the tilting beam pivot, so that a different approach was attempted.

2.2 Horizontal antagonistic testing using fixed sensors

During April 2019, the two prototype RDAs were attached to a beam facing one another with their rod ends connected and compressed to half stroke. The RDAs were connected to the directional sensors as before and the movement of the coupling and time of day were monitored from 12 April 2019 in a series of tests to compare movement with the ideal. The results show positive response and approximate the ideal curve, when used with low pressures up to 75 kPa. Deficiencies with the prototype RDAs were evident at higher pressures and the units eventually became unresponsive and repeatedly jammed above 1 Bar (g).
The ideal curve was created using the product of an energy approximation for each hour of the solar day based on typical values of the daily solar insolation bell curve and the insolated area of two sides of the square tube sensor using the sum of the sine and cosine of the azimuth angle for the corresponding hour of the day for April 2019. The actual curve corresponded to this ideal within a 78% compliance as depicted by the clear day readings of 15 April 2019 despite some early morning mist. This result includes a correction for the early morning ‘thermal inertia’ of a cold system with considerable metal mass, a small input energy value and a seasonally changing sunrise time. The results are plotted as Displacement vs Hour of Day

curves and clearly show the effect of mist, cloud and rain on the sensor, which is essentially a partly insulated solar collector without glass cover.

Figure 2.2 (a-e) serve to illustrate these effects –

Figure 2.2(a)

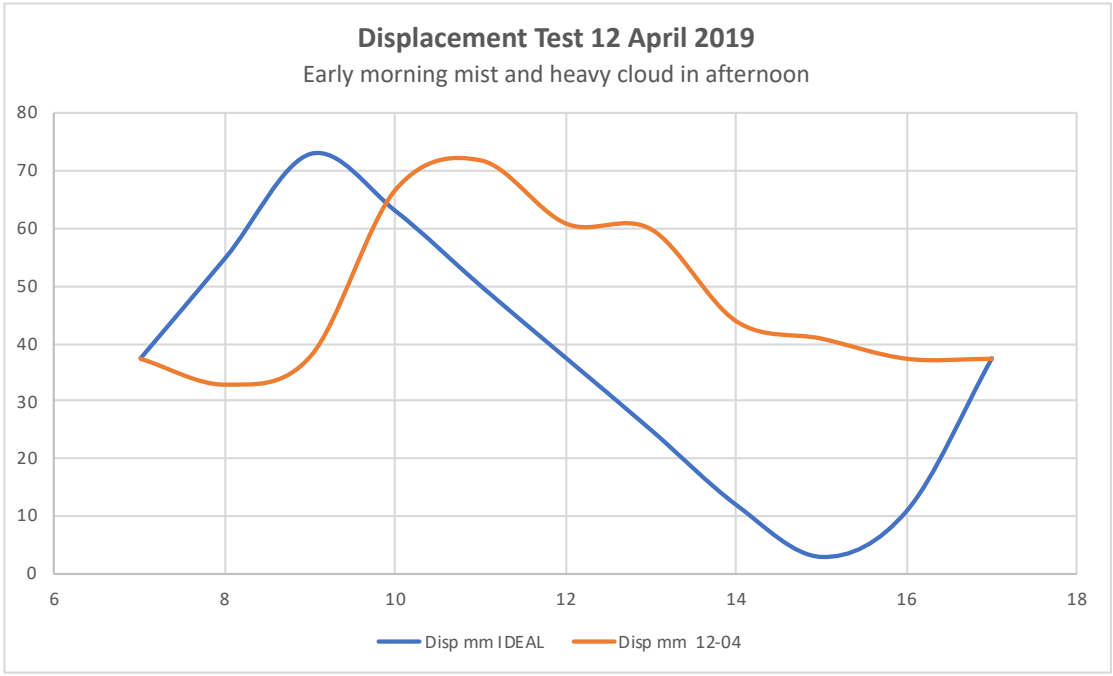

Figure 2.2(b)

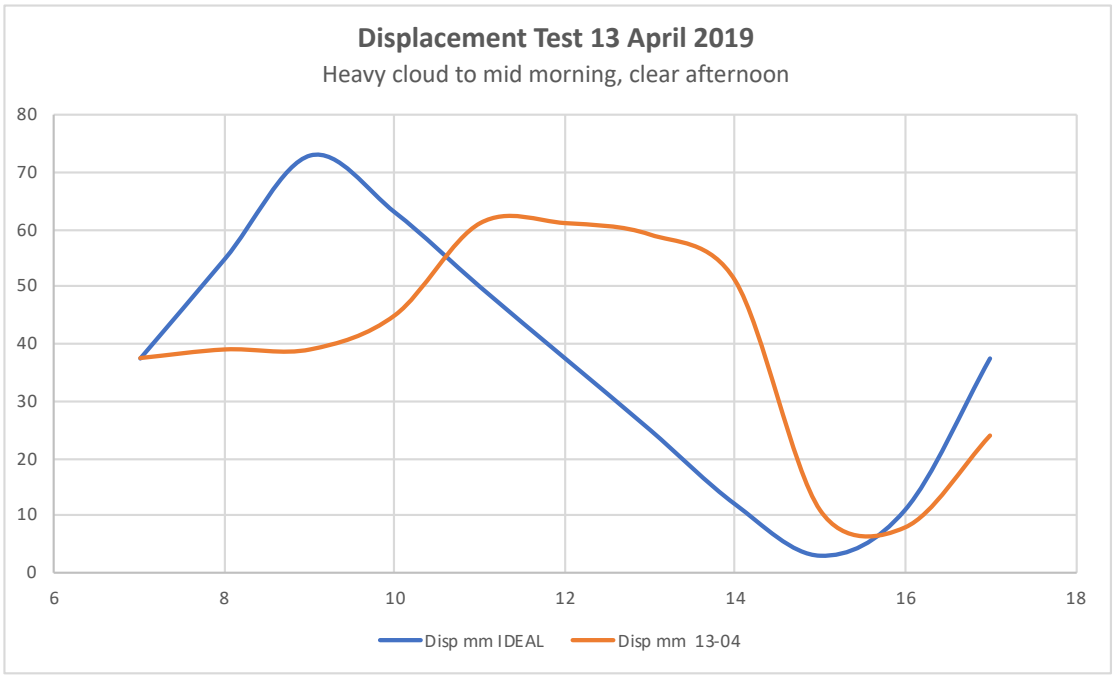

Figure 2.2(c)

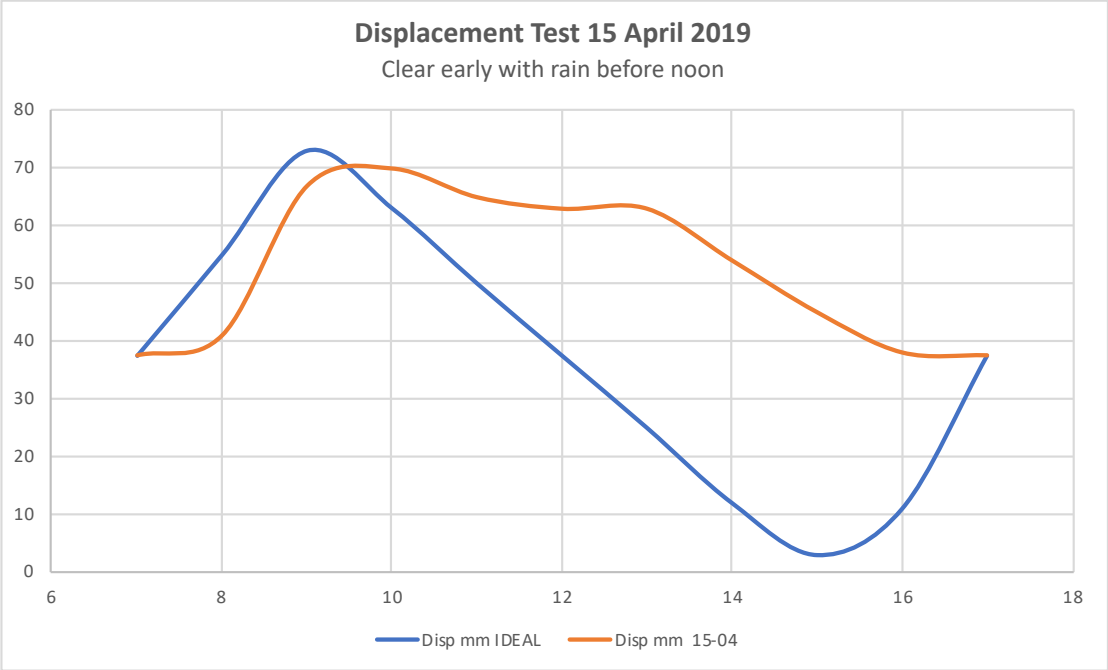

Figure 2.2(d)

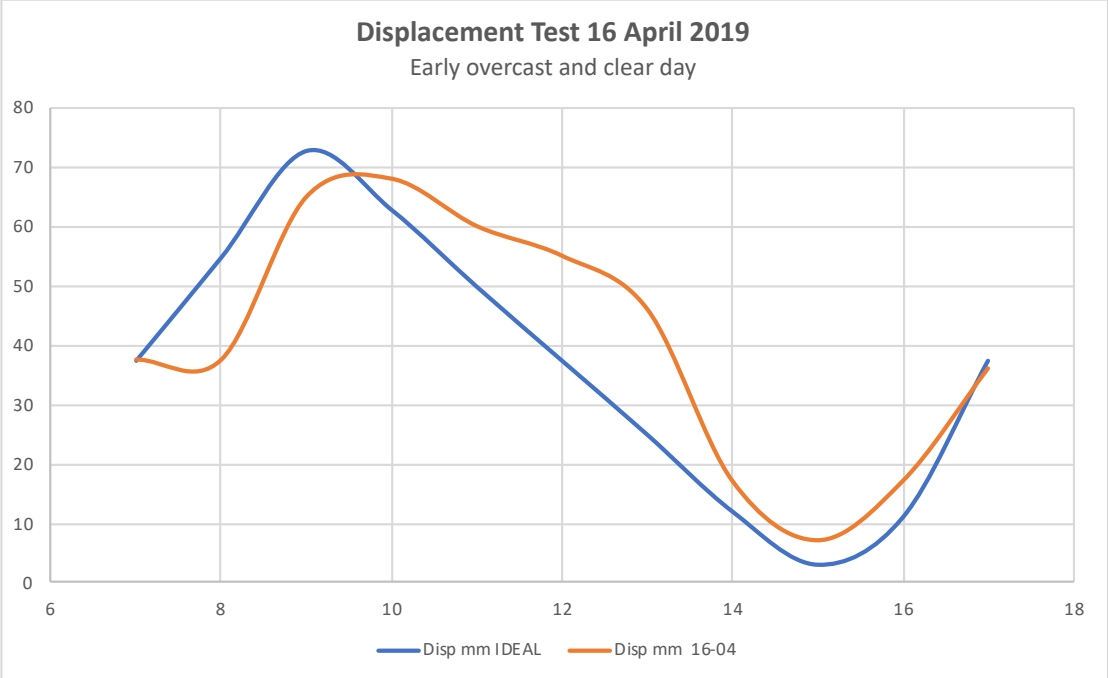

Despite these encouraging results, the pre-charge pressure was limited due to the actuator construction hence the actuation forces were small, heightening the effect of friction in the guide bushes. It is also clear that the performance is heavily dependent on clear weather due to the threshold friction.

Figure 2.2(e) Summary of antagonistic heated air tests

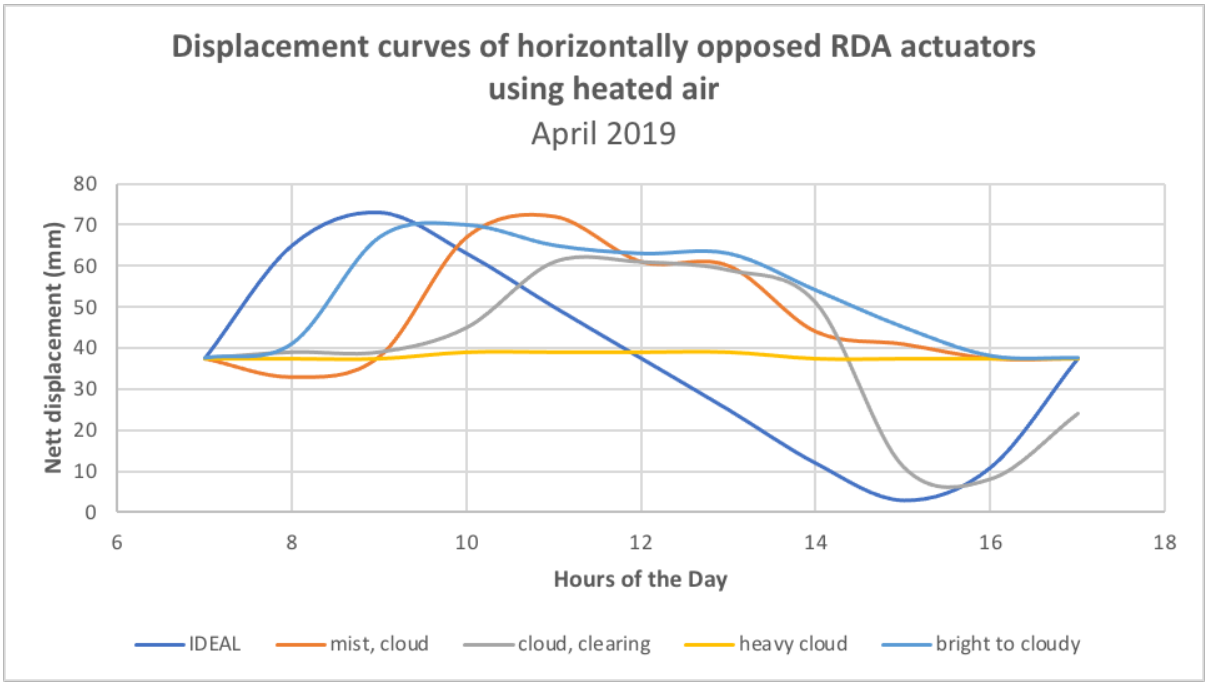

The first prototype RDAs were observed to have these deficiencies –

- Permanent deformation of the diaphragm. Once inflated regularly above 1 Bar (g) the butyl elastic material deforms permanently and fouls over the front of the piston.
- The bearing length of 50mm and the 0.2mm clearance of the rod allows a minor angular misalignment. The cast shape of the diaphragm as well as this clearance allows enough misalignment to cause fouling between the piston back end and the diaphragm outer, especially when the actuator has some bending moment applied, as with the tilting beam arrangement.
- At pressures above 65 kPa the material stretches and ‘balloons’ into the available space. This distorts the pressure and volume relationship between the two cylinders i.e. the relationship between volume and actuator rod stroke is not linear.
- The membrane stretch displacement at various stroke lengths and pressures causes frictional work against the cylinder wall, reducing the amount of available work for actuation.

Considered solutions to these issues are the use of a conical diaphragm, a non-elastic but flexible diaphragm membrane and a longer or more rigid guide bearing. There is also the possibility of a centralising guide rod sliding within the hollow

actuator rod and rigidly attached to the back actuator plug, although this requires a diaphragm with a seal ring at both ends.

The poor frictional response from standard pneumatic cylinders and the encouraging results using a preliminary rolling diaphragm actuator concept led to a higher specification actuator which reduced the frictional losses substantially and utilised a low cost replaceable diaphragm with limited elasticity, more rigid than the butyl rubber tubing used in the trials.

The new diaphragm is closed at one end with a locating nub to position the diaphragm centrally at all times. The rear is fitted with an extrusion ring which locks the diaphragm in position and provides an airtight seal.

The membrane is a composite of high grade silicon rubber impregnated into a fabric blank.

The fabric selected is a raw cotton weave which has excellent wicking qualities to assist with impregnation of the silicon, as well as adequate strength. The cotton fibres are 0.2mm in diameter with a minimum breaking strain of 327g. Tensile testing produces a strength of the fabric in excess of 8kg/cm when applied in the weft direction.

The membrane was pressure tested and the result compared to various other materials. The test membrane fractured in tension at a pressure of 9.6 Bar with a permanent deformation of 5% at failure. By comparison a sample of membrane from a life saving device failed at 2.1 Bar and a sample from a brand name inflatable boat failed at 3.5 Bar. Both of these materials deformed in excess of 20% at failure.

The diaphragms were hand made by the author due to lack of a supplier for small batch prototype rubber parts within the required time frame. The final diaphragm design is cylindrical in the static end and conical at the rolling end in order to enhance the rolling clearance. To take advantage of the small elasticity difference between the two fabric dimensions, the weave is placed circumferentially where it is supported by the cylinder wall and the weft placed longitudinally where the smaller elasticity limits the frictional work done. The unavoidable fabric joints are effected using a raw latex bonding agent which is vulcanised by ironing. The fabric blank seams are placed and oriented in such a way as to confirm the seam using internal pressure and to ensure stressed seams are always in shear, i.e. the bond is not subjected to tensile stress.

The cylinder friction is well below the 3% of applied force as specified in commercially available versions and has the added benefits of the correct stroke and a pressure rating comparable with the commercial offerings, however reliability and air retention of the handmade diaphragm were not up to standard.

3.0 TESTING USING THE TEST RIG

The test rig was assembled without solar panels fitted until a reliable tracking of the frame could be achieved. The RDA concept had proven to be not reliable without extensive development of the diaphragm.
A radial version of the RDA was produced with a double acting linkage to the test rig and tested using various types of flexible lay-flat hose as the diaphragm with various designs of end clamping and inlet porting within the clamps. These actuators worked extremely well with compressed air, producing very high output forces across a relatively short stroke. Performance with the small pressure available from plain tube heating produced disappointing results due to the small forces and short stroke. A magnifying linkage increased the stroke at the cost of even smaller output force.

The use of standard pneumatic equipment was considered, provided the issues of leakage, chemical compatibility, damping and ‘sticky’ motion could be resolved.

In February 2020 the test assembly was stripped down, maintained and lubricated for a new series of tests using pneumatic cylinders. The test rig was rotated 90° to facilitate the vertical actuator configuration and the necessary mountings and attachments designed and fabricated. The frame was balanced and aligned to be very slightly underslung so as to return to the horizontal without external assistance.

3.1 Air testing using the plain frame

On **15 February 2020**, the assembly was completed for the East/West actuation tests with two 25mm x 200mm pneumatic cylinders installed rod side down. This configuration had the intent to limit any potential leakage to only one seal as well as ensuring a wet seal by introducing a viscous fluid on top of the piston. Glycerine was introduced into the upper chamber of both actuators to provide the wet seal of around 2cm in depth, or 5cm^3 in volume, which ensures full stroke operation without

fluid carryover. Both rod end ports were connected together without a restrictor, to prevent dirt ingress.
To estimate the baseline data, an air pump was connected to one cylinder port whilst the other was left open. A pressure of 25 kPa(g) was required to initiate movement, equating to a force of 12.2 N at a radius of 90 mm which represents a total frictional moment of 1.1 Nm. Considering that the bearing frictional moment is only 6.32 $x10^{-3}$ Nm each (SKF Bearing Friction Calculator) it appears that the cylinder seal static friction force is around 6N per cylinder. The dynamic co-efficient of friction was observed to be much lower, once in motion the frame continued to move to its maximum incline but if halted, would remain in that position.
A differential pressure of 25kPa equates to a sensor temperature of 93°C above ambient for a pre-charge pressure of 0 kPa(g) and initial charge temperature of 20°C, which is impractical for plain heating surfaces.
Using a 5 Bar(g) pre-charge pressure would require differential heating of only 32°C but with the higher stresses and potential leaks at this maximum pressure for the system.
The above threshold pressure and temperature only allows initial movement, control and actuation require higher values.

On **16 February 2020** the apparatus was set up with two cylinders opposed antagonistically, using natural air at barometric pressure, prior to sunrise. The East sensor was connected to the West cylinder and vice versa. Both systems were connected by a connecting line with a blocking valve (Partition valve) and the common line was routed to atmosphere via a second blocking valve (Atmospheric valve).
The frame was set horizontal with both blocking valves open so as to equalise pressures and volumes in both systems at ambient temperature of 20°C. The Atmospheric valve was shut followed by the Partition valve at 07h15. The rod end ports were left connected to each other to prevent dirt ingress, i.e. no damping.
The West sensor was covered with loose tissue paper to prevent heating. Despite frequent light cloud cover, the differential temperature was measured at 8-15 am to be 12°C (36°C hot side, 24°C cold side). The derived pressures would correspond to 105.46 kPa versus 101.36 kPa, a differential of 4.1 kPa. Clearly the pressure

differential falls way short of the friction threshold pressure of 25 kPa as measured previously and predictably the frame failed to move despite the temperature differential increasing with time.
The system was pressurised to the full 5 Bar(g) limit to soak overnight and confirm zero leakage.
On **17 February 2020** the apparatus was set up as before with the exception that the system was manually pressurised through the Atmospheric valve before being partitioned. Successive planned tests at 1 Bar(g) through 4 Bar(g) were omitted due to the obvious inadequacy of small differential temperatures to overcome the friction force of the cylinder seals.
Further delays were due to the need to design, fabricate and fit a locking system for the North/South axis in order to evaluate motion of the East/West axis in isolation. A second modification was a stopper to limit East/West movement and prevent damage to the pneumatic cylinders. Excessive wind and cloud further delayed testing at the site. Polystyrene shade strips were also installed on the East and West sensors to ensure selective shading.
On **1 March 2020** and the following two weeks, the system was tested at various pre-charge pressures, air only, and plain heating. Despite the increased charge pressure, the actuation force dropped away rapidly with an increase in cylinder stroke. Overall angular displacement was in the region of 10 degrees of arc on the best day, shown in **Figure 3.1**, far short of any useful travel.

3.2 Acetone mixture volume tests

Pure acetone has a very low vapour pressure at low ambient pressures, hence the air mixture moderates this low temperature situation by a Daltons law addition of partial pressures and ensuring that the mixture pressure remains positive. This is clear from **Figure 3.2** below, which is the result of a 2.5 :: 1 by mass mixture of acetone to air in a steel lined solar collector. With the insert sealed, the partial pressures combine to produce a more moderate response, where the maximum air pressure is around 40 kPa(g) at maximum collector temperature.
A separate apparatus was set up to investigate the effects of Acetone $(CH_2)_3CO$ vapour as an air mixture, using a solar tube with a steel insert with gypsum wick and connected to a pressure gauge and a 50mm pneumatic cylinder.

Figure 3.1

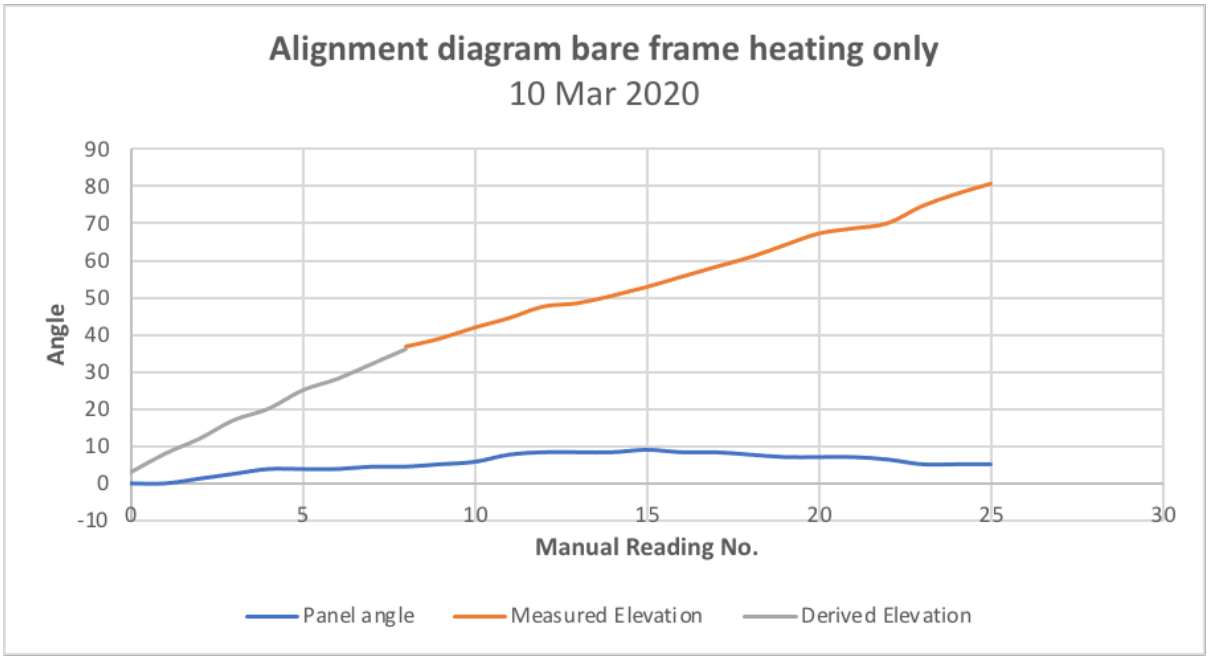

The cylinder rod-end volume remained open to atmosphere via bronze strainers. Into the feed tube a measure of 10cc of pure Acetone was added to create a mixture ratio of 5 :: 1 kg acetone to air.

The tube was rocked to disperse the fluid to the wick. The block valve was then opened to the cylinder. The result was dramatic, with the cylinder opening with some force.

It is clear that the acetone mixture creates a response very different to that of the plain air, whilst it is still liquid in the hot tube, however the data clearly shows that the effect decreases once a saturated mixture is achieved with the existent air due to the loss of acetone in the mix as it condenses in the cooler regions inside the actuator.

It was suspected that the excess liquid acetone condenses above the glycerine layer in the cylinder and remains there as an inert fluid, having neither the pressure or heat to become re-entrained. This suspicion was proven when the cylinders were drained at the end of test and the contents inspected. The Acetone was allowed to separate naturally in a closed container which formed a clear separation layer and then evaporated in air to leave the clean Glycerine behind.

Figure 3.2

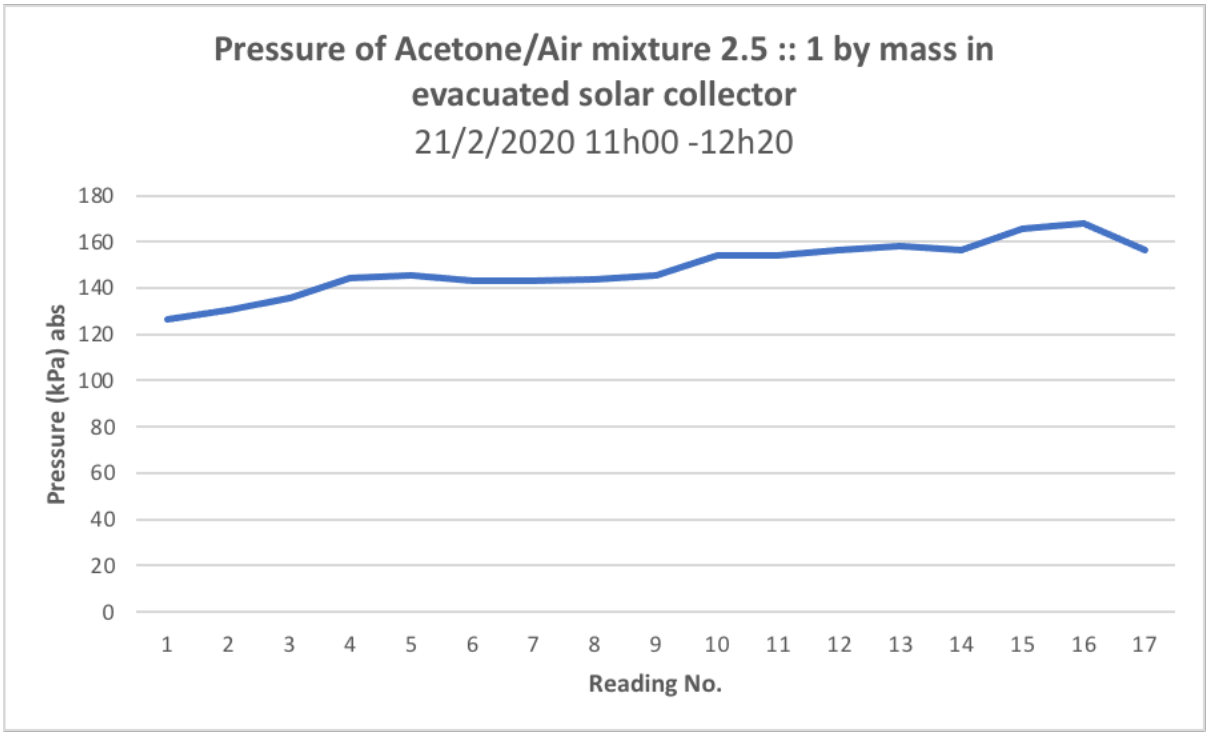

This test illustrates that an Acetone vapour pressure generator can produce good results under the following conditions -

- The destination should be located above the generator to ensure gravity return of the condensate.
- The feed pipe should be large enough to allow dual flow of vapour and condensate.
- The cylinder being pressurised should be arranged such that any condensate formed inside can be effectively drained away.
- The feed line requires insulation to prevent significant heat loss to condensation with resultant pressure reduction.

3.2.1 Acetone mixture testing on the test rig using bare frame tubing

The test rig was further adapted to use acetone mixtures and damping. The rod-end volumes of the cylinders were charged with glycerine into a common connecting line. The connecting line was fitted with a restrictor in the form of an aluminium rod machined and tapped on both ends to fit a 6mm pneumatic tube connector. The 2mm wall between the connectors was drilled through to 0.8 mm and further restricted to 0.26 mm by casting a brass wire into the orifice with epoxy, then

removing the wire. The damping response was dramatic, the frame was difficult to manipulate by hand but the Acetone vapour pressure managed to move the frame almost imperceptibly.

Tests at barometric pressure using 10g liquid acetone/3litres air produced movement which was sporadic and unpredictable. The results of two tests are illustrated below as Figure 3.2.1(a) and (b) which show the relationship between the temperature differential (East to West) and displacement antagonistically opposed small bore pneumatic cylinders. Although the graphs show a definite correlation, the displacements achieved are impractically small. For example, the biggest tilt angle achievable on a 50mm radius is around 11° of arc and providing a correcting torque around zero Nm at equilibrium.

Figure 3.2.1(a)

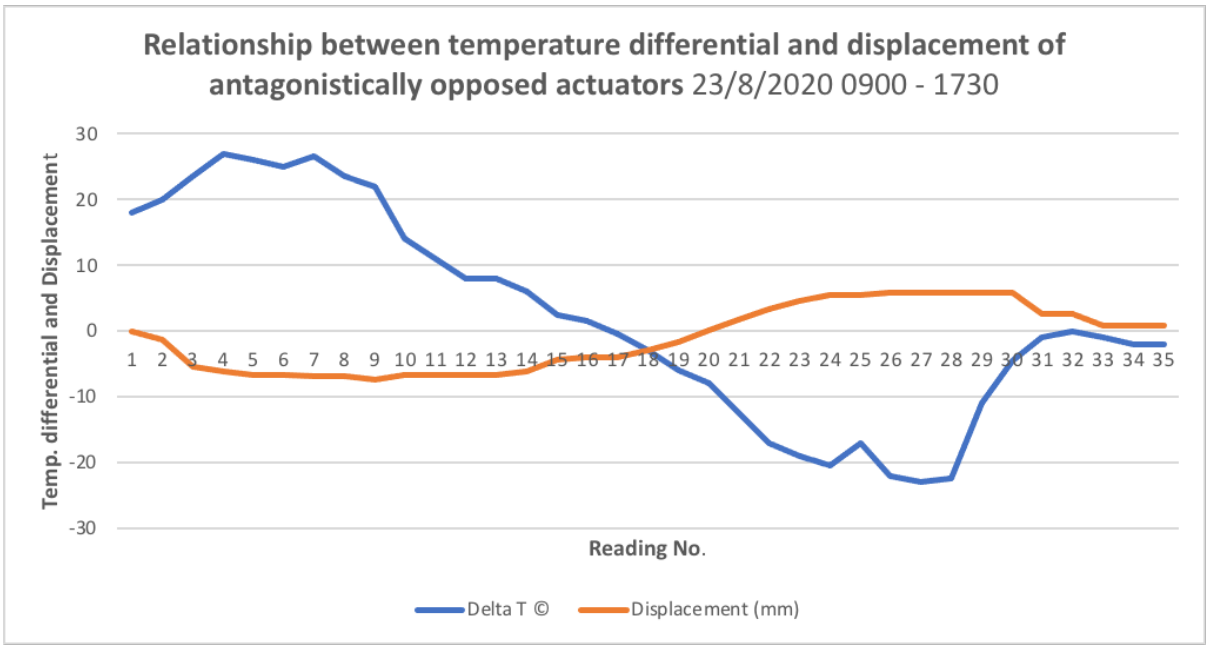

Figure 3.2.1(b)

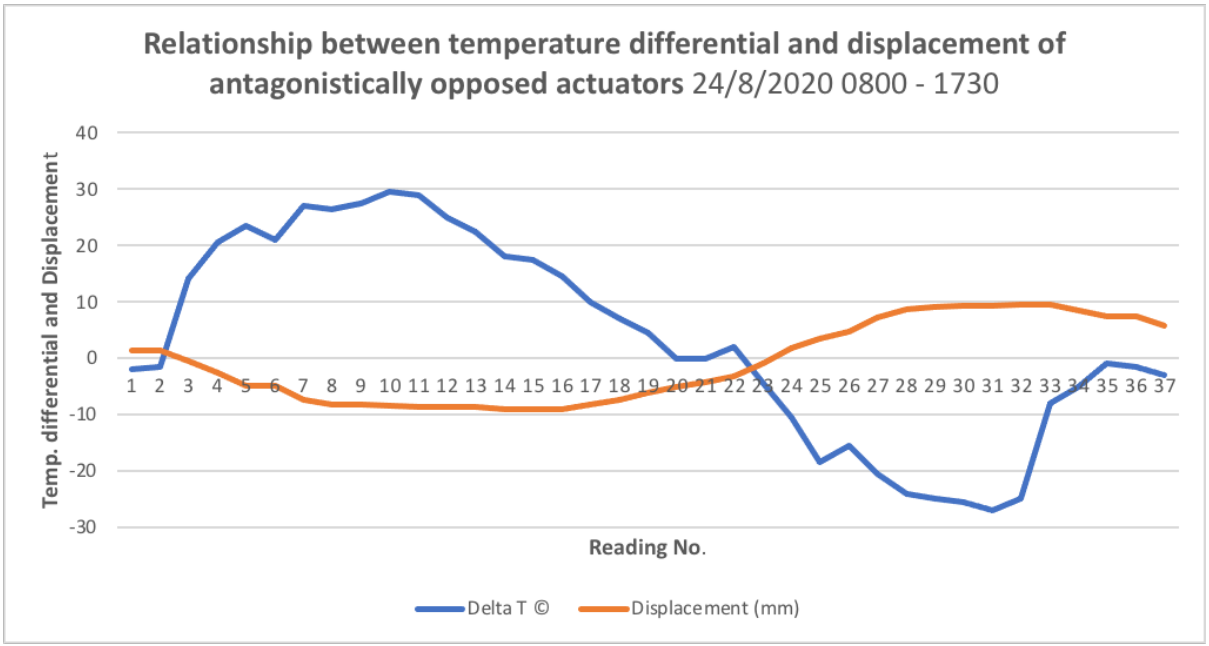

4.0 ENHANCED HEATING TESTS

During **January 2020** four steel evaporator pipes were constructed for enhanced heating testing with solar heating tubes. Two pipes were fabricated plain and the other two were fitted with an internal gypsum wick. The evaporators with the wick system were exposed to sunshine for several days to eliminate moisture, during which time it was observed that they produced visible steam when the outlet was restricted.

On **23 February 2020** the first wick evaporator tube was exposed in a North/South horizontal position and the outlet routed to a pressure gauge. The gauge pressure was initially zero, Barometric pressure for the morning was 101.27 kPa and ambient temperature was 19.9°C at the time of sealing the system.

The device was exposed between 10h00 and 11h50, during which time the trapped volume generated a pressure of 119 kPa(g).

At 11h50 the device was shaded with a loose PVC cover and pressures monitored at 5 minute intervals. The response over 30 minutes was a pressure reduction to 90 kPa(g).

The cover was again removed at 12h30 and the pressure was seen to rise steadily to 135 kPa at 13h00.

The device was left exposed in an attempt to find the stagnation pressure. The captive gas pressure continued to rise up to 14h25 when the pressure became stagnant at 245 kPa.
On release of the hot gas, some vapour and condensate was emitted at first, indicating that the captive air and gypsum wick had still possessed some moisture. Despite the test having failed as an air test, the dramatic result implies that the device has potential to be used as a steam generator for actuation purposes.

On **29 February 2020** a plain heat pipe assembly, charged at 22°C and atmospheric pressure was exposed at 09h30. The first readings were obscured due to leakage, however the leak was cured and the system recovered at 15 kPa(g) at 10h30. Over the following three hours the dry air pressure increased and plateaued at 41 kPa(g). A calculation of the air temperature at constant volume indicates that the temperature of the concealed heat pipe parts reached a maximum of 143°C. A further calculation of tube mass and air mass indicates that the average heat absorption during this time was only 14 Watts with a maximum during the initial heating stage of 22 Watts, due to the higher differential temperature..
Insulation of the protruding section of the heat pipe resulted in a 2 kPa improvement to 43 kPa, equivalent to the conversion of an additional 9.5 Watt. This value compares closely to the calculated convection loss of 9.9 Watt.

During early March 2020 the test rig was fitted with two holders for solar tubes as well as shade plates.

On **10 March 2020** the frame and solar tube system was set up to be level and charged at 0 kPa(g) at 07h00 with the North/South axis blocked. The system responded by tilting towards the East after a warmup period of 80 minutes.
The response was slow and the West solar tube received sun before the system matched the sun angle, resulting in a premature levelling-out of the panel angle before noon.

Calculations of the heating cycle revealed some problems with the steel insert such as the low emissivity of bright galvanised tube but mainly the mass and wall

thickness require much heating time. This situation is exacerbated by the fact that the heat transfer reduces as the surface temperature of the insert rises.
The above two issues are compounded by the extended cooling response due to the same factors.
The actions following this test were threefold -

- a faster responding insert was designed using aluminium with a roughened surface to improve heating response and which would be fitted to a new, longer solar tube. The insert is still a necessity for using refrigerants due to the potentially high pressures reached.
- the second initiative was to extend the shade plate to shade the westerly solar tube for a longer period as well as polish the inner surface to provide some additional heat to improve response.
- a third initiative was to eliminate the heating delay of the insert entirely by designing an expanding plug, using only the inner tube for both air heater and receiver functions for dry air testing. This measure was considered safe insofar as expected pressures are below 50 kPa(g) and the glass strength provides a large safety factor even at elevated temperatures.

These changes were effected by **12 March 2020** and a second set of the 1.8m tubes were sourced to prepare for the test without inserts.
Response and reaction were noticeably improved using the aluminium inserts with modified shades. The overall response at 23 minutes produced the same small changes as before, albeit much quicker. It was noted that response to meet the sun was far greater than any response to lock on and track the solar path.

On the morning of **14 March 2020** a set of solar tubes with cemented plugs and no inserts were mounted before daybreak and the platform balanced and pressures balanced with barometric pressure. The initial response was very quick, well within the 15 minute reading interval and estimated to be just 2 minutes. As the platform tilted toward the sun, the East tube shattered. In the belief that there had perhaps been a stress raiser in the tube, a second tube was prepared and the exercise repeated the next day **15 March 2020**, with the same result. Testing of this idea was halted before any results could be recorded, for safety reasons.

On **12 March 2020** the two aluminium inserts were fitted and pressurised to 500 kPa(g) and soaked overnight. On the morning of **13 March 2020** it was found that the pressure in the West circuit had leaked away. The pressures were balanced and the system left on test for the day. Attempts to find the leak indicated that both East and West cylinder seals were passing, despite the wet seal provided.
Despite the leakage some movement was observed which reduced as the day warmed up, leaving the rig frozen at a slight tilt to the east.

At this time it was concluded that the use of heated gas was a problematic solution due to the small available energy and practical issues of response, loss of heat and leakage.

5 .0 UNBALANCED MASS TEST

5.1 Unbalanced water weights using heated air

This variant pumps water from a low reservoir to an eccentrically placed reservoir at the edge of the platform using the pressure and expansion of the solar heated air.

The platform is weighted to face East overnight. The heated air from one solar tube aluminium insert displaces the water from the airtight low reservoir up to the variable mass reservoir which encourages tilting of the platform, in turn causing shading of the solar tube and a resultant cooling of the gas, in turn draining fluid from the variable reservoir and reversing the tilt. The intent is that the alternate tilting increments follow the angle of the sun until sundown, when heating is lost and the fluid drains back to the reservoir, allowing the platform to return to its East bias by gravity.
This theory was tested during the week starting **16 March 2020.** The platform was fitted up with two glass jars of 500 ml capacity, the first jar had been modified to accept pressurised air via a sealed tube through the lid. A second sealed tube originated in the base of the jar and extended to the second bottle. This second bottle was hung from the platform at its western end and its lid was perforated to prevent airlocks. The platform was weighted to stay tilted to the East when the second bottle was empty.

A function test using only lung pressure easily displaced water to the second reservoir and effected a successful full tilting motion. The water was then allowed to siphon back to the airtight bottle with the air hose disconnected.
The air tube was connected to the aluminium insert on 17 March. The system responded as expected and water was pumped to the second reservoir, initiating some tilt. The air pressure was noted to increase to approximate the head difference and stabilised there for some time, however the pressure started to decrease rapidly thereafter and the fluid seen to be siphoning back to the lower reservoir despite full sun exposure, indicating a leak. The leak was found and sealed. The test was repeated with a similar result where the water flow would slow and stop, having reached an equilibrium between the air expanded into the water bottle and the remaining mass of air in the insert having expanded to its maximum capacity for the available temperature. The second solar tube was connected in parallel with the first and the shade plate turned around, so as to double the available volume of air. This measure allowed a further movement which was exaggerated due to the slow cooling response of the solar tubes. The position reverted and again was exaggerated by the slow heating response of the tubes. Further testing during the latter part of March 2020 was hindered by preparations and limitations imposed by government to curb the global pandemic.

6.0 HYDRAULIC ACTUATION WITH PV POSITIONER

During the national level 5 lockdown of 2020, a scaled down facsimile of the test rig was created for testing under lockdown at the author's home.

6.1 Proportional control of pump speed

On **30 March 2020** a successful actuation was achieved using a potable water pump and solar panel connected to a pneumatic cylinder and using controlled shading of the panel as positioner. The pump started up once the shading of the first row of cells reduced to expose a 2cm strip. With a 12.5cm high shade tilted away from East at 14°, the panel alignment consistently advanced the elevation angle by 7°, well within the 10° target alignment. Initially the pump was unable to move the panel and ran at low speed. As the shade retreated due to solar movement, the pump speed increased until the panel started to move. Due to this movement, the shade advanced on the panel and the pump slowed down again, allowing the movement to

stop. This mechanism maintained a proportional relationship between the panel position and the length of the shaded area, in turn maintaining a fixed relationship with the position of the sun. A plasticised protractor was attached to the frame to monitor the accuracy of the system, an indication of the alignment is visible on the shadow from the frame where 90° indicates perfect alignment.

On **31 March 2020** the system was re-configured for better balance and less effort required to move the panel. The system performed as well as on the previous day and it was resolved to provide some form of automatic stop/start of the pump to prevent it running constantly as this system was not ideal from a reliability perspective. In the interim the system was fitted with a manual switch. Closing the switch initiated the above control mechanism, correcting the alignment to 90° and slowing the pump due to low current, at which time the pump was stopped manually.

6.2 Pilot circuit for 'Bang-Bang' control

In the following days the apparatus was upgraded to start and stop the pump by means of a manual relay whose secondary circuit switched the pump drive circuit. The relay primary circuit was activated by lack of shading of the panel, as before, but stopped the pump when the desired length of shade was achieved. On **1 April 2020** it was attempted to run the system using a relay wired into the circuit but using the same power source, during which time the relay locked up and the panel actuator ran to full stroke. Work was done to split the power supplies to provide for a pilot circuit.

During this time the pump was powered by a lead-acid battery to separate the circuits.

On **3 April 2020** the actuation radius was reduced from 210mm to 140mm, the minimum for this design. this change increased total tracking range from 42° to 60°. The setup produced a very satisfactory result which cycled between the same limits as previously, but with around 10 minutes between pump starts. The range increased and the tracking time which had initiated around 10h30 proceeded until around 14h40. The pump ran on as noticed the previous day and was again stopped manually.

A further development was the use of a 5 Volt PV cell in a shaded and angularly adjustable compartment and which energised a micro relay connected to the pump circuit. The main PV panel was then used to power the pump. The 5V trigger system

was installed on **6 May 2020** and produced the required sensitivity to reduce the control range within 4° on cloudy days and 2° on sunny days, for the duration of the test period.

6.3 Shutdown switch

At the end of the solar day, the pump was found to run on as the cylinder had reached end of stroke and the trigger PV cell remained fully exposed. On **5 April 2020** a special switch was fitted to shut the system down once the platform reaches its maximum tilt towards the West. The switch comprises a steel roller within a confined track under which a microswitch has been fitted. The switch is mounted on a sheet metal strip so that the set angle can be adjusted. Once the platform angle exceeds the set angle, the roller rolls forward and triggers the microswitch. The platform begins to return to the rest position and the roller only resets after the pilot trigger is in shade, to prevent the panel repeatedly attempting to tilt west until sundown. This hysteresis is achieved by placing a 1mm wire across the roller path, which keeps the circuit open until the PV sensor is fully shaded by the retreating panel.

6.4 Leak-off and overnight reset

The pump discharge was initially throttled to allow reverse flow leak-off, to return the frame to the east at night. This measure also ensured that the panel hunts across the ideal angle constantly, but resulted in excessive stop and starts of the pump.

This system was upgraded with a check valve and tee in the pump discharge, with a leak-off throttle valve to control leak-off, so that response was quick and subsidence was slow.

The throttled valve in the leak-off line often clogged with contaminants in the water. A water change and fitting of a pump inlet filter reduced this issue. The throttling valve was replaced with an in-line filter and restrictor orifice to produce good repeatability of subsidence time. Current leak-off and damping permit the payload to move from fully deployed west to park in 30 minutes.

6.5 Heavy duty pump and low pressure hydraulic actuator

The test pump used was a water pump designed for recreational vehicles, of plastic construction. With concern for the longevity of the pump, a dedicated heavy duty

pump with high head and low flow characteristics and with the capacity for many starts was designed, manufactured and tested for this specific application. The pump was installed on **26 April 2020** for daily use until the system was stopped on **8 May 2020** for upgrades.
The pump design concept became the subject of an article submitted to the Journal for New Generation Sciences.
Due to lack of a suitable actuator during the level 5 lockdown, a 45mm single acting hydraulic cylinder was designed and manufactured from available materials and used between March and June 2020, when it was transferred to the main test rig at campus and run for a further month with the forward bladed heavy duty pump. Drawings of this actuator are provided in the final specification, **Appendix D** to the thesis.

The above system was run during the above developments from **30 March 2020** and run daily with exception of 3 days of bad weather until **8 May 2020,** at which time it was dismantled to develop the Northern tilting axis linkage. The upgrades and changes were effected in the evenings and early mornings.

On **20 April 2020** a design was done of a linkage system to tilt the rig towards the north during the day, using the effort provided by the hydraulic azimuthal tracking. A model was built during the pandemic lockdown to test the design and a full sized set of components manufactured in anticipation of eventual access to the test site. The design was upgraded to provide sufficient strength for the full size test rig and installed during July 2020 on return to campus.

The linkage system tilts the payload north in sympathy with the position of the main Hookes joint member, thus maintaining a relationship between the polar equivalents of Azimuth and Elevation throughout the day.

The linkage system was set for the winter solstice and later adjusted to the equinox setting. At the time of writing the linkage is set to the summer solstice position.

Using the shadow pin method described in the thesis, spot checks of the shadow during full sunshine and medium overcast maintained the alignment within the 90%

target during the active hours, with the panel ‘locking on’ at 10h20 and reaching full travel at 15h20 during the period across the winter solstice.

Measurements were taken from a matched pair of PV cells during the period April to November 2020 to gauge the comparison between a horizontal cell and a tracked cell. During the winter months the tracked cell peaked at 20% more energy than the flat cell at noon. The tracked cell ramped up to full power very quickly and exhibited an almost flat characteristic throughout the day, whereas the flat panel exhibited the typical inverse parabolic shape.

The area under the tracked cell curve (Current vs Time) shows clearly a marked increase in full day energy production over the flat curve, see **Figures 6.5(a) to (e).** These figures illustrate the advantage of early and late day alignment with the solar path.

Figures 6.5(a)

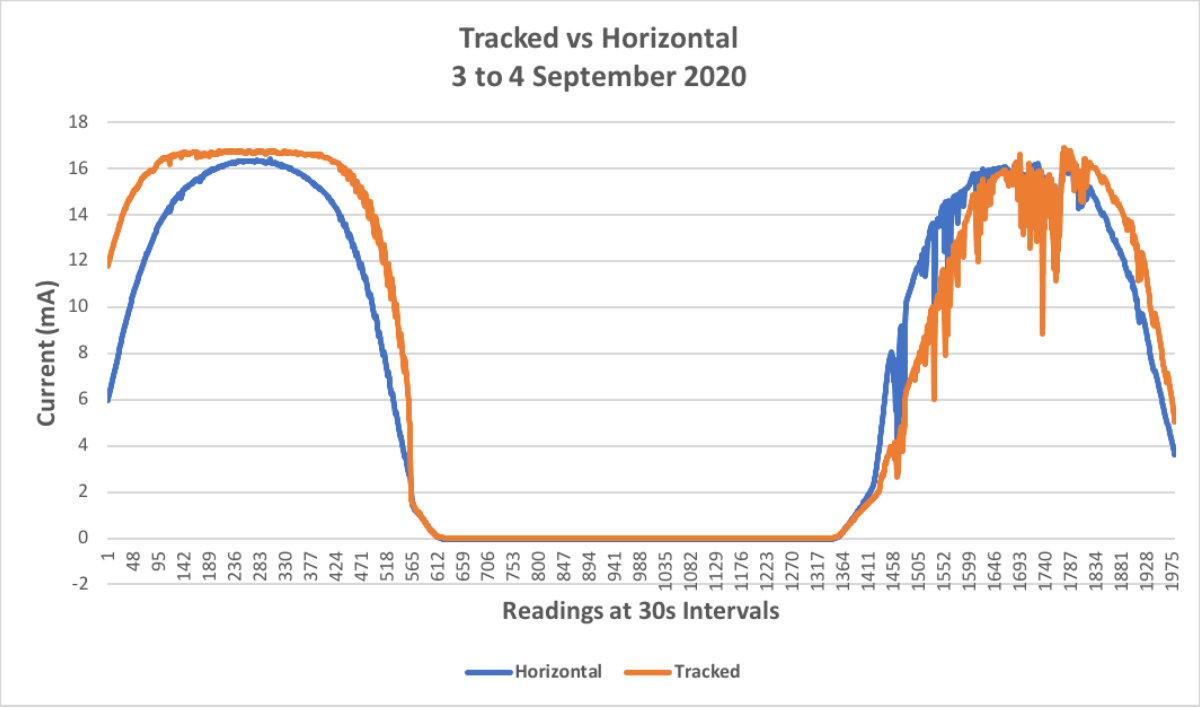

Figure 6.5(a) shows the comparison on 3 September where the fixed cell peak daily output closely approximates the tracked cell. This is due to the tracked panel still aligned to the winter setting (35° above horizon). The curves for 4 September show

the effects of inclement weather - heavy intermittent cloud and high winds - which unsettle the tracker until late afternoon.

Figure 6.5(b)

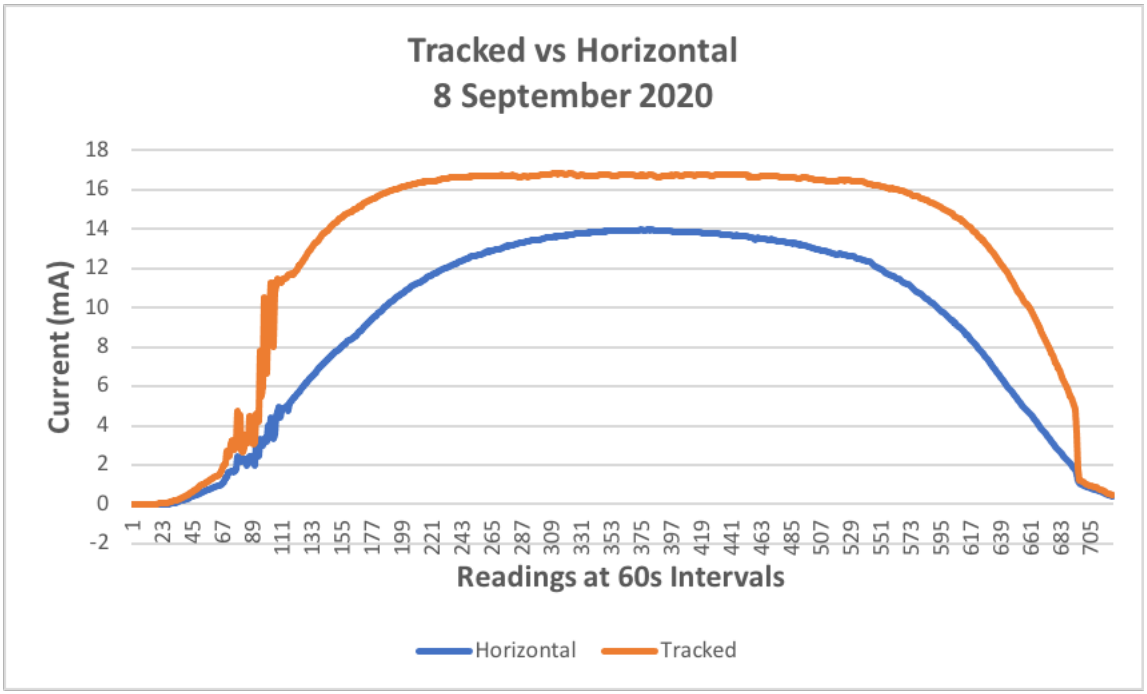

Figure 6.5 (b) shows the power output improvement when the panel was re-aligned to the Equinox setting. On a day of high cloud and relatively low radiation, the tracked panel increased overall output by 40% despite early morning shading issues from the adjacent buildings.

Figure 6.5 (c) and (d) illustrate the improvement at the Equinox setting with readings measured from 06h00 to 16h30. The energy absorbed by the tracked cell shows an increase over the horizontal cell of 57.5% and 58.8% on the respective days of 17 September and 30 September 2020, respectively.

Figure 6.5(e) illustrates a typical week of comparisons during the final week of September 2020. The horizontal panel consistently returned peaks around 11mA whereas the tracked cell consistently returned peaks of around 16mA. The flatter arc of the tracked cell power curve is evident when the chart is expanded, the earlier ramp-up to peak and the later ramp-down in the afternoons contribute greatly towards the 58% overall daily increase in output illustrated here.

Figure 6.5(c)

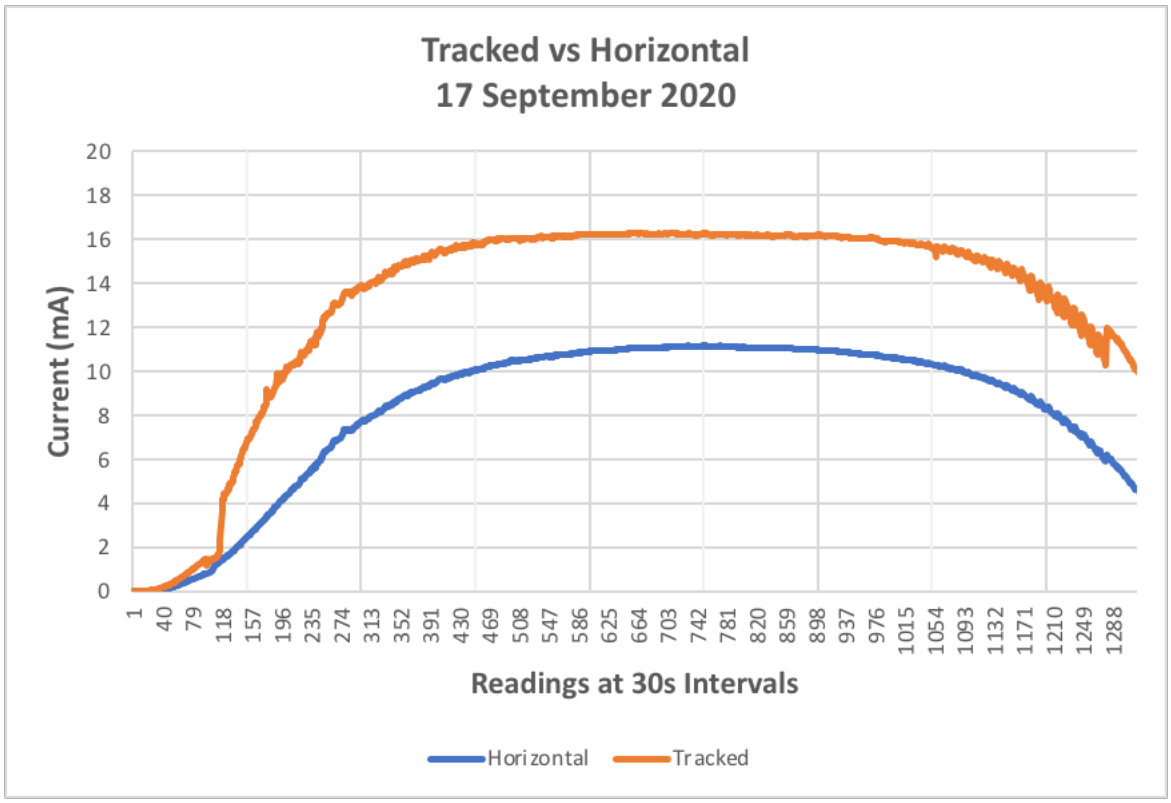

Figure 6.5 (d)

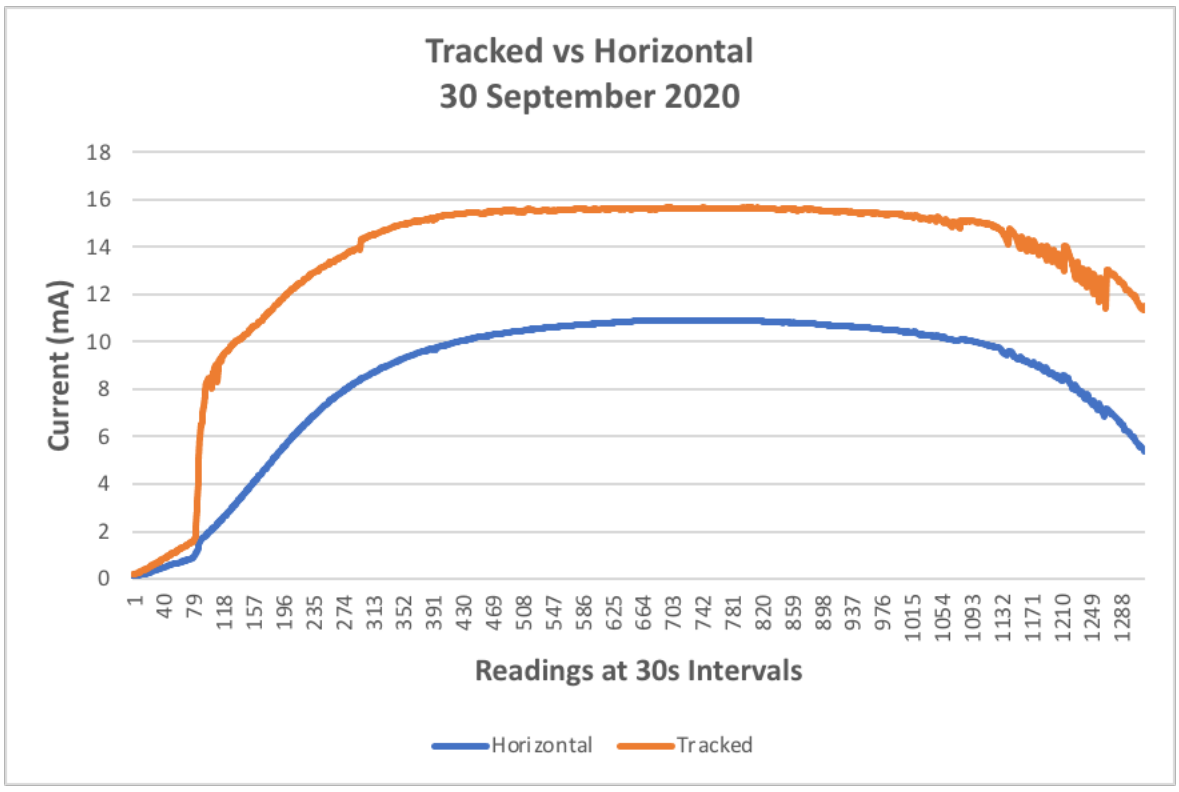

Figure 6.5(e)

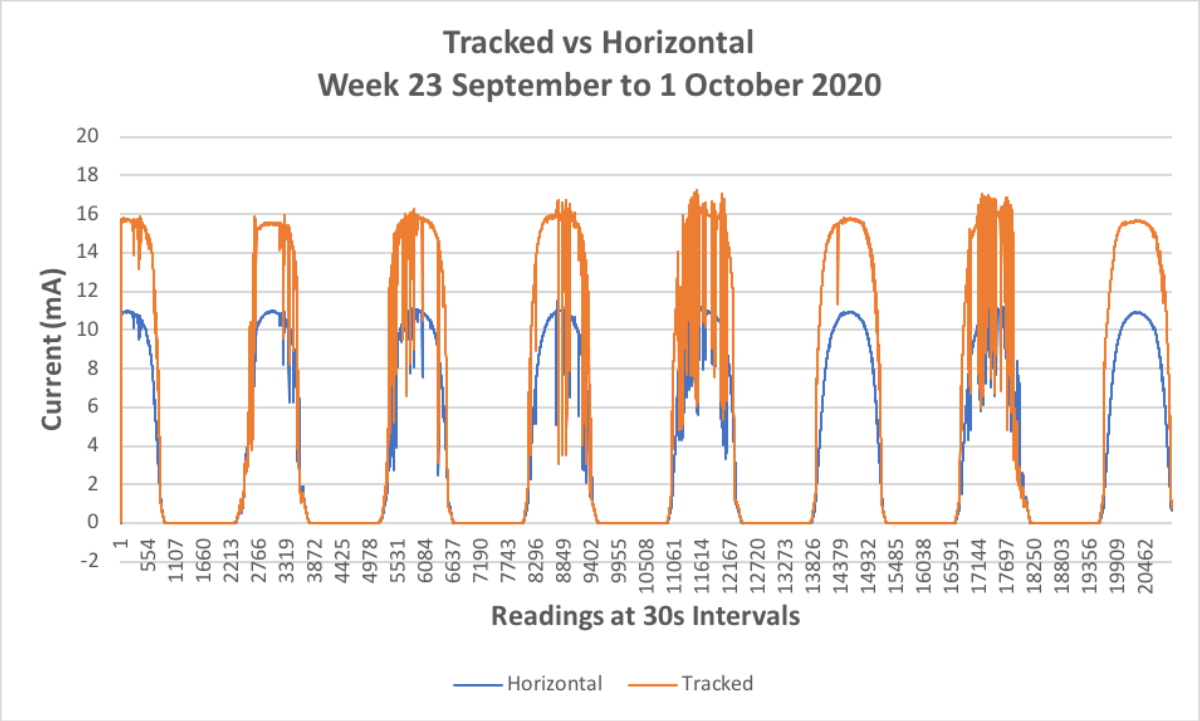

POSTSCRIPT

The system was fitted with 2 x 325W panels during late November 2020. The payload platform was re-balanced to accommodate the new centre of gravity and the bias weights adjusted.

The system continues to track as before but with greater fluctuations on windy days due to the reactive wind loads.

NELSON MANDELA UNIVERSITY

FACULTY OF ENGINEERING, THE BUILT ENVIRONMENT AND INFORMATION TECHNOLOGY

C - DETAILED DESIGN OF TEST RIG
APPENDIX TO THE RESEARCH THESIS -

'Enhancement of domestic solar photovoltaic unit productivity through the use of a cost effective tracking system '

John Henry Cawood
Student Number: 213282909

Final Design of Two Axis Actuated Photovoltaic Panel Structure for Tracked Photovoltaic Panels

(i) Background

An articulated framework is required to align a pair of solar panels with the sun. The system comprises two main components; a fixed base comprising a foot and centre column with fluid reservoir, and a PV panel support framework with integrated ballast tank. A universal joint joins these major components to complete the system.
This document contains the basic design which may be reproduced to duplicate the structure and its mechanisms. Detailed drawings of the structure and its components is to be found in **Appendix D**.

(ii) Symbols

Symbol	Quantity	Units
A	Area	m^2
B	Breadth of section	m
D	Depth of section	m
I	Second moment of area, stiffness	m^4
$I_{xx/yy}$	Second moment through plane XX or YY	m^4
L	Length	m
m	mass	kg
M	Bending moment	Nm
P	Pressure	Pa
P_b	Barometric pressure	Pa
P_v	Velocity pressure	Pa
ρ	Density	kg/m^3
σ	Stress	MPa
σ_t	Tensile stress	MPa
σ_p	Permissible stress	MPa
τ	Shear stress	MPa
V	Velocity	m/s
W	Point load	N

(iii) Abbreviations

CG	Centre of gravity
EW	East to West plane
NS	North to South plane
PV	Photovoltaic
ULA	Unequal leg angle section
TFC	Tapered Flange Channel section

CONTENT

1.0 Framework

1.1 Description

The PV panels are supported on an articulated frame. The chosen configuration is two 325W panels of 2m x 1m mounted on a framework of approximately 2m x 2.5m with the longer dimension along the EW plane and an open area between the panels to allow admit the auxiliary control PV panel and clearance for movement without interference with the centre support column. The outer members are inverted angle sections with the corners pinned and bolted by corner braces of the same section material. The frame is supported in the centre by two parallel channels, also held in place by the same corner cleats. The highest stressed portion of the frame is the centre parts of the angle section frame which is boxed at both ends for strength.
The selection of this configuration is enables very large angles of articulation up to 140° in both planes, however the end user may choose to operate on a range of their choice, dependent on their geographic location.

1.2 Loading

The loading capacity for this feature is taken from the PV panel typical specification and includes consideration for snow loading, despite the fact that the test site is not in a snowy location but has considerable wind loadings. A worst case scenario is considered whereby the Cd of the wind loading is taken as unity and the wind is considered at 160 km/h at 20°C and 1 Atmosphere barometric pressure.
Static loading is made from mass estimates of 130 kg (1275 N) for the suspended payload. Dynamic loading is estimated at the above conditions -

Wind Velocity	$v = 160/3.6 = 44.44$ m/s
Air Density	$\rho = PV/RT = 1.2$ kg/m^3
Baro Pressure	$P_b = 101.3$ kPa
Projected Area	$A = 4$ m^2
Velocity head	$h_v = v^2/2g = 100.66$ m
Velocity Pressure	$P_v = \rho g h_v = 1185$ Pa
Projected Force	$P_v \times A = 4740$ N

Total Force assuming all loads in one direction = 6015 N (say 6 kN).

Figure 1.2 - Wind Loading

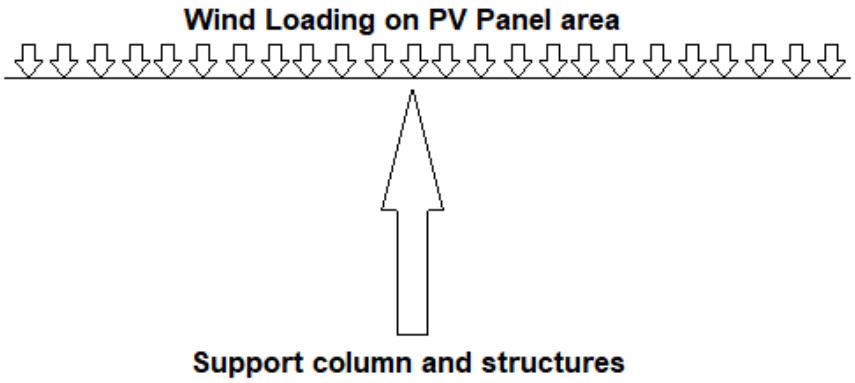

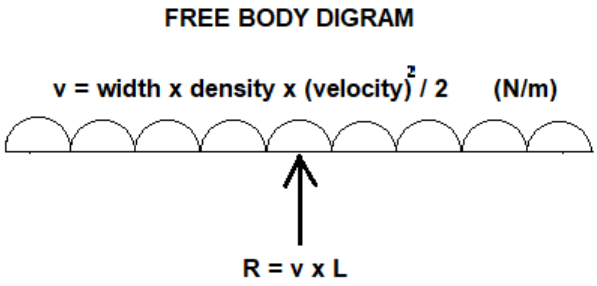

1.3 Loading about EW axis

The highest stress is experienced in the centre of the two longer frame members, all sections being identical and the wind loading UDL exerted across a longer length of platform.

Consider the loading as a cantilever system with a concentrated load of 3 kN at a radius of 0.625 m from the centreline, representing one half of the structure.

Figure 1.3 - Cantilever analogy for wind loaded frame

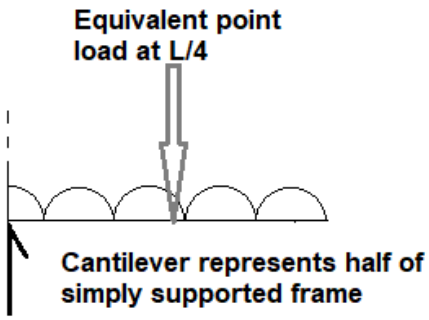

Assuming 75 x 50 x 6mm unequal leg angles material 350W structural steel, I = 0.405e-6 m^4 and y = 23.7mm -

Bending Moment M = WL = 3E3 x 0.625 = 1.875kNm

Area Moment I = 0.405E-6 m^4 from steel tables

From general beam equation -

σ_t = My/I = 1875 x 0.0237/0.405E-6

σ_t = 109.72 MPa

For fatigue strength, σ_t should not exceed 40% of Yield -

109.72/350 = 0.314 or 31.4%

[This stress is not excessive, the section requires no additional strengthening.]

1.4 Loading about the NS axis

The load is again considered to be a cantilever representing one half of the structure, acted on by a 3 kN point load at a radius of 0.5m. The load is resisted by a ULA 75 x 50 x 6mm section and a centre beam of TFC 76 x 38 profile.

M = 3000 x 0.5 = 1500 Nm

Stiffness of ULA sections = (2 x 0.405E-6) = 0.810E-6 m^4
Stiffness of TFC sections = (2 x 0.743E-6) = 1.486E-6 m^4
Total Stiffness = 2.296E-6m^4

Using average beam radius of 31 mm, median stress in system is -

σ = 1500 x .031 / 2.296E-6 = 20.25 MPa

As loading is proportional to stiffness -

- Portion of load carried by TFC = 1.486E-6 / 2.296E-6 = 64.7% or 1.94 kN

Stress in TFC = 1940 x 1 x 0.038 / (2 x 2 x 0.743E-6) = 24.8 MPa

- Portion of load carried by ULA = 1.06 kN

Stress in ULA = 1060 x 1 x .0237 / (2 x 2 x 0.405-6) = 15.5 MPa

[This plane strength is adequate.]

2.0 Hookes Joint

2.1 Description

Actuation in two planes requires that the centre pivotal device is rotationally stable, i.e. that actuator movement is dedicated to its own plane and cannot influence the other plane. For this reason the pivot must take the shape of a Hookes Joint with sufficient angular clearance to allow large movements.
To achieve minimum work to actuate the system, the payload must be balanced about the centreline of the centre pivot. The CG of a complex frame is difficult to predict accurately so that the height of the payload must be adjustable above the centre pivot i.e. where the pivot meets the frame.

2.2 Angular Requirement

The pivot is considered in the two planes EW and NS, in a direction normal to the payload. For the test site, the range for the EW plane is 140° or 20° above the horizon in both directions and that of the NS plane is 70° in the northerly direction or 20° above the north horizon.
For simplicity and universal utility, the NS plane requirement is set at 20° above the horizon in both north and south directions.
To facilitate the movements, the Hookes joint will comprise a relatively long central beam placed in direction EW as part of the UJ cross, housing a short central intersecting pin in the beam centre in the NS direction and which comprises the second axis of the UJ.

2.3 Loading and centre pin stress

The loading as determined in Paragraph 1 above is used for the pivot design. The EW beam section will be analysed as a simply supported beam with a centre loading without assistance from the NS pin, and vice versa.

The load is transmitted from frame to UJ via the centre cross pins. The shorter pin is evaluated for shear and bending stress, assuming a diameter of 25mm and using 800MPa Grade 8.8 bolting steel -

Permissible shear $\sigma_p = 0.56 \times 0.4 \times 800$

$\sigma_p = 179.2$ MPa

In double shear only -

$\sigma_s = W/A$

$\sigma_s = 6000 / (2 \times \pi \times 0.025^2 / 4)$

$\sigma_s = 6.11$ MPa

Permissible tension - $\sigma_p = \sigma_u \times 0.4$

$\sigma_p = 320$ MPa

Assumption - length of pin L = 150 mm and diameter of pin 25 mm, loading as 6kN at unsupported centre, in bending only -

$\sigma_t = My/I$

$\sigma_t = (WL/2)y/I$

$\sigma_t = 293.35$ MPa

Compounded stress = $[(3x(6.112)^2 + (293.352)^2)]^{0.5} = 293.5$ MPa

[The pin is adequately sized at 25mm and material 8.8 Grade with σ_u 800 MPa]

2.4 Strength of centre beam

Assumption - spacing of centre beams L = 500 mm.

Point load W = 6 kN

Moment M = WL/2 = 6E3 x 0.5/2 = 1500 Nm

Ultimate stress σ = 455 MPa (350W, minimum)

Permissible stress $\sigma_p = 0.4\ \sigma$ = 182 MPa

From general beam formula -

σ_p = My/I

Required Stiffness **$I_{xx} = My/\sigma_p = 0.247E\text{-}6\ m^4$**

A rectangular hollow section 60 x 40 x 3mm is selected from tables with stiffness 0.254E-6 m^4.

Maximum stress is σ = 177.2 MPa < σ_p

[Section RHS 60 X 40 X 3mm is suitable]

2.5 Strength of pin mountings

Consider highest stress loading at junction of pin and beam -

Applied Load W = 6 kN

Diameter of pins d = 25 mm

Applied shear stress τ = (6E3 / (π/4) x.025^2)2 for double shear

τ = 6.1 MPa

Applied bending σ = My/I = (3E3 x .05) x 0.0125 / ($\pi/64$) x 0.025^4

σ = 97.8 MPa

Combined stress $\sigma = (3(6.1^2) + 97.8^2)^{0.5}$ using Von Mises

σ = 98.4 MPa

For a safety factor > 5 :: 1, use 8.8 Grade carbon steel with yield stress 64 MPa.

2.6 Bearing Selection

Spherically mounted 2-hole Y bearings, shaft diameter 25mm

Static load ratings 6.55 kN each

Dynamic load ratings > 12 kN each

Resistance 30 Nmm, total resistance 60E-3 Nm per plane.
Rotational velocity is negligible - use static load ratings.
[Bearing safety factor = 2]

3.0 Centre Support Column

3.1 Description

The payload and associated loading is supported by a single central column. The column loading is considered as vertical cantilever bending only as a result of horizontal wind load.

3.2 Basic Geometry and Height

The height of column must not allow interference between frame and ground level.
The longest dimension of the frame from the centre pivot is half the diagonal of the frame between corners. Due to the as yet unknown total outside dimension and the high articulation, this diagonal is taken as the minimum height of column to centre pivot, plus a small safety factor.
The diagonal dimension is $(L^2 + H^2)^{0.5}$; using basic frame dimensions of 2.0 m x 2.5 m, the half of the diagonal is 1.6 m. A safety factor of 100mm is added to round this dimension to **1.7m.**

3.3 Strength at Base of Column

Previously determined worst case loading in the horizontal direction was stated at 6 kN. The moment about the base -

$$M = WL \text{ for cantilever,}$$

$$\underline{\mathbf{M = 6000 \times 1.7 = 10\ 200\ Nm}}$$

Required stiffness at the base, using limiting stress at 140 MPa for steel 350W and a dimension of 120mm

$$\underline{\mathbf{I_{xx} = My/\sigma_p = 10\ 200 \times 0.06 / 140E6 = 4.37E\text{-}6m^4}}$$

This is a large loading for a single section, however it is planned to support the centre column with knee braces to a height of 0.5m, reducing the bending moment to -

$$\underline{\mathbf{M = 6000 \times 1.2 = 7\ 200\ Nm}}$$

The new stiffness requirement for the reduced moment will be -

$$\underline{\mathbf{I_{xx} = 7\ 200 \times 0.06 / 140E6 = 3.09E\text{-}6m^4}}$$

A suitable section shape for the purpose is a square section which accommodates the mountings coincident to the compass points.
The section 100 x 100 x 6mm has a similar stiffness but has some 7kg more mass per metre.
[A suitable stiffness section is a SHS 120 x 120 x 3mm at stiffness of $3.123E\text{-}6m^4$.]

3.4 Centre column bracing

The dimension of the knee braces can be determined from the permissible strength of the economical steel S 235 JR with permissible stress of 160 MPa. Assuming a 45 degree brace angle to limit the footprint to one square metre and the brace is in tension only i.e. a tie, then the tensile force in the brace will be -

$$\mathbf{F = (M / r \cos 45)}$$
$$\mathbf{F = 10\ 200/(0.5 \cos 45) = 28.9\ kN}$$

A suitable brace section area -

$$\mathbf{A = F / \sigma_p = 1.8E\text{-}4\ m^2}$$

[This dimension equates to a standard tie rod of 16mm diameter.]

NOTE - It is sensible to attach the ties to the centre of the flats of the column in the weakest plane I_{xx} and I_{yy}.

The attachment must necessarily be by means of a bolted yoke around the column.

3.5 Footing shape and strength

The imposed horizontal load of 6kN translates into a base moment of 10.2kNm (M) when the load applied at the UJ cross which is 1.7m above base level.

It is desired to construct the foot structures from RC, pre-cast in 32 MPa concrete with reinforcing and foundation fixings guaranteed by the manufacturer.

An estimate of the base mass is 600kg. This mass is made up of two sleeper sections of identical shape which interlock to form the foundation cross.
A four bolt centre hole pattern coincides with both parts allowing the centre joint to be firmly bolted in compression. Similarly, holes at the extremities allow bracing anchors to be hand fitted prior to placement. All holes are located with 20mm PVC tubing cast in and located with the necessary precision by the factory mould shape.

The members may also be cast in situ using a constructed wooden former to plan, in which case the centre joint is redundant and the four hole pattern is cast in with foundation bolts and a baseplate.

It is also suggested to drape the finished and as yet uncovered frame with a stainless or galvanised steel mesh prior to backfill to form an earth anchor. The compacted backfill adds a huge inertial mass to the frame when the compacted soil volume is added to the inertial surcharge.

Foundation bolt dimension is estimated at 16mm diameter which implies a bolt stress of 80 MPa for a minimum yield of 200MPa for galvanised bolts Grade 4.2.

Where the base is to be chemically anchored in a concrete slab, the recommended slab thickness is 100mm with welded wire mesh (5mm wire x 150 aperture) placed 40mm above the screed.

The chemical anchors rely on the permissible shear of the bond for strength, specified by Hilti® as 3.5 MPa in shear. The minimum depth of the bolt holes, assuming worst case wind gust at right angles to the column -

Tension on each bolt = 6E3 x 1.7 / 0.2 = 51 kN or 17 kN per bolt

Bond in shear is 17 000 / 3.5E6 = 0.0048 m^2 per bolt

[Bolt depth = 0.0048 / (π x0.016) = 0.095 m say 100 mm depth.]

3.6 North - South Actuator Tie Bar

Using the worst case wind loading as 6kN for the whole payload area and assuming no balanced loading from one half of the panel -

Load on half payload area = 3kN
Radius of exerted loading = 2.5/2 = 1.25m
Moment on payload structure = 3.75 kNm

Estimated radial location of the tie bar = 180mm from the fulcrum (to allow maximum articulation from 200mm cylinder stroke)
Force on tie bar W = 3.75E3 / 0.18 = 20.8 kN

Length of tie bar = 0.5m (from payload platform drawing)
Bending moment assuming fixed ends, M = WL/4

M = 20.8E3*.5/4

M = 2.6 kNm

For permissible stress of 350WA steel at 140 MPa

$I / y = M / \sigma = Zx$

$Zx = 2.6E3 / 140E6$

$\underline{Zx = 18.6E\text{-}6\ m^3}$

[Suitable Angle section is 70 x 70 x 6mm, Zx = 17.32E-6 m3]

$\sigma = My / I = 150.12$ MPa, SF = 2.3 to Yield

NELSON MANDELA UNIVERSITY

FACULTY OF ENGINEERING, THE BUILT ENVIRONMENT AND INFORMATION TECHNOLOGY

D - DRAWINGS

APPENDIX TO THE RESEARCH THESIS -

'Enhancement of domestic solar photovoltaic unit productivity through the use of a cost effective tracking system '

John Henry Cawood

Student Number: 213282909

1.0 Drawing List

Drawings fall under the headings relevant to the component where they are located on the structure. The list of drawings is provided below and the drawings are reproduced on successive pages.

A - Attachments

A0010	Cylinder mounting clamp
A0011	Cylinder mount
A0012	Cylinder mount spacer
A0013	Bell crank
A0014	Bell crank cover
A0015	Cylinder rod clevis
A0016	Cylinder rod clevis base
A0017	Cylinder rod clevis leg

C - Centre column

C0010	Centre Column GA
C0011	Column detail
C0012	Stiffener
C0013	Base Plate
C0014	Foot brace
C0015	Foot brace part 1
C0016	Foot brace part 2
C0017	Foot brace part 3

E - Electrical and Instrumentation

E0010	Roller switch
E0011	Roller switch holder
E0012	Roller switch bracket
E0013	Roller
E0014	Sensor plate
E0015	Sensor plate profile
E0016	Sensor plate mounting bar
E0017	Sensor plate bracket

F - Foundation pre-cast members

F0010 GA Foundation beam

F0013 Rebar Assembly and profiles

G - General views

G0002 - Piping diagram

G0003 - Electrical Circuit diagram

J - Hookes joint

J0010 GA Hookes joint

J0011 Beam

J0012 End pin assembly

J0013 Centre stiffener

J0014 Cross pin

P - Panel main frame

P0000 GA Test Rig

P0010 GA Main frame

P0011 North members

P0012 East members

P0013 Centre beam

P0014 Corner cleats

P0015 Height adjuster plate

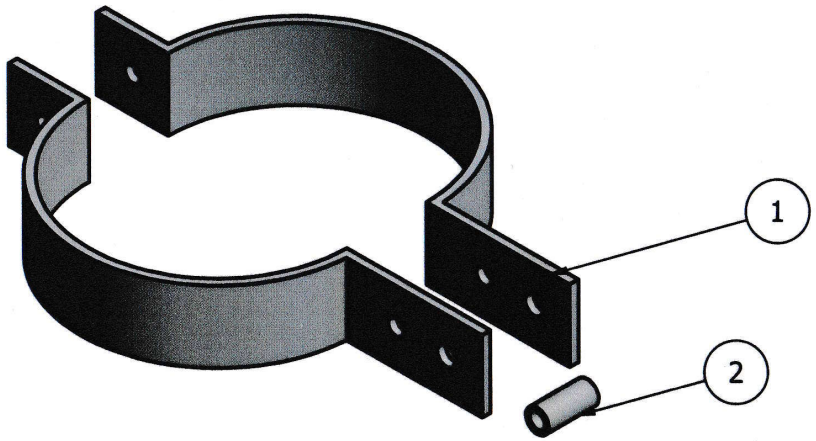

PARTS LIST				
ITEM	QTY	STOCK NUMBER	PART NUMBER	DESCRIPTION
1	2	Cylinder mount	A0011	MS Flat bar
2	1	Cylinder mount spacer	A0012	MS

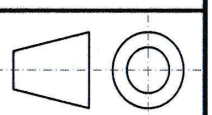

LIN TOL. (mm):
(0-250) ± 0.1
(250-500) ± 0.25
(500-1000) ±0.5

ANGULAR TOL.:
±0.25°

BREAK SHARP EDGES
ALL DIMENSIONS IN MM

Drawn by:	Checked by	Approved by	Project:
K Mpurwana	J Cawood	J Cawood	Solar Tracking System

NELSON MANDELA UNIVERSITY

Title:		Material:	--
Cylinder mount		Scale:	1 : 3
Part Number: A0010	Rev 00	Sheet size A4	Sheet 1

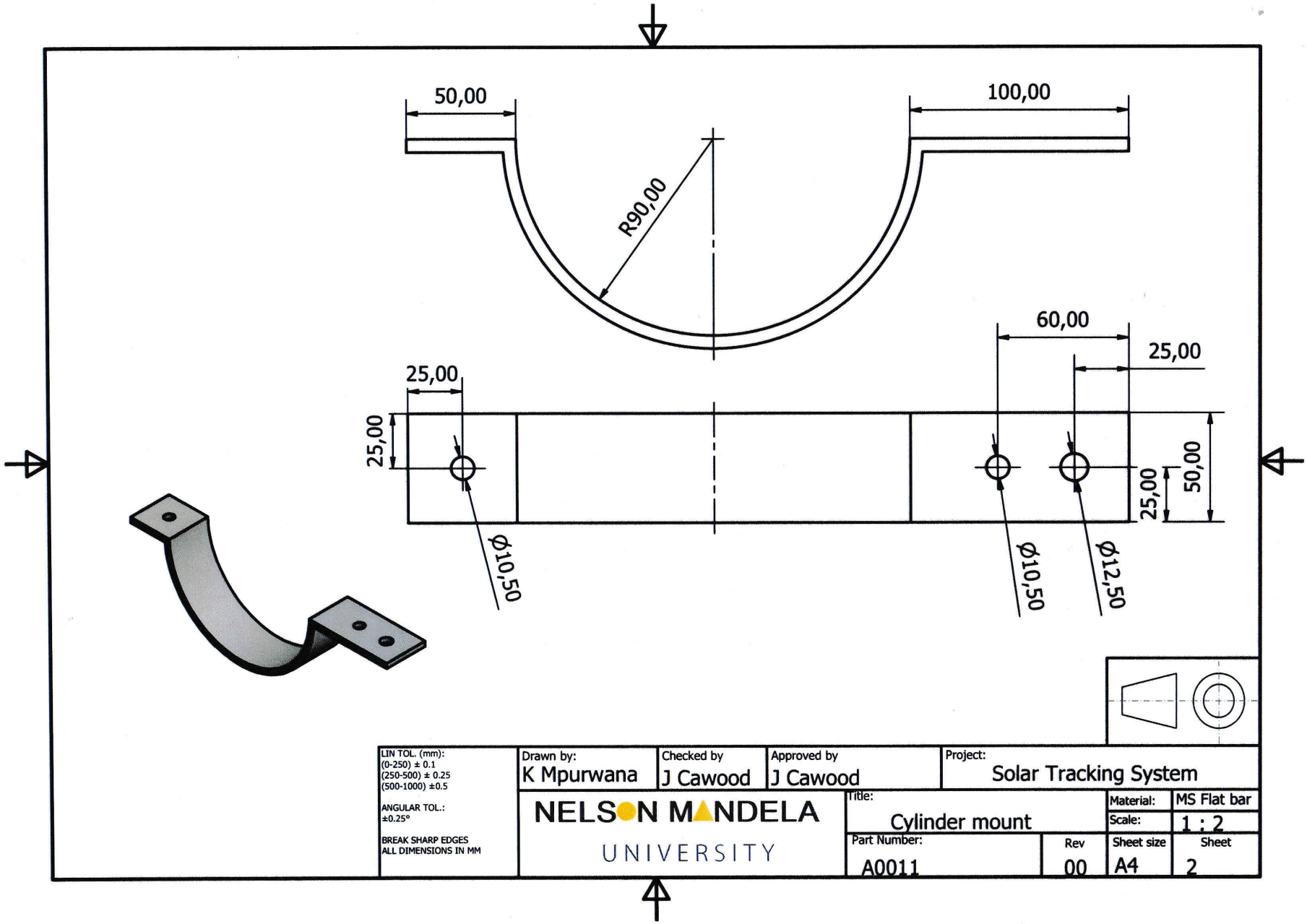

LIN TOL. (mm): (0-250) ± 0.1 (250-500) ± 0.25 (500-1000) ±0.5 ANGULAR TOL.: ±0.25° BREAK SHARP EDGES ALL DIMENSIONS IN MM	Drawn by: K Mpurwana	Checked by J Cawood	Approved by J Cawood	Project: Solar Tracking System	
NELSON MANDELA UNIVERSITY	Title: Cylinder mount			Material:	MS Flat bar
				Scale:	1 : 2
	Part Number: A0011	Rev 00	Sheet size A4	Sheet 2	

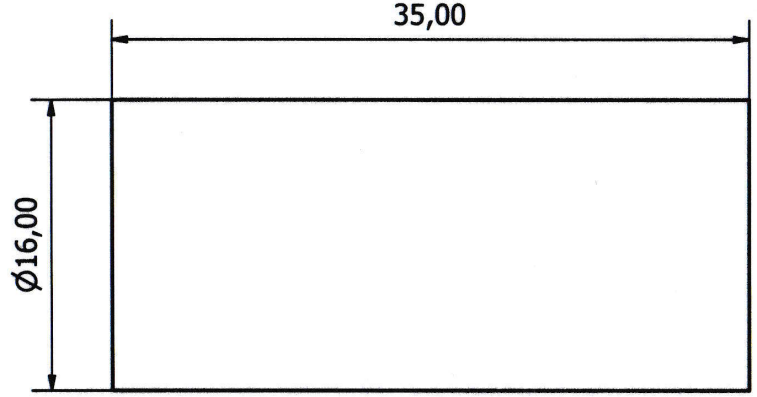

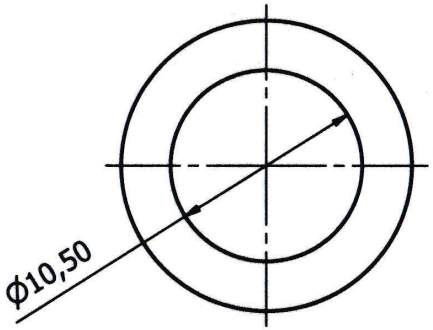

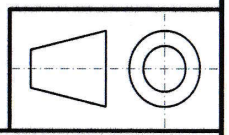

LIN TOL. (mm): (0-250) ± 0.1 (250-500) ± 0.25 (500-1000) ±0.5 ANGULAR TOL.: ±0.25° BREAK SHARP EDGES ALL DIMENSIONS IN MM	Drawn by: K Mpurwana	Checked by J Cawood	Approved by J Cawood	Project: Solar Tracking System
NELSON MANDELA UNIVERSITY	Title: Cylinder mount spacer		Material: MS	Scale: 3 : 1
	Part Number: A0012	Rev 00	Sheet size A4	Sheet 3

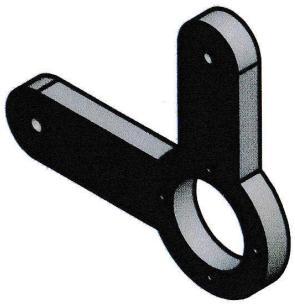

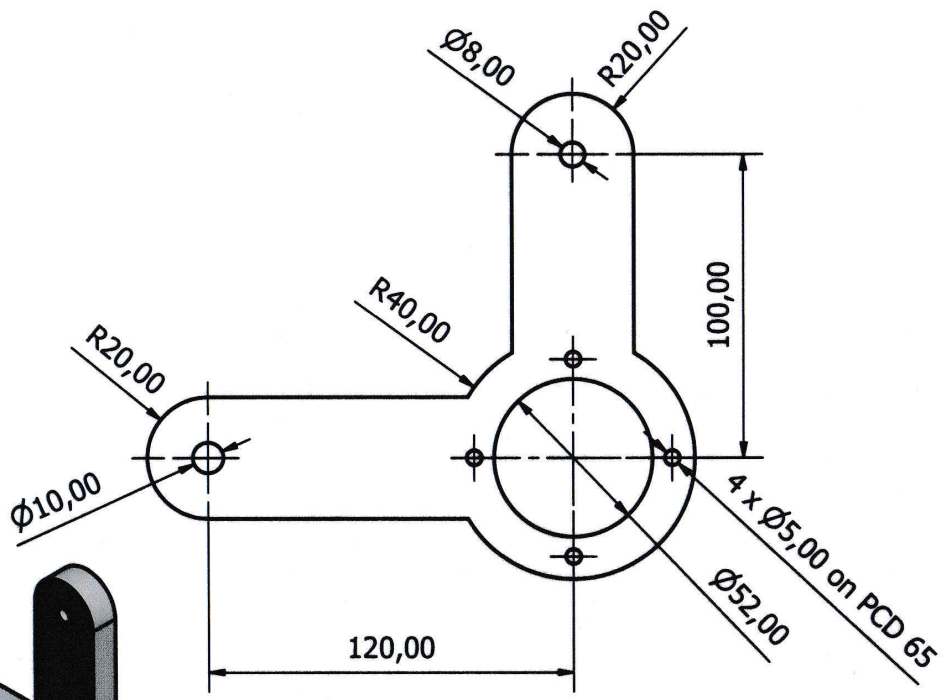

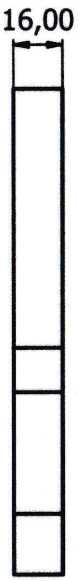

Note: NB
Mark small holes for
drilling by others

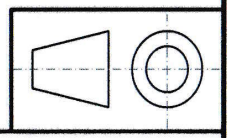

LIN TOL. (mm): (0-250) ± 0.1 (250-500) ± 0.25 (500-1000) ±0.5 ANGULAR TOL.: ±0.25° BREAK SHARP EDGES ALL DIMENSIONS IN MM	Drawn by: K Mpurwana	Checked by J Cawood	Approved by J Cawood	Project: Solar Tracking System		
NELSON MANDELA UNIVERSITY	Title: Bell crank R3			Material: MS	Scale: 1 : 2	
	Part Number: A0013	Rev 00		Sheet size A4	Sheet 4	

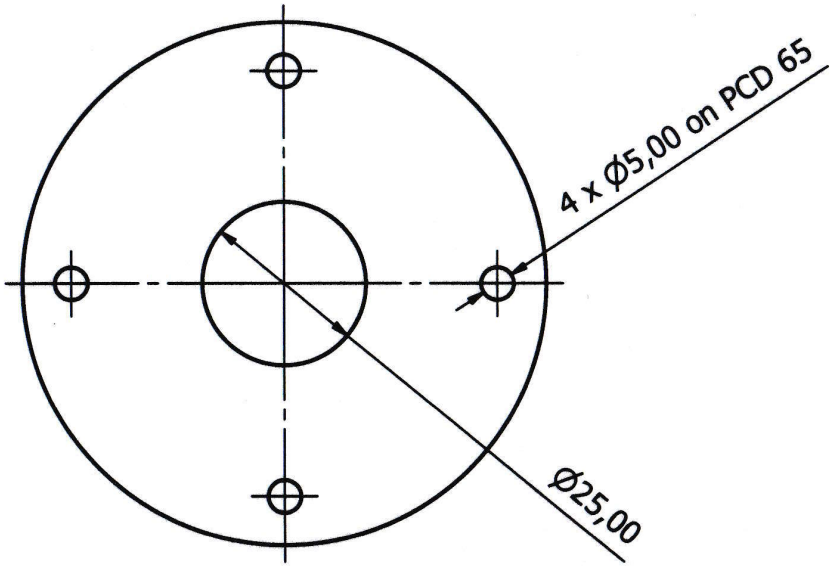

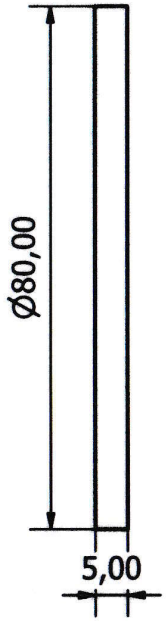

Note:
2-off

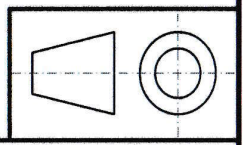

LIN TOL. (mm): (0-250) ± 0.1 (250-500) ± 0.25 (500-1000) ±0.5 ANGULAR TOL.: ±0.25° BREAK SHARP EDGES ALL DIMENSIONS IN MM	Drawn by: K Mpurwana	Checked by J Cawood	Approved by J Cawood	Project: Solar Tracking System	
NELSON MANDELA UNIVERSITY				Title: Bell crank cover	Material: MS Scale: 1 : 1
				Part Number: A0014	Rev 00 / Sheet size A4 / Sheet 5

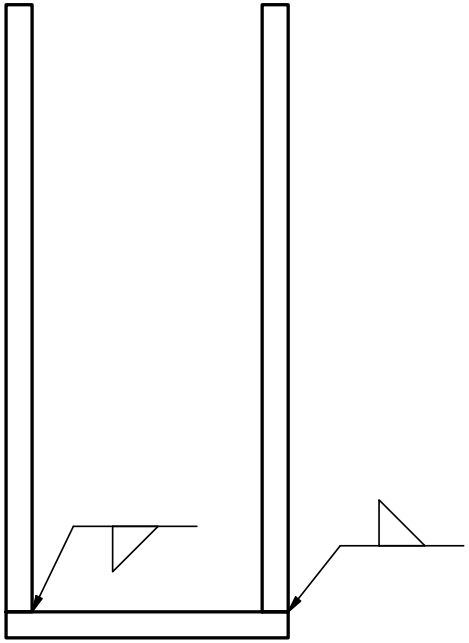

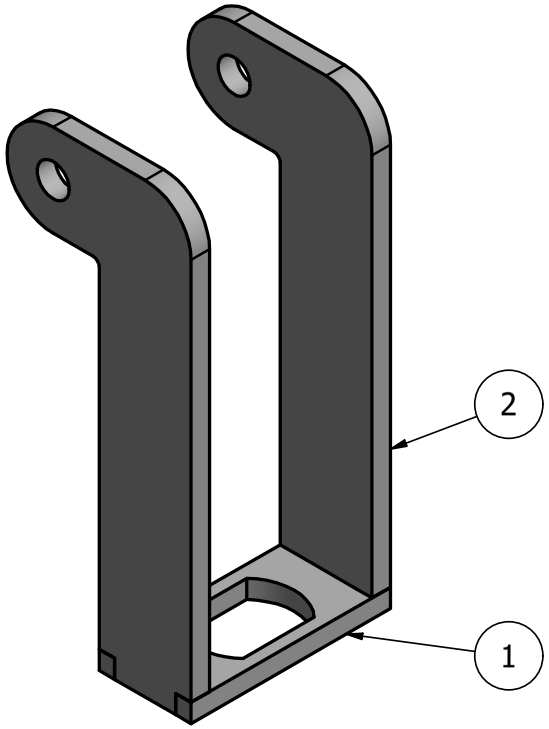

PARTS LIST				
ITEM	QTY	STOCK NUMBER	PART NUMBER	DESCRIPTION
1	1	Cylinder rod clevis base	A0016	MS Plate
2	2	Cylinder rod clevis leg	A0017	MS plate

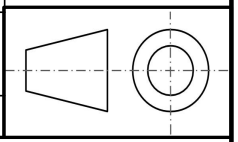

LIN TOL. (mm):
(0-250) ± 0.1
(250-500) ± 0.25
(500-1000) ±0.5

ANGULAR TOL.:
±0.25°

BREAK SHARP EDGES
ALL DIMENSIONS IN MM

Drawn by:	Checked by	Approved by	Project:
K Mpurwana	J Cawood	J Cawood	Solar Tracking System

NELSON MANDELA UNIVERSITY

Title:		Material:	MS Plate
Cylinder rod clevis		Scale:	1 : 1.5
Part Number:	Rev	Sheet size	Sheet
A0015	00	A4	1

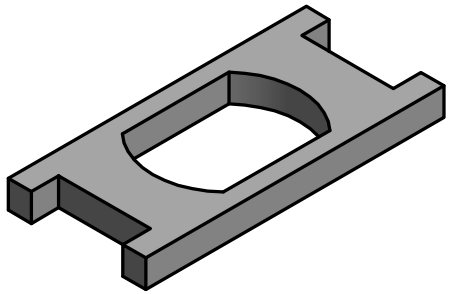

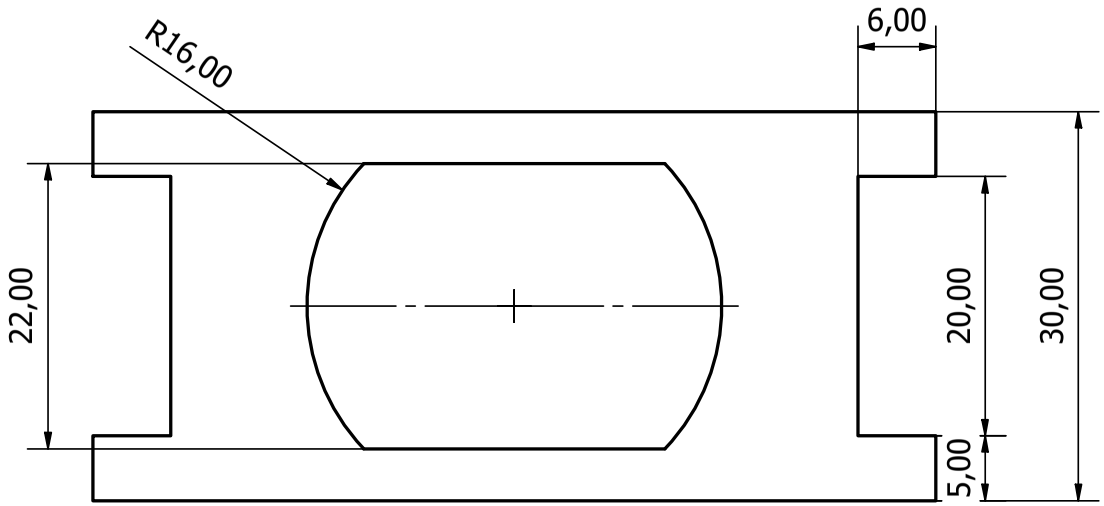

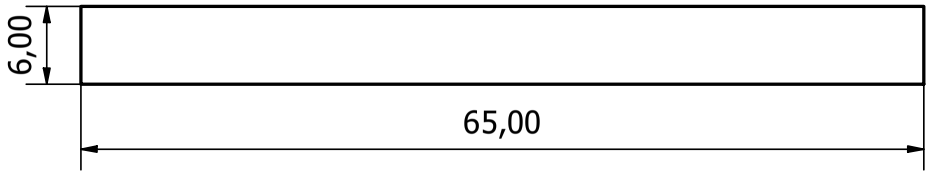

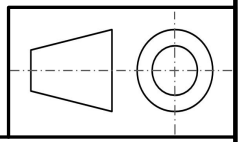

LIN TOL. (mm): (0-250) ± 0.1 (250-500) ± 0.25 (500-1000) ±0.5 ANGULAR TOL.: ±0.25° BREAK SHARP EDGES ALL DIMENSIONS IN MM	Drawn by: K Mpurwana	Checked by J Cawood	Approved by J Cawood	Project: Solar Tracking System		
NELSON MANDELA UNIVERSITY	Title: Cylinder rod clevis base			Material:	MS Plate	
				Scale:	2 : 1	
	Part Number: A0016	Rev 00		Sheet size A4	Sheet 3	

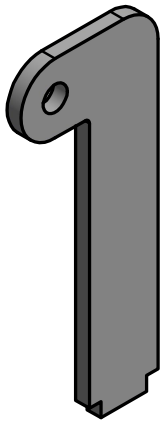

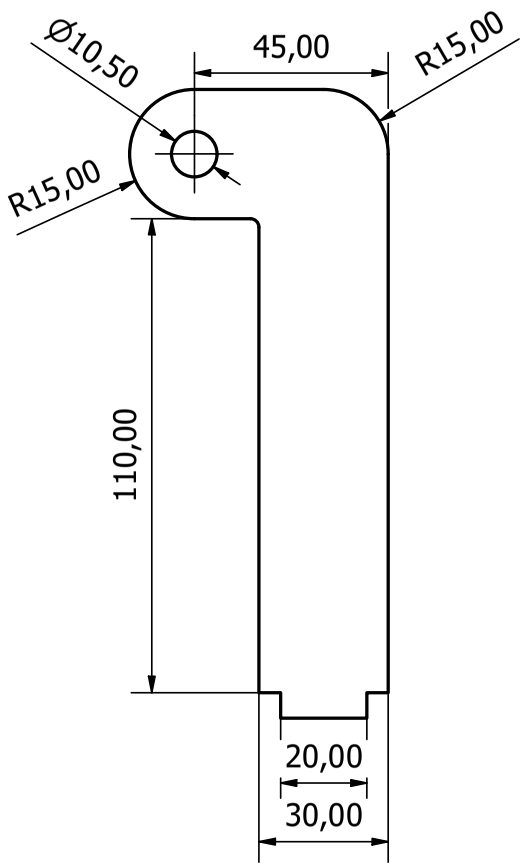

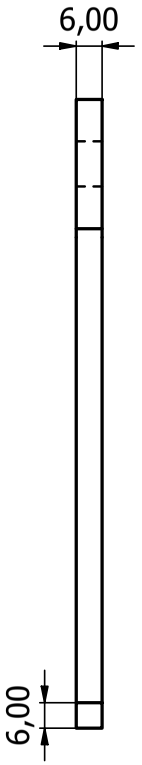

Note:
2-off

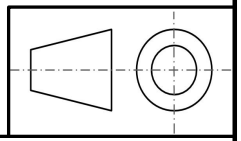

LIN TOL. (mm): (0-250) ± 0.1 (250-500) ± 0.25 (500-1000) ±0.5 ANGULAR TOL.: ±0.25° BREAK SHARP EDGES ALL DIMENSIONS IN MM	Drawn by: K Mpurwana	Checked by J Cawood	Approved by J Cawood	Project: Solar Tracking System	
NELSON MANDELA UNIVERSITY	Title: Cylinder rod clevis leg			Material: MS plate	
				Scale: 1 : 1.5	
	Part Number: A0017	Rev 00	Sheet size A4	Sheet 2	

11

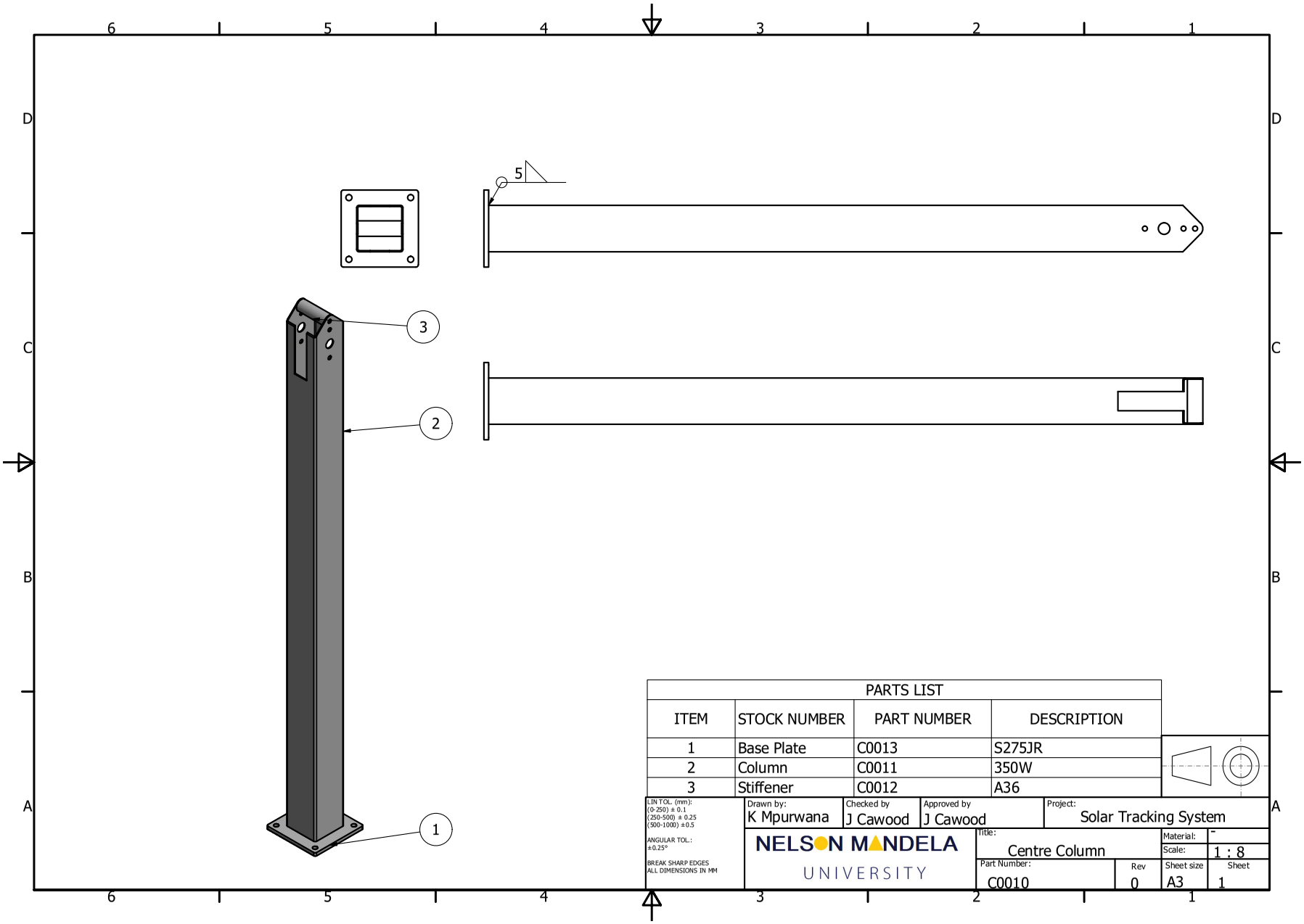

PARTS LIST			
ITEM	STOCK NUMBER	PART NUMBER	DESCRIPTION
1	Base Plate	C0013	S275JR
2	Column	C0011	350W
3	Stiffener	C0012	A36

LIN TOL. (mm):
(0-250) ± 0.1
(250-500) ± 0.25
(500-1000) ±0.5

ANGULAR TOL.:
±0.25°

BREAK SHARP EDGES
ALL DIMENSIONS IN MM

Drawn by: K Mpurwana	Checked by J Cawood	Approved by J Cawood	Project: Solar Tracking System

NELSON MANDELA UNIVERSITY

Title: Centre Column		Material:	-
		Scale:	1 : 8
Part Number: C0010	Rev 0	Sheet size A3	Sheet 1

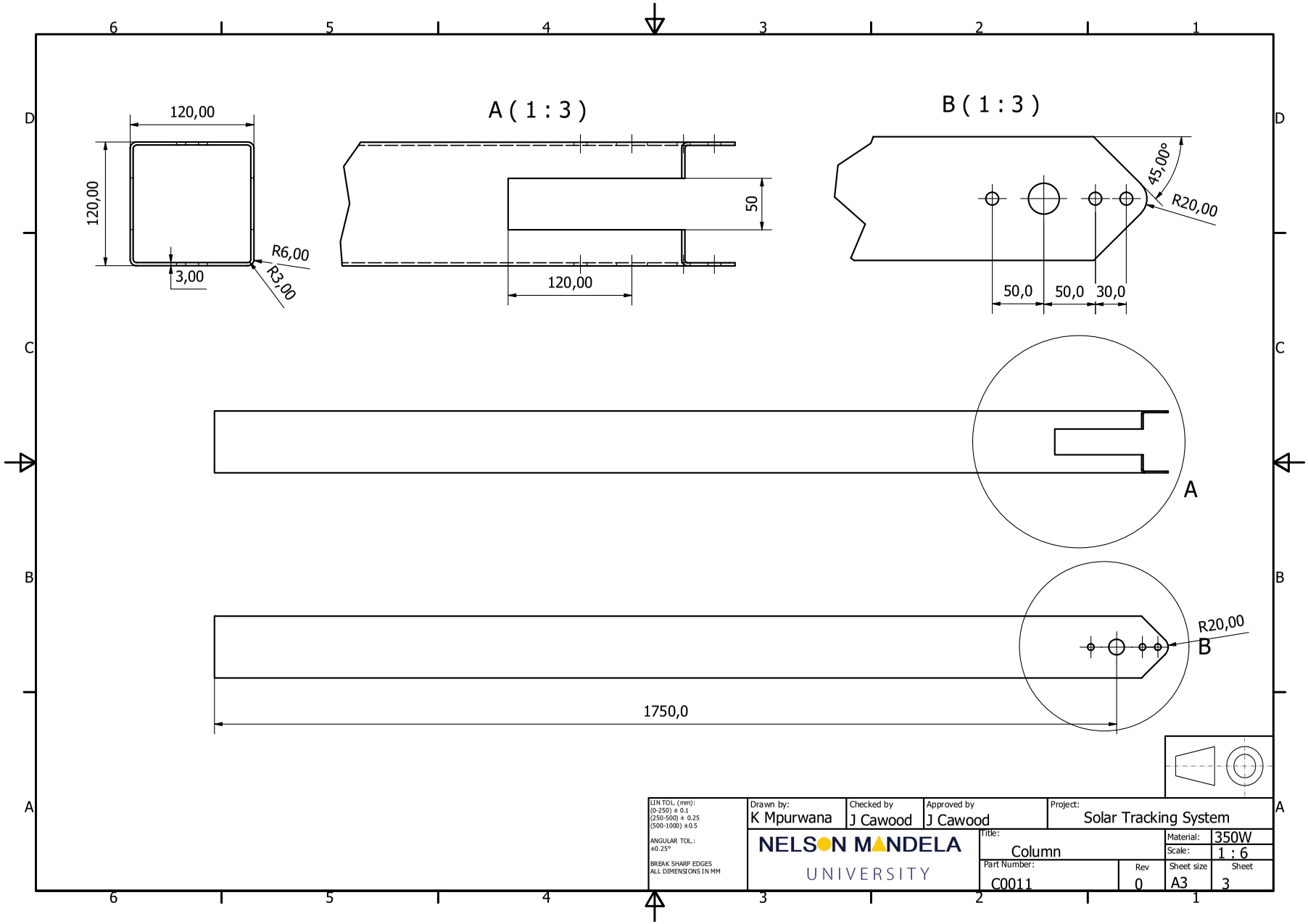
120,00
120,00
3,00
R6,00
R3,00
A (1 : 3)
50
120,00
B (1 : 3)
45,00°
R20,00
50,0
50,0
30,0
A
R20,00
B
1750,0
LIN TOL. (mm):
(0-250) ± 0.1
(250-500) ± 0.25
(500-1000) ± 0.5
ANGULAR TOL.:
±0.25°
BREAK SHARP EDGES
ALL DIMENSIONS IN MM
Drawn by:
K Mpurwana
Checked by
J Cawood
Approved by
J Cawood
Project:
Solar Tracking System
NELSON MANDELA
UNIVERSITY
Title:
Column
Material:
350W
Scale:
1 : 6
Part Number:
C0011
Rev
0
Sheet size
A3
Sheet
3

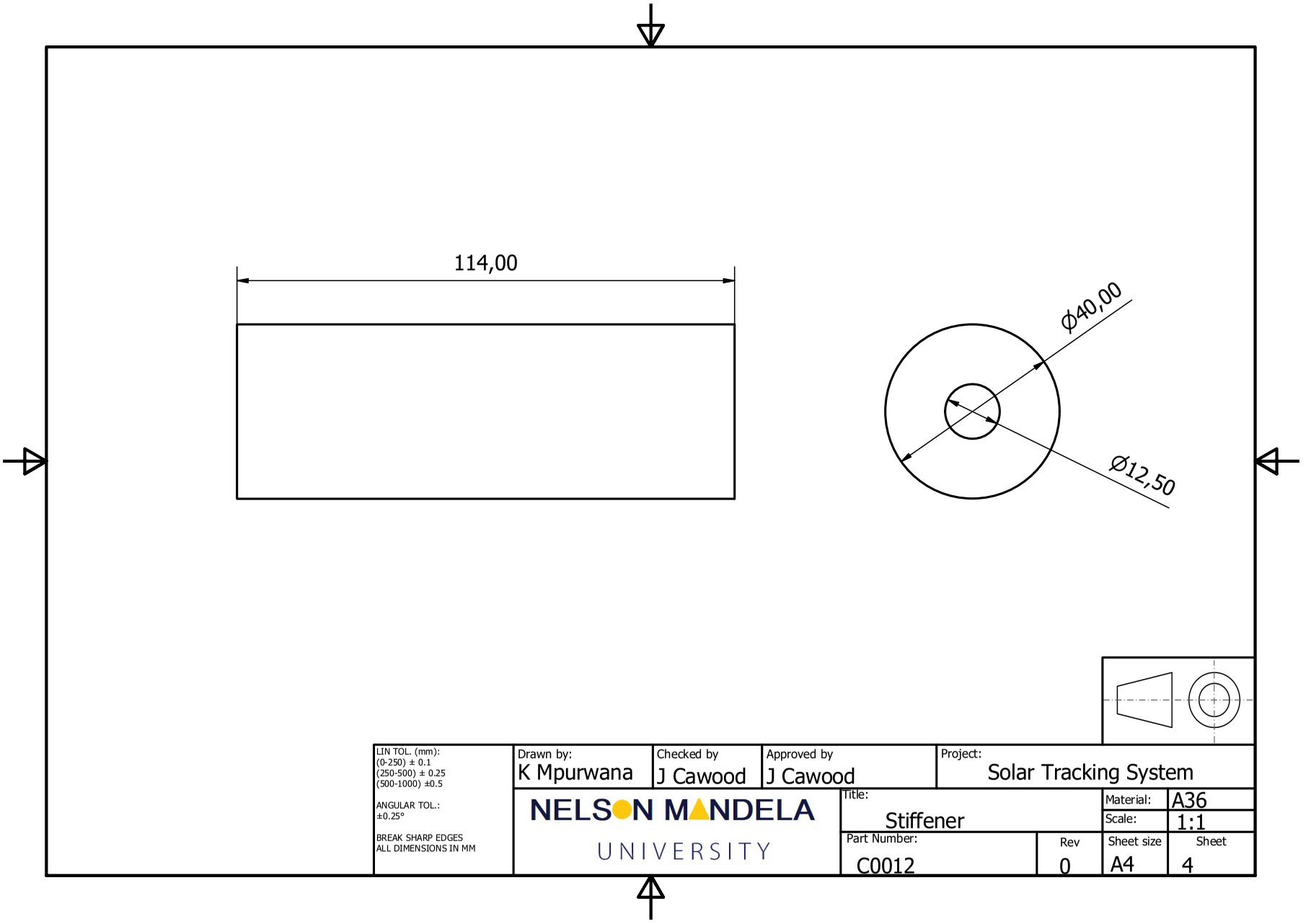

LIN TOL. (mm): (0-250) ± 0.1 (250-500) ± 0.25 (500-1000) ±0.5 ANGULAR TOL.: ±0.25° BREAK SHARP EDGES ALL DIMENSIONS IN MM	Drawn by: K Mpurwana	Checked by J Cawood	Approved by J Cawood	Project: Solar Tracking System		
NELSON MANDELA UNIVERSITY	Title: Stiffener			Material: A36		
				Scale: 1:1		
	Part Number: C0012	Rev 0		Sheet size A4	Sheet 4	

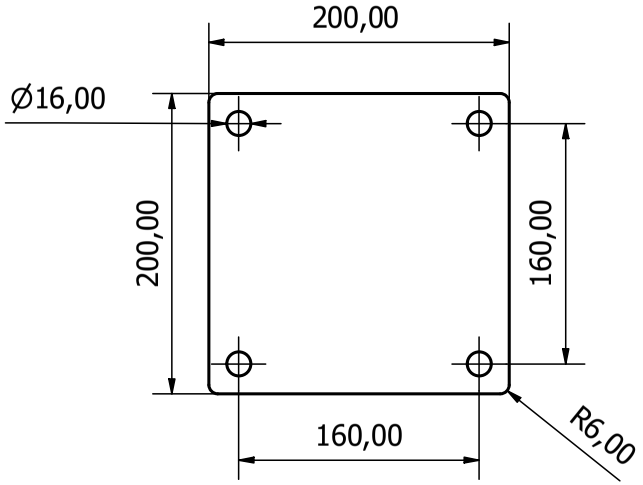

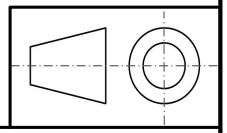

LIN TOL. (mm): (0-250) ± 0.1 (250-500) ± 0.25 (500-1000) ±0.5 ANGULAR TOL.: ±0.25° BREAK SHARP EDGES ALL DIMENSIONS IN MM	Drawn by: K Mpurwana	Checked by J Cawood	Approved by J Cawood	Project: Solar Tracking System	
NELSON MANDELA UNIVERSITY			Title: Base Plate	Material: S275JR	
				Scale: 1 : 4	
			Part Number: C0013	Rev 0	Sheet size A4 / Sheet 2

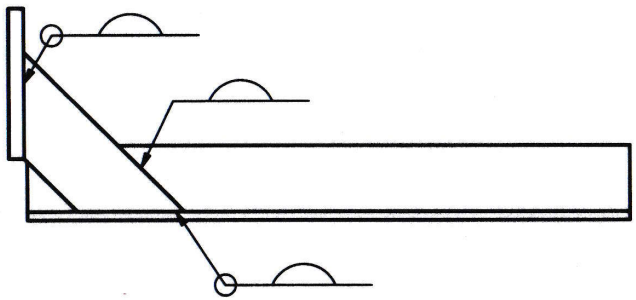

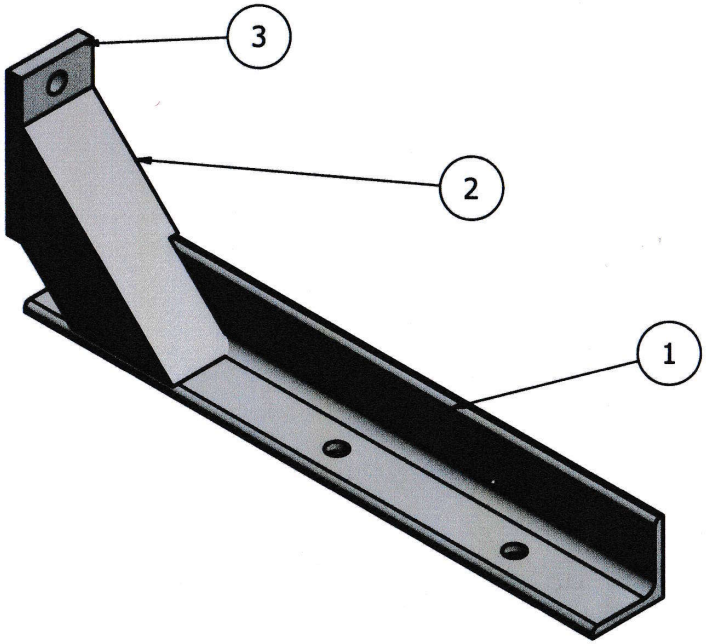

PARTS LIST				
ITEM	QTY	STOCK NUMBER	PART NUMBER	DESCRIPTION
1	1	Foot brace 1	C0015	MS
2	1	Foot brace 2	C0016	MS
3	1	Foot brace 3	C0017	MS

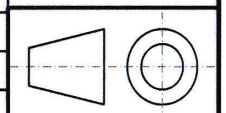

LIN TOL. (mm):
(0-250) ± 0.1
(250-500) ± 0.25
(500-1000) ±0.5

ANGULAR TOL.:
±0.25°

BREAK SHARP EDGES
ALL DIMENSIONS IN MM

Drawn by:	Checked by	Approved by	Project:
K Mpurwana	J Cawood	J Cawood	Solar Tracking System

NELSON MANDELA UNIVERSITY

Title:		Material:	--
Foot brace		Scale:	1 : 3
Part Number: C0014	Rev 00	Sheet size A4	Sheet 1

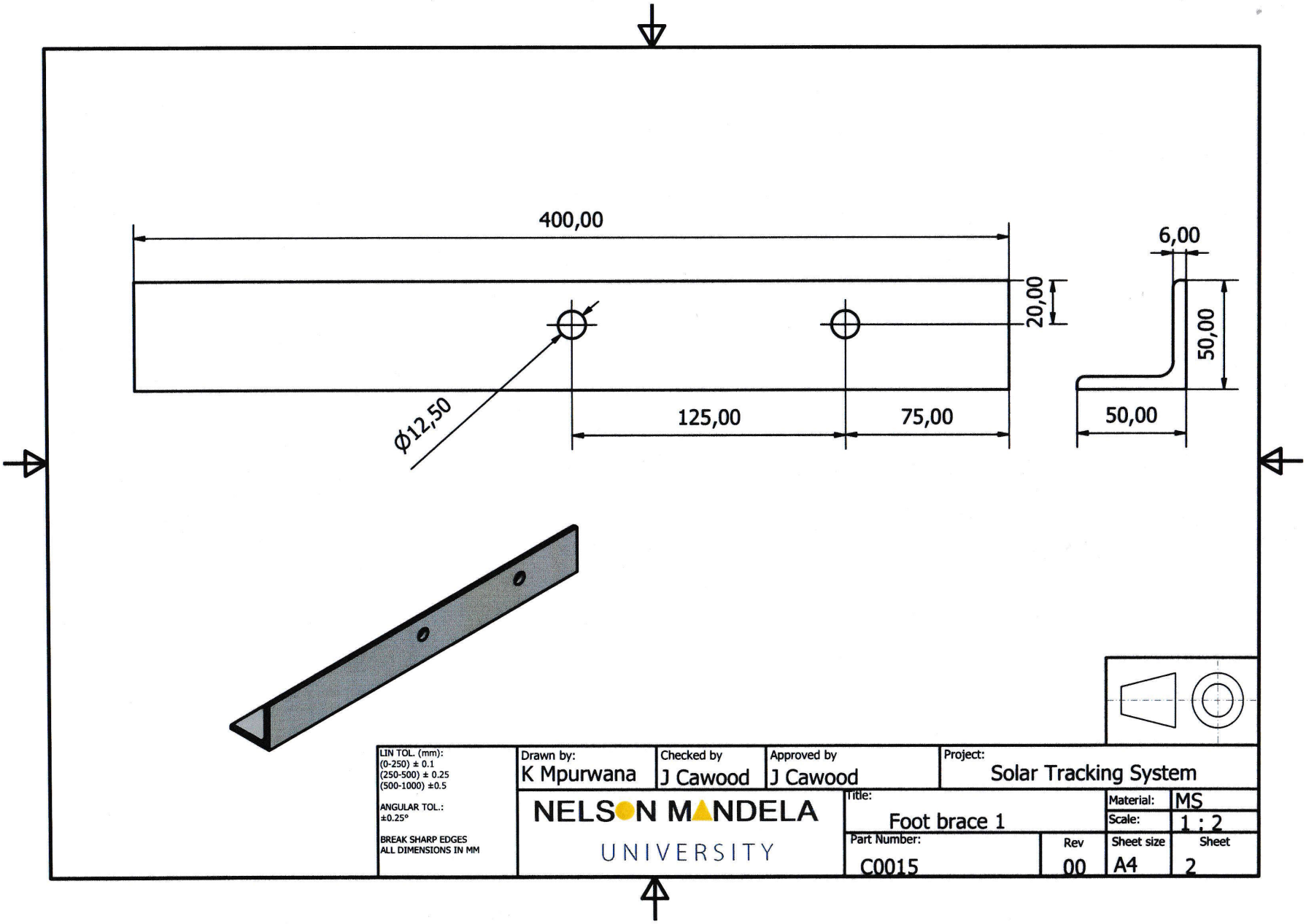

LIN TOL. (mm): (0-250) ± 0.1 (250-500) ± 0.25 (500-1000) ±0.5 ANGULAR TOL.: ±0.25° BREAK SHARP EDGES ALL DIMENSIONS IN MM	Drawn by: K Mpurwana	Checked by J Cawood	Approved by J Cawood	Project: Solar Tracking System	
NELSON MANDELA UNIVERSITY	Title: Foot brace 1			Material: MS	Scale: 1 : 2
	Part Number: C0015	Rev 00	Sheet size A4	Sheet 2	

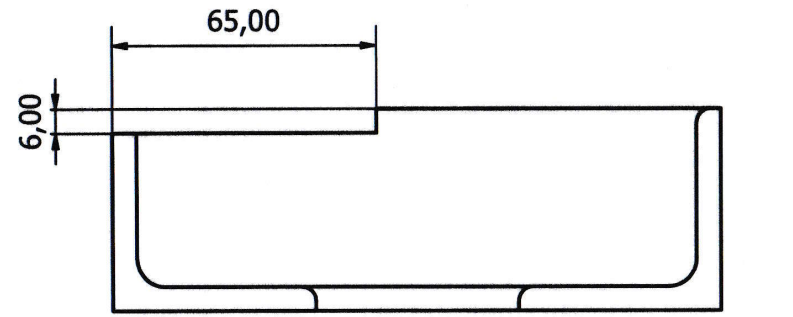

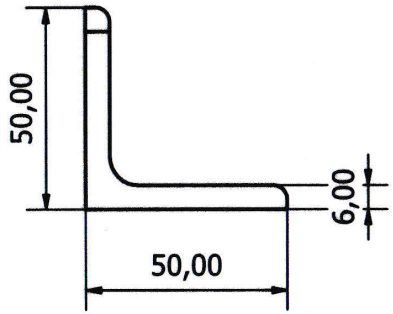

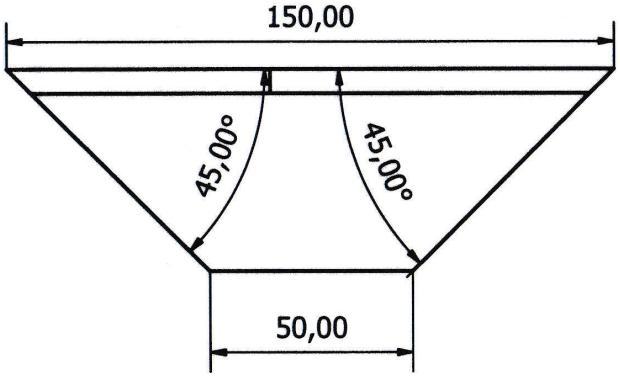

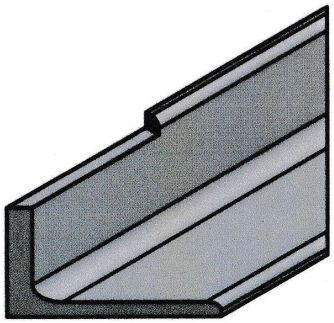

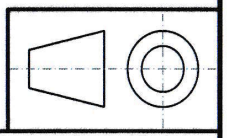

LIN TOL. (mm): (0-250) ± 0.1 (250-500) ± 0.25 (500-1000) ±0.5 ANGULAR TOL.: ±0.25° BREAK SHARP EDGES ALL DIMENSIONS IN MM	Drawn by: K Mpurwana	Checked by J Cawood	Approved by J Cawood	Project: Solar Tracking System		
NELSON MANDELA UNIVERSITY	Title: Foot brace 2				Material:	MS
					Scale:	1 : 1.5
	Part Number: C0016		Rev 00		Sheet size A4	Sheet 3

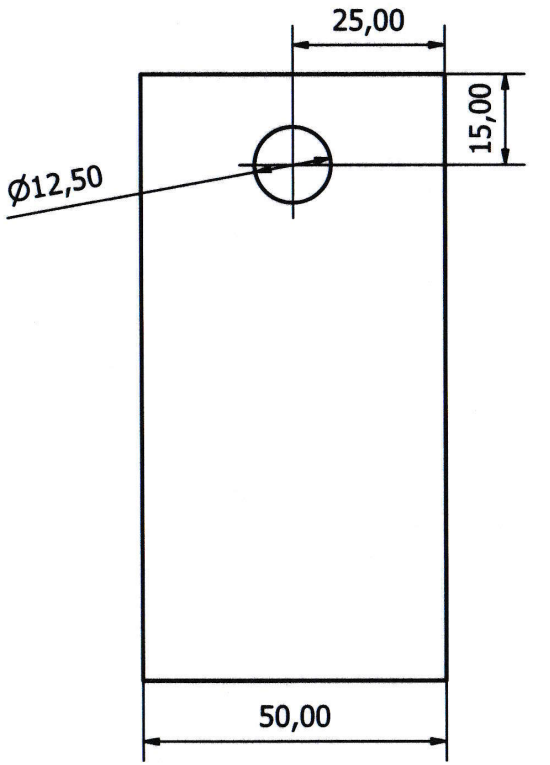

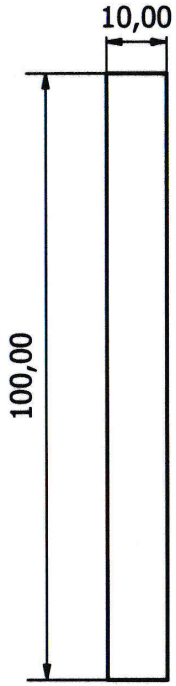

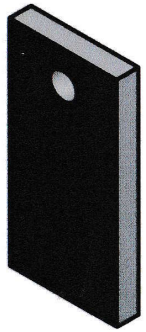

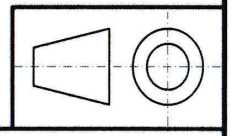

LIN TOL. (mm): (0-250) ± 0.1 (250-500) ± 0.25 (500-1000) ±0.5 ANGULAR TOL.: ±0.25° BREAK SHARP EDGES ALL DIMENSIONS IN MM	Drawn by: K Mpurwana	Checked by J Cawood	Approved by J Cawood	Project: Solar Tracking System
NELSON MANDELA UNIVERSITY	Title: Foot brace 3			Material: MS Scale: 1 : 1
	Part Number: C0017	Rev 00	Sheet size A4	Sheet 4

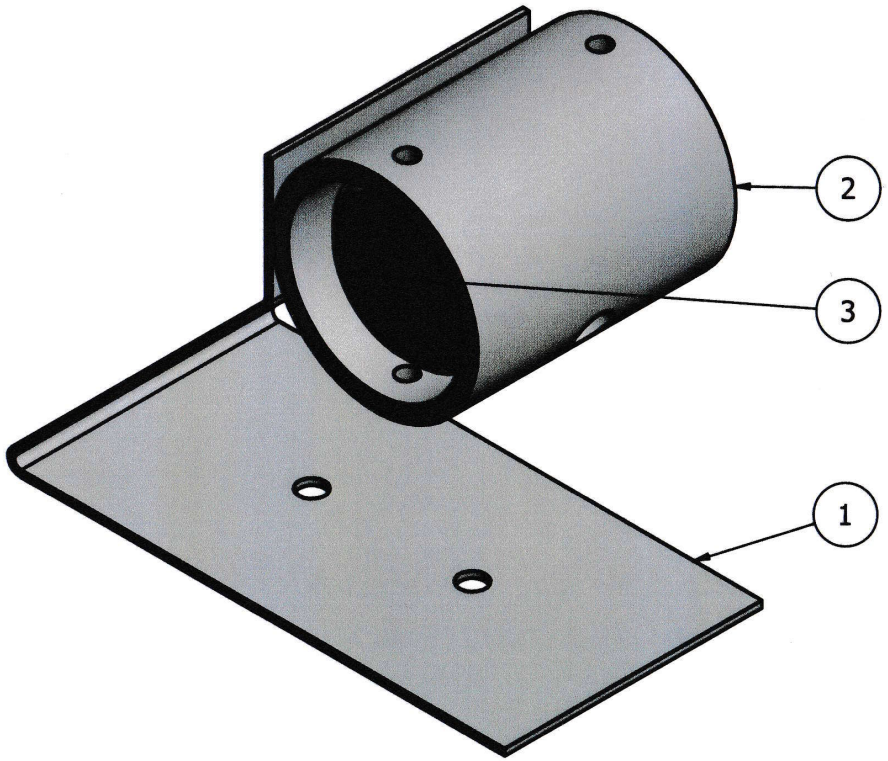

PARTS LIST			
ITEM	STOCK NUMBER	PART NUMBER	DESCRIPTION
1	Roller switch bracket	E0012	Galv. sheet
2	Roller switch holder	E0011	304 SS tube
3	Roller	E0013	304 SS

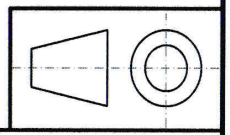

LIN TOL. (mm):
(0-250) ± 0.1
(250-500) ± 0.25
(500-1000) ±0.5

ANGULAR TOL.:
±0.25°

BREAK SHARP EDGES
ALL DIMENSIONS IN MM

Drawn by: K Mpurwana
Checked by: J Cawood
Approved by: J Cawood
Project: Solar Tracking System

NELSON MANDELA UNIVERSITY

Title: Roller Switch
Material: --
Scale: 1.5 : 1
Part Number: E0010
Rev: 00
Sheet size: A4
Sheet: 1

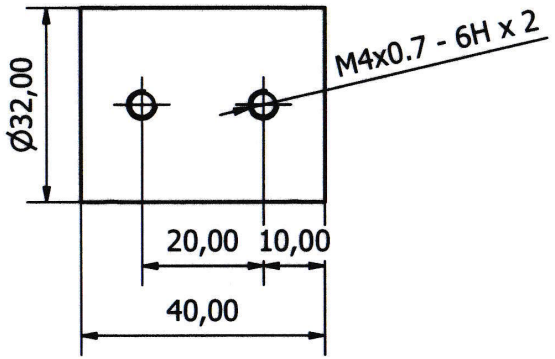

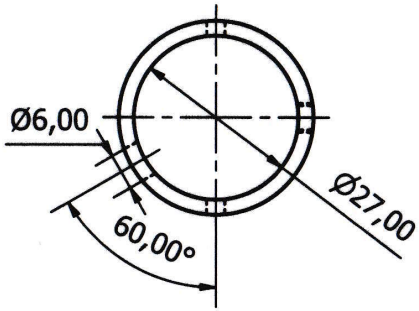

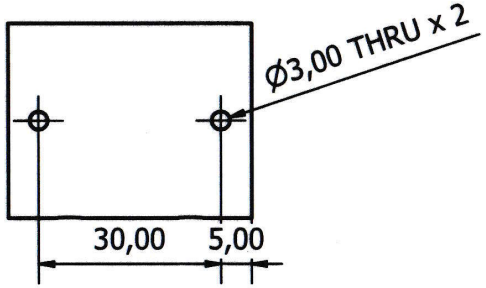

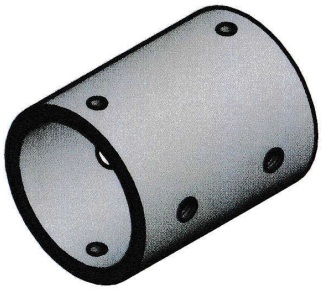

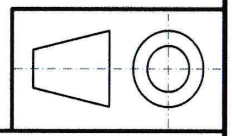

LIN TOL. (mm): (0-250) ± 0.1 (250-500) ± 0.25 (500-1000) ±0.5 ANGULAR TOL.: ±0.25° BREAK SHARP EDGES ALL DIMENSIONS IN MM	Drawn by: K Mpurwana	Checked by J Cawood	Approved by J Cawood	Project: Solar Tracking System	
NELSON MANDELA UNIVERSITY	Title: Roller switch holder			Material: 304 SS tube	Scale: 1:1
	Part Number: E0011	Rev 00	Sheet size A4	Sheet 3	

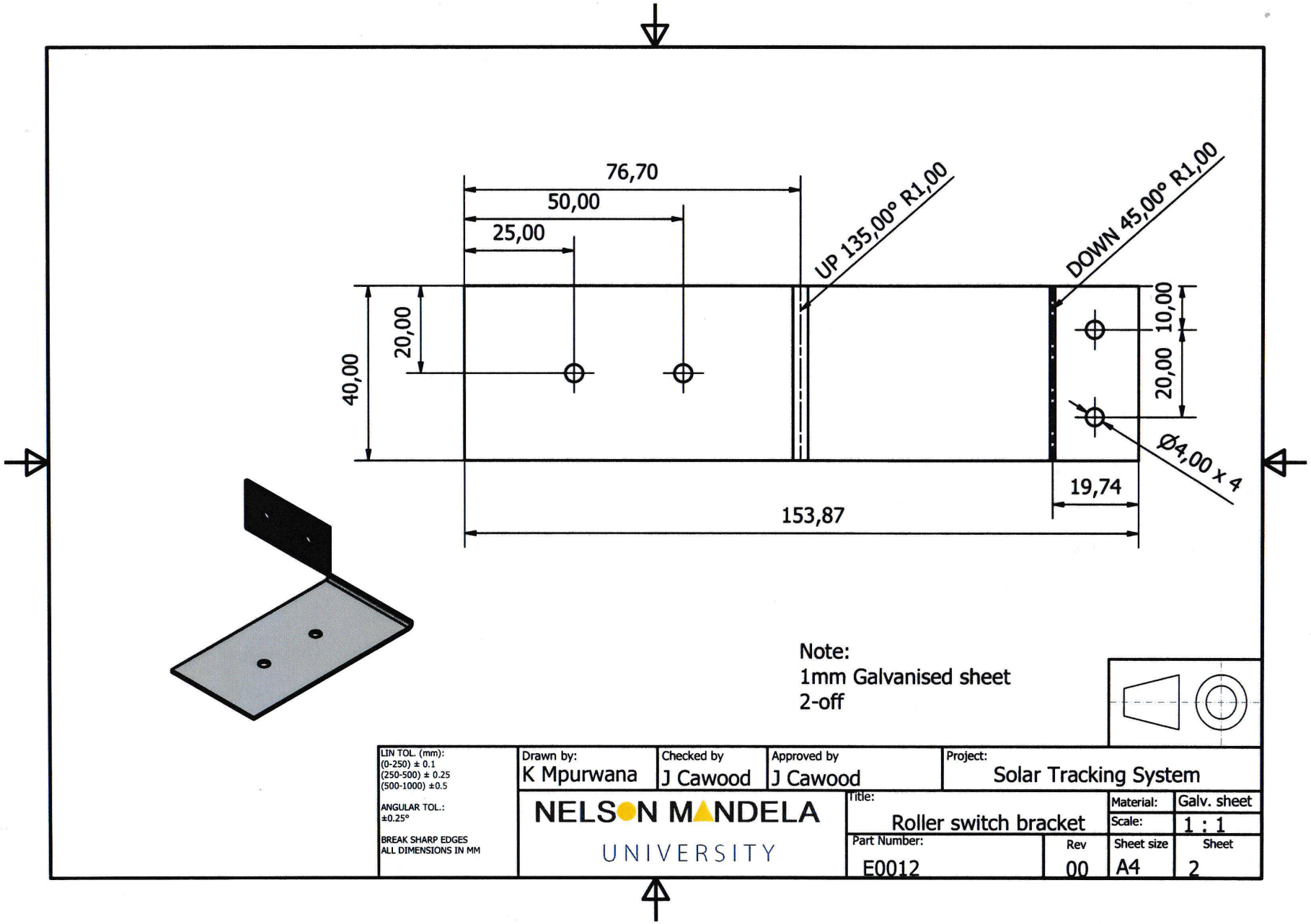

Note:
1mm Galvanised sheet
2-off

LIN TOL. (mm): (0-250) ± 0.1 (250-500) ± 0.25 (500-1000) ±0.5 ANGULAR TOL.: ±0.25° BREAK SHARP EDGES ALL DIMENSIONS IN MM	Drawn by: K Mpurwana	Checked by J Cawood	Approved by J Cawood	Project: Solar Tracking System	
NELSON MANDELA UNIVERSITY	Title: Roller switch bracket			Material: Galv. sheet	Scale: 1 : 1
	Part Number: E0012	Rev 00	Sheet size A4	Sheet 2	

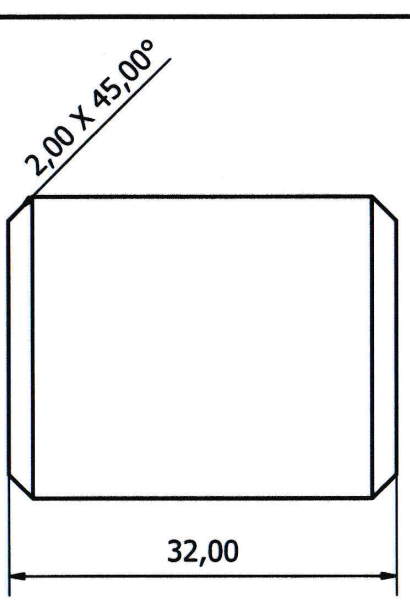

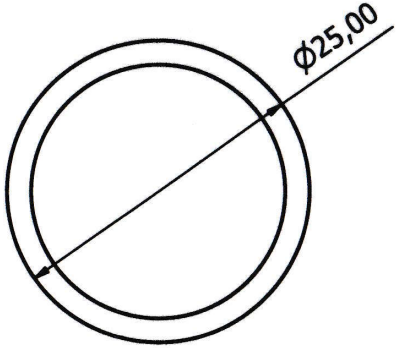

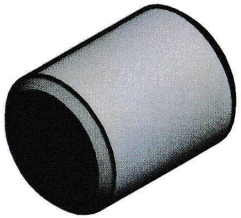

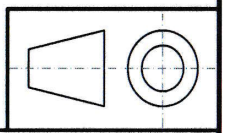

LIN TOL. (mm): (0-250) ± 0.1 (250-500) ± 0.25 (500-1000) ±0.5 ANGULAR TOL.: ±0.25° BREAK SHARP EDGES ALL DIMENSIONS IN MM	Drawn by: K Mpurwana	Checked by J Cawood	Approved by J Cawood	Project: Solar Tracking System	
NELSON MANDELA UNIVERSITY	Title: Roller			Material: 304 SS	
				Scale: 2:1	
	Part Number: E0013	Rev 00	Sheet size A4	Sheet 4	

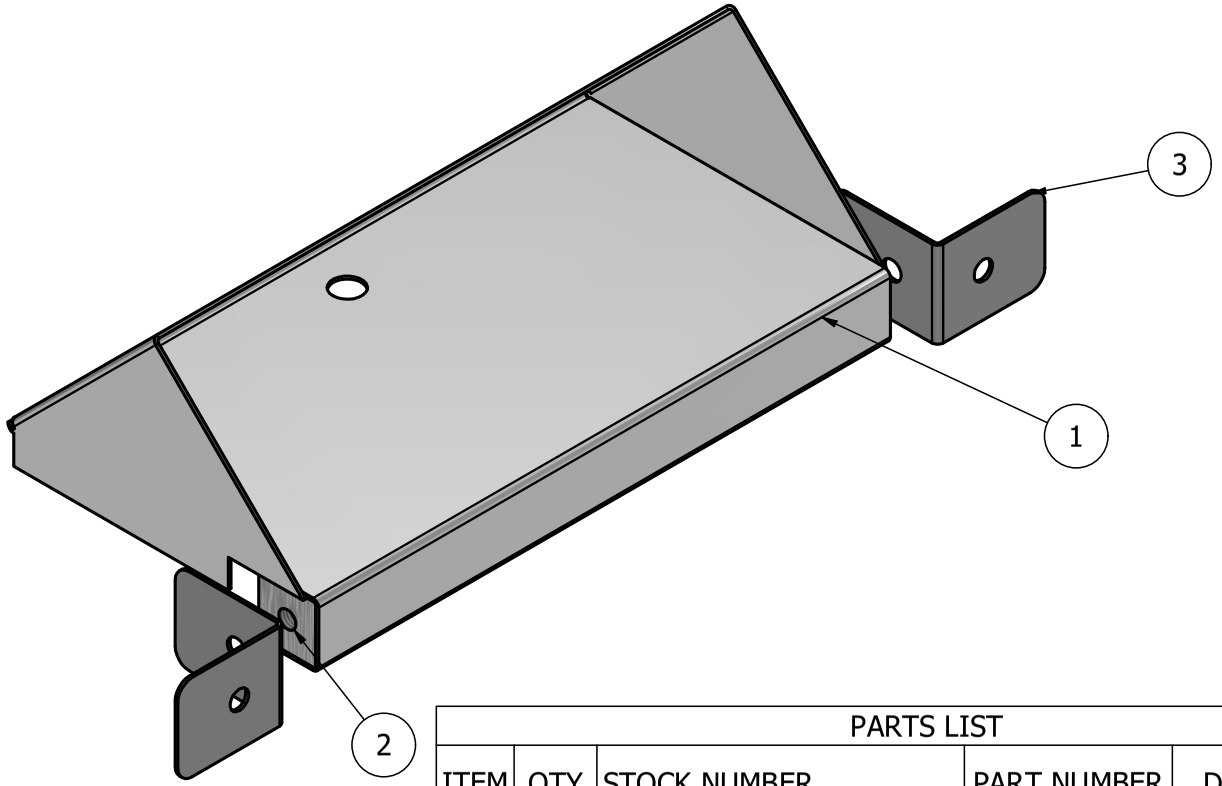

PARTS LIST				
ITEM	QTY	STOCK NUMBER	PART NUMBER	DESCRIPTION
1	1	Sensor plate	E0015	Galv. sheet
2	1	Sensor plate mounting bar	E0016	Al bar
3	2	Sensor plate bracket	E0017	Galv. sheet

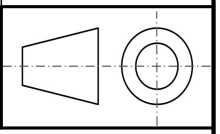

LIN TOL. (mm):
(0-250) ± 0.1
(250-500) ± 0.25
(500-1000) ±0.5

ANGULAR TOL.:
±0.25°

BREAK SHARP EDGES
ALL DIMENSIONS IN MM

Drawn by:	Checked by	Approved by	Project:
K Mpurwana	J Cawood	J Cawood	Solar Tracking System

NELSON MANDELA UNIVERSITY

Title:		Material:	--
Sensor plate		Scale:	1 :1.5
Part Number:	Rev	Sheet size	Sheet
E0014	00	A4	1

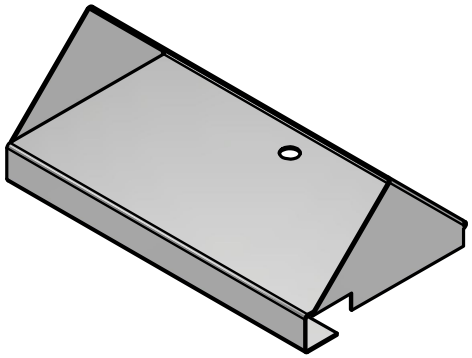

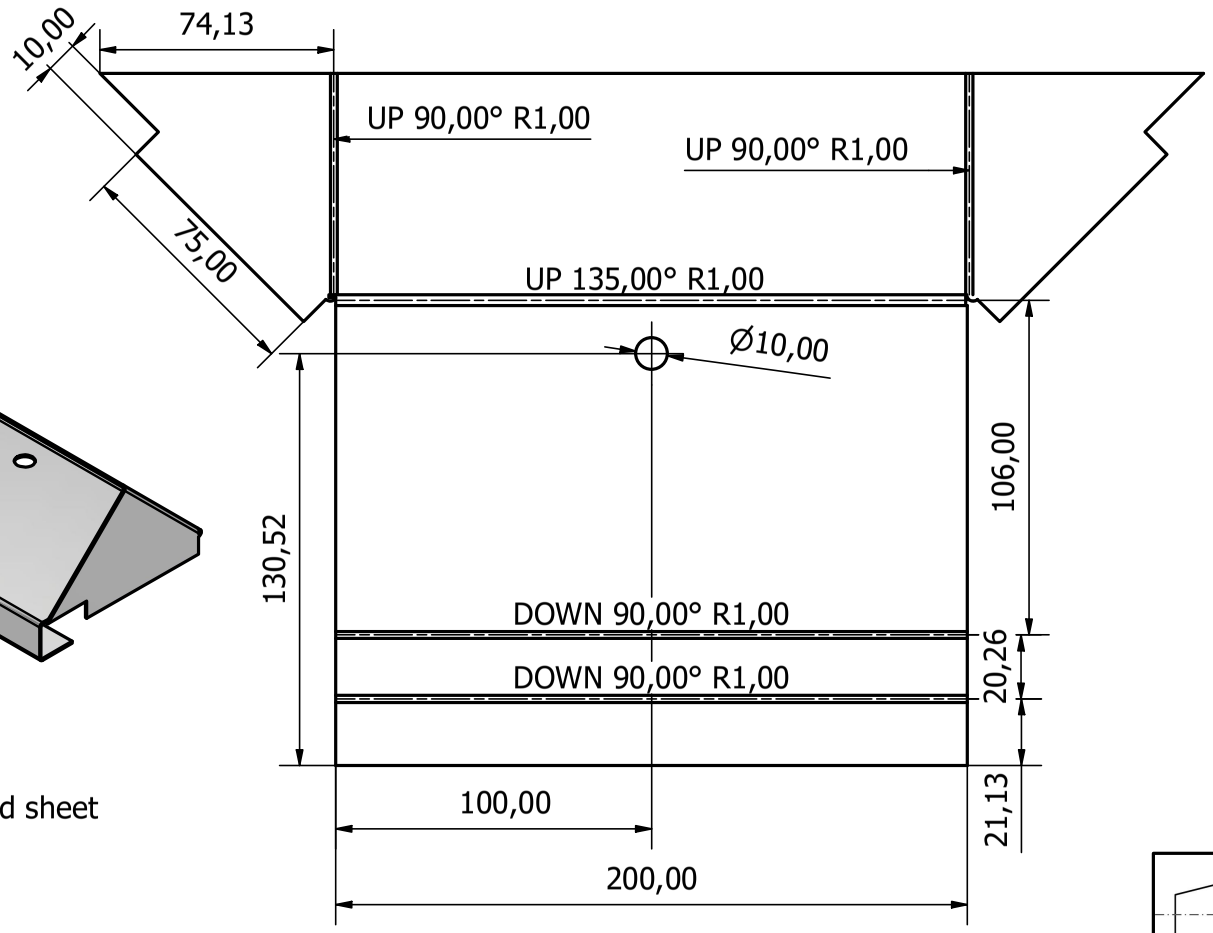

Note:
1mm Galvanised sheet

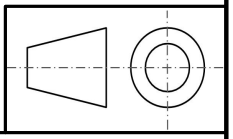

LIN TOL. (mm): (0-250) ± 0.1 (250-500) ± 0.25 (500-1000) ±0.5 ANGULAR TOL.: ±0.25° BREAK SHARP EDGES ALL DIMENSIONS IN MM	Drawn by: K Mpurwana	Checked by J Cawood	Approved by J Cawood	Project: Solar Tracking System		
NELSON MANDELA UNIVERSITY	Title: Sensor plate			Material:	Galv. sheet	
				Scale:	1 : 2	
	Part Number: E0015	Rev 00		Sheet size A4	Sheet 2	

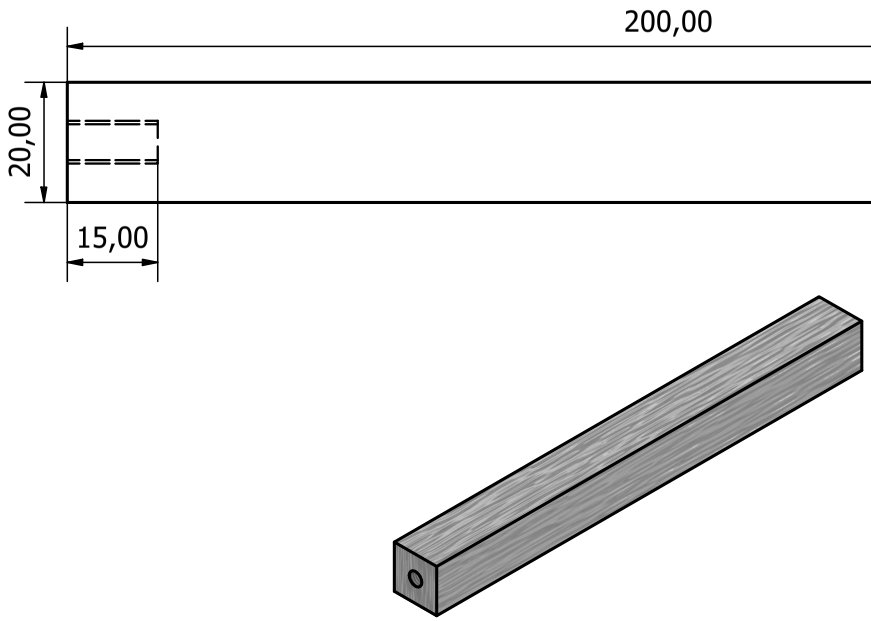

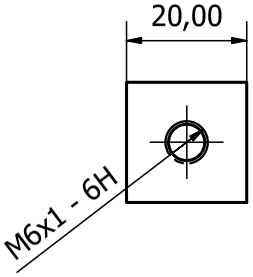

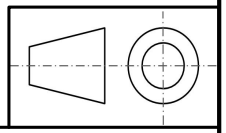

LIN TOL. (mm): (0-250) ± 0.1 (250-500) ± 0.25 (500-1000) ±0.5 ANGULAR TOL.: ±0.25° BREAK SHARP EDGES ALL DIMENSIONS IN MM	Drawn by: K Mpurwana	Checked by J Cawood	Approved by J Cawood	Project: Solar Tracking System
NELSON MANDELA UNIVERSITY	Title: Sensor plate mounting bar		Material: Al bar	
			Scale: 1 : 1	
	Part Number: E0016	Rev 00	Sheet size A4	Sheet 4

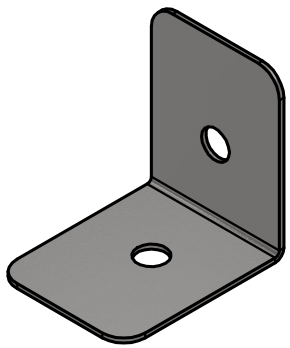

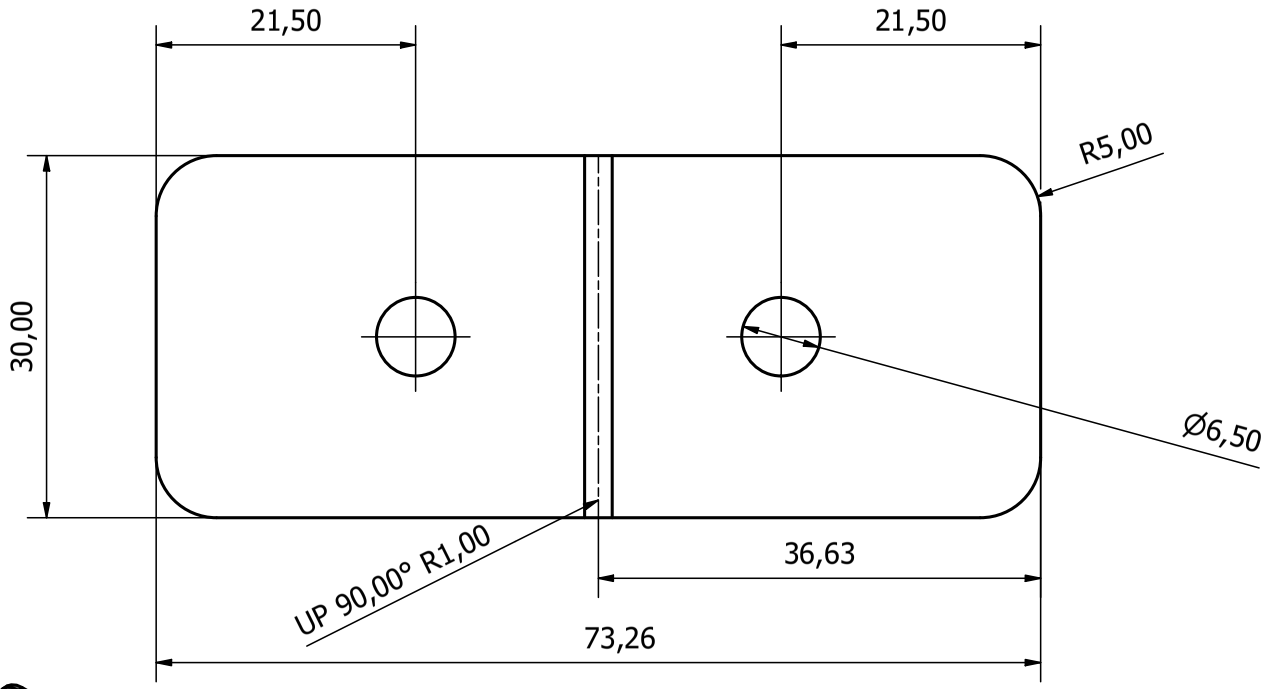

Note:
1mm Galvanised sheet
2-off

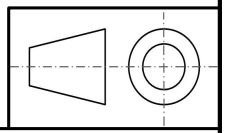

LIN TOL. (mm): (0-250) ± 0.1 (250-500) ± 0.25 (500-1000) ±0.5 ANGULAR TOL.: ±0.25° BREAK SHARP EDGES ALL DIMENSIONS IN MM	Drawn by: K Mpurwana	Checked by J Cawood	Approved by J Cawood	Project: Solar Tracking System	
NELSON MANDELA UNIVERSITY	Title: Sensor plate bracket			Material:	Galv. sheet
				Scale:	2 : 1
	Part Number: E0017	Rev 00		Sheet size A4	Sheet 3

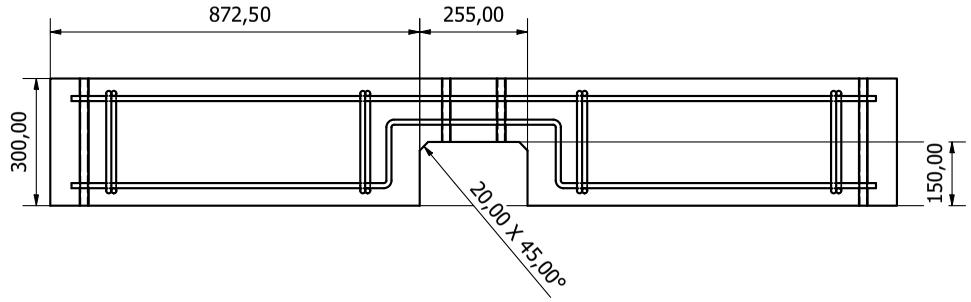

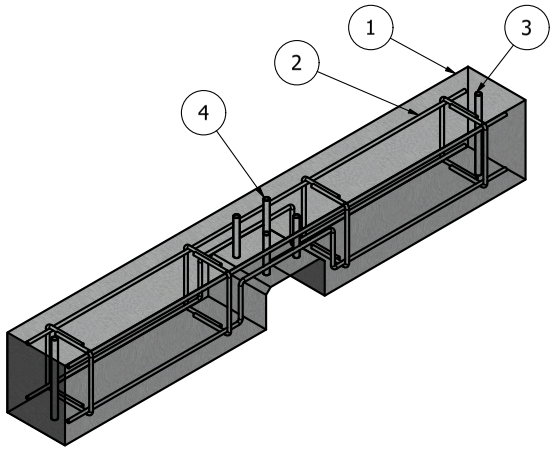

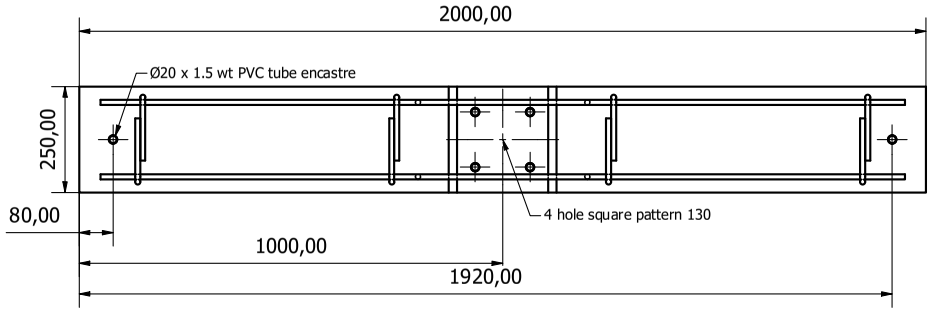

PARTS LIST				
ITEM	QTY	STOCK NUMBER	PART NUMBER	DESCRIPTION
1	1	Cast concrete	F0011	Concrete Mix C40 fine
2	1	Rebar Assembly	F0013	-
3	2	PVC Blind Tube	F00121	PVC
4	4	PVC 150	F00122	PVC

LIN TOL. (mm):
(0-250) ± 0.1
(250-500) ± 0.25
(500-1000) ±0.5

ANGULAR TOL.:
±0.25°

BREAK SHARP EDGES
ALL DIMENSIONS IN MM

Drawn by: K Mpurwana	Checked by J Cawood	Approved by J Cawood	Project: Solar Tracking System

NELSON MANDELA UNIVERSITY

Title: Foundation		Material:	-
		Scale:	1 : 10
Part Number: F0010	Rev 00	Sheet size A3	Sheet 1

Y12 C (1 : 9)

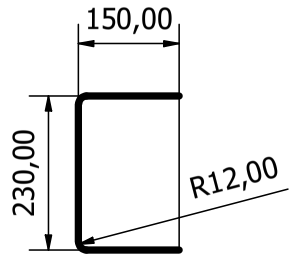

Y12 Straight (1 : 25)

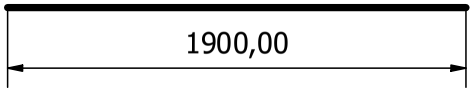

Y12 Loop (1 : 25)

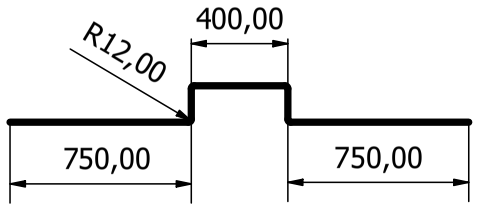

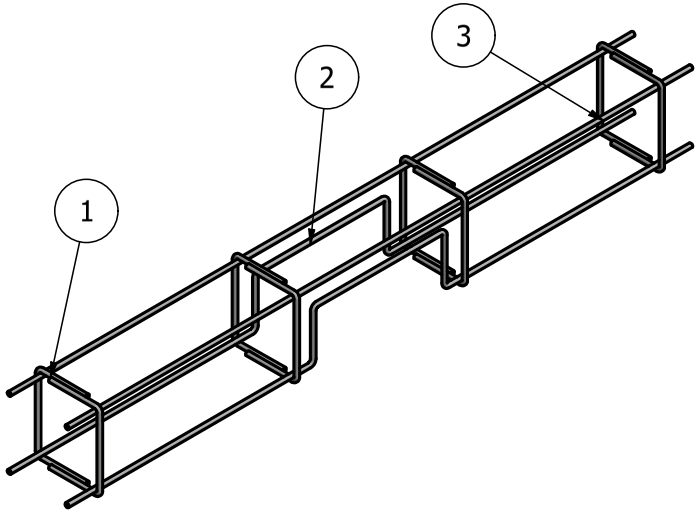

PARTS LIST			
ITEM	QTY	STOCK NUMBER	PART NUMBER
1	8	Y12 C	F00131
2	1	Y12 Loop	F00132
3	1	Y12 Straight	F00133

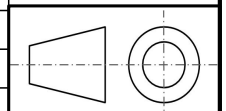

LIN TOL. (mm):
(0-250) ± 0.1
(250-500) ± 0.25
(500-1000) ±0.5

ANGULAR TOL.:
±0.25°

BREAK SHARP EDGES
ALL DIMENSIONS IN MM

Drawn by: K Mpurwana	Checked by J Cawood	Approved by J Cawood	Project: Solar Tracking System

NELSON MANDELA UNIVERSITY

Title: Rebar Assembly			Material:	-
			Scale:	1 : 13
Part Number: F0013	Rev 00	Sheet size A4	Sheet 2	

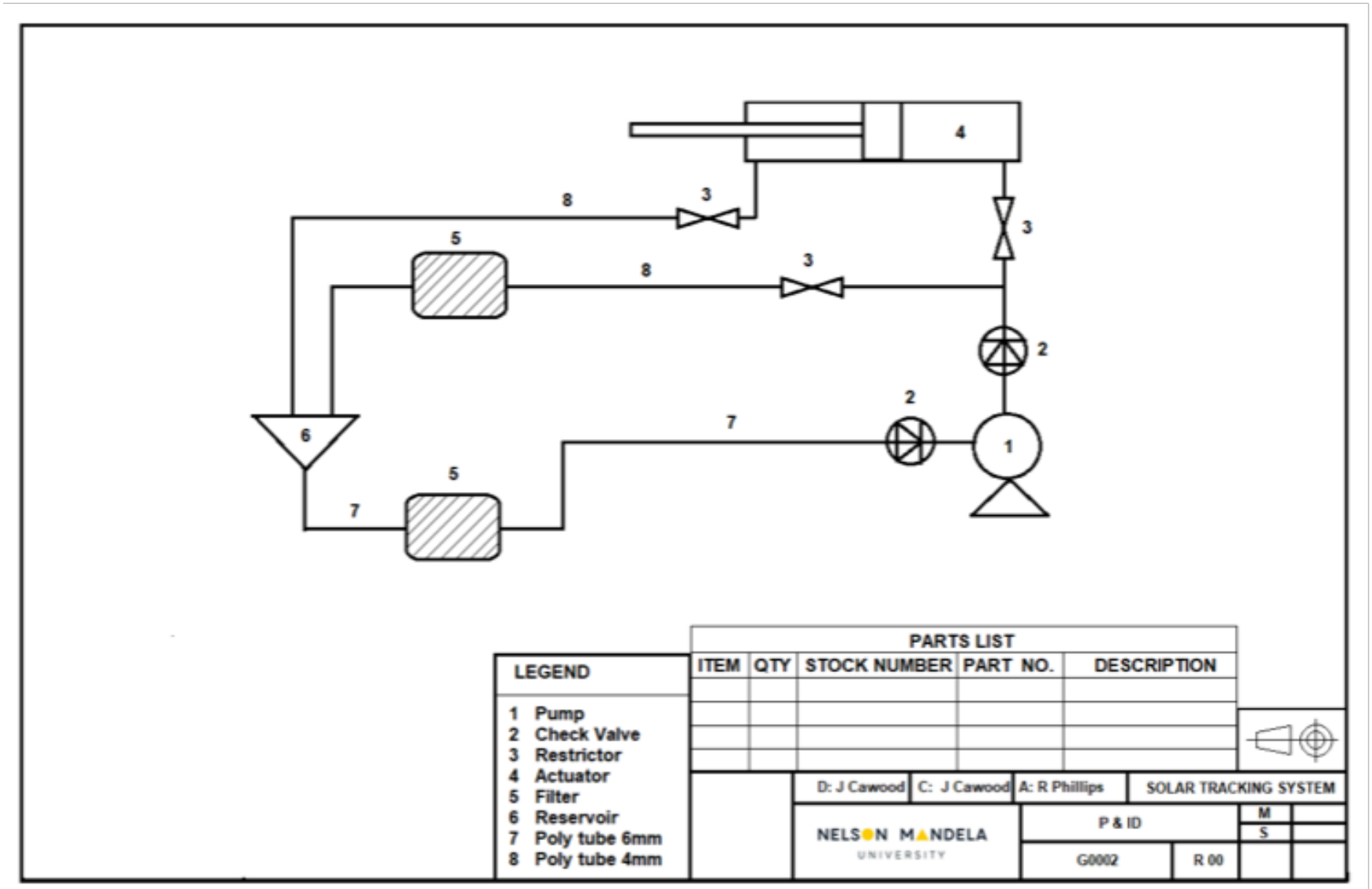
4
8
3
3
5
8
3
2
2
7
6
1
5
7
LEGEND
1 Pump
2 Check Valve
3 Restrictor
4 Actuator
5 Filter
6 Reservoir
7 Poly tube 6mm
8 Poly tube 4mm
PARTS LIST
ITEM
QTY
STOCK NUMBER
PART NO.
DESCRIPTION
D: J Cawood
C: J Cawood
A: R Phillips
SOLAR TRACKING SYSTEM
NELSON MANDELA UNIVERSITY
P & ID
M
S
G0002
R 00

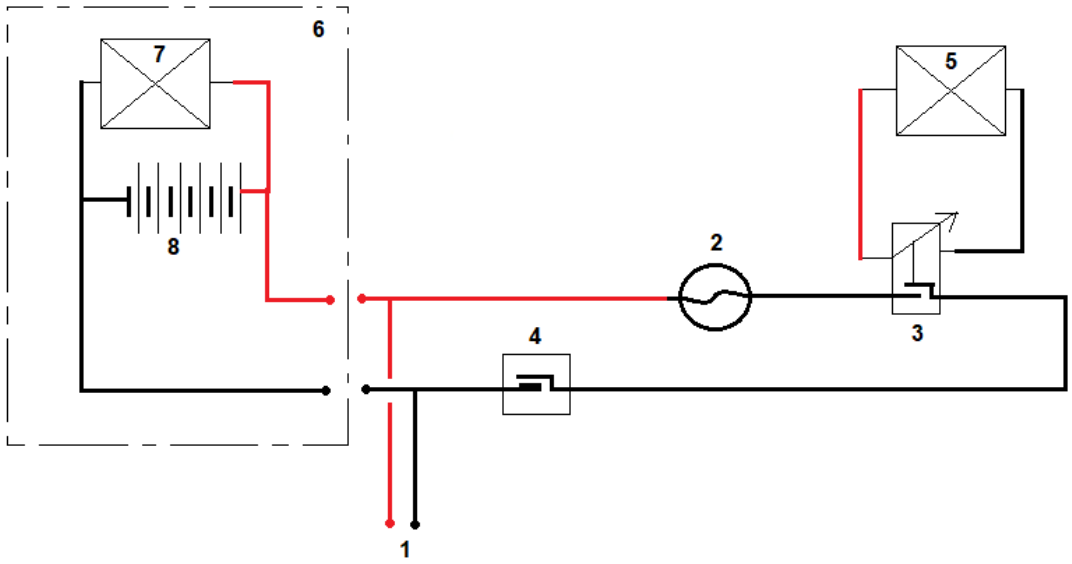

LEGEND

1 DC power 12V supply stepped down from main PV panel cct
2 Pump drive 12V 1.5A solenoid pulse motor
3 Relay 240V/5V5A (SCHRACK Part No. PE014005)
4 Contactor DC 12V 8A
5 5V 500mA Solar cell
6 Optional auxilliary power supply
7 Solar mono PV panel 15W 12V
8 Battery pack 12V 7.5Ah

PARTS LIST

ITEM	QTY	STOCK NUMBER	PART NO.	DESCRIPTION

D: J Cawood C: J Cawood A: R Phillips

SOLAR TRACKING SYSTEM

NELSON MANDELA UNIVERSITY

Electrical Circuit Diagram

M S

G0003 R 00

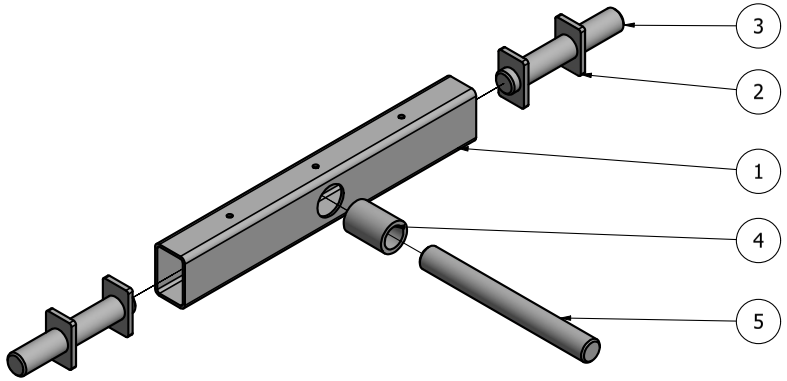

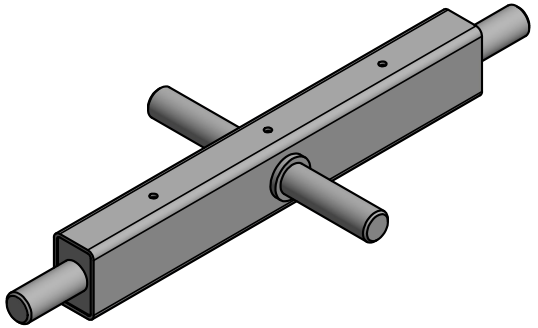

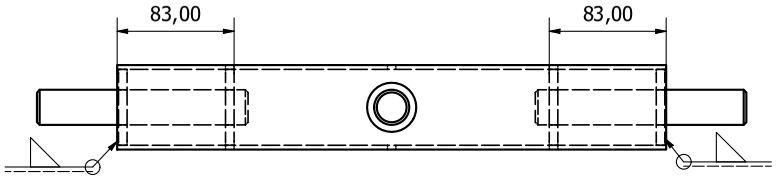

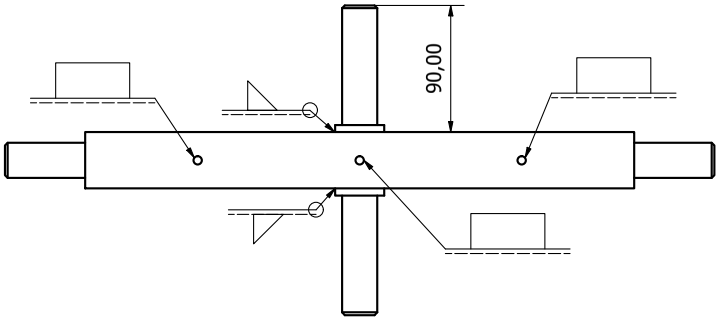

PARTS LIST				
ITEM	QTY	STOCK NUMBER	PART NUMBER	DESCRIPTION
1	1	Beam	J0011	300W
2	4	End Pin Gussets	J00122	A36
3	2	End Pin	J00121	Gr 8.8
4	1	Centre Stiffener	J0013	A36
5	1	Cross Pin	J0014	Gr 8.8

LIN TOL. (mm):
(0-250) ± 0.1
(250-500) ± 0.25
(500-1000) ±0.5

ANGULAR TOL.:
±0.25°

BREAK SHARP EDGES
ALL DIMENSIONS IN MM

Drawn by: K Mpurwana
Checked by: J Cawood
Approved by: J Cawood
Project: Solar Tracking System

NELSON MANDELA UNIVERSITY

Title: Hookes Joint
Material: -
Scale: 1 : 4
Part Number: J0010
Rev: 0
Sheet size: A3
Sheet: 1

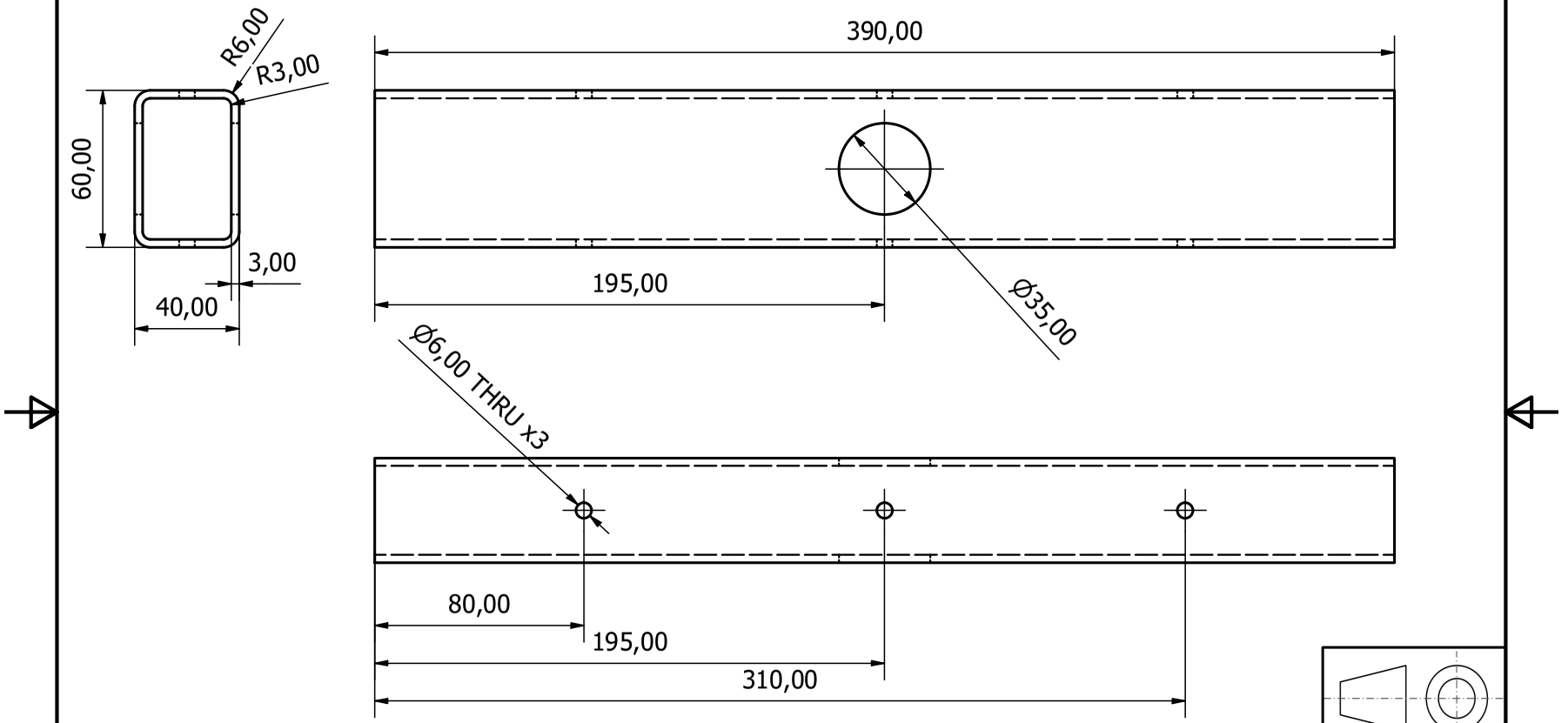

LIN TOL. (mm): (0-250) ± 0.1 (250-500) ± 0.25 (500-1000) ±0.5 ANGULAR TOL.: ±0.25° BREAK SHARP EDGES ALL DIMENSIONS IN MM	Drawn by: K Mpurwana	Checked by J Cawood	Approved by J Cawood	Project: Solar Tracking System	
NELSON MANDELA UNIVERSITY	Title: Beam			Material: 300W	
				Scale: 1 : 2	
	Part Number: J0011	Rev 0	Sheet size A4	Sheet 2	

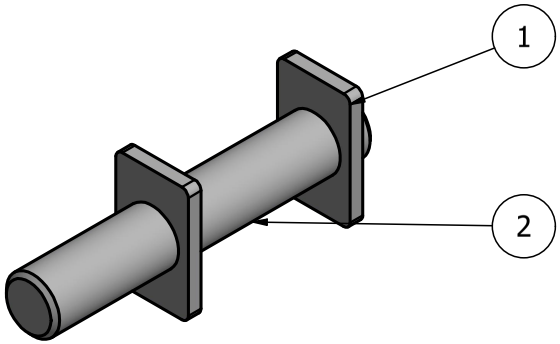

End Pin Assembly (1 : 2)

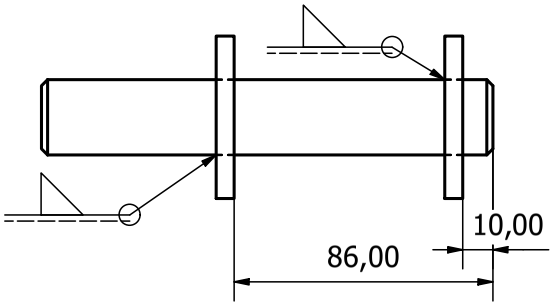

End Pin Gusset (1 : 2)

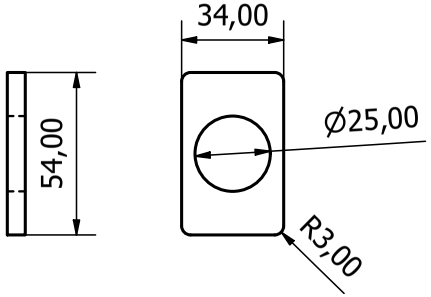

End Pin (1 : 2)

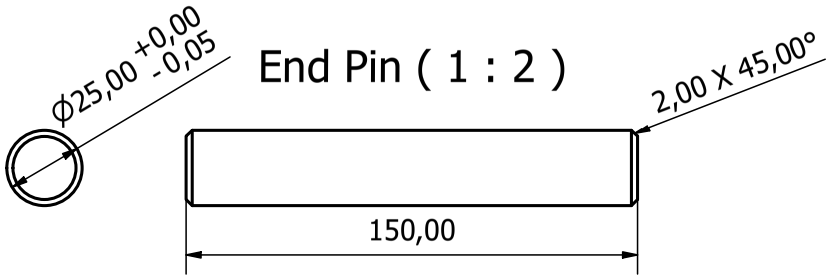

PARTS LIST				
ITEM	QTY	STOCK NUMBER	PART NUMBER	DESCRIPTION
1	2	End Pin Gussets	J00122	A36
2	1	End Pin	J00121	Gr 8.8

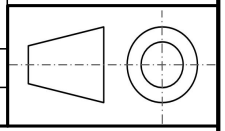

LIN TOL. (mm):
(0-250) ± 0.1
(250-500) ± 0.25
(500-1000) ±0.5

ANGULAR TOL.:
±0.25°

BREAK SHARP EDGES
ALL DIMENSIONS IN MM

Drawn by:	Checked by	Approved by	Project:
K Mpurwana	J Cawood	J Cawood	Solar Tracking System

NELSON MANDELA UNIVERSITY

Title:		Material:	-
End Pin Assembly		Scale:	1 : 2
Part Number:	Rev	Sheet size	Sheet
J0012	0	A4	3

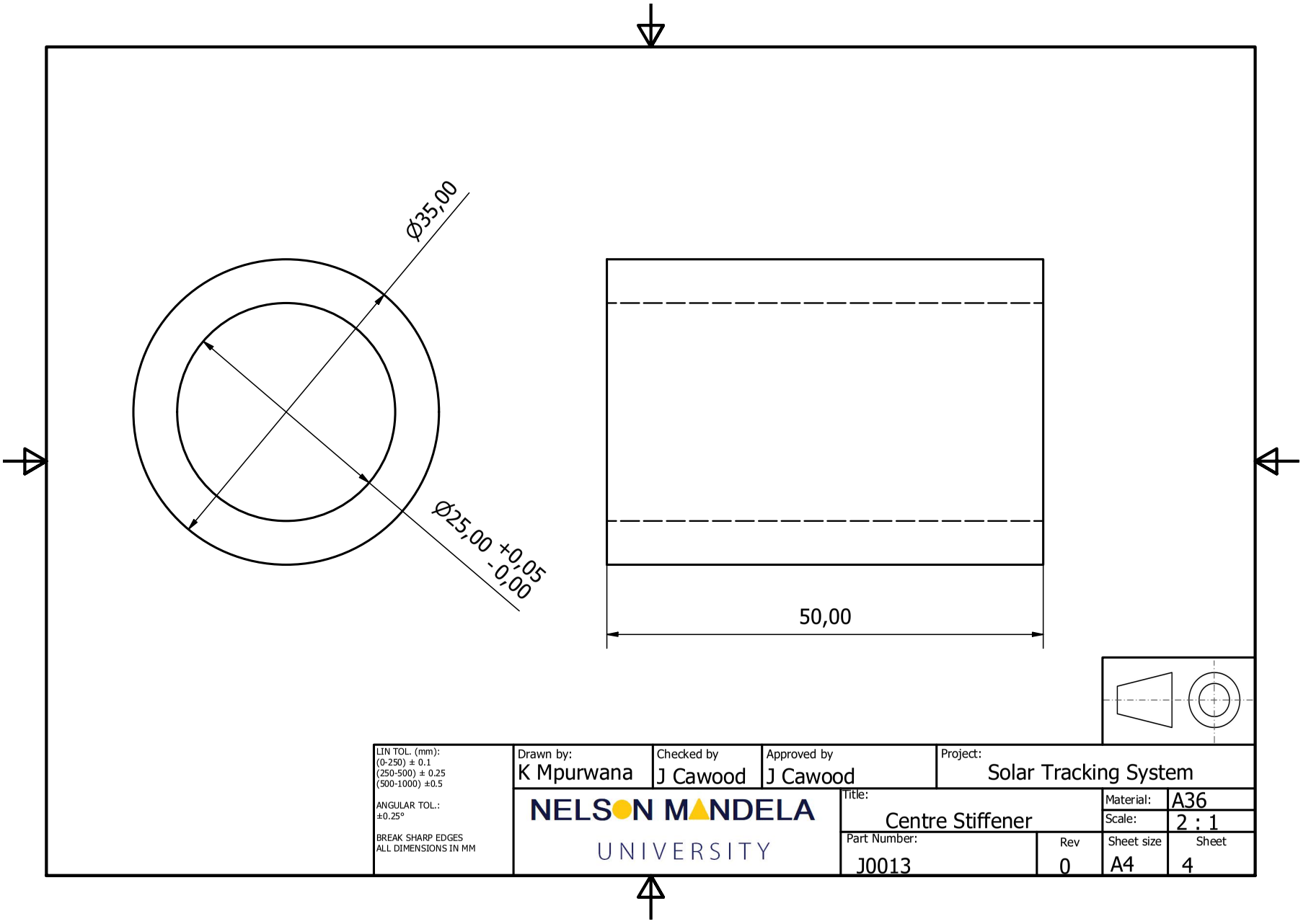

LIN TOL. (mm): (0-250) ± 0.1 (250-500) ± 0.25 (500-1000) ±0.5 ANGULAR TOL.: ±0.25° BREAK SHARP EDGES ALL DIMENSIONS IN MM	Drawn by: K Mpurwana	Checked by J Cawood	Approved by J Cawood	Project: Solar Tracking System	
	NELSON MANDELA UNIVERSITY		Title: Centre Stiffener	Material: A36	
				Scale: 2 : 1	
			Part Number: J0013	Rev 0	Sheet size A4 / Sheet 4

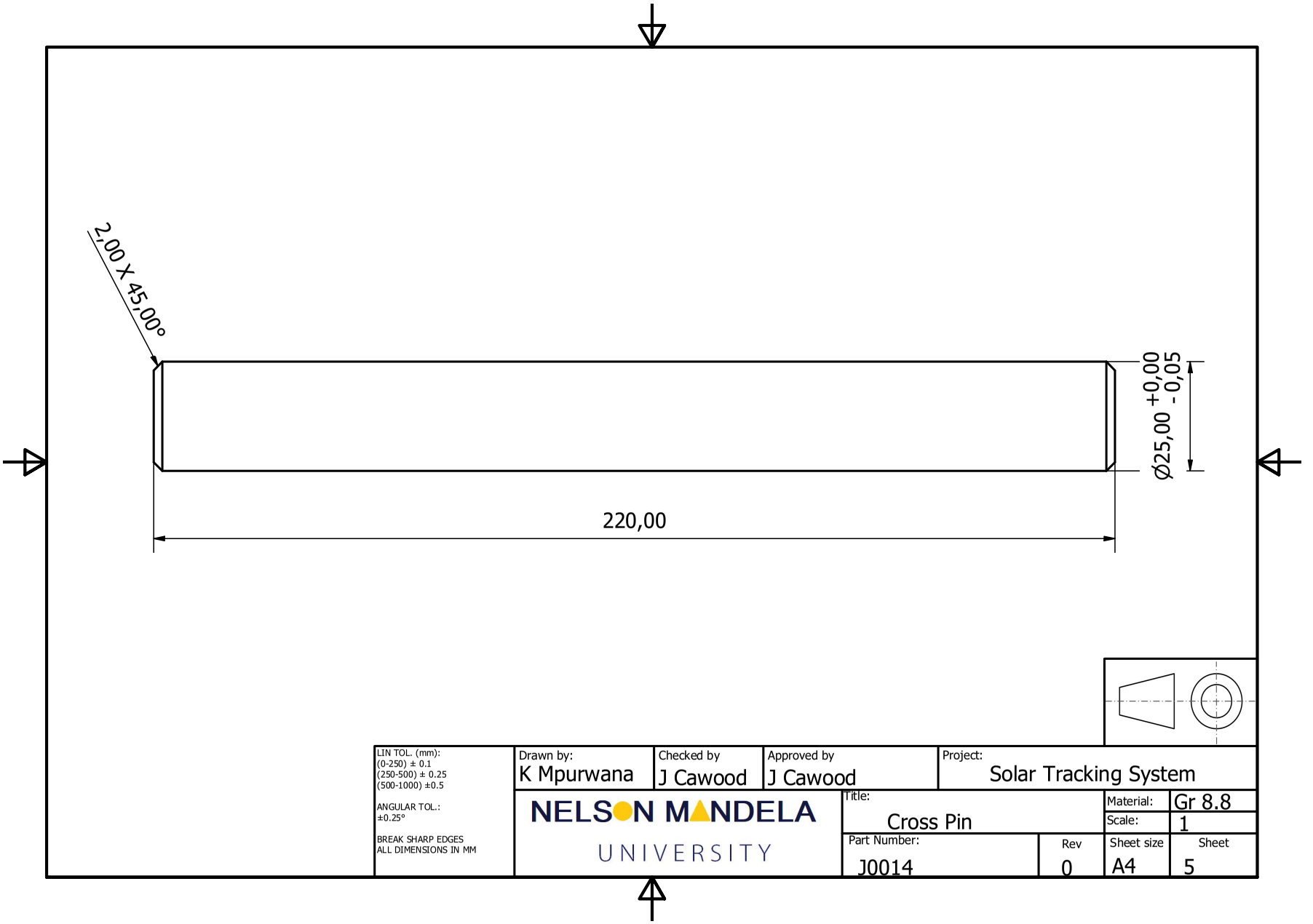

LIN TOL. (mm): (0-250) ± 0.1 (250-500) ± 0.25 (500-1000) ±0.5 ANGULAR TOL.: ±0.25° BREAK SHARP EDGES ALL DIMENSIONS IN MM	Drawn by: K Mpurwana	Checked by J Cawood	Approved by J Cawood	Project: Solar Tracking System
NELSON MANDELA UNIVERSITY	Title: Cross Pin			Material: Gr 8.8 / Scale: 1
	Part Number: J0014	Rev 0	Sheet size A4	Sheet 5

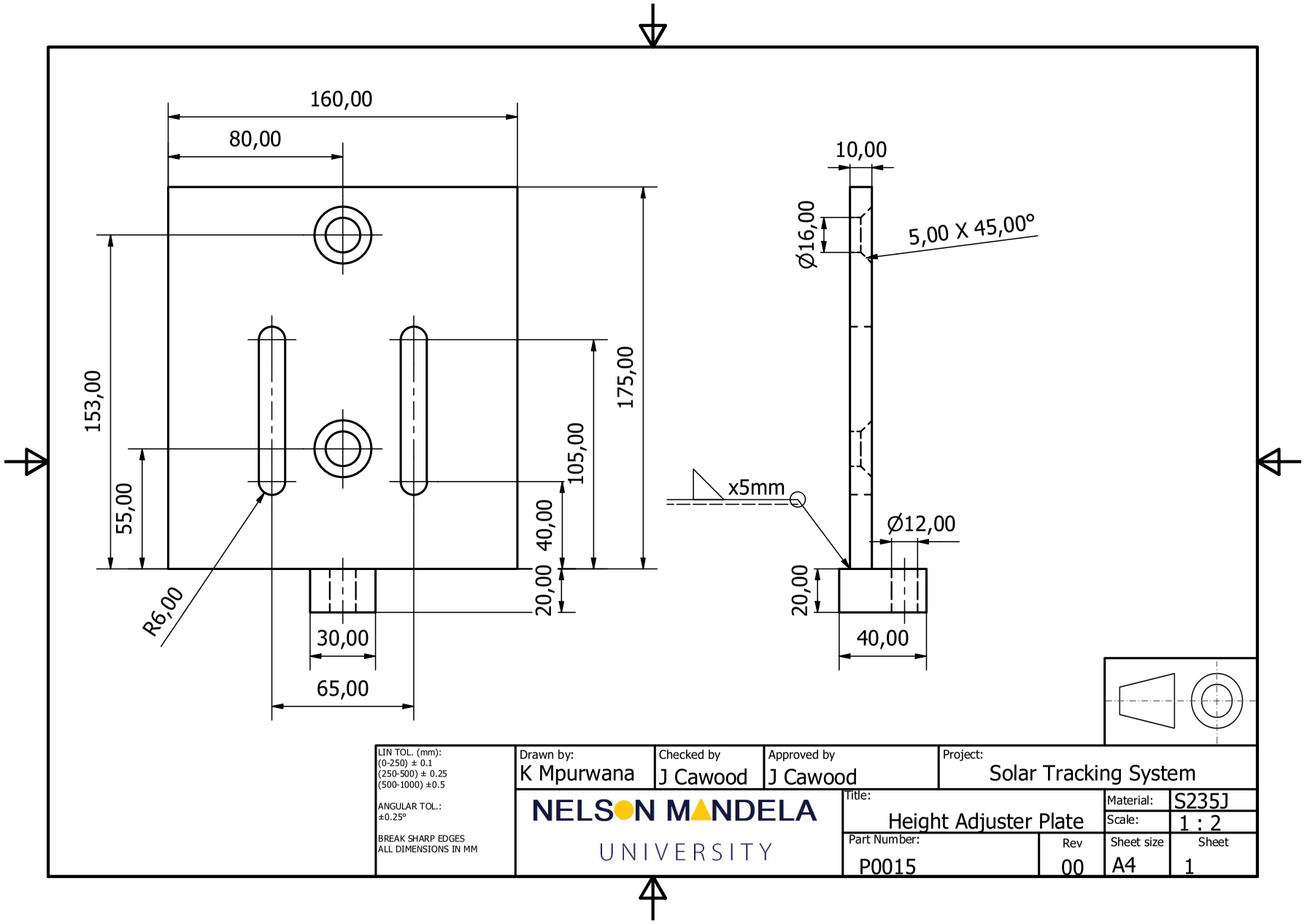

LIN TOL. (mm): (0-250) ± 0.1 (250-500) ± 0.25 (500-1000) ±0.5 ANGULAR TOL.: ±0.25° BREAK SHARP EDGES ALL DIMENSIONS IN MM	Drawn by: K Mpurwana	Checked by J Cawood	Approved by J Cawood	Project: Solar Tracking System	
NELSON MANDELA UNIVERSITY	Title: Height Adjuster Plate			Material: S235J	Scale: 1 : 2
	Part Number: P0015	Rev 00	Sheet size A4	Sheet 1	

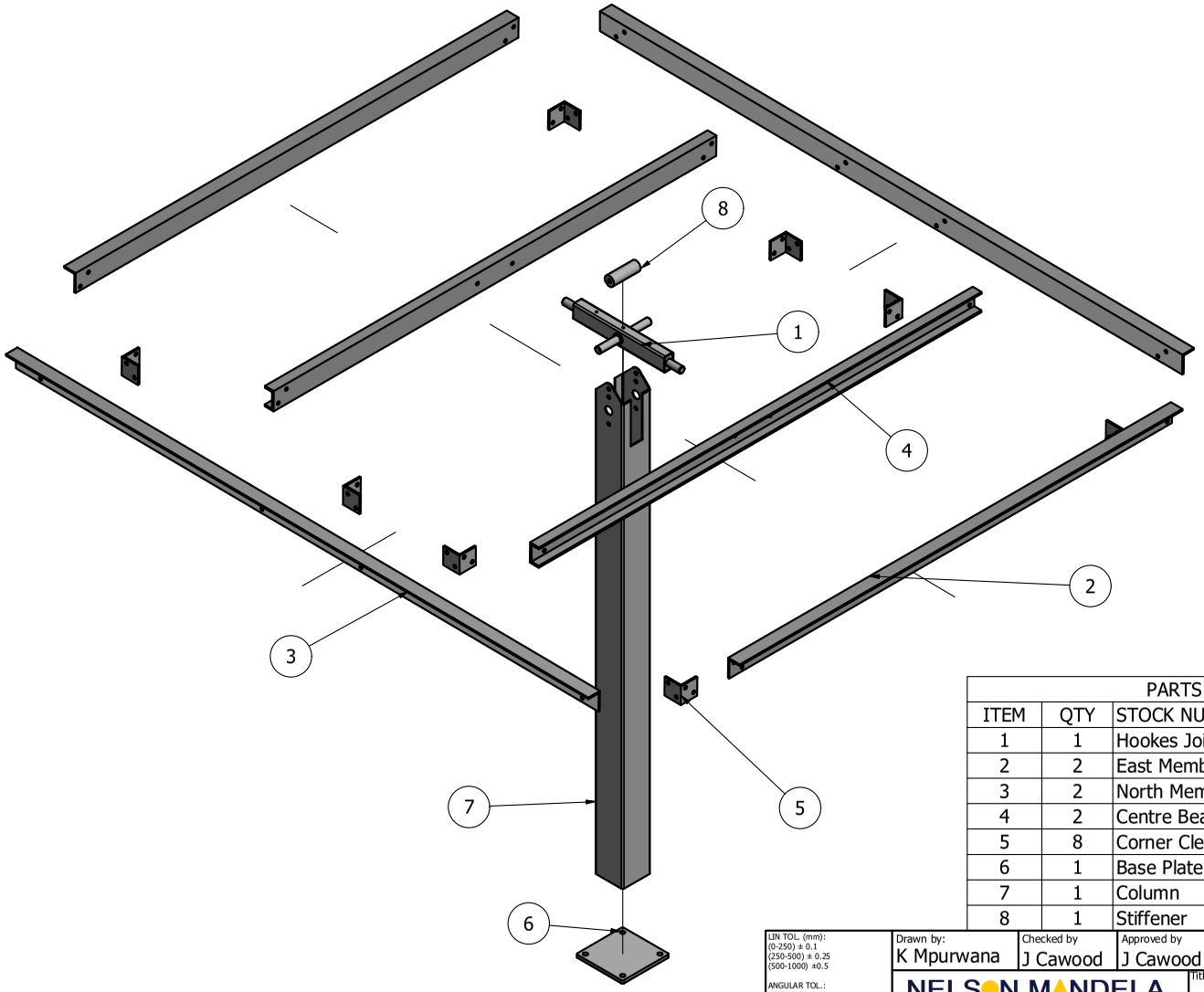

PARTS LIST			
ITEM	QTY	STOCK NUMBER	PART NUMBER
1	1	Hookes Joint	J0010
2	2	East Member	P0012
3	2	North Member	P0011
4	2	Centre Beam	P0013
5	8	Corner Cleats	P0014
6	1	Base Plate	C0013
7	1	Column	C0011
8	1	Stiffener	C0012

LIN TOL. (mm):
(0-250) ± 0.1
(250-500) ± 0.25
(500-1000) ±0.5

ANGULAR TOL.:
±0.25°

BREAK SHARP EDGES
ALL DIMENSIONS IN MM

Drawn by: K Mpurwana	Checked by J Cawood	Approved by J Cawood	Project: Solar Tracking System

NELSON MANDELA UNIVERSITY

Title: Main frame		Material:	--
		Scale:	1 : 12
Part Number: P0000	Rev 00	Sheet size A3	Sheet 1

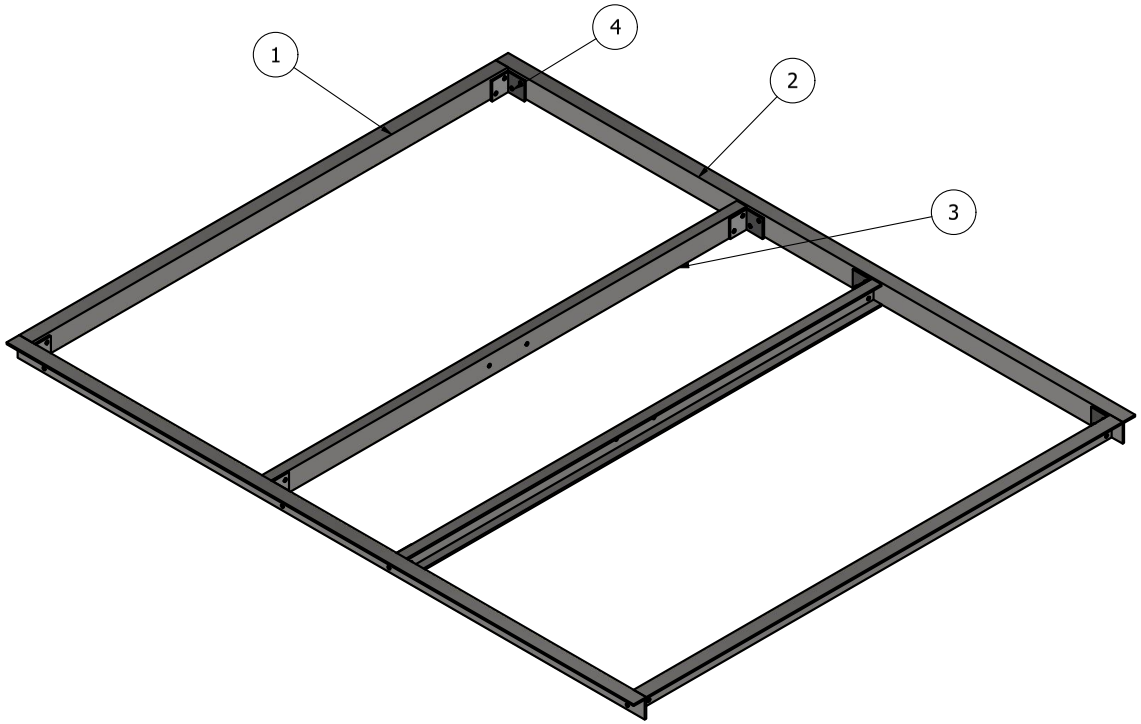

PARTS LIST				
ITEM	QTY	STOCK NUMBER	PART NUMBER	DESCRIPTION
1	2	East Member	P0012	300W
2	2	North Member	P0011	300W
3	2	Centre Beam	P0013	300W
4	8	Corner Cleats	P0014	300W

LIN TOL. (mm):
(0-250) ± 0.1
(250-500) ± 0.25
(500-1000) ±0.5

ANGULAR TOL.:
±0.25°

BREAK SHARP EDGES
ALL DIMENSIONS IN MM

Drawn by: K Mpurwana
Checked by: J Cawood
Approved by: J Cawood
Project: Solar Tracking System

NELSON MANDELA UNIVERSITY

Title: Main Frame
Material: -
Scale: 1 :12
Part Number: P0010
Rev: 0
Sheet size: A3
Sheet: 1

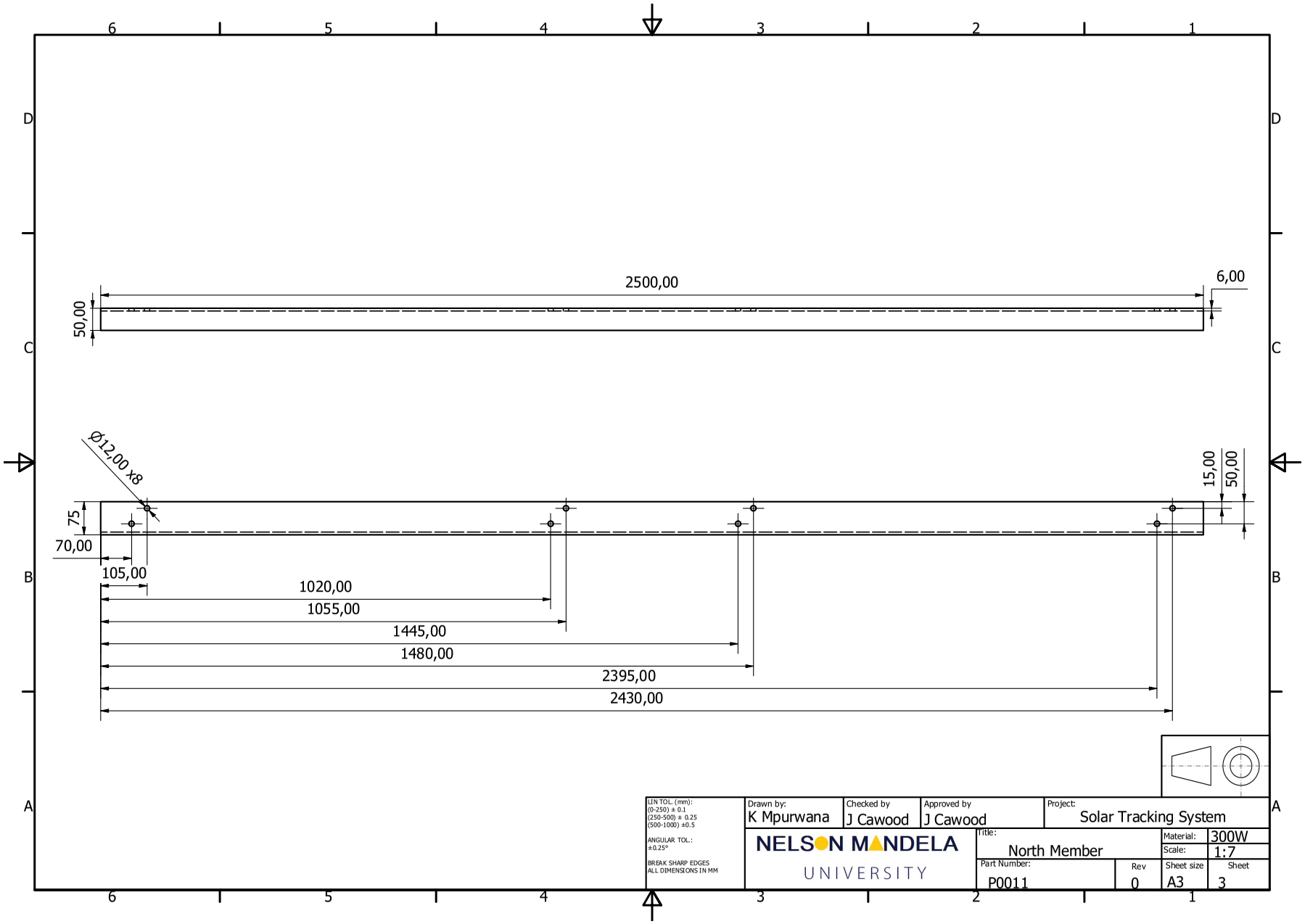

LIN TOL. (mm): (0-250) ± 0.1 (250-500) ± 0.25 (500-1000) ±0.5 ANGULAR TOL.: ±0.25° BREAK SHARP EDGES ALL DIMENSIONS IN MM	Drawn by: K Mpurwana	Checked by J Cawood	Approved by J Cawood	Project: Solar Tracking System
NELSON MANDELA UNIVERSITY	Title: North Member			Material: 300W Scale: 1:7
	Part Number: P0011	Rev 0	Sheet size A3	Sheet 3

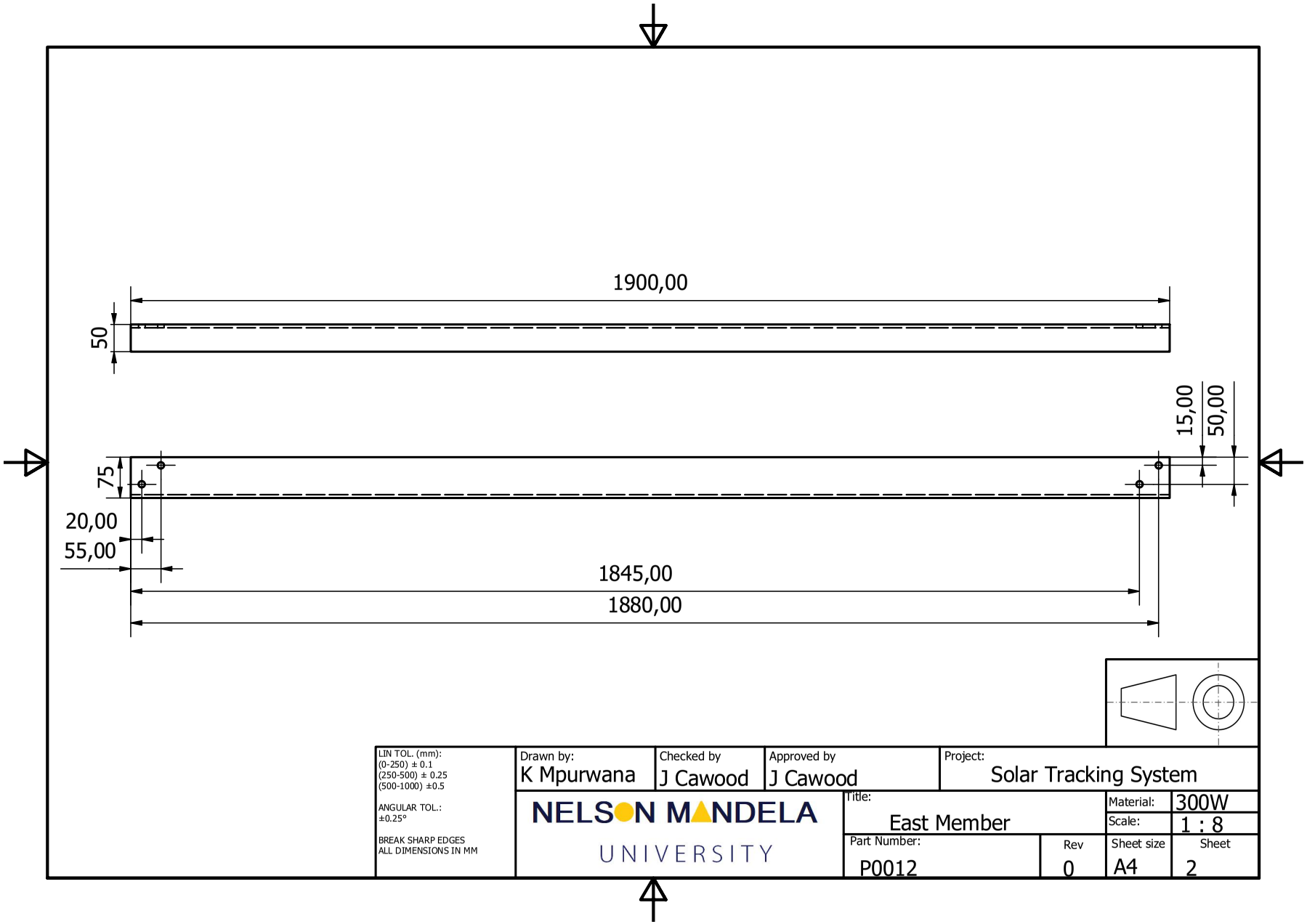

LIN TOL. (mm): (0-250) ± 0.1 (250-500) ± 0.25 (500-1000) ±0.5 ANGULAR TOL.: ±0.25° BREAK SHARP EDGES ALL DIMENSIONS IN MM	Drawn by: K Mpurwana	Checked by J Cawood	Approved by J Cawood	Project: Solar Tracking System		
NELSON MANDELA UNIVERSITY				Title: East Member	Material: Scale:	300W 1 : 8
				Part Number: P0012	Rev 0	Sheet size A4 / Sheet 2

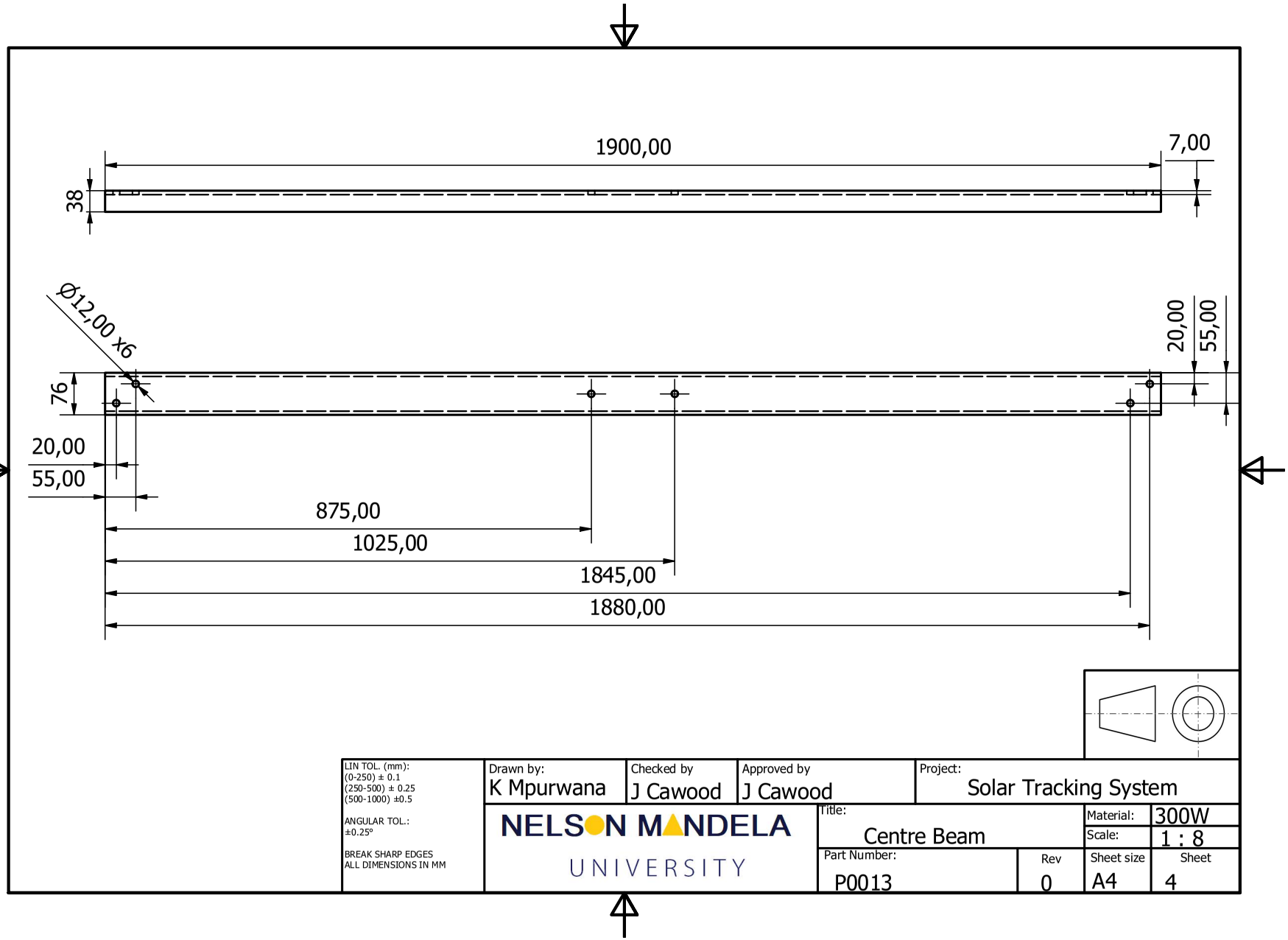

LIN TOL. (mm): (0-250) ± 0.1 (250-500) ± 0.25 (500-1000) ±0.5 ANGULAR TOL.: ±0.25° BREAK SHARP EDGES ALL DIMENSIONS IN MM	Drawn by: K Mpurwana	Checked by J Cawood	Approved by J Cawood	Project: Solar Tracking System		
NELSON MANDELA UNIVERSITY	Title: Centre Beam			Material: 300W	Scale: 1 : 8	
	Part Number: P0013	Rev 0		Sheet size A4	Sheet 4	

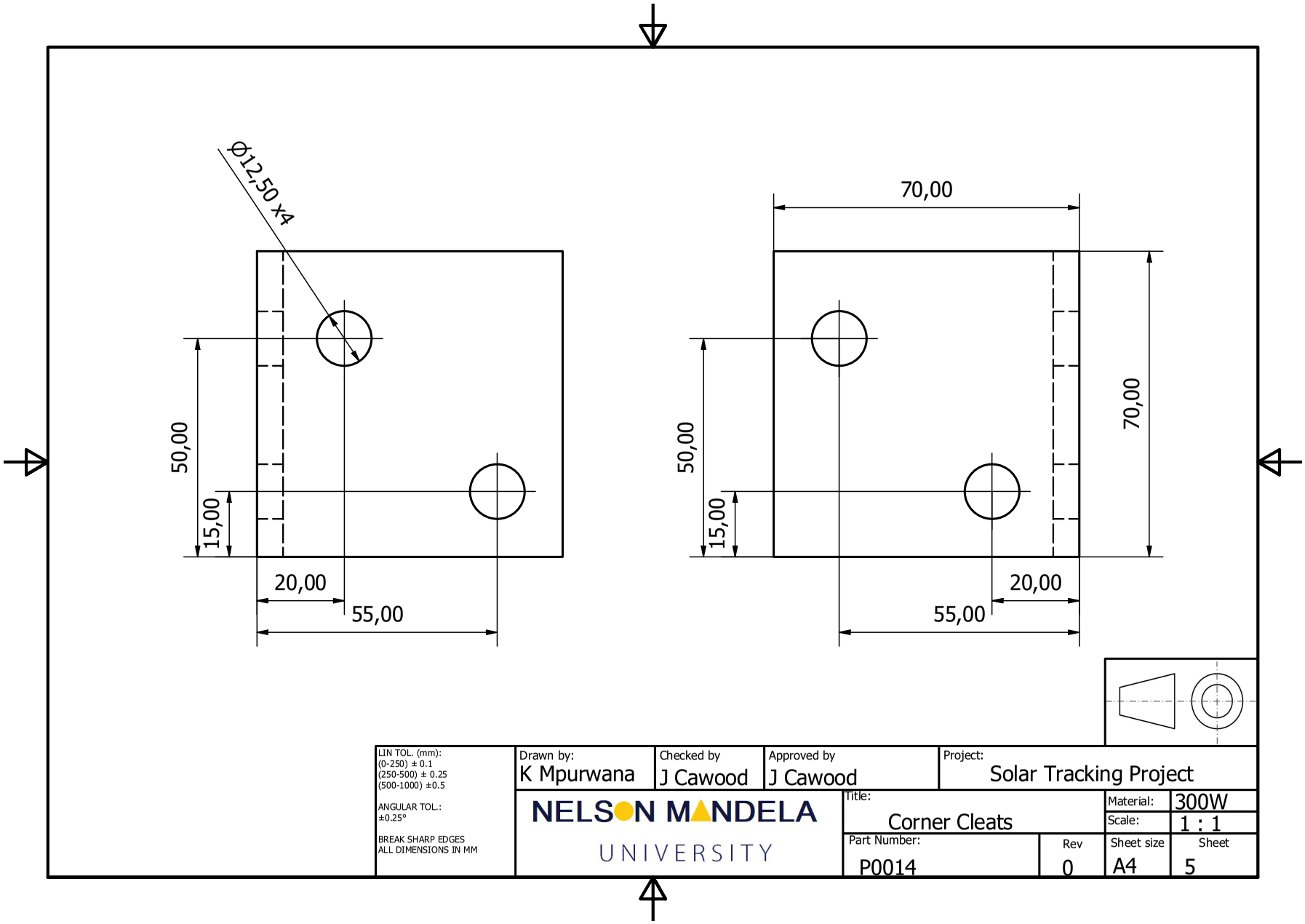

LIN TOL. (mm): (0-250) ± 0.1 (250-500) ± 0.25 (500-1000) ±0.5 ANGULAR TOL.: ±0.25° BREAK SHARP EDGES ALL DIMENSIONS IN MM	Drawn by: K Mpurwana	Checked by J Cawood	Approved by J Cawood	Project: Solar Tracking Project		
NELSON MANDELA UNIVERSITY	Title: Corner Cleats			Material: 300W	Scale: 1 : 1	
	Part Number: P0014	Rev 0	Sheet size A4	Sheet 5		

NELSON MANDELA UNIVERSITY

FACULTY OF ENGINEERING, THE BUILT ENVIRONMENT AND INFORMATION TECHNOLOGY

APPENDIX E - COST ESTIMATE
TO THE RESEARCH THESIS -

'Enhancement of domestic solar photovoltaic unit productivity through the use of a cost effective tracking system '

John Henry Cawood
Student Number: 213282909

The costing estimate **Table E** below reflects the landed cost of materials and manufactured components for the 650W tilt/tilt articulated platform with panels and hydraulic drive. Source of costing is **SEIFSA PIPS 4/2017** with compounded CPI up to December 2020.

Table E - Estimated costing - ZAR December 2020

					Processes							
Steel												
Description	**Unit mass**	**Quantity**	**Mass**	**Matl. Cost**	**Cut / shape**	**Weld**	**Machining**	**Galvanise**	**Transport**	**Proc. Cost**	**Comp. Cost**	
Square tube section 120 x 120 x6	21.478	2.000	42.955	902.06	0.200	0.500	0.000	558.42	180.41	850.27	1752.33	
Round 40	9.865	0.120	1.184	24.86	0.200	0.000	0.300	15.39	4.97	99.96	124.82	
Plate 12	94.200	0.040	3.768	79.13	0.500	0.500	0.500	48.98	15.83	303.61	382.74	
Rect tube 40 x 60	4.427	0.400	1.771	37.19	0.200	0.500	0.200	23.02	7.44	173.74	210.93	
Round 25 8.8	3.851	0.550	2.118	44.48	0.100	0.000	0.100	27.54	8.90	68.27	112.76	
Plate 10	78.500	0.056	4.396	92.32	0.200	0.100	1.000	57.15	18.46	282.57	374.89	
ULA 75 X 50 X 6	5.605	9.000	50.444	1059.33	1.000	0.000	1.000	655.77	211.87	1186.04	2245.36	
TFC 76 X 38	7.976	4.000	31.902	669.95	0.500	0.000	0.500	414.73	133.99	707.92	1377.87	
ELA 70 x 70 x 6	6.217	0.600	3.730	78.34	1.000	0.000	1.000	48.49	15.67	382.56	460.90	Sub - Steel
ELA 50 x 50 x 5	3.690	3.500	12.913	271.18	0.500	1.000	0.500	167.87	54.24	540.51	811.69	**7854.28**
Frame Components		**Quantity**	**Unit cost**	**Matl. Cost**	**Cut / shape**	**Weld**	**Machining**	**Galvanise**	**Transport**	**Proc. Cost**	**Comp. Cost**	
Bearings Flanged sphericals		4.000	185.000	740.00	0.000	0.000	0.000	0.00	14.80	14.80	754.80	
Bell crank assy		1.000	247.000	247.00	0.000	0.100	0.100	52.00	4.94	88.78	335.78	
Bell crank bearing		1.000	34.000	34.00	0.000	0.000	0.000	0.00	0.68	0.68	34.68	
Rod ends		2.000	55.000	110.00	0.000	0.000	0.000	0.00	2.20	2.20	112.20	
Threaded bar		1.000	65.000	65.00	0.000	0.000	0.000	0.00	1.30	1.30	66.30	Sub - Frame components
Fasteners		40.000	3.500	140.00	0.000	0.000	0.000	0.00	2.80	2.80	142.80	**1446.56**
Actuation components		**Quantity**	**Unit cost**	**Matl. Cost**	**Cut / shape**	**Weld**	**Machining**	**Galvanise**	**Transport**	**Proc. Cost**	**Comp. Cost**	
Pneumatic cylinder 63mm x 200mm		1.000	2320.000	2320.00	0.000	0.000	0.000	0.00	46.40	46.40	2366.40	
Pump		1.000	450.000	450.00	0.000	0.000	0.000	0.00	9.00	9.00	459.00	
Relay		1.000	35.000	35.00	0.000	0.000	0.000	0.00	0.70	0.70	35.70	
Wiring		1.000	120.000	120.00	0.000	0.000	0.000	0.00	2.40	2.40	122.40	
Cabinet		1.000	140.000	140.00	0.000	0.000	0.000	0.00	2.80	2.80	142.80	
Tubing		6.000	35.000	210.00	0.000	0.000	0.000	0.00	4.20	4.20	214.20	
Connectors		10.000	35.000	350.00	0.000	0.000	0.000	0.00	7.00	7.00	357.00	
Sensor frame		1.000	85.000	85.00	0.000	0.000	0.000	0.00	1.70	1.70	86.70	
Sensor PV cell		1.000	125.000	125.00	0.000	0.000	0.000	0.00	2.50	2.50	127.50	
Switch		1.000	36.000	36.00	0.000	0.000	0.000	0.00	0.72	0.72	36.72	Sub - Actuation
Clevis		1.000	155.000	155.00	0.000	0.000	0.000	0.00	3.10	3.10	158.10	**4106.52**
Panels		**Quantity**	**Unit cost**	**Matl. Cost**	**Cut / shape**	**Weld**	**Machining**	**Galvanise**	**Transport**	**Proc. Cost**	**Comp. Cost**	
325 W 48V PV		2.000	1840.000	3680.00	0.000	0.000	0.000	0.00	73.60	73.60	3753.60	Sub - Electrical
DC 48/12 converter		1.000	235.000	235.00	0.000	0.000	0.000	0.00	4.70	4.70	239.70	**3993.30**
Total landed cost - Materials and Manufacture												**17400.6622**

NELSON MANDELA UNIVERSITY

FACULTY OF ENGINEERING, THE BUILT ENVIRONMENT AND INFORMATION TECHNOLOGY

APPENDIX F - MODEL
TO THE RESEARCH THESIS -

'Enhancement of domestic solar photovoltaic unit productivity through the use of a cost effective tracking system '

John Henry Cawood
Student Number: 213282909

Guide to the model calculations -

Table F1

The first calculation, **Table F1** is made to determine the Northern Elevation (NE) of the payload platform using a mimic linkage of known lengths, relative to an assumed East Elevation (EE) angle. The adjustable linkage is part C. The philosophy is to provide a linkage with three possible drillings - the owner may prefer to improve production by altering the position of link C during the change of seasons, alternately he may prefer to set up once only on the Equinox position for the entire year and accept the alignment errors with their associated production losses.

The calculation is performed for the three milestone conditions, the summer and winter Solstices as well as for the interim Equinox period.

Table F2 and **Table F3** use known values of Azimuth and Elevation on the days of the solstices as inputs for conversion to values of East Elevation(EE) and North Elevation(NE) i.e. the degree of tilt of a tilt/tilt payload required to match the position of the sun at right angles. The calculation is anchored by the assumption that the East Elevation tracking is exact i.e. the Cosine of the error angle =1. This assumption is considered to be safe as the actual accuracy of the shaded PV sensor system has proven to be within 2° or Cosine of error angle = 0.999391. The calculation is applied for each hour of the solar day. The final columns relate the compounded error angle with the aperture error of a horizontal panel.
A second assumption made is that background radiation at the summer solstice has less relative effect on the calculation due to the tracked and horizontal panels having only 12° difference at noon, whereas in the winter situation the indirect attitude of the horizontal panel will allow it to benefit more from ambient radiation than it would in summer.

Table F1 - Linkage calculation to set North Elevation from given East Elevation

EQUINOX SETTINGS			NOON NE IS 54 DEGREES, PANEL ANGLE 36 DEGREES					
R=120, A=200, B=120, D=175 ONLY C IS ADJUSTABLE					AUG/SEP/OCT + FEB/MAR/APR			
EE	C	l1	x	l2	V	D	h	NE
60	130	65	112.583302	133.97761	198.97761	175	-1.0223899	-0.3254386
57	130	70.8030746	109.027174	136.88709	207.690164	175	7.6901644	2.44860063
54	130	76.4120828	105.172209	139.870677	216.28276	175	16.2827602	5.19005838
51	130	81.8116508	101.028975	142.892079	224.70373	175	24.7037297	7.88833848
48	130	86.9869788	96.6088273	145.916875	232.903854	175	32.9038541	10.5328473
45	130	91.9238816	91.9238816	148.912726	240.836608	175	40.8366077	13.1128678
42	130	96.6088273	86.9869788	151.849483	248.45831	175	48.4583104	15.6174314
39	130	101.028975	81.8116508	154.699237	255.728212	175	55.7282115	18.0351971
36	130	105.172209	76.4120828	157.436316	262.608525	175	62.6085253	20.3543486
33	130	109.027174	70.8030746	160.03726	269.064434	175	69.064434	22.5625186
30	130	112.583302	65	162.480768	275.064071	175	75.0640706	24.6467549
27	130	115.830848	59.018765	164.747642	280.57849	175	80.5784897	26.5935403
24	130	118.760909	52.8757636	166.820723	285.581632	175	85.5816325	28.3888824
21	130	121.365455	46.5878334	168.684836	290.050291	175	90.0502911	30.0184863
18	130	123.637347	40.1722093	170.326726	293.964073	175	93.9640732	31.4680235
15	130	125.570357	33.6464759	171.735013	297.30537	175	97.3053703	32.7234978
12	130	127.159188	27.0285198	172.900142	300.05933	175	100.05933	33.7717046
9	130	128.399484	20.3364805	173.814348	302.213832	175	102.213832	34.6007572
6	130	129.287846	13.5887002	174.471623	303.759469	175	103.759469	35.2006437
3	130	129.82184	6.80367431	174.867693	304.689532	175	104.689532	35.5637566
0	130	130	0	175	305	175	105	35.6853347
SUMMER SOLSTICE SETTING			NOON NE IS 78 DEGREES, PANEL ANGLE IS 12 DEGREES					
R=120, A=200, B=120, D=175 ONLY C IS ADJUSTABLE					NOV/DEC/JAN			
EE	C	l1	x	l2	V	D	h	NE
60	60	30	51.9615242	167.10775	197.10775	175	-2.8922503	-0.9206715
57	60	32.6783421	50.3202341	167.60929	200.287632	175	0.28763195	0.09155613
54	60	35.2671151	48.5410197	168.133189	203.400305	175	3.40030463	1.08241496
51	60	37.7592235	46.6287577	168.673528	206.432751	175	6.43275119	2.04804441
48	60	40.1478364	44.5886895	169.224256	209.372092	175	9.37209223	2.98457917
45	60	42.4264069	42.4264069	169.779268	212.205675	175	12.2056753	3.88817072
42	60	44.5886895	40.1478364	170.332473	214.921162	175	14.9211622	4.75500985
39	60	46.6287577	37.7592235	170.877854	217.506612	175	17.5066119	5.58135061
36	60	48.5410197	35.2671151	171.409541	219.95056	175	19.9505602	6.36353523
33	60	50.3202341	32.6783421	171.92186	222.242094	175	22.2420941	7.09802031
30	60	51.9615242	30	172.409396	224.370921	175	24.3709207	7.78140384
27	60	53.4603915	27.23943	172.86704	226.327431	175	26.3274313	8.41045293
24	60	54.8127275	24.4041986	173.290032	228.102759	175	28.1027592	8.98213191
21	60	56.0148256	21.502077	173.674007	229.688833	175	29.6888325	9.49363037
18	60	57.063391	18.5410197	174.01503	231.078421	175	31.0784208	9.94239068
15	60	57.9555496	15.5291427	174.309626	232.265176	175	32.2651756	10.3261343
12	60	58.688856	12.4747014	174.55481	233.243666	175	33.2436664	10.6428864
9	60	59.2613004	9.3860679	174.748109	234.00941	175	34.0094098	10.8909983
6	60	59.6713137	6.2717078	174.88758	234.558894	175	34.5588938	11.0691662
3	60	59.9177721	3.14015737	174.971825	234.889597	175	34.8895967	11.1764474
0	60	60	0	175	235	175	35	11.2122714
WINTER SOLSTICE SETTING			NOON NE IS 34 DEGREES, PANEL ANGLE IS 56 DEGREES					
R=120, A=200, B=120, D=175 ONLY C IS ADJUSTABLE					MAY/JUN/JUL			
EE	C	l1	x	l2	V	D	h	NE
60	170	85	147.224319	94.6044396	179.60444	175	-20.39556	-6.5060812
57	170	92.588636	142.573997	101.477365	194.066	175	-5.9339995	-1.889193
54	170	99.9234929	137.532889	108.211388	208.134881	175	8.13488061	2.5902952
51	170	106.984466	132.114813	114.763566	221.748032	175	21.7480324	6.93956812
48	170	113.752203	126.33462	121.097332	234.849535	175	34.8495346	11.163449
45	170	120.208153	120.208153	127.180973	247.389126	175	47.3891262	15.2643549
42	170	126.33462	113.752203	132.986602	259.321222	175	59.3212223	19.2422138
39	170	132.114813	106.984466	138.489436	270.60425	175	70.6042496	23.0943139
36	170	137.532889	99.9234929	143.667309	281.200198	175	81.2001977	26.8150646
33	170	142.573997	92.588636	148.500318	291.074315	175	91.0743147	30.395659
30	170	147.224319	85	152.970585	300.194904	175	100.194904	33.823635
27	170	151.471109	77.178385	157.06208	308.533189	175	108.533189	37.0823426
24	170	155.302728	69.1452293	160.760497	316.063224	175	116.063224	40.1503588
21	170	158.708673	60.9225514	164.05317	322.761843	175	122.761843	43.0009306
18	170	161.679608	52.532889	166.929014	328.608621	175	128.608621	45.6016101
15	170	164.20739	43.9992377	169.378473	333.585863	175	133.585863	47.9143463
12	170	166.285092	35.3449874	171.3935	337.678592	175	137.678592	49.8964124
9	170	167.907018	26.5938591	172.967531	340.874549	175	140.874549	51.5025978
6	170	169.068722	17.7698388	174.09547	343.164193	175	143.164193	52.6889528
3	170	169.767021	8.89711256	174.773686	344.540707	175	144.540707	53.4179215
0	170	170	0	175	345	175	145	53.6639425

Table F2 - Comparison of Actual vs Predicted alignments - Winter Solstice

Solar Position during winter solstice (EA Range 30 to 150 degrees)									PANEL			(EA matches actual by 5% angle error, Cos Error = 99.7% Cos error assumed = 1)											
time	Azimuth	Az Rad	Elevation	El Rad	Eq NA	NA	Eq EA	EA	EA	EA Sinus	C	I1	x	I2	V	D	h	NA			NA X EA	FLAT
9	33	0.57595865	6	0.10471976	0.19063617	10.9226482	0.12467245	7.14320541	7.14320541	7.14320541	130	16.1654657	128.990999	118.263783	134.429248		175	-65.570752	-21.3634		0.84539193	0.02356223
	36.6666667	0.63995406	8.33333333	0.1454441	0.24054305	13.7821013	0.18062315	10.3489441	10.3489441	10.3489441	130	23.3535405	127.885152	119.458729	142.812269		175	-57.187731	-18.524469		0.84520056	0.04279627
	40.3333333	0.70394946	10.6666667	0.18616845	0.28318611	16.2253688	0.24223151	13.8788429	13.8788429	13.8788429	130	31.1830452	126.204666	121.232761	152.415806		175	-47.584194	-15.328727		0.85214646	0.06702346
10	44	0.76794487	13	0.2268928	0.32086333	18.3841143	0.31055953	17.7937501	17.7937501	17.7937501	130	39.7268876	123.781155	123.706207	163.433094		175	-36.566906	-11.721193		0.86510497	0.09637925
	48	0.83775804	16.3333333	0.28507044	0.37561799	21.5213255	0.41279604	23.651471	23.651471	23.651471	130	52.1523698	119.080352	128.237552	180.389922		175	-19.610078	-6.2544961		0.88477771	0.14716897
	52	0.90757121	19.6666667	0.34324809	0.42579517	24.3962662	0.52596287	30.1354524	30.1354524	30.1354524	130	65.2659751	112.429322	134.106851	199.372826		175	-0.6271738	-0.199636		0.90926588	0.20736762
11	56	0.97738438	23	0.40142573	0.4732087	27.1128614	0.64929005	37.2015797	37.2015797	37.2015797	130	78.6007398	103.546722	141.078263	219.679003		175	19.6790029	6.27656728		0.93460055	0.27555287
	60.3333333	1.05301532	25	0.43633231	0.49253769	28.2203309	0.75560698	43.2930908	43.2930908	43.2930908	130	89.1449763	94.6212091	147.213541	236.358518		175	36.3585177	11.6534563		0.95848758	0.33425694
	64.6666667	1.12864625	27	0.4712389	0.51332941	29.4116086	0.87227185	49.9774957	49.9774957	49.9774957	130	99.5529488	83.6014974	153.739356	253.292305		175	53.292305	17.221612		0.97745278	0.37606529
12	69	1.20427718	29	0.50614548	0.53580781	30.6995262	0.99687641	57.1168107	57.1168107	57.1168107	130	109.171296	70.5806504	160.135479	269.306775		175	69.3067751	22.646077		0.99013781	0.42873735
	78.3333333	1.36717458	30.6666667	0.5352343	0.54443826	31.1940146	1.12413932	71.1693407	71.1693407	71.1693407	130	123.041968	41.9603868	169.895044	292.937012		175	92.9370121	31.085508		0.9999821	0.49021591
	87.6666667	1.53007198	32.3333333	0.56432312	0.56469804	32.3548144	1.50656593	86.3198695	86.3198695	86.3198695	130	129.731932	8.34421103	174.800956	304.532888		175	104.532888	35.502485		0.99849133	0.53405723
13	97	1.69296937	34	0.59341195	0.59688527	34.1990068	1.74954662	100.241637	100.241637	100.241637	130	127.928666	23.1139891	173.466837	301.395503		175	101.395503	34.2849022		0.99999888	0.5531134
	98.3333333	1.71624043	33	0.57595865	0.58081747	33.2783897	1.7903735	102.580845	102.580845	102.580845	130	126.878653	28.3162058	172.693927	299.57258		175	99.5725798	33.5855177		0.99998563	0.53553287
	99.6666667	1.73951149	32	0.55850536	0.56495194	32.369362	1.83331624	105.041283	105.041283	105.041283	130	125.546082	33.7369439	171.717264	297.263345		175	97.2633452	32.7075986		0.99998258	0.51703278
14	101	1.76278254	31	0.54105207	0.54927399	31.4710815	1.8782839	107.61774	107.61774	107.61774	130	123.90261	39.3464505	170.519374	294.421984		175	94.4219841	31.6390701		0.9999957	0.49758159
	106	1.85004901	30	0.52359878	0.54087317	30.9897499	2.01621561	115.520645	115.520645	115.520645	130	117.315913	56.0087176	165.795125	283.111039		175	83.1110387	27.498668		0.99814429	0.46464747
	111	1.93731547	29	0.50614548	0.53580781	30.6995262	2.14471625	122.883189	122.883189	122.883189	130	109.171296	70.5806504	160.135479	269.306775		175	69.3067751	22.646077		0.99013781	0.42873735
15	116	2.02458193	28	0.48869219	0.53420602	30.6077503	2.26027273	129.504088	129.504088	129.504088	130	100.305296	82.697325	154.227599	254.532896		175	54.5328956	17.6355066		0.97447893	0.3928556
	120.333333	2.10021287	25.6666667	0.44796784	0.50802776	29.1078465	2.38102617	136.422751	136.422751	136.422751	130	89.613152	94.1779326	147.497515	237.110667		175	37.1106673	11.8980202		0.95522763	0.33532899
	124.666667	2.1758438	23.3333333	0.40724349	0.48302607	27.6753552	2.49276049	142.824655	142.824655	142.824655	130	78.5533189	103.582702	141.051848	219.605167		175	19.6051673	6.25292349		0.93091289	0.28065359
16	129	2.25147474	21	0.36651914	0.45878845	26.2866416	2.59387743	148.618229	148.618229	148.618229	130	67.6959453	110.983147	135.306101	203.002046		175	3.00204643	0.95562536		0.90385107	0.23061518
	133	2.32128791	18	0.31415927	0.41808001	23.9542198	2.69698393	154.525796	154.525796	154.525796	130	55.9136083	117.361273	129.812679	185.726287		175	-14.273713	-4.5482392		0.87879663	0.17462533
	137	2.39110108	15	0.26179939	0.37436063	21.449284	2.79040561	159.878465	159.878465	159.878465	130	44.7216433	122.065452	125.399463	170.121106		175	-29.878894	-9.5549743		0.85712902	0.12579769
17	141	2.46091425	12	0.20943951	0.32572541	18.6626911	2.87461297	164.703191	164.703191	164.703191	130	34.2965137	125.394374	122.07068	156.367193		175	-43.632807	-14.028498		0.84159385	0.08442117
	144	2.51327412	8.66666667	0.15126187	0.2537337	14.53787	2.95536663	169.330035	169.330035	169.330035	130	24.0696945	127.752299	119.600795	143.67049		175	-56.32951	-18.236602		0.84080788	0.0464767
	147	2.565634	5.33333333	0.09308423	0.16975565	9.72628252	3.0307371	173.648445	173.648445	173.648445	130	14.3817234	129.202036	118.03319	132.414914		175	-67.585086	-22.053532		0.85007829	0.01868977
18	150	2.61799388	2	0.03490659	0.06972831	3.99513796	3.10129146	177.690911	177.690911	177.690911	130	5.23773766	129.894442	117.270772	122.508509		175	-77.491491	-25.499821		0.87039901	0.0028071
																				direct	17.3999462	7.04697735
																				ambient	0	1.73999462
																				increase	**1.98019821**	

Table F3 - Comparison of Actual vs Predicted alignments - Summer Solstice

Solar Position during summer solstice (EA Range 30 to 150 degrees)											PANEL		(EA matches actual by 5% angle error, Cos Error = 99.7% Cos error assumed = 1)												Cos Error	
time	Azimuth	Az Rad	Elevation	El Rad		Eq NA	NA	Eq EA	EA		EA	EA Sinus	C	I1	x	I2	V	D	h	NA					NE X EE	FLAT
6	-28	-0.4886922	0	0			0	0	0			0	60	3.6754E-15		60	164.392822	164.392822	175	-35.607178	101.40937				-0.1978177	3.7525E-33
	-26	-0.4537856	3.33333333	0.05817764		-0.1320895	7.56817227	0.06471121	3.70767894		3.70767894	3.70767894	60	3.87996307	59.8744176	60	164.438603	168.318566	175	-31.681434	100.137321				-0.0448251	0.00851689
	-24	-0.418879	6.66666667	0.11635528		-0.2798282	16.0329758	0.12725327	7.29107503		7.29107503	7.29107503	60	7.61460598	59.5148534	60	164.56908	172.183686	175	-27.816314	98.8898332				0.12434865	0.03505137
7	-22	-0.3839724	10	0.17453293		-0.4399333	25.2063231	0.18793063	10.7676317		10.7676317	10.7676317	60	11.2095815	58.9435771	60	164.774557	175.984139	175	-24.015861	97.66735				0.30135446	0.07956545
	-19.333333	-0.3374303	14	0.2443461		-0.6454901	36.9838609	0.25832446	14.8009014		14.8009014	14.8009014	60	15.3276581	58.0091622	60	165.105836	180.433494	175	-19.566506	96.2405437				0.51119284	0.15368277
	-16.666667	-0.2908882	18	0.31415927		-0.8476277	48.5654911	0.32699282	18.7353085		18.7353085	18.7353085	60	19.2717989	56.8207512	60	165.518586	184.790385	175	-15.209615	94.8471507				0.69111138	0.24080518
8	-14	-0.2443461	22	0.38397244		-1.0312761	59.0877657	0.39455956	22.6065977		22.6065977	22.6065977	60	23.0640978	55.3899575	60	166.002869	189.066967	175	-10.933033	93.4822359				0.82516802	0.32979939
	-11.666667	-0.2036217	26	0.45378561		-1.1777611	67.4807389	0.46206348	26.4742871		26.4742871	26.4742871	60	26.7477687	53.7080708	60	166.554625	193.302394	175	-6.6976063	92.1324065				0.90886035	0.41180456
	-9.3333333	-0.1628974	30	0.52359878		-1.2969529	74.309926	0.52938862	30.3317338		30.3317338	30.3317338	60	30.3003448	51.7869588	60	167.16193	197.462275	175	-2.5377251	90.8078097				0.95883022	0.48618853
9	-7	-0.122173	34	0.59341195		-1.392046	79.7583627	0.59688527	34.1990068		34.1990068	34.1990068	60	33.7241424	49.6254191	60	167.816322	201.540464	175	1.54046401	89.5096491				0.98555226	0.5531134
	-4.6333333	-0.0808669	38	0.66322512		-1.4677702	84.0970397	0.66481378	38.0910235		38.0910235	38.0910235	60	37.0147548	47.221901	60	168.508433	205.523188	175	5.523188	88.2416387				0.99738483	0.6136414
	-2.2666667	-0.0395608	42	0.73303829		-1.5268993	87.484885	0.73342752	42.0223017		42.0223017	42.0223017	60	40.165189	44.5730591	60	169.228374	209.393562	175	9.39356248	87.0085773				0.99996545	0.66877495
10	0.1	0.00174533	46	0.80285146		1.569111088	89.9034313	0.80285222	46.0000436		46.0000436	133.999956	60	43.1604197	41.6794694	60	169.964178	213.124598	175	13.1245978	85.8186001				0.99745968	0.71933931
	3.4	0.05934119	50.3333333	0.87848239		1.52165707	87.1845282	0.87934789	50.3829228		50.3829228	129.617077	60	46.2193933	38.2592169	60	170.766602	216.985995	175	16.9859952	84.5851328				0.99897105	0.76939337
	6.7	0.11693706	54.6666667	0.95411332		1.48827472	85.2718605	0.95734281	54.8517024		54.8517024	125.148298	60	49.0598835	34.5416826	60	171.557198	220.617081	175	20.6170814	83.4229443				0.99947938	0.81488223
11	10	0.17453293	59	1.02974426		1.46683415	84.0434059	1.03647827	59.3858307		59.3858307	120.614169	60	51.6369668	30.5552558	60	172.311858	223.948825	175	23.9488247	82.3541804				0.99956542	0.85596947
	16.6666667	0.29088821	63	1.09955743		1.42568988	81.686013	1.11669778	63.9820696		63.9820696	116.01793	60	53.919409	26.3191439	60	173.009545	226.928954	175	26.928954	81.3959462				0.99998718	0.8892124
	23.3333333	0.40724349	67	1.1693706		1.40422821	80.4563496	1.19914892	68.7061722		68.7061722	111.293828	60	55.9038212	21.7890517	60	173.638237	229.542058	175	29.5420578	80.553735				0.99999856	0.91883481
12	30	0.52359878	71	1.23918377		1.4003039	80.2315032	1.28099498	73.3956057		73.3956057	106.604394	60	57.4980396	17.1457119	60	174.158045	231.656084	175	31.6560844	79.870876				0.99998019	0.94440658
	46	0.80285146	73.3333333	1.27990812		1.35867973	77.8466143	1.365752	78.2518253		78.2518253	101.748175	60	58.7431176	12.2166337	60	174.573062	233.316179	175	33.3161792	79.3336271				0.99966323	0.95710896
	62	1.08210414	75.6666667	1.32063247		1.34890359	77.2864825	1.45140908	83.1596148		83.1596148	96.8403852	60	59.5729082	7.14623008	60	174.854029	234.426937	175	34.4269371	78.9736301				0.99956649	0.96853897
13	78	1.36135682	78	1.36135682		1.36580507	78.2548664	1.52663207	87.4695744		87.4695744	92.5304256	60	59.9414951	2.64899414	60	174.97995	234.921445	175	34.9214449	78.8132189				0.99995252	0.9781081
	97.3333333	1.69878714	77	1.34390352		1.34569713	77.1027658	-1.5413365	88.3120737		88.3120737	91.6879263	60	59.5739654	1.76733658	60	174.991076	234.965041	175	34.9650409	78.7990727				0.99956177	0.97434901
	116.666667	2.03621746	76	1.32645023		1.35156958	77.4392327	-1.4593617	83.615265		83.615265	96.384735	60	59.6278549	6.67224983	60	174.872757	234.500612	175	34.5006118	78.9497366				0.99965251	0.97001194
14	136	2.37364778	75	1.30899694		1.38676913	79.4560184	-1.3803849	79.0902287		79.0902287	100.909771	60	58.915587	11.3557743	60	174.631172	233.546759	175	33.5467594	79.2589315				0.99999408	0.96534636
	144	2.51327412	71.3333333	1.24500153		1.374773	78.7686907	-1.3039995	74.7136679		74.7136679	105.286332	60	57.8772203	15.8185768	60	174.283598	232.160819	175	32.1608185	79.7076286				0.99986573	0.94614677
	152	2.65290046	67.6666667	1.18100613		1.38027214	79.0837683	-1.2228319	70.0631057		70.0631057	109.936894	60	56.4041251	20.4590974	60	173.799958	230.204083	175	30.204083	80.3400422				0.99975963	0.92305831
15	160	2.7925268	64	1.11701072		1.40550394	80.5294439	-1.1410461	65.3771274		65.3771274	114.622873	60	54.5441914	24.9986237	60	173.205279	227.749471	175	27.7494708	81.1317016				0.99994476	0.8966795
	165	2.87979327	60.3333333	1.05301532		1.42442245	81.6133948	-1.067792	61.1799769		61.1799769	118.820023	60	52.5682961	28.9235932	60	172.593238	225.161534	175	25.1615339	81.9645195				0.99998122	0.86676925
	170	2.96705973	56.6666667	0.98901991		1.45707886	83.484469	-0.9960268	57.0681332		57.0681332	122.931867	60	50.3590579	32.6184808	60	171.933227	222.292285	175	22.2922854	82.8858796				0.99994543	0.83389659
16	175	3.05432619	53	0.9250245		1.50521395	86.2424066	-0.926856	53.1049354		53.1049354	126.895065	60	47.9841825	36.0210804	60	171.252684	219.236866	175	19.2368665	83.8649987				0.99913926	0.79801714
	178	3.10668607	48.6666667	0.84939357		1.54011001	88.2418037	-0.8496957	48.68398		48.68398	131.31602	60	45.064774	39.6127018	60	170.457719	215.522493	175	15.5224927	85.0528925				0.99845155	0.75072597
	181	3.15904595	44.3333333	0.77376264		-1.5529349	88.9766147	-0.7738388	44.3376957		44.3376957	135.662304	60	41.9331599	42.9139849	60	169.65682	211.589842	175	11.5898424	86.3082847				0.99891576	0.69877452
17	184	3.21140582	40	0.6981317		-1.4878545	85.2477844	-0.6993329	40.068823		40.068823	139.931177	60	38.6224385	45.9163069	60	168.868863	207.491301	175	7.49130114	87.6147559				0.9991468	0.64149444
	186.33333	3.25213017	36	0.62831853		-1.420115	81.3665944	-0.6312323	36.1669488		36.1669488	143.833051	60	35.4084043	48.4380522	60	168.162883	203.571287	175	3.57128694	88.8631495				0.99145271	0.58345321
	188.666667	3.29285452	32	0.55850536		-1.3341666	76.4421142	-0.5636791	32.2964359		32.2964359	147.703564	60	32.0579861	50.7177043	60	167.489446	199.547432	175	-0.4525681	90.144057				0.97154109	0.51941074
18	191	3.33357887	28	0.48869219		-1.2262507	70.2589919	-0.4964186	28.4426898		28.4426898	151.55731	60	28.576769	52.7576371	60	166.858119	195.434888	175	-4.5651125	91.4532763				0.93235987	0.44828808
	193.333333	3.37430322	24	0.41887902		-1.0928749	62.6171206	-0.4291249	24.5870481		24.5870481	155.412952	60	24.9645148	54.5598112	60	166.27756	191.242075	175	-8.7579251	92.7888352				0.86452302	0.3694552
	195.666667	3.41502757	20	0.34906585		-0.9324802	53.4271825	-0.3614103	20.707285		20.707285	159.292715	60	21.2156268	56.1239448	60	165.756155	186.971782	175	-13.028218	94.1506401				0.7578673	0.28397125
19	198	3.45575192	16	0.27925268		-0.7480322	42.8590873	-0.2928342	16.778161		16.778161	163.221839	60	17.3200129	57.4457758	60	165.302701	182.622714	175	-17.377286	95.5399904				0.6062535	0.19635052
	201	3.50811718	12	0.20943951		-0.5353481	30.6731886	-0.2238628	12.8263929		12.8263929	167.173607	60	13.3198602	58.5028318	60	164.931558	178.251418	175	-21.748582	96.9397444				0.40248219	0.11325
	204	3.56047167	8	0.13962634		-0.3326896	19.061708	-0.1526444	8.74587919		8.74587919	171.254121	60	9.12313806	59.3023469	60	164.645776	173.768914	175	-26.231086	98.379453				0.18536228	0.0496582
20	207	3.61283155	4	0.06981317		-0.152826	8.75628626	-0.0783202	4.48741473		4.48741473	175.512585	60	4.694407	59.8160726	60	164.459835	169.154242	175	-30.845758	99.8672111				-0.0193881	0.01191064
																								direct	27.8937088	22.5056462
																								ambient	0	0
																								increase	1.23940937	

Postscript

Values measured during the solar day during September 2020 indicate an improvement of the energy absorbed by the tracked cell vs the horizontal cell to be in the region of 58% at the equinox. Considering our assumption of summertime background radiation having little effect on the horizontal panel, the effect during the equinox would be the midpoint between summertime and wintertime improvements, implying a wintertime background radiation advantage of 11.2% and not the assumed 10%.

NELSON MANDELA UNIVERSITY

FACULTY OF ENGINEERING, THE BUILT ENVIRONMENT AND INFORMATION TECHNOLOGY

APPENDIX G - CONVERSION OF AZIMUTH AND ELEVATION TO POLAR ELEVATIONS EA AND NA-
TO THE RESEARCH THESIS -

'Enhancement of domestic solar photovoltaic unit productivity through the use of a cost effective tracking system '

John Henry Cawood
Student Number: 213282909

CONTENT

Notation

Symbol	*Description*
A	Conventional azimuth angle
α	Converted azimuth angle
θ	Elevation angle

1. Introduction

The basis of the authors original research stems from the productivity gains to be made from solar tracking of PV installations on the one hand and the need for a simple and preferably independently passive system to actuate and position panels to follow the solar path.

The paper provides the proof and conversion equations for adapting historical and seasonal azimuth and altitude records to their polar equivalents for setting up the range and calibrations of a tilt/tilt installation.
The use of tilt/tilt systems appear to be an option of choice for small scale installations due to their reduced land footprint and higher production per unit area.

This article is written from a southern hemisphere perspective to address the sun's northerly arc, readers in the northern hemisphere will need to exchange the descriptions to cater for the sun's southerly arc from their perspective.

2. Concepts to define the position of the sun

2.1. Traditional measurements

The convention of Azimuth is the radial angle of the sun position about true North, thus North is the zero position and the azimuthal angle increases in a clockwise direction past East, South and West until 360 degrees coincides again with 0 degrees in the Northern direction. This is easily measured with a compass if the magnetic declination is known and accurate.
Elevation is the angle between the horizon and the sun, measured on the azimuthal line.
The ideal tracking solution at any time and date can be read from a polar plot of Azimuth (radial axis) against Elevation (concentric axis) for that particular day. These values have been used by travellers and mariners for centuries for time and navigation purposes. Historical sun position data is stored in this format.
To interpret the above measurements and historical data into useful units for a Tilt/Tilt system requires that the values are converted to two polar measures which describe arcs in the East to West direction and the North to South direction.

2.2. The two altitude notation

The primary axis is the largest movement and is the vertical arc corresponding to the East/West daily path of the sun irrespective of its northerly bias due to its seasonal limits, i.e. it assumes that the sun passes directly overhead every day. This axis is deemed to be the East Altitude (EA), where 0EA faces directly due East, 90EA is vertical at solar noon and 180EA faces directly West. With the knowledge that one unit of EA equals one degree of arc, the degree symbol is omitted for simplicity.

The secondary axis describes the sun's angle above the horizon strictly in the northerly direction, irrespective of the azimuth angle. At sunrise and sunset this angle is small and grows until its vertex is reached at true noon, according to the day of the year. At solar noon this angle corresponds to the conventional Elevation data between winter solstice and summer solstice. This angle is designated North Altitude (NA) where 0NA faces the horizon and 90NA is vertical. The position 90NA meets 90EA directly above the observer. Again the degree symbol is omitted for the polar terms.

At any time, the sun position can be accurately described by a two-part angular solution which would appear as, for example, 45EA16NA, indicating that the sun position coincides with 45 degrees above the East horizon and 16 degrees above the North horizon. A solar payload adjusted in two planes normal to these values will face the sun at right angles.

Degrees of arc are stated as round numbers, fractions of a degree are rounded to the nearest whole number. This is due to the negligible value of fractions of a degree when considered as change in PV output. A 0.5 degree alignment error changes the PV output by the Cosine of that angle, a value of 3.8×10^{-3} %.

2.3. Preparation of historical data

To enable conversion the conventional values of both Elevation and Azimuth need to be known. Symbol θ is assigned to Elevation and symbol A is assigned to Azimuth. It is assumed the observer is at ground level on an infinite horizontal plane at a point designated 'O'.

During a solar day in the southern hemisphere, the conventional azimuth angle at sunrise originates around 90° or due East, the exact angle being dependent on season and latitude of the site. This angle then recedes as the sun path veers northwards, at solar noon the azimuth is 0° (and 360°) or due North, whereupon the angle counts down from 360° to around 270° at sunset. To simplify this notation, the conventional azimuth angle A is converted to the value α which originates due East or 0° and increases anti-clockwise throughout the day to 180° at sunset.

To convert from standard azimuth data, the historical morning values between 90° and 0° (360°) are modified by -

$$\alpha = \sqrt{((\text{morning A} - 90)^2)}$$

Afternoon values of azimuth between 360° and 270° are modified by -

$$\alpha = \sqrt{((\text{afternoon A} - 270)^2 + 90)}$$

These changes produce a range of modified azimuth values that progress from around 0° to around 180° progressively during the day which are in a form conducive to further computation.

The historical data for elevation exists in the form of degrees of arc above the horizon and is used as is, assigned the symbol θ.

3. Conversion of converted azimuth angles to polar units of EA

With reference to **Figure 2**, consider a vertical right angled triangle with its base along the azimuthal line for an assumed base length of R linear units, i.e. the base originates at the observer and ends after R units at a right angle, point 'V', which then extends vertically. From the observer, point 'O', the elevation line extends directly towards the sun until it intersects the vertical line at point 'S'. These lines form a triangle SOV with angle SOV = θ, co-incident with the conventional elevation angle.

The importance of line VS is that it establishes the universal height of the sun above the horizontal plane relative to line length R and which is common in all directions.
Deductions made from this triangle of known dimensions are -

OS = R / Cos θ

VS = R Tan θ

Figure 2- Conventional Azimuth-Elevation triangle

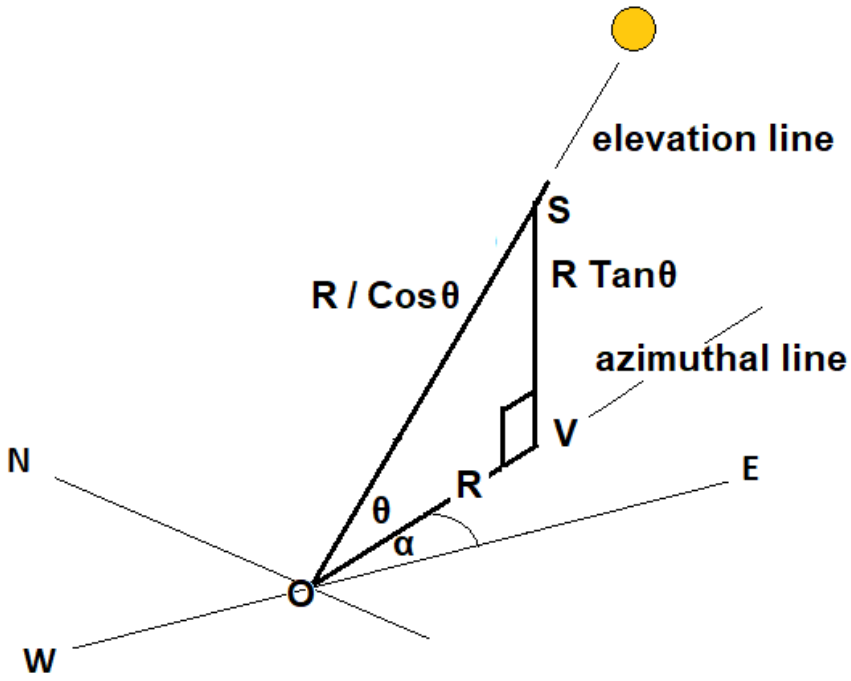

The second relationship as illustrated in **Figure 3** is a horizontal triangle bounded by the line VO and a line due East from the observer and terminating at point E which is level with point V and forms the triangle EOV where angle EOV = α. Deductions made from this triangle are -

OE = R Cos α

The height of VS is projected across to a position above point E, creating the vertical component of the East Altitude triangle.

Figure 3 - Basis of EA triangle

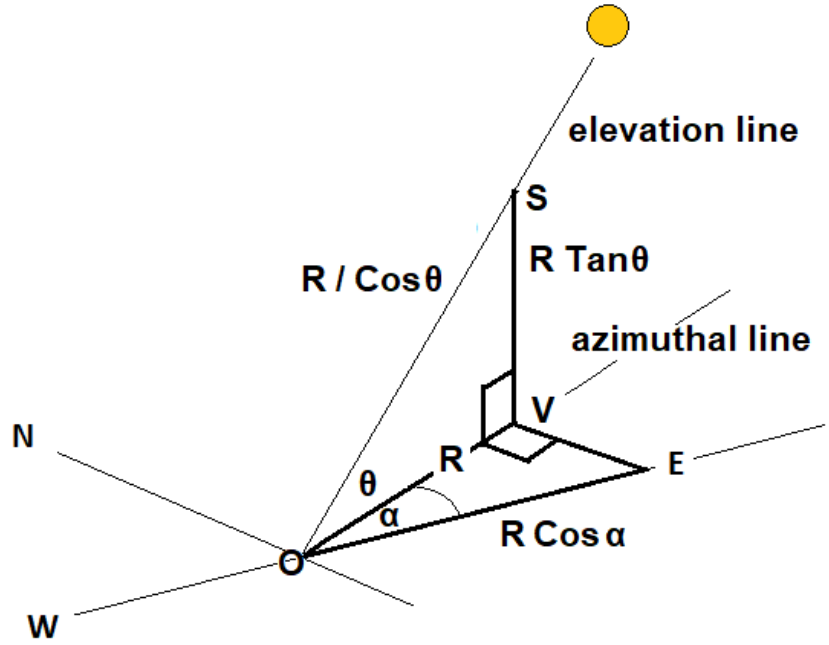

Angle EA is found as -

$$EA = Tan^{-1} (VS / OE)$$

Condensing the process -

$$\mathbf{EA = Tan^{-1} (Tan\ \theta / Cos\ \alpha) \quad . \ . \ . \ . \ . \ (2.1)}$$

Figure 4 - The EA triangle

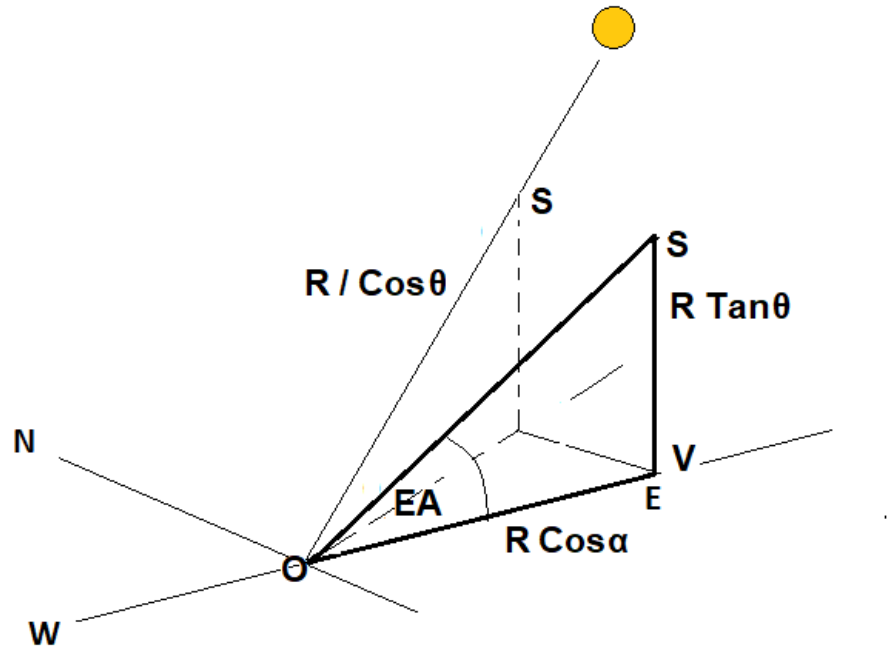

4.0 Conversion of elevation to polar units of NA

A similar exercise is followed to determine the angle NA, whereby the horizontal triangle is bounded by line VO and a line running North from O and ending level with the northern extent of VO at point N, the included angle being (90 - α). It is clear that the shape of the base ONVE is a rectangle. This is illustrated in **Figure 5**.

The line ON is defined as -

ON = R Cos (90 - α)

also -

ON = R Sin α

The equivalent northerly elevation is determined using the universal height VS and the base ON -

$NA = Tan^{-1} (VS / ON)$

$NA = Tan^{-1} (Tan \theta / Sin \alpha)$ . . (2.2)

Figure 5 - The NA triangle

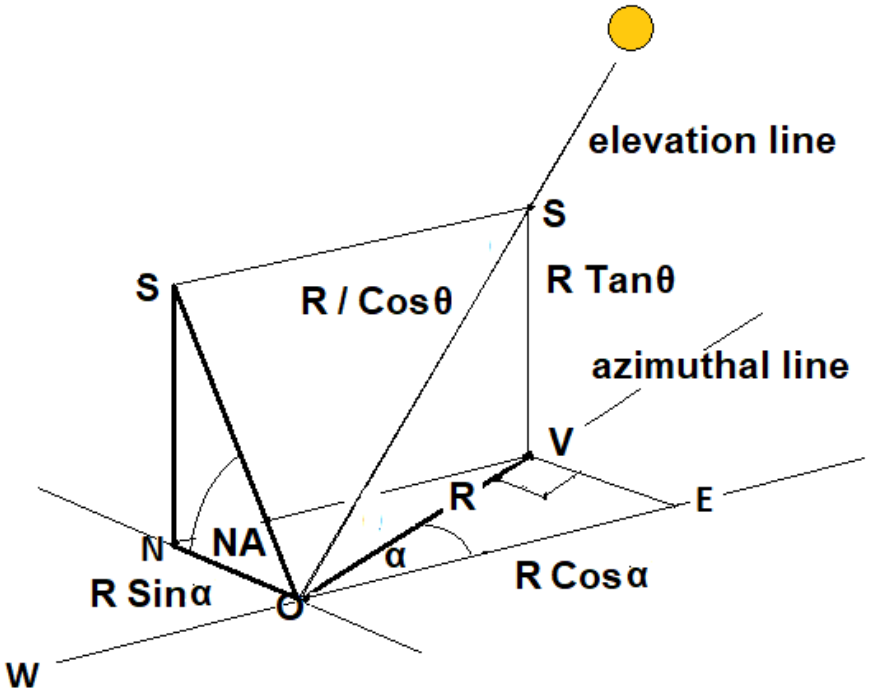

Through the use of equations **2.1** and **2.2**, historical data can be converted to polar units of EA and NA to relate to a tilt/tilt solar payload.

NELSON MANDELA UNIVERSITY

FACULTY OF ENGINEERING, THE BUILT ENVIRONMENT AND INFORMATION TECHNOLOGY

H - PROPRIETARY PART DRAWINGS - APPENDIX TO THE RESEARCH THESIS -

'Enhancement of domestic solar photovoltaic unit productivity through the use of a cost effective tracking system '

John Henry Cawood

Student Number: 213282909

DRAWING LIST

H0001- Hydraulic cylinder

H0001A Exploded view of cylinder

H0001B Seal mould

H0010 Rod end plug

H0011 Piston rod

H0012 Front bushing

H0013 Bearing

H0014 Piston

H0015 O-ring

H0016 Back Bush

H0017 Body tube

H0018 Mould cap

H0019 Positioning tube

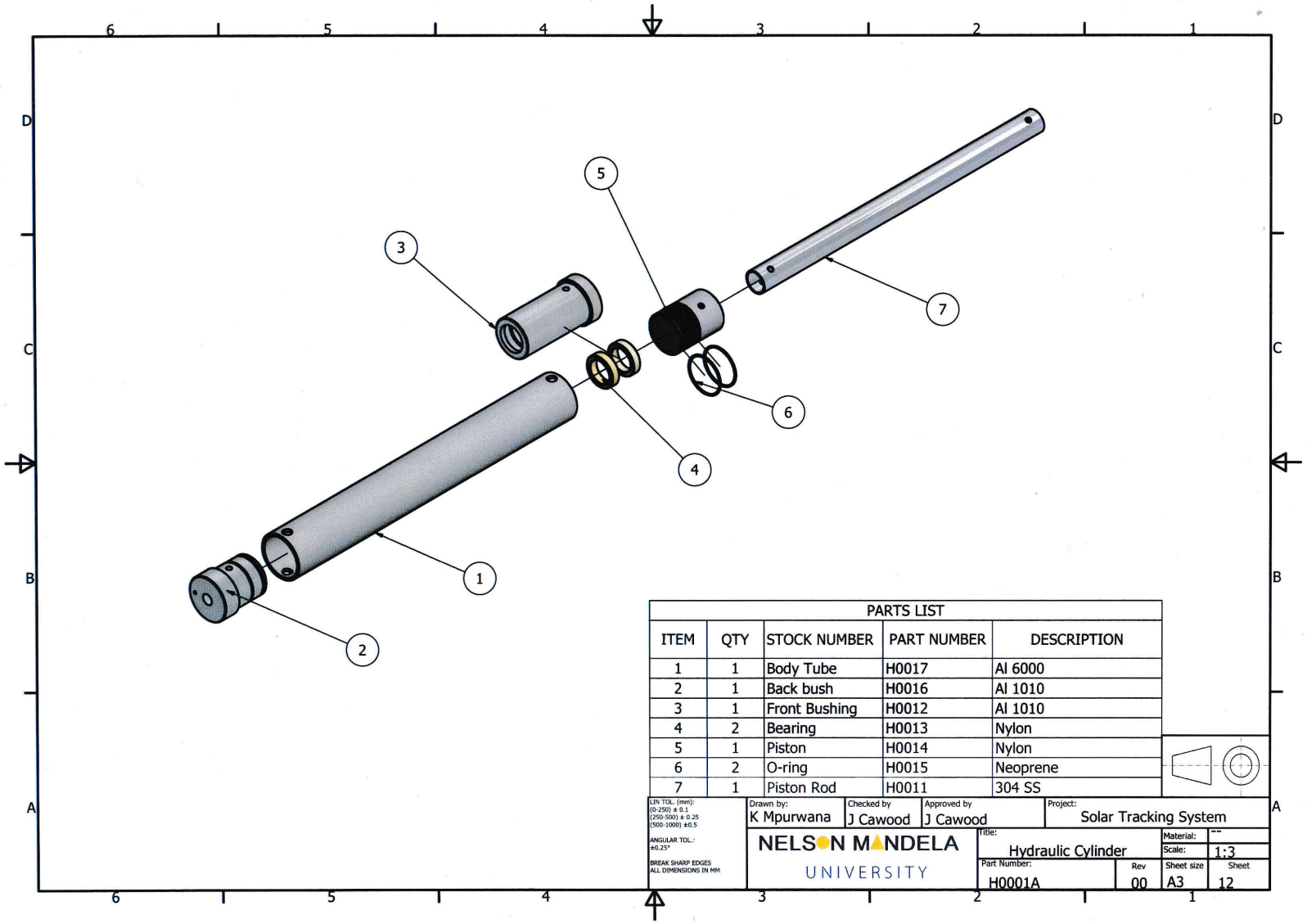

PARTS LIST				
ITEM	QTY	STOCK NUMBER	PART NUMBER	DESCRIPTION
1	1	Body Tube	H0017	Al 6000
2	1	Back bush	H0016	Al 1010
3	1	Front Bushing	H0012	Al 1010
4	2	Bearing	H0013	Nylon
5	1	Piston	H0014	Nylon
6	2	O-ring	H0015	Neoprene
7	1	Piston Rod	H0011	304 SS

LIN TOL. (mm):
(0-250) ± 0.1
(250-500) ± 0.25
(500-1000) ±0.5

ANGULAR TOL.:
±0.25°

BREAK SHARP EDGES
ALL DIMENSIONS IN MM

Drawn by: K Mpurwana	Checked by J Cawood	Approved by J Cawood	Project: Solar Tracking System

NELSON MANDELA UNIVERSITY

Title: Hydraulic Cylinder		Material:	--
		Scale:	1:3
Part Number: H0001A	Rev 00	Sheet size A3	Sheet 12

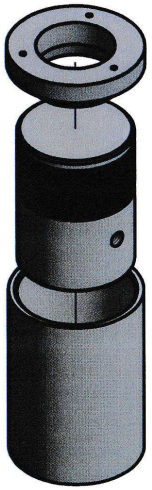

Notes: Seal Casting Procedure

1. Place positioning tube on a level surface.
2. Wet the internal bore with a light mineral oil.
3. Wipe off excess oil. Similarly treat the cap.
4. Wash down the piston crown with alcohol or lacquer thinner.
5. Insert the piston crown uppermost into the tube using latex gloves. Ensure no oil contaminates the crown.
6. Fill the cavity above the crown with high grade Silicone rubber solution. Ensure no air cavities and full wetting of the the crown.
7. Place the cap onto the tube and press down until the spigot seats. Scoop out excess material from the centre and allow to set.
8. Allow 48 hours before dismantling. Prise the seal edges free and push the piston out from behind.

PARTS LIST				
ITEM	QTY	STOCK NUMBER	PART NUMBER	DESCRIPTION
1	1	Positioning Tube	H0019	Al 1010
2	1	Piston	H0014	Nylon
3	1	Cap	H0018	Al 1010

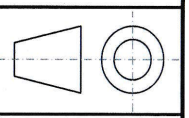

LIN TOL. (mm):
(0-250) ± 0.1
(250-500) ± 0.25
(500-1000) ±0.5

ANGULAR TOL.:
±0.25°

BREAK SHARP EDGES
ALL DIMENSIONS IN MM

Drawn by:	Checked by	Approved by	Project:
K Mpurwana	J Cawood	J Cawood	Solar Tracking System

NELSON MANDELA UNIVERSITY

Title:		Material:	-
Seal mold		Scale:	1 : 2
Part Number: H0001B	Rev 00	Sheet size A4	Sheet 11

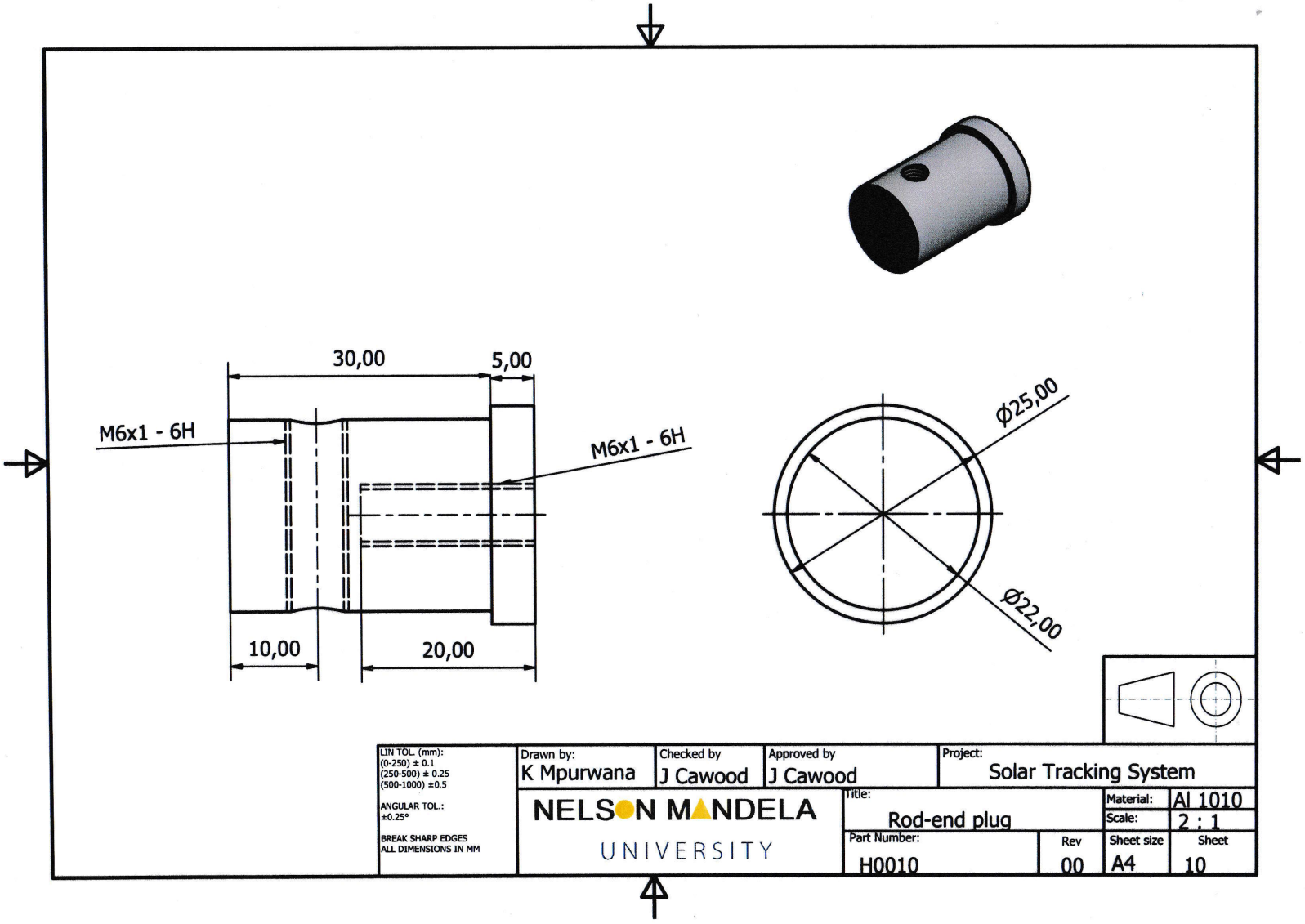

LIN TOL. (mm): (0-250) ± 0.1 (250-500) ± 0.25 (500-1000) ±0.5 ANGULAR TOL.: ±0.25° BREAK SHARP EDGES ALL DIMENSIONS IN MM	Drawn by: K Mpurwana	Checked by J Cawood	Approved by J Cawood	Project: Solar Tracking System	
NELSON MANDELA UNIVERSITY	Title: Rod-end plug			Material: Al 1010	Scale: 2 : 1
	Part Number: H0010	Rev 00	Sheet size A4	Sheet 10	

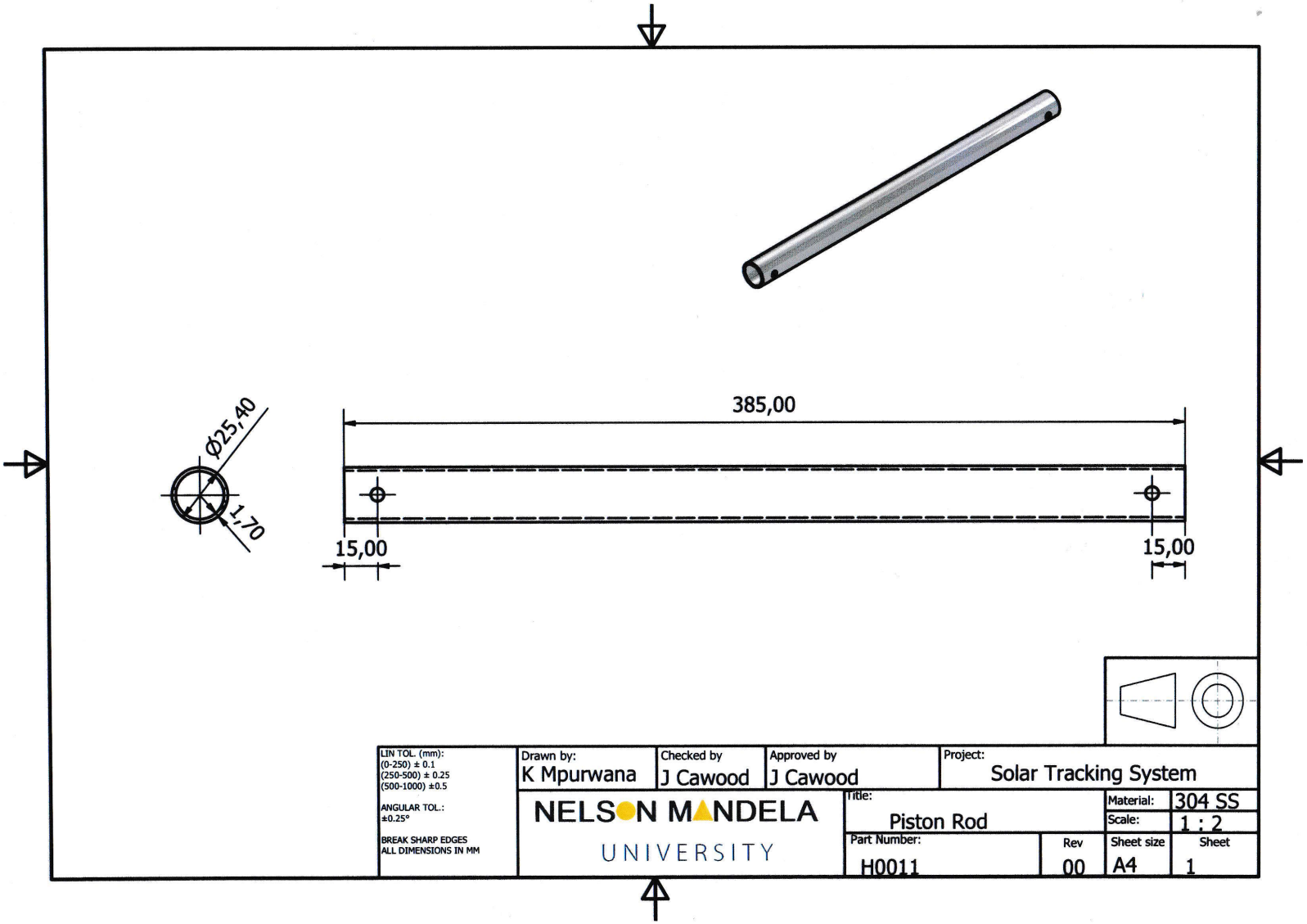

LIN TOL. (mm): (0-250) ± 0.1 (250-500) ± 0.25 (500-1000) ±0.5 ANGULAR TOL.: ±0.25° BREAK SHARP EDGES ALL DIMENSIONS IN MM	Drawn by: K Mpurwana	Checked by J Cawood	Approved by J Cawood	Project: Solar Tracking System		
NELSON MANDELA UNIVERSITY	Title: Piston Rod			Material: 304 SS		
				Scale: 1 : 2		
	Part Number: H0011	Rev 00		Sheet size A4	Sheet 1	

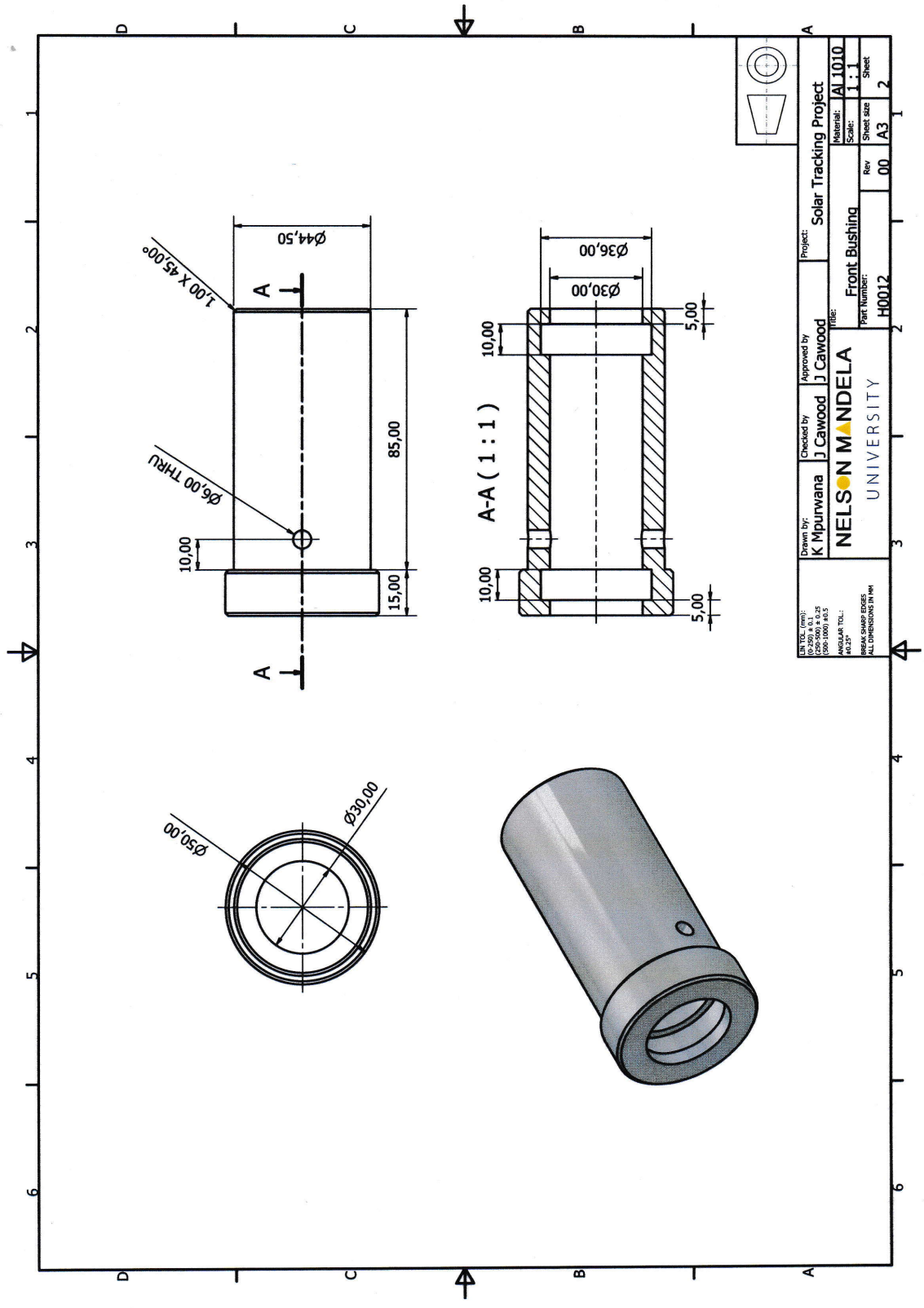
Ø44,50
1,00 X 45,00°
A
Ø6,00 THRU
10,00
85,00
15,00
A
A-A (1 : 1)
Ø36,00
Ø30,00
10,00
5,00
10,00
5,00
Ø50,00
Ø30,00
Drawn by: K Mpurwana
Checked by J Cawood
Approved by J Cawood
Project: Solar Tracking Project
Title: Front Bushing
Material: AL1010
Scale: 1 : 1
Sheet size A3
Sheet 2
Part Number: H0012
Rev 00
NELSON MANDELA UNIVERSITY
LIN TOL. (mm): (0-250) ± 0.1 (250-500) ± 0.25 (500-1000) ±0.5
ANGULAR TOL.: ±0.25°
BREAK SHARP EDGES
ALL DIMENSIONS IN MM

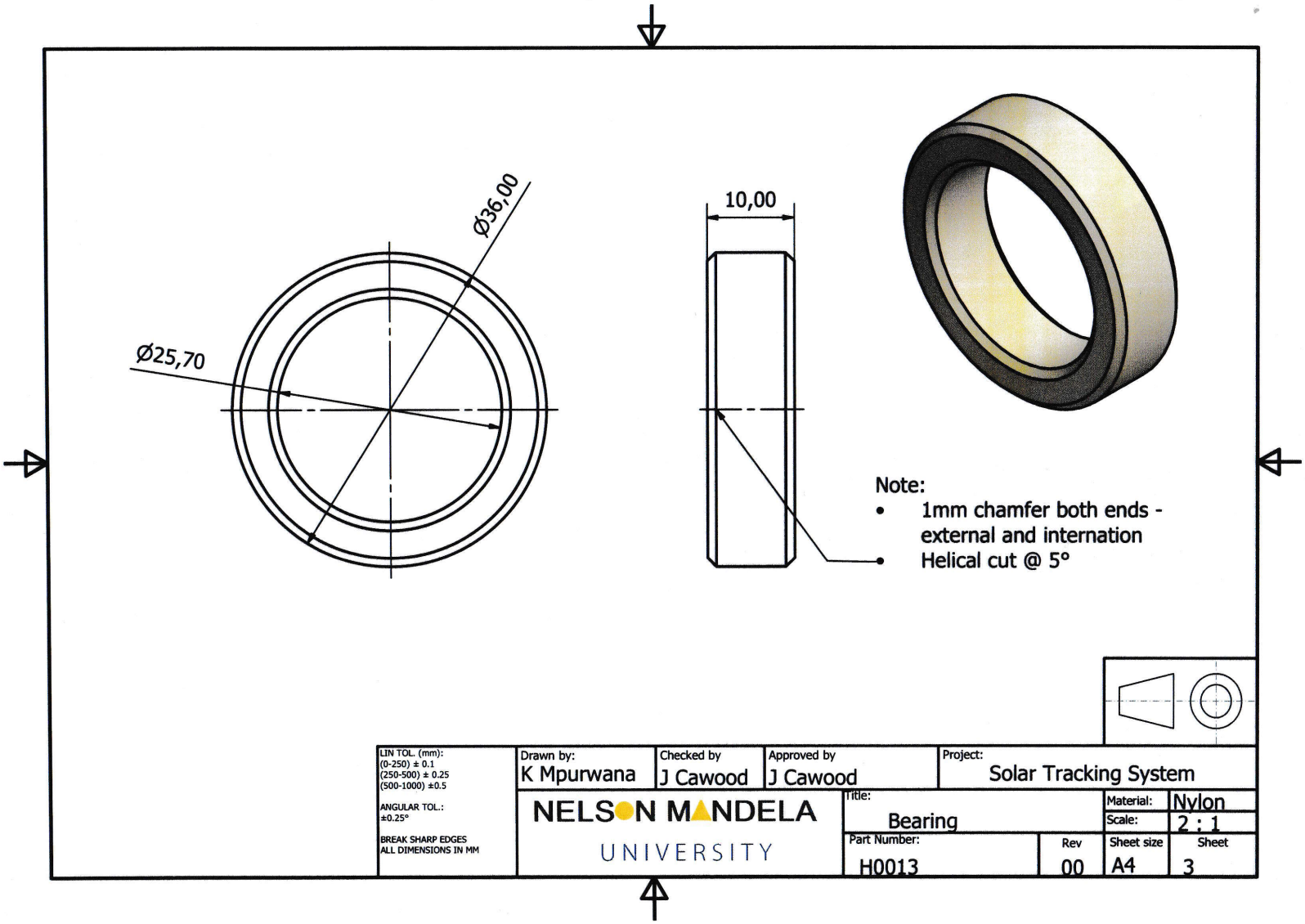
Ø36,00
Ø25,70
10,00
Note:
• 1mm chamfer both ends - external and internation
• Helical cut @ 5°
LIN TOL. (mm):
(0-250) ± 0.1
(250-500) ± 0.25
(500-1000) ±0.5
ANGULAR TOL.:
±0.25°
BREAK SHARP EDGES
ALL DIMENSIONS IN MM
Drawn by: K Mpurwana
Checked by J Cawood
Approved by J Cawood
Project: Solar Tracking System
NELSON MANDELA UNIVERSITY
Title: Bearing
Material: Nylon
Scale: 2 : 1
Part Number: H0013
Rev 00
Sheet size A4
Sheet 3

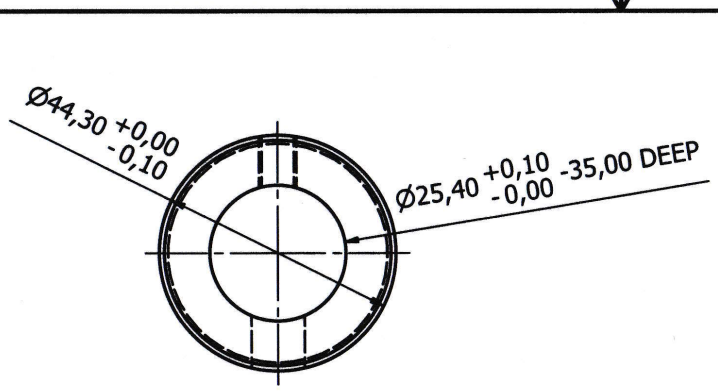

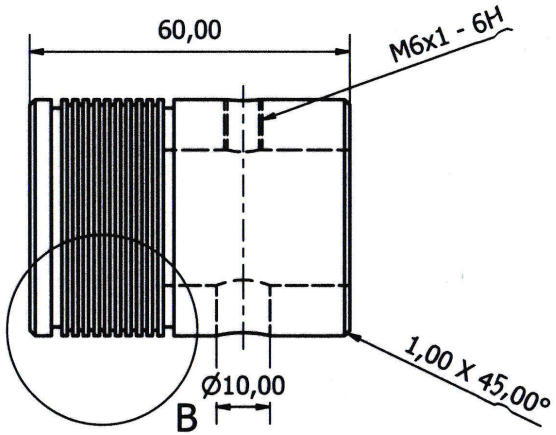

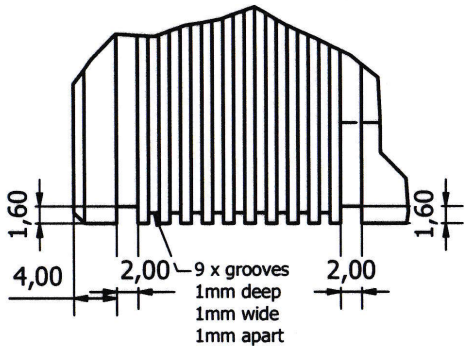

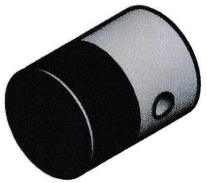

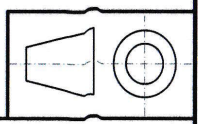

LIN TOL. (mm): (0-250) ± 0.1 (250-500) ± 0.25 (500-1000) ±0.5 ANGULAR TOL.: ±0.25° BREAK SHARP EDGES ALL DIMENSIONS IN MM	Drawn by: K Mpurwana	Checked by J Cawood	Approved by J Cawood	Project: Solar Tracking System
NELSON MANDELA UNIVERSITY	Title: Piston		Material: Nylon	Scale: 1 : 1
	Part Number: H0014	Rev 00	Sheet size A4	Sheet 4

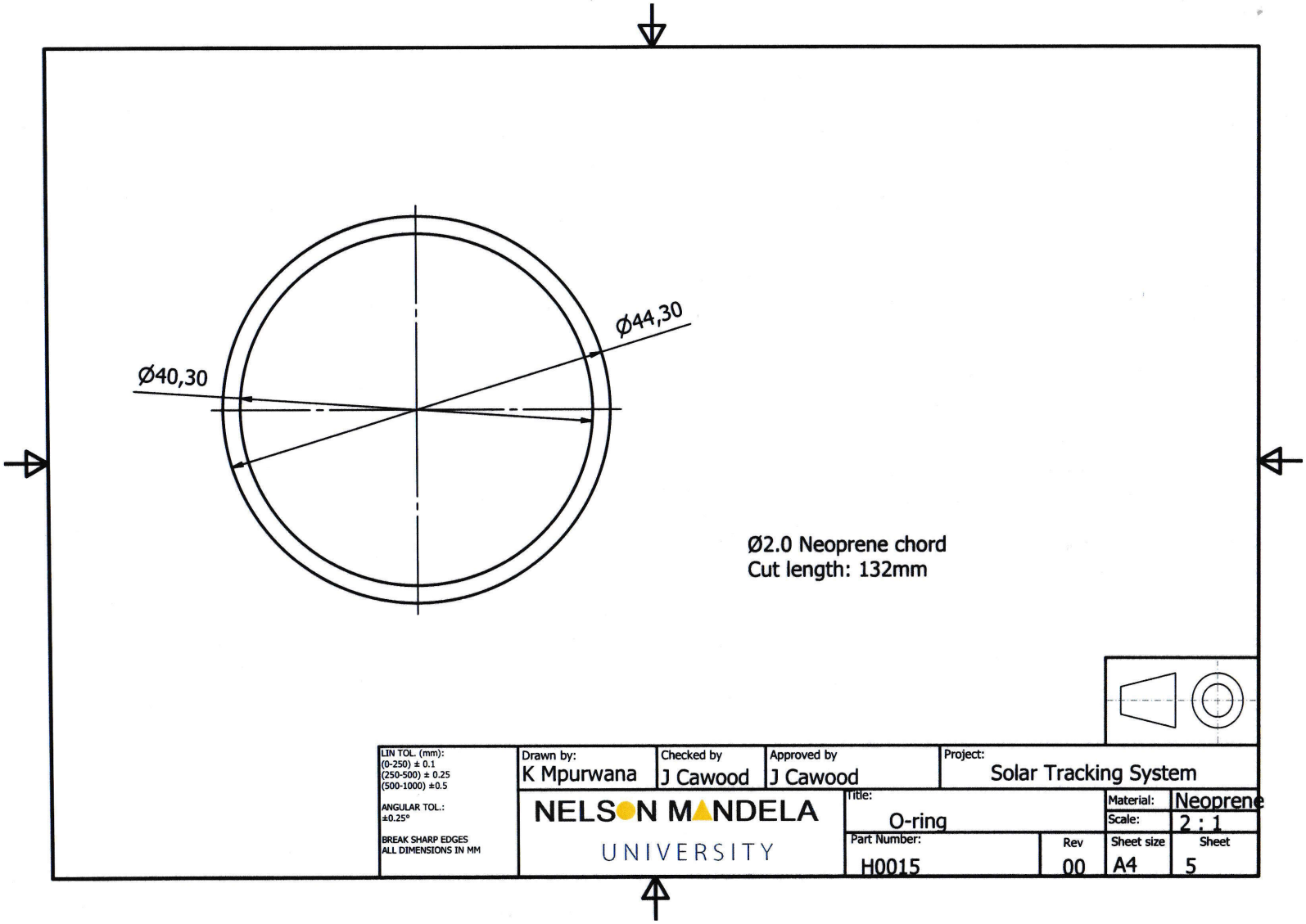
Ø40,30
Ø44,30
Ø2.0 Neoprene chord
Cut length: 132mm
LIN TOL. (mm):
(0-250) ± 0.1
(250-500) ± 0.25
(500-1000) ±0.5
ANGULAR TOL.:
±0.25°
BREAK SHARP EDGES
ALL DIMENSIONS IN MM
Drawn by:
K Mpurwana
Checked by
J Cawood
Approved by
J Cawood
Project:
Solar Tracking System
NELSON MANDELA
UNIVERSITY
Title:
O-ring
Material:
Neoprene
Scale:
2 : 1
Part Number:
H0015
Rev
00
Sheet size
A4
Sheet
5

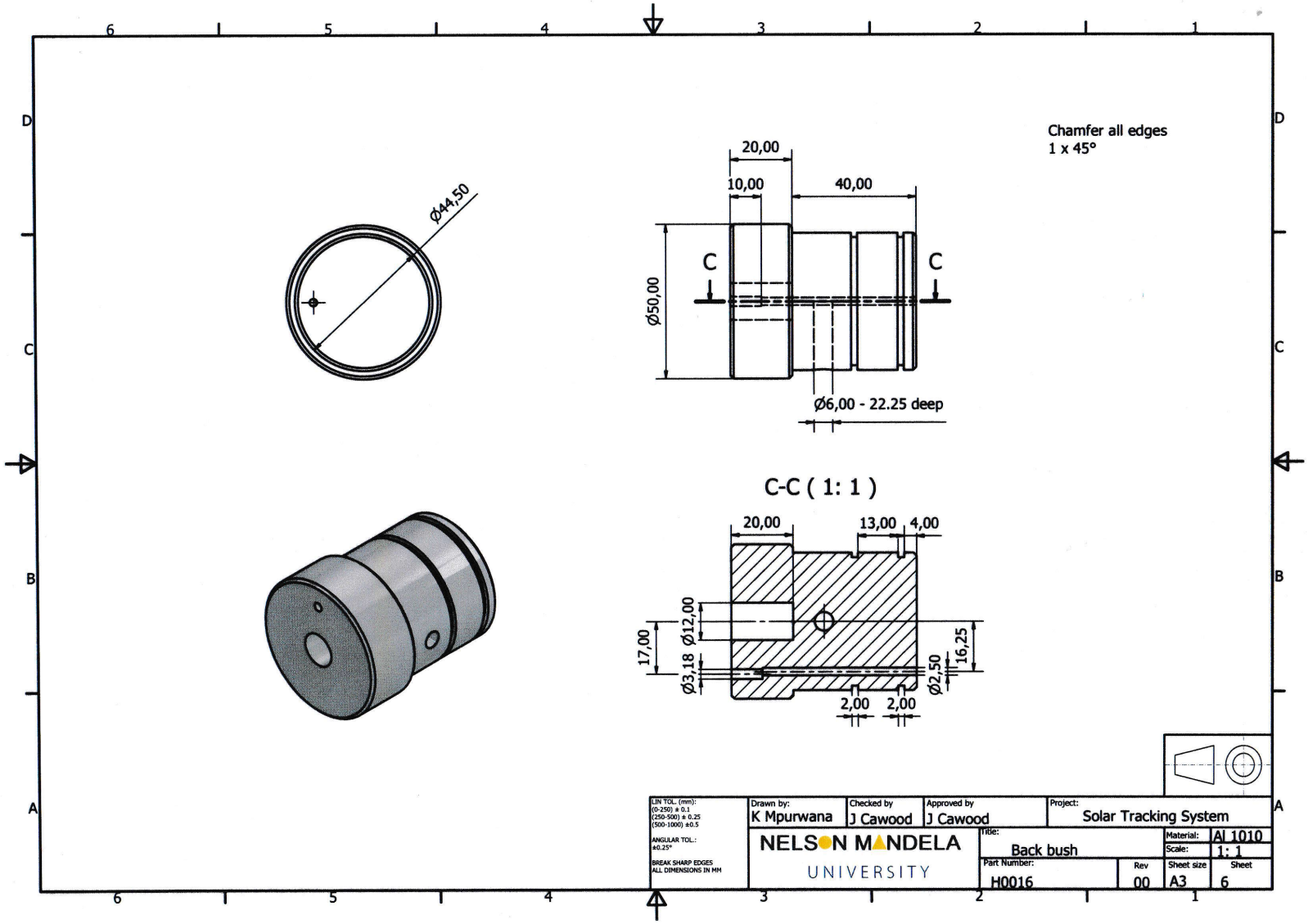
Chamfer all edges
1 x 45°
Ø44,50
20,00
10,00
40,00
C
C
Ø50,00
Ø6,00 - 22.25 deep
C-C (1: 1)
20,00
13,00
4,00
17,00
Ø12,00
Ø3,18
Ø2,50
16,25
2,00
2,00
LIN TOL. (mm):
(0-250) ± 0.1
(250-500) ± 0.25
(500-1000) ±0.5
ANGULAR TOL.:
±0.25°
BREAK SHARP EDGES
ALL DIMENSIONS IN MM
Drawn by:
K Mpurwana
Checked by
J Cawood
Approved by
J Cawood
Project:
Solar Tracking System
NELSON MANDELA
UNIVERSITY
Title:
Back bush
Material:
Al 1010
Scale:
1: 1
Part Number:
H0016
Rev
00
Sheet size
A3
Sheet
6

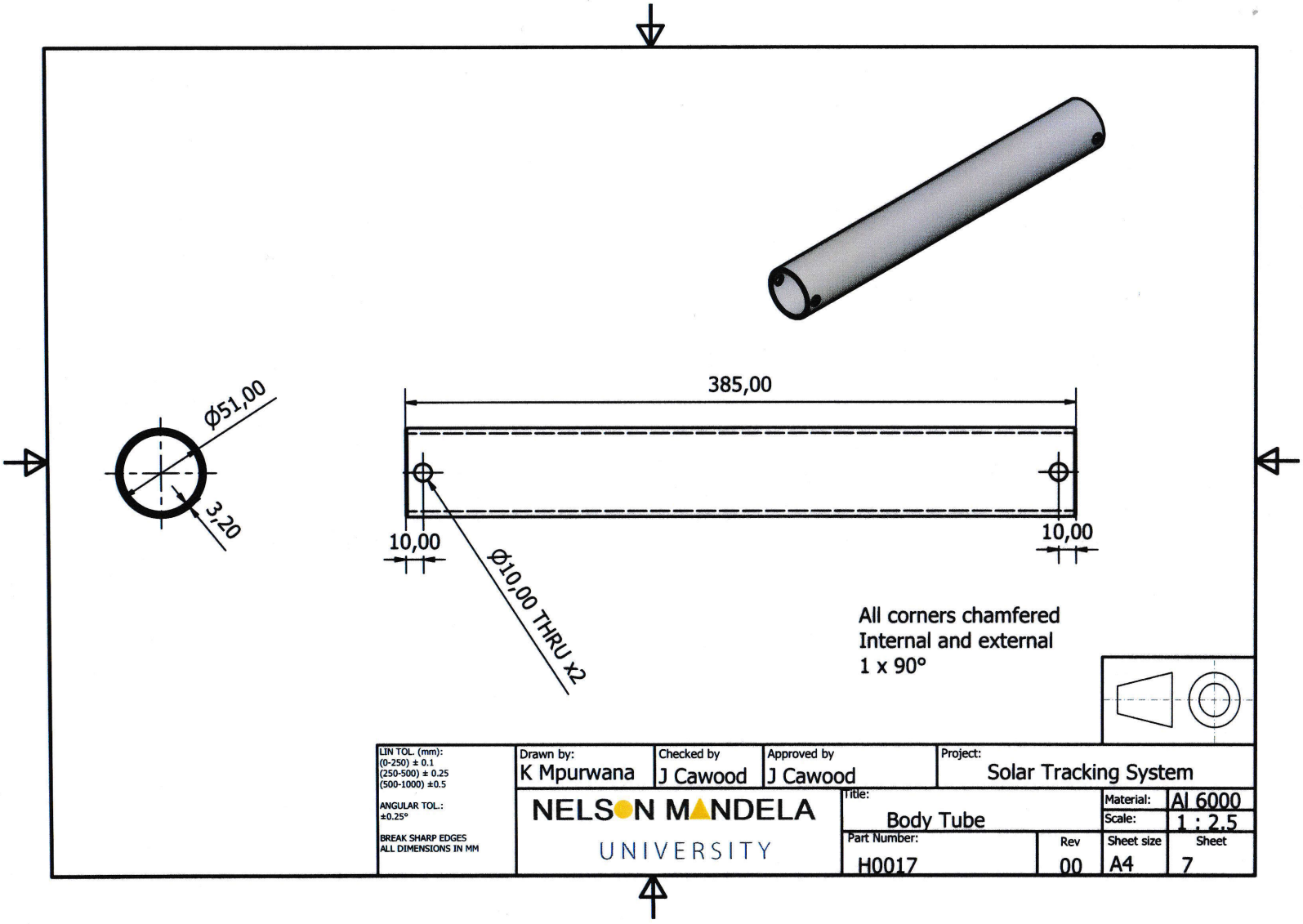
Ø51,00
3,20
385,00
10,00
10,00
Ø10,00 THRU x2
All corners chamfered
Internal and external
1 x 90°
LIN TOL. (mm):
(0-250) ± 0.1
(250-500) ± 0.25
(500-1000) ±0.5
ANGULAR TOL.:
±0.25°
BREAK SHARP EDGES
ALL DIMENSIONS IN MM
Drawn by:
K Mpurwana
Checked by
J Cawood
Approved by
J Cawood
Project:
Solar Tracking System
NELSON MANDELA
UNIVERSITY
Title:
Body Tube
Material:
Al 6000
Scale:
1 : 2.5
Part Number:
H0017
Rev
00
Sheet size
A4
Sheet
7

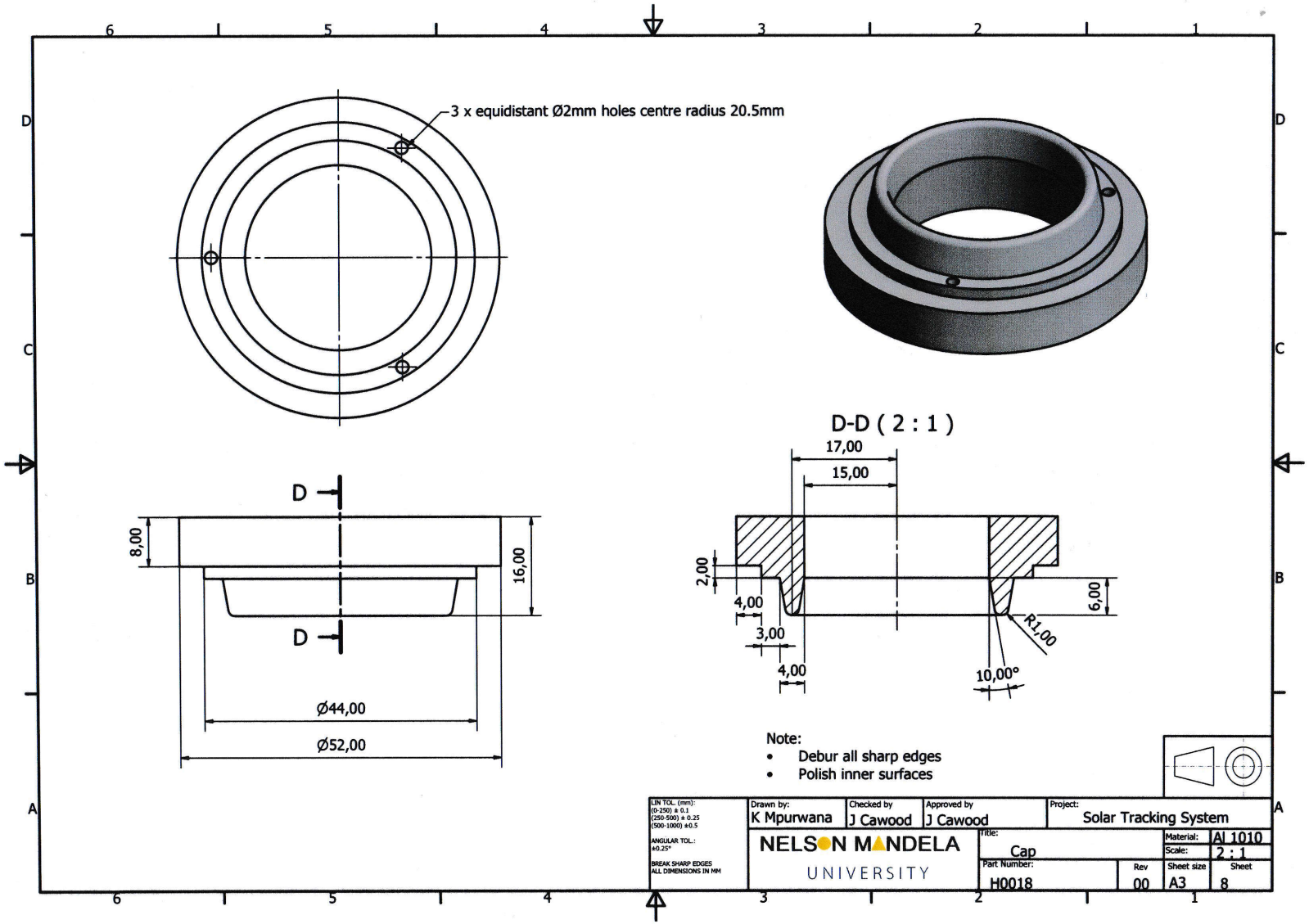
3 x equidistant Ø2mm holes centre radius 20.5mm
D
D
8,00
16,00
Ø44,00
Ø52,00
D-D (2 : 1)
17,00
15,00
2,00
4,00
3,00
4,00
6,00
R1,00
10,00°
Note:
• Debur all sharp edges
• Polish inner surfaces
LIN TOL. (mm):
(0-250) ± 0.1
(250-500) ± 0.25
(500-1000) ±0.5
ANGULAR TOL.:
±0.25°
BREAK SHARP EDGES
ALL DIMENSIONS IN MM
Drawn by: K Mpurwana
Checked by J Cawood
Approved by J Cawood
Project: Solar Tracking System
NELSON MANDELA UNIVERSITY
Title: Cap
Material: Al 1010
Scale: 2 : 1
Part Number: H0018
Rev 00
Sheet size A3
Sheet 8

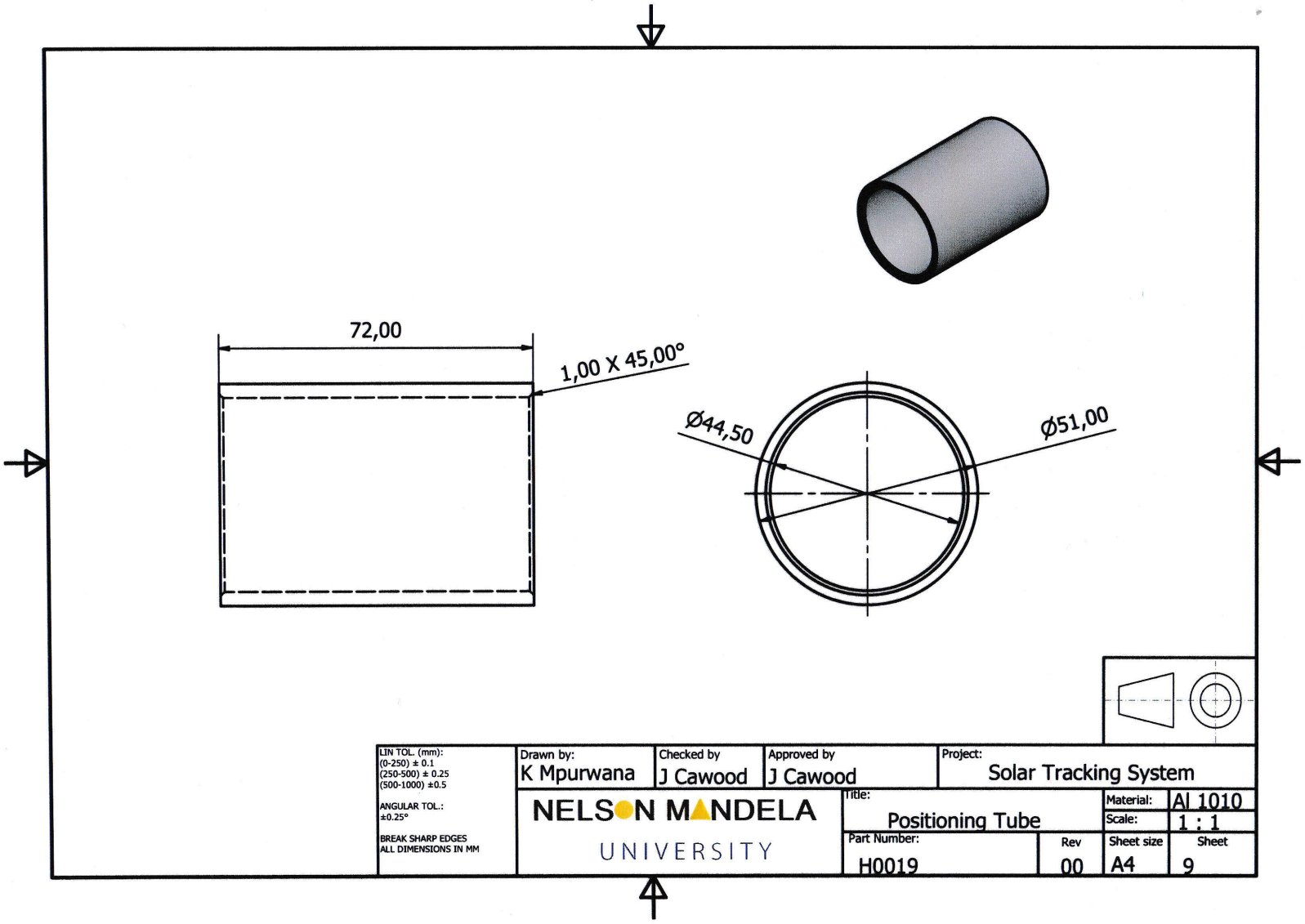
72,00
1,00 X 45,00°
Ø44,50
Ø51,00
LIN TOL. (mm):
(0-250) ± 0.1
(250-500) ± 0.25
(500-1000) ±0.5
ANGULAR TOL.:
±0.25°
BREAK SHARP EDGES
ALL DIMENSIONS IN MM
Drawn by:
K Mpurwana
Checked by
J Cawood
Approved by
J Cawood
Project:
Solar Tracking System
NELSON MANDELA
UNIVERSITY
Title:
Positioning Tube
Material:
Al 1010
Scale:
1 : 1
Part Number:
H0019
Rev
00
Sheet size
A4
Sheet
9

H002 - Hydraulic pump

H0002 Exploded view of pump

H00201 Inlet Flange

H00202 Top flange

H00203 Vortex chamber

H00204 Mesh

H00205 Body tube

H00206 Body tube flange

H00207 Discharge tube

H00208 Impeller

H00209 Drive shaft

H00210 Motor coupling

H00211 Main bearing

H00212 Thrust bearing

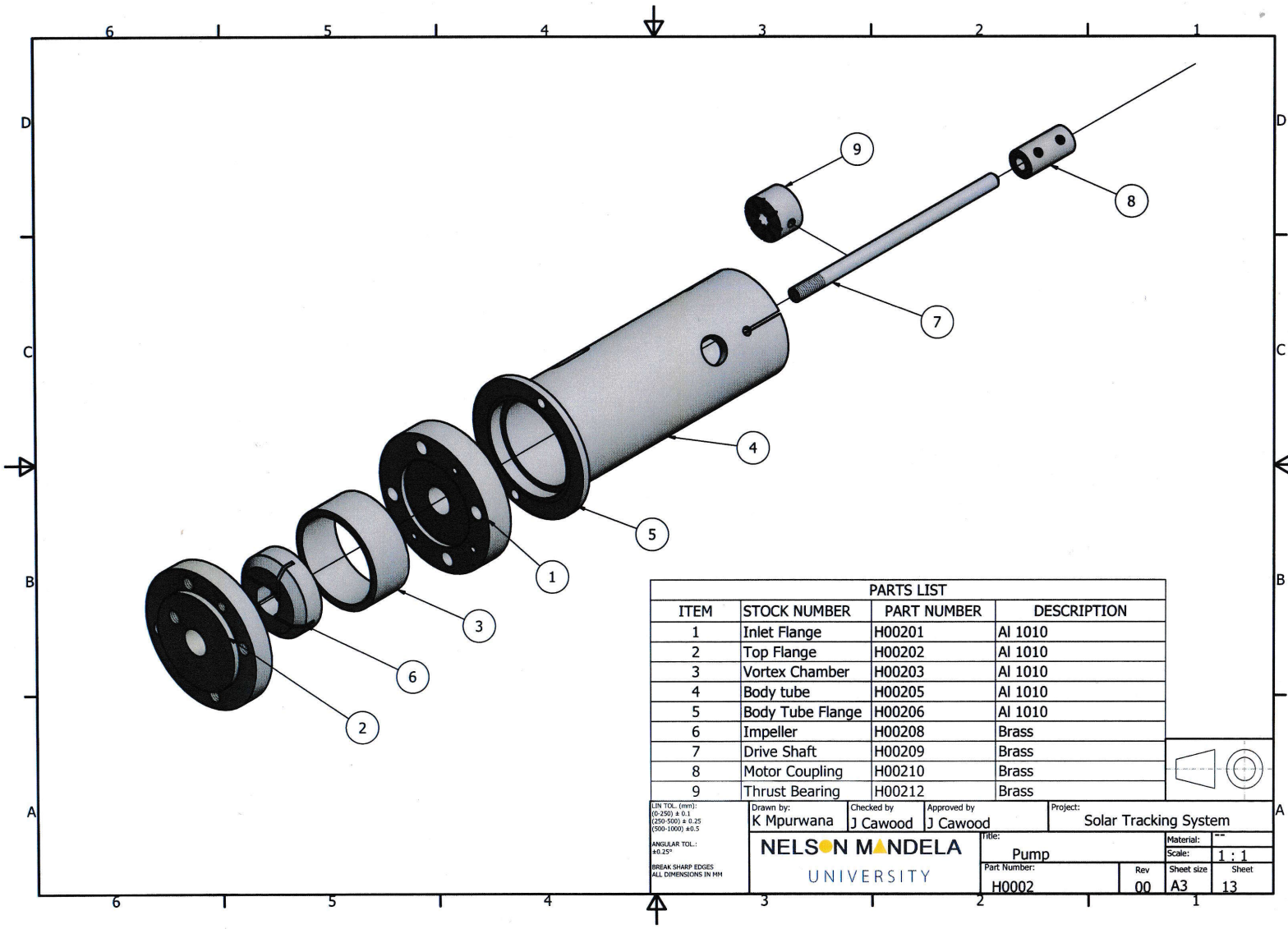

PARTS LIST			
ITEM	STOCK NUMBER	PART NUMBER	DESCRIPTION
1	Inlet Flange	H00201	Al 1010
2	Top Flange	H00202	Al 1010
3	Vortex Chamber	H00203	Al 1010
4	Body tube	H00205	Al 1010
5	Body Tube Flange	H00206	Al 1010
6	Impeller	H00208	Brass
7	Drive Shaft	H00209	Brass
8	Motor Coupling	H00210	Brass
9	Thrust Bearing	H00212	Brass

LIN TOL. (mm):
(0-250) ± 0.1
(250-500) ± 0.25
(500-1000) ±0.5

ANGULAR TOL.:
±0.25°

BREAK SHARP EDGES
ALL DIMENSIONS IN MM

Drawn by: K Mpurwana
Checked by: J Cawood
Approved by: J Cawood
Project: Solar Tracking System

NELSON MANDELA UNIVERSITY

Title: Pump
Material: --
Scale: 1 : 1
Part Number: H0002
Rev: 00
Sheet size: A3
Sheet: 13

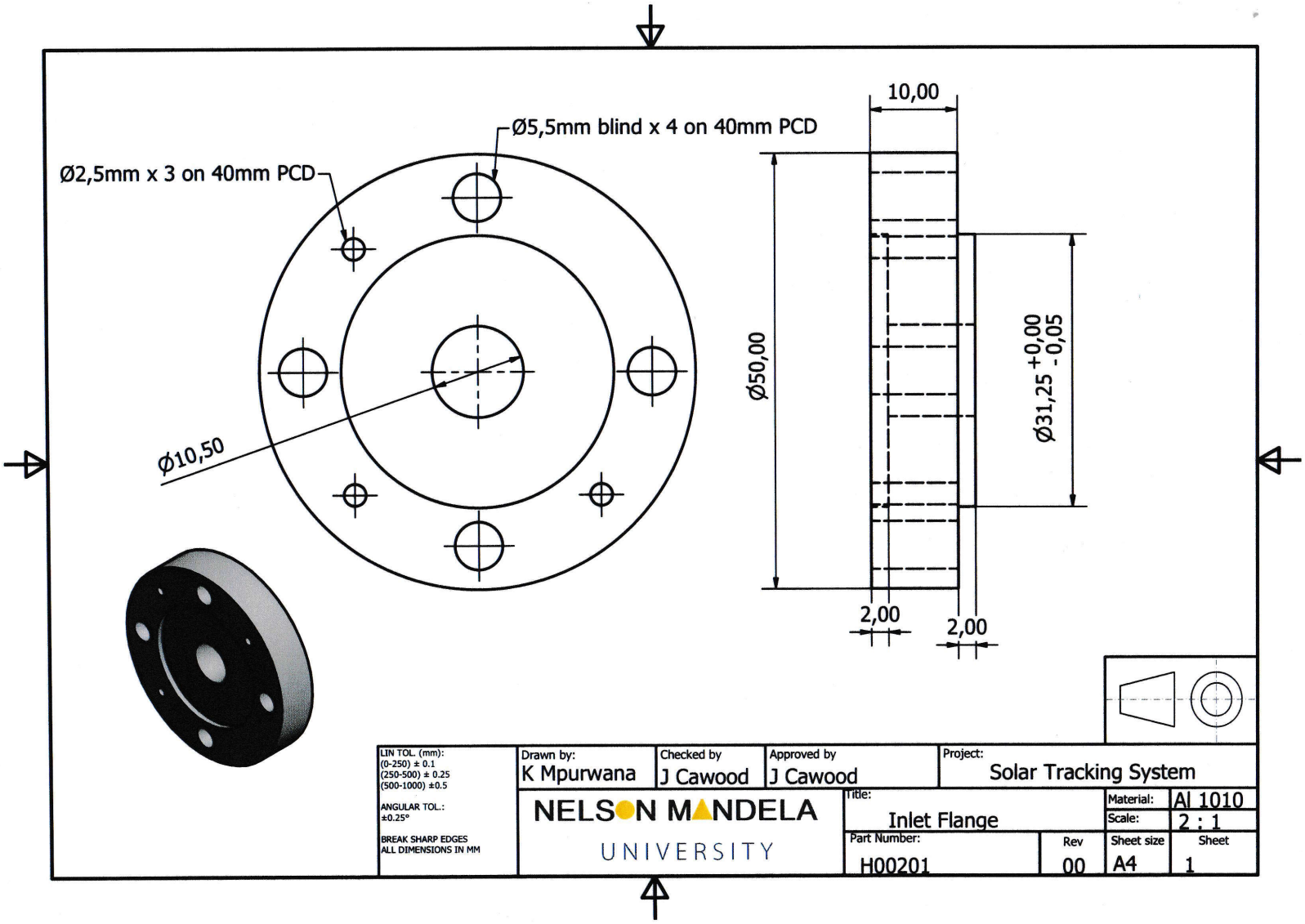

LIN TOL. (mm): (0-250) ± 0.1 (250-500) ± 0.25 (500-1000) ±0.5 ANGULAR TOL.: ±0.25° BREAK SHARP EDGES ALL DIMENSIONS IN MM	Drawn by: K Mpurwana	Checked by J Cawood	Approved by J Cawood	Project: Solar Tracking System
NELSON MANDELA UNIVERSITY	Title: Inlet Flange		Material: Al 1010	Scale: 2 : 1
	Part Number: H00201	Rev 00	Sheet size A4	Sheet 1

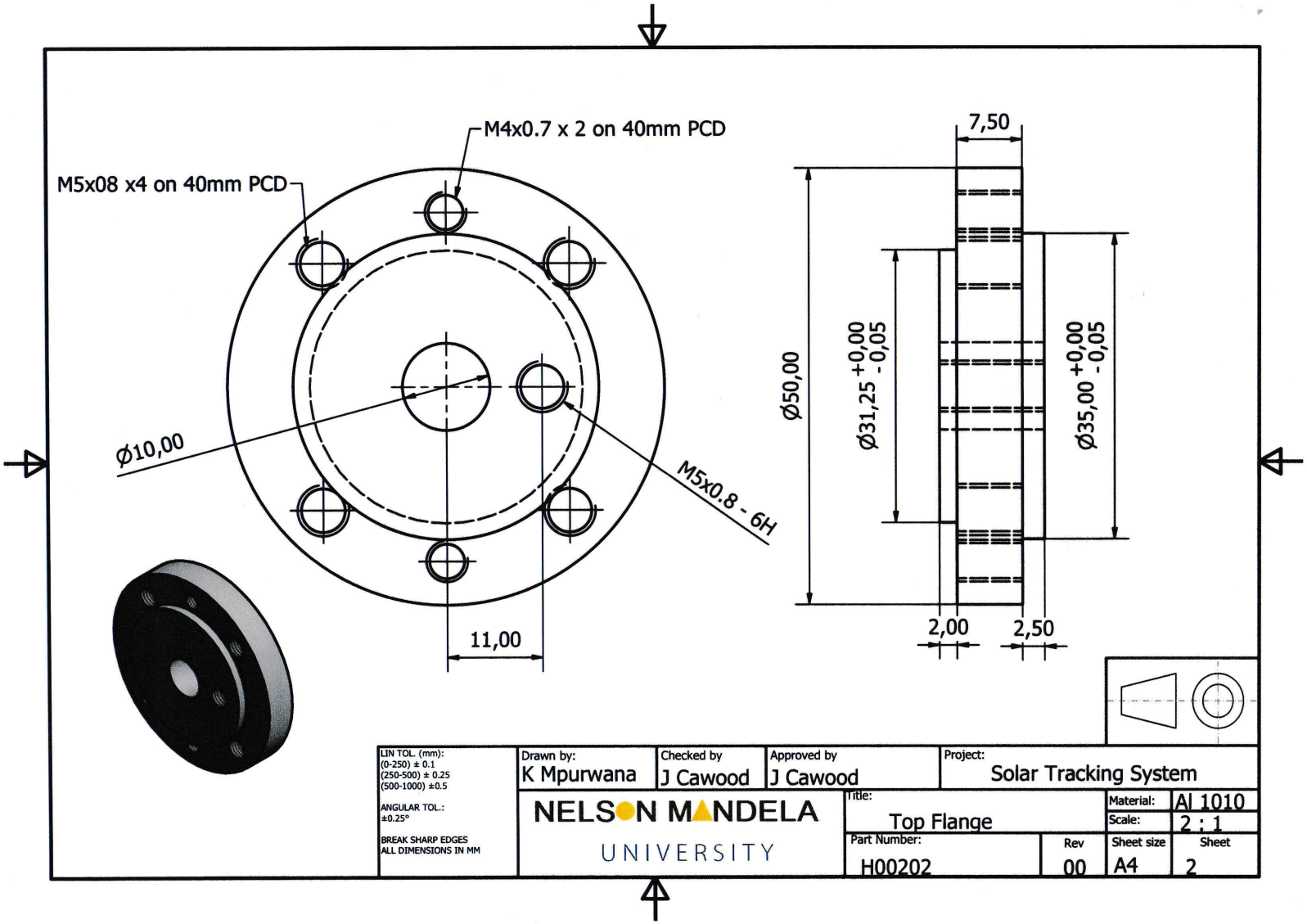
M4x0.7 x 2 on 40mm PCD
M5x08 x4 on 40mm PCD
Ø10,00
M5x0.8 - 6H
11,00
7,50
Ø50,00
Ø31,25 +0,00 -0,05
Ø35,00 +0,00 -0,05
2,00
2,50
LIN TOL. (mm):
(0-250) ± 0.1
(250-500) ± 0.25
(500-1000) ±0.5
ANGULAR TOL.:
±0.25°
BREAK SHARP EDGES
ALL DIMENSIONS IN MM
Drawn by:
K Mpurwana
Checked by
J Cawood
Approved by
J Cawood
Project:
Solar Tracking System
NELSON MANDELA
UNIVERSITY
Title:
Top Flange
Material:
Al 1010
Scale:
2 : 1
Part Number:
H00202
Rev
00
Sheet size
A4
Sheet
2

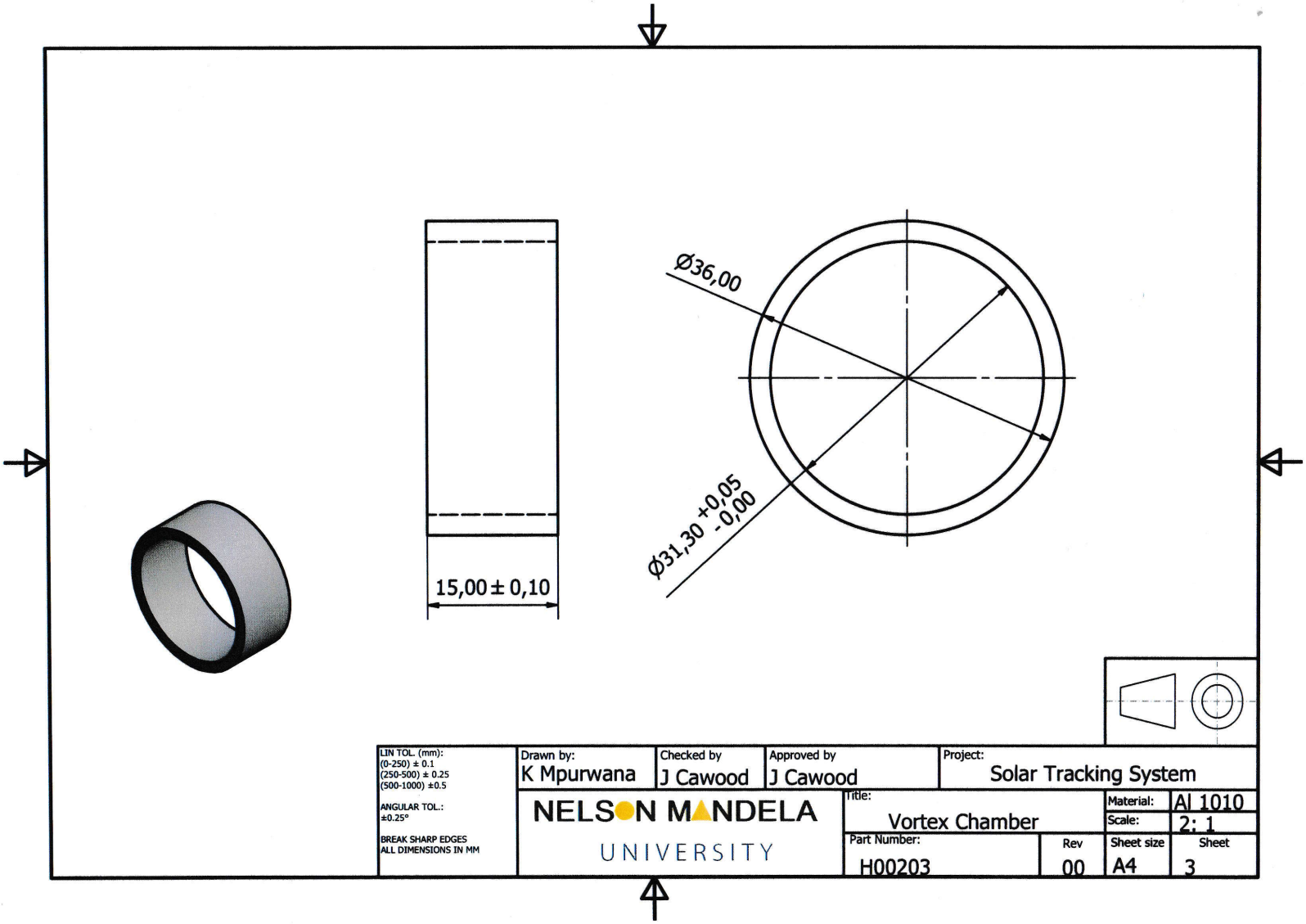
Ø36,00
Ø31,30 +0,05 -0,00
15,00 ± 0,10
LIN TOL. (mm):
(0-250) ± 0.1
(250-500) ± 0.25
(500-1000) ±0.5
ANGULAR TOL.:
±0.25°
BREAK SHARP EDGES
ALL DIMENSIONS IN MM
Drawn by:
K Mpurwana
Checked by
J Cawood
Approved by
J Cawood
Project:
Solar Tracking System
NELSON MANDELA
UNIVERSITY
Title:
Vortex Chamber
Material:
Al 1010
Scale:
2: 1
Part Number:
H00203
Rev
00
Sheet size
A4
Sheet
3

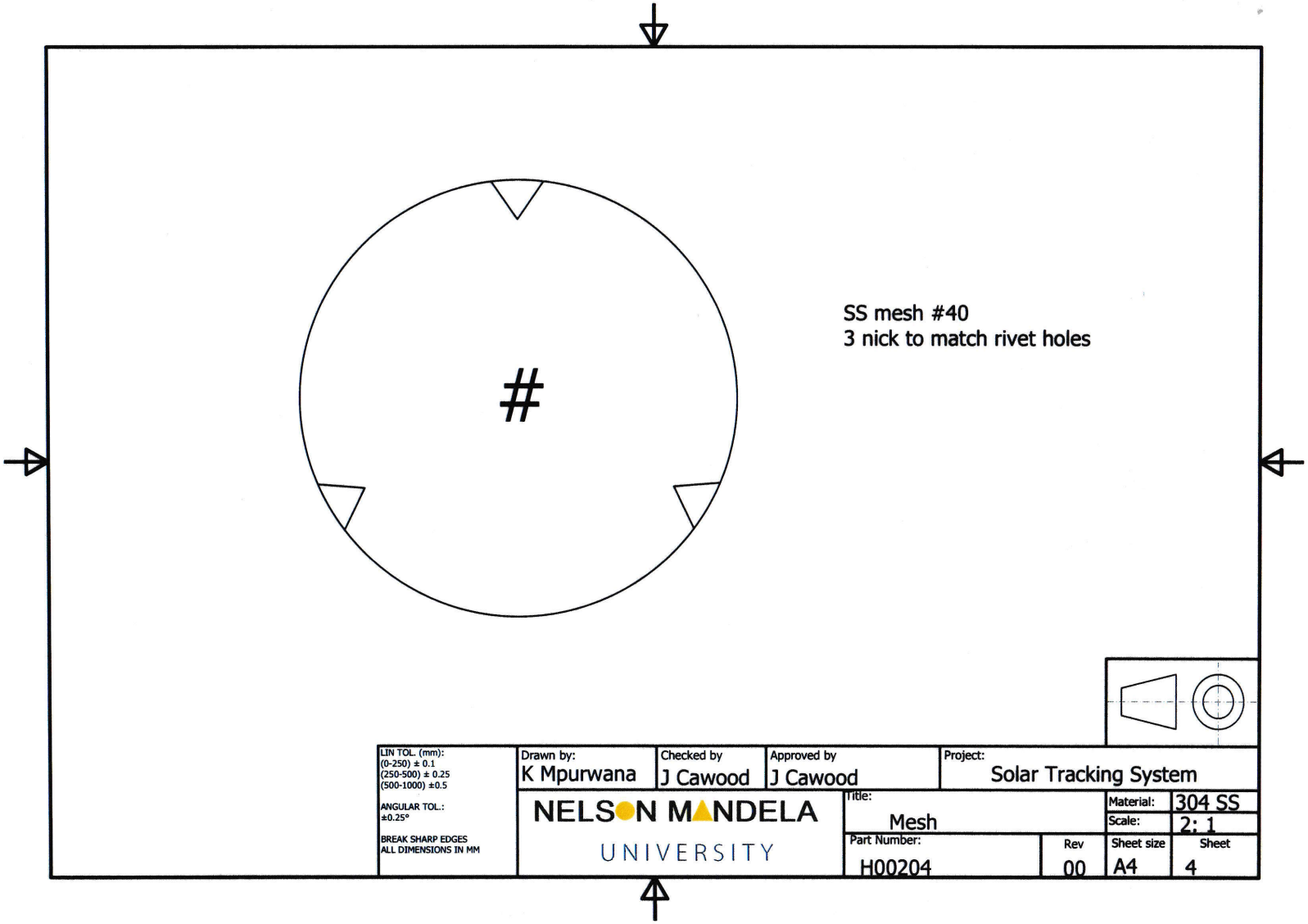
#
SS mesh #40
3 nick to match rivet holes
LIN TOL. (mm):
(0-250) ± 0.1
(250-500) ± 0.25
(500-1000) ±0.5
ANGULAR TOL.:
±0.25°
BREAK SHARP EDGES
ALL DIMENSIONS IN MM
Drawn by:
K Mpurwana
Checked by
J Cawood
Approved by
J Cawood
Project:
Solar Tracking System
NELSON MANDELA
UNIVERSITY
Title:
Mesh
Material:
304 SS
Scale:
2: 1
Part Number:
H00204
Rev
00
Sheet size
A4
Sheet
4

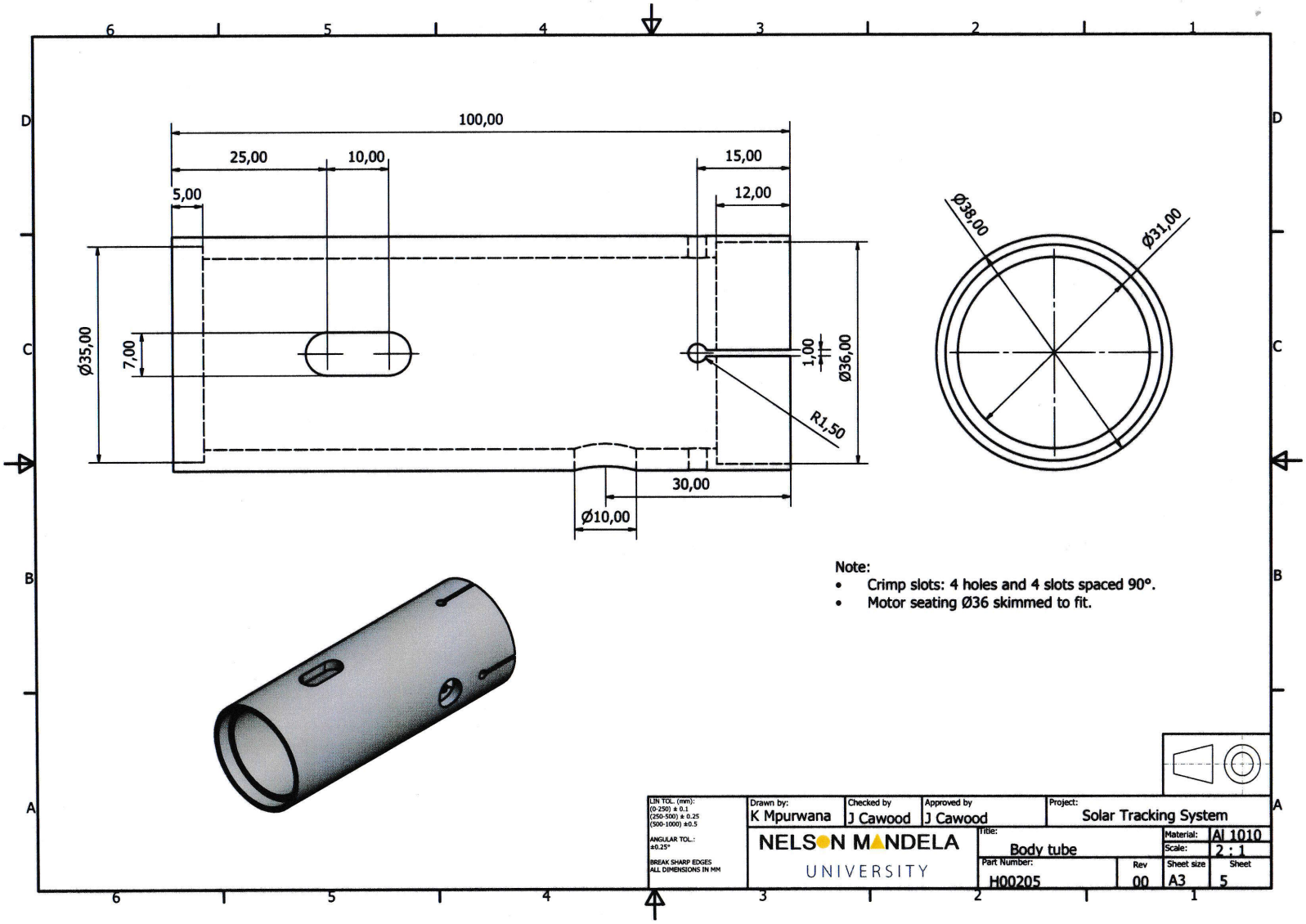
100,00
25,00
10,00
15,00
5,00
12,00
Ø35,00
7,00
1,00
Ø36,00
R1,50
30,00
Ø10,00
Ø38,00
Ø31,00
Note:
• Crimp slots: 4 holes and 4 slots spaced 90°.
• Motor seating Ø36 skimmed to fit.
LIN TOL. (mm):
(0-250) ± 0.1
(250-500) ± 0.25
(500-1000) ±0.5
ANGULAR TOL.:
±0.25°
BREAK SHARP EDGES
ALL DIMENSIONS IN MM
Drawn by:
K Mpurwana
Checked by
J Cawood
Approved by
J Cawood
Project:
Solar Tracking System
NELSON MANDELA
UNIVERSITY
Title:
Body tube
Material:
Al 1010
Scale:
2 : 1
Part Number:
H00205
Rev
00
Sheet size
A3
Sheet
5

Body tube and flange (1 : 2)

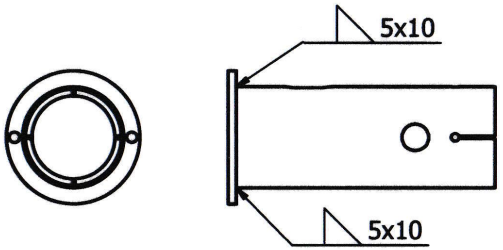

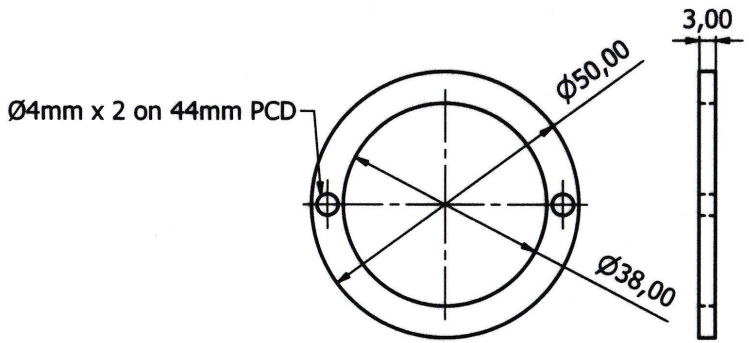

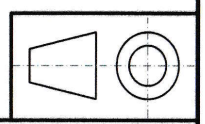

LIN TOL. (mm): (0-250) ± 0.1 (250-500) ± 0.25 (500-1000) ±0.5 ANGULAR TOL.: ±0.25° BREAK SHARP EDGES ALL DIMENSIONS IN MM	Drawn by: K Mpurwana	Checked by J Cawood	Approved by J Cawood	Project: Solar Tracking System		
NELSON MANDELA UNIVERSITY	Title: Body Tube Flange				Material:	Al 1010
					Scale:	1 : 1
	Part Number: H00206		Rev 00	Sheet size A4	Sheet 6	

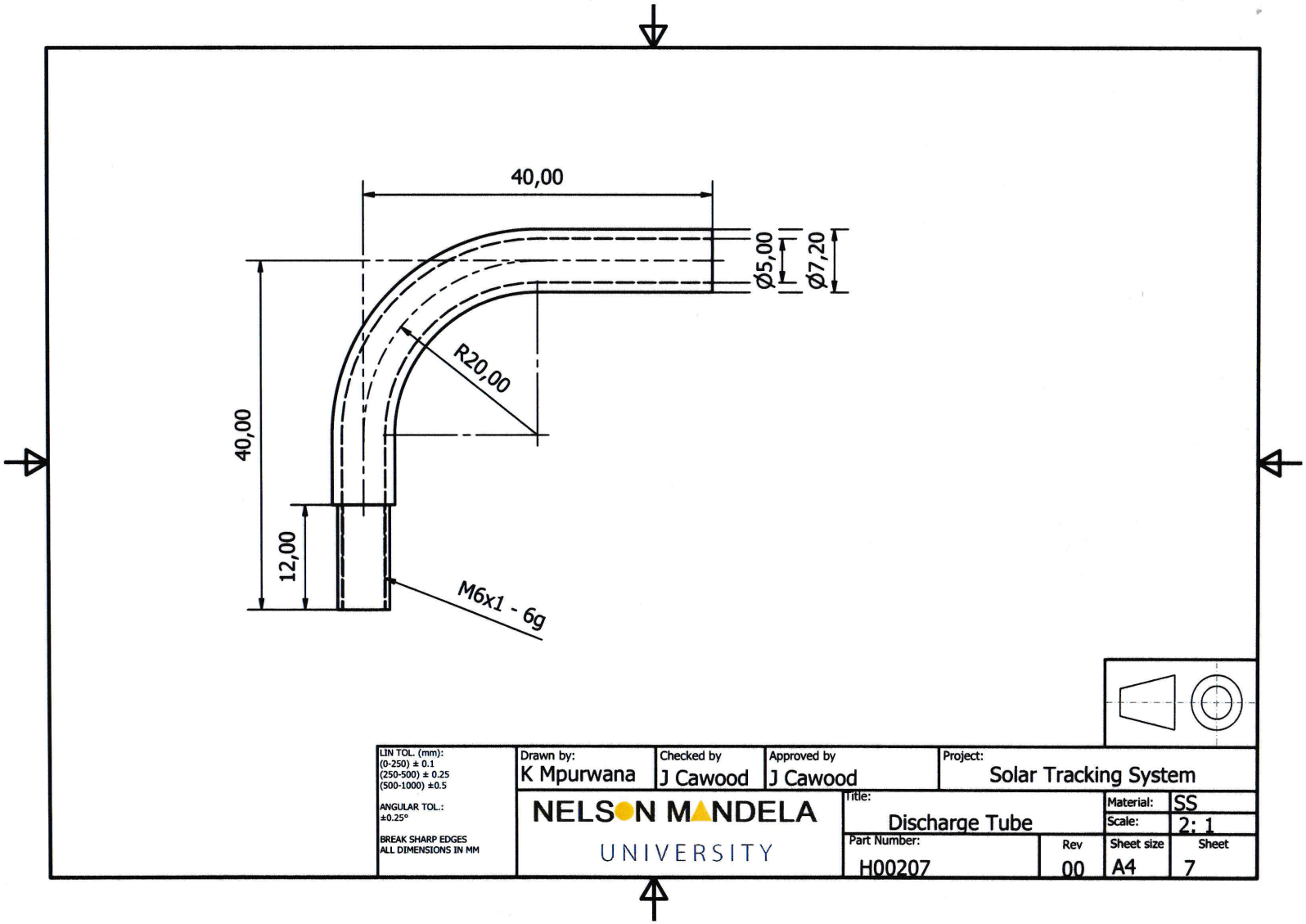
40,00
Ø5,00
Ø7,20
R20,00
40,00
12,00
M6x1 - 6g
LIN TOL. (mm):
(0-250) ± 0.1
(250-500) ± 0.25
(500-1000) ±0.5
ANGULAR TOL.:
±0.25°
BREAK SHARP EDGES
ALL DIMENSIONS IN MM
Drawn by:
K Mpurwana
Checked by
J Cawood
Approved by
J Cawood
Project:
Solar Tracking System
NELSON MANDELA
UNIVERSITY
Title:
Discharge Tube
Material:
SS
Scale:
2: 1
Part Number:
H00207
Rev
00
Sheet size
A4
Sheet
7

Note:
4 Flutes milled/ground tangential to inlet.

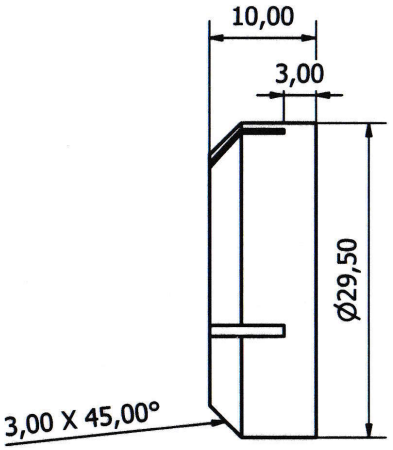

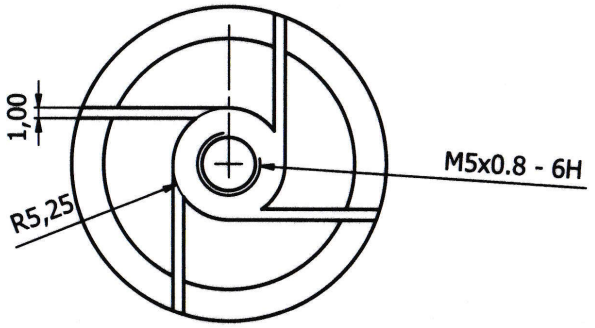

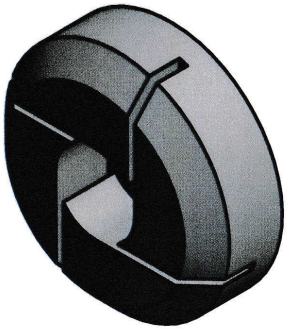

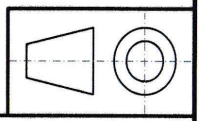

LIN TOL. (mm): (0-250) ± 0.1 (250-500) ± 0.25 (500-1000) ±0.5 ANGULAR TOL.: ±0.25° BREAK SHARP EDGES ALL DIMENSIONS IN MM	Drawn by: K Mpurwana	Checked by J Cawood	Approved by J Cawood	Project: Solar Tracking System		
NELSON MANDELA UNIVERSITY	Title: Impeller				Material:	Brass
					Scale:	2: 1
	Part Number: H00208		Rev 00	Sheet size A4	Sheet 8	

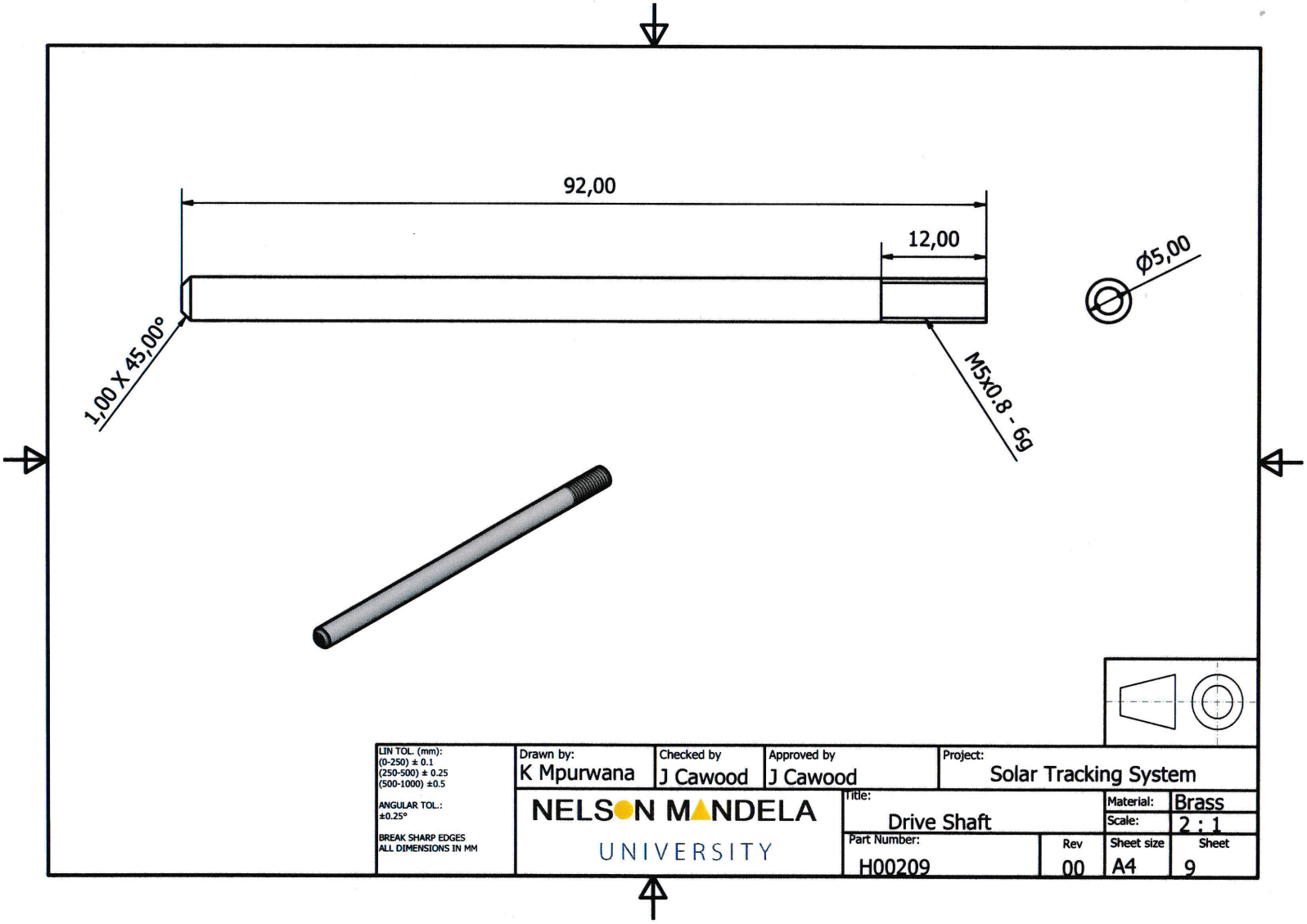
92,00
12,00
Ø5,00
1,00 X 45,00°
M5x0.8 - 6g
LIN TOL. (mm):
(0-250) ± 0.1
(250-500) ± 0.25
(500-1000) ±0.5
ANGULAR TOL.:
±0.25°
BREAK SHARP EDGES
ALL DIMENSIONS IN MM
Drawn by:
K Mpurwana
Checked by
J Cawood
Approved by
J Cawood
Project:
Solar Tracking System
NELSON MANDELA
UNIVERSITY
Title:
Drive Shaft
Material:
Brass
Scale:
2 : 1
Part Number:
H00209
Rev
00
Sheet size
A4
Sheet
9

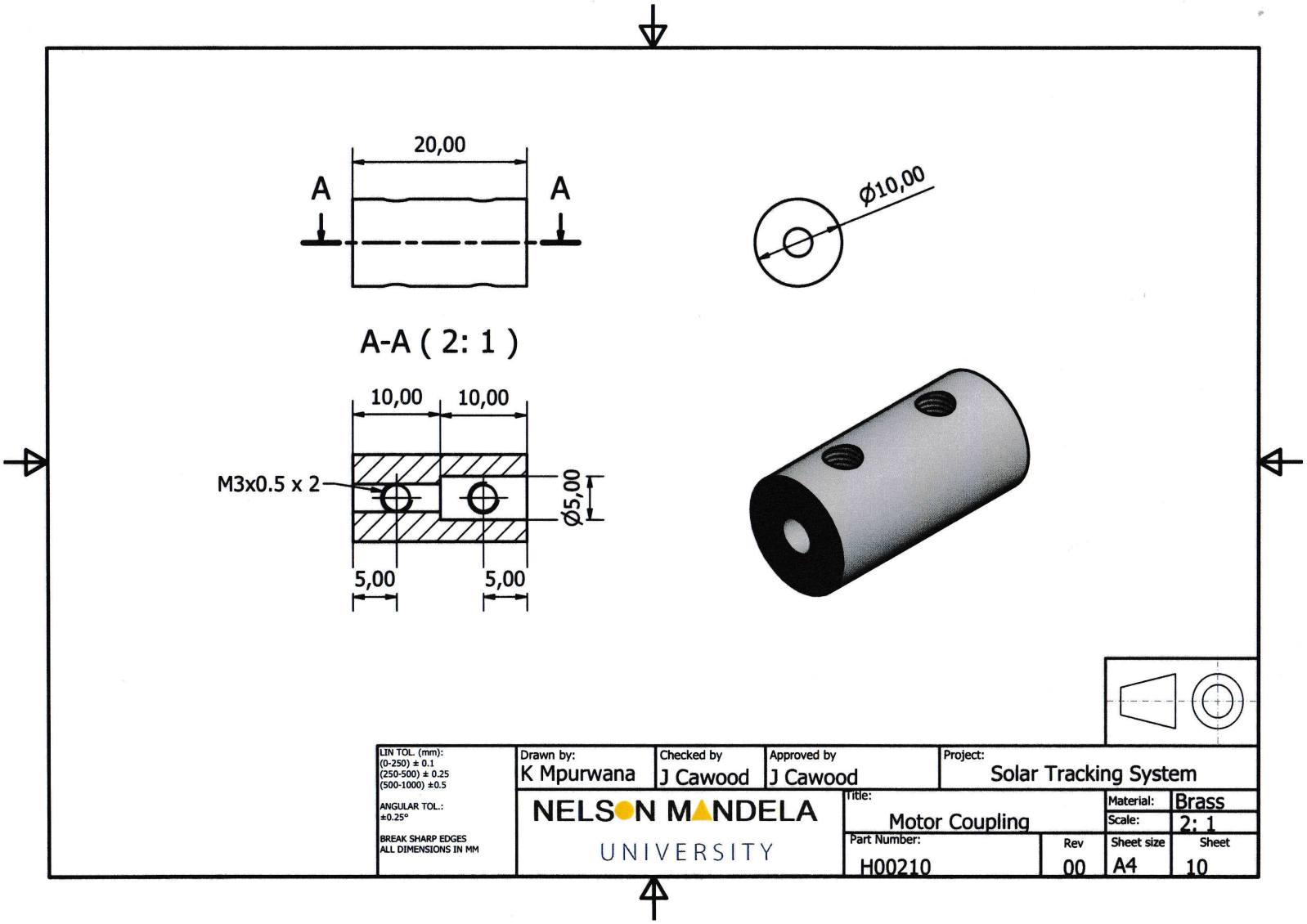

LIN TOL. (mm): (0-250) ± 0.1 (250-500) ± 0.25 (500-1000) ±0.5 ANGULAR TOL.: ±0.25° BREAK SHARP EDGES ALL DIMENSIONS IN MM	Drawn by: K Mpurwana	Checked by J Cawood	Approved by J Cawood	Project: Solar Tracking System	
NELSON MANDELA UNIVERSITY	Title: Motor Coupling			Material: Brass	Scale: 2: 1
	Part Number: H00210	Rev 00	Sheet size A4	Sheet 10	

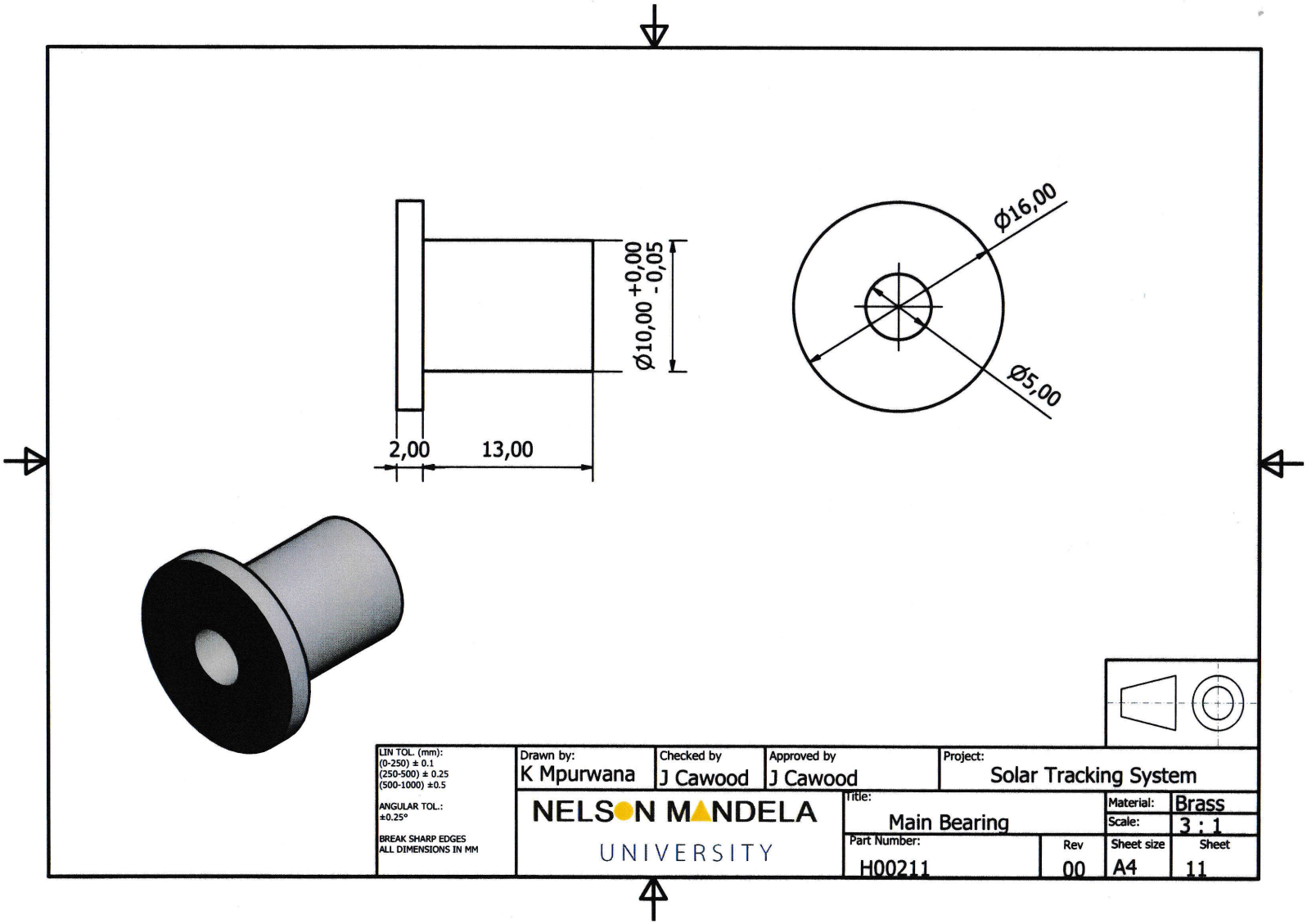
Ø10,00 +0,00 -0,05
2,00
13,00
Ø16,00
Ø5,00
LIN TOL. (mm):
(0-250) ± 0.1
(250-500) ± 0.25
(500-1000) ±0.5
ANGULAR TOL.:
±0.25°
BREAK SHARP EDGES
ALL DIMENSIONS IN MM
Drawn by:
K Mpurwana
Checked by
J Cawood
Approved by
J Cawood
Project:
Solar Tracking System
NELSON MANDELA
UNIVERSITY
Title:
Main Bearing
Material:
Brass
Scale:
3 : 1
Part Number:
H00211
Rev
00
Sheet size
A4
Sheet
11

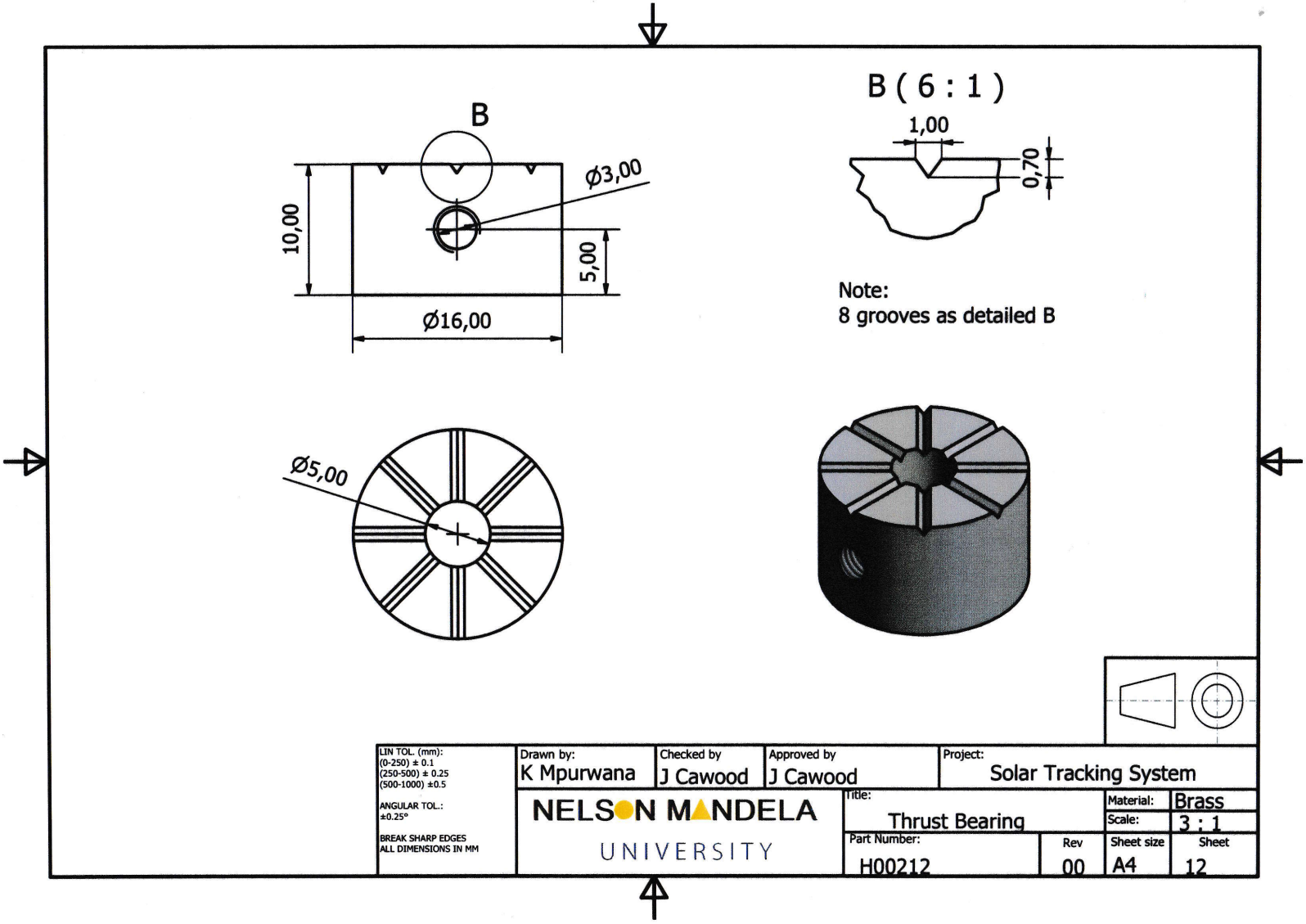
B
Ø3,00
10,00
5,00
Ø16,00
B (6 : 1)
1,00
0,70
Note:
8 grooves as detailed B
Ø5,00
LIN TOL. (mm):
(0-250) ± 0.1
(250-500) ± 0.25
(500-1000) ±0.5
ANGULAR TOL.:
±0.25°
BREAK SHARP EDGES
ALL DIMENSIONS IN MM
Drawn by:
K Mpurwana
Checked by
J Cawood
Approved by
J Cawood
Project:
Solar Tracking System
NELSON MANDELA
UNIVERSITY
Title:
Thrust Bearing
Material:
Brass
Scale:
3 : 1
Part Number:
H00212
Rev
00
Sheet size
A4
Sheet
12